Joint Channel and Frequency Offset Estimation for Wireless Communications

Rami Khal

Doctor of Philosophy (Ph.D.)

University of York

Department of Electronics

August 2011

Abstract

This thesis deals with joint channel and frequency offset estimation in many scenarios of wireless communications. In additive white Gaussian noise (AWGN) channels, a general literature survey of channel and frequency offset estimators based on the data-aided maximum likelihood (ML) principle is presented. The Cramer-Rao lower bounds (CRLB)s of the joint estimators are presented. Performance analysis of advanced frequency estimators recently proposed in the literature is provided. The performance of the estimators is compared for different application scenarios so that to get a better understanding of the differences, in terms of accuracy, complexity, frequency estimation range, signal to noise ratio (SNR) threshold. The dichotomous search (DS) frequency estimator is found to be the best practical choice. The DS frequency estimator emploies a fast Fourier transform (FFT)-based coarse search and dichotomous fine search of the periodogram peak to approximate the ML optimal estimator. This algorithm achieves the ML-like accuracy over a wide range of SNRs and throughout the wide frequency estimation range. As it relies entirely on linear operations, it is perfectly suitable for real-time implementation.

In time-invariant frequency-selective channels, the joint data-aided estimation of channel and frequency offset for signals exploiting multipath diversity is considered. This diversity improves the estimation performance by searching for the peak of the combined periodograms of multipath components. The first estimator is based on the Bayesian approach and can be used when certain prior statistical knowledge about the channel is available. The second estimator is based on the ML approach and can operate when these channel statistics are not available. Both estimators employ the DS frequency estimation technique. These estimators have a high-accuracy performance with an estimation error very close to the CRLBs over a wide range of SNRs and throughout the wide frequency acquisition range.

In frequency-flat time-variant fading channels, new joint data-aided channel and frequency offset estimators are derived. The proposed estimators are based on the basis expansion model (BEM) of the fading process and the DS frequency estimation technique. The first estimator is based on the Bayesian approach and exploits prior channel statistics to provide a high performance. The second estimator relies on the ML approach, and with a slightly lower accuracy, can operate when the prior statistics are unknown. The performance of the proposed joint estimators is examined for different scenarios in Rayleigh fading channels. The sensitivity of the Bayesian estimator to the knowledge of the Doppler frequency is investigated using such BEMs as Karhunen-Loève (KL), discrete prolate spheroidal (DPS), generalised complex exponential (GCE), and B-spline (BS) functions. The BS-BEM is found to be the most robust and the best practical choice.

In doubly-selective fading channels, a joint data-aided channel and frequency offset Bayesian estimator is proposed. The joint estimator is based on the BS-BEM representation of the fading process and the DS frequency estimation technique. Simulation results for different scenarios in Rayleigh fading channels show that the proposed estimator achieves a high accuracy performance, which is close to that with perfect knowledge of the frequency offset, over a wide range of SNRs, for different Doppler frequencies and throughout all the frequency acquisition range.

Iterative turbo receivers are developed for frequency-flat time-variant fading channels which jointly perform channel and frequency offset estimation together with data detection and decoding. The estimation and detection are based on the BS-BEM of the fading time variations and use the DS frequency estimation. Soft information generated in the turbo decoder is used to improve the quality of detection in the subsequent iterations. Depending on how much knowledge of channel statistics is available, three versions of the joint estimator, the Bayesian, ML and regularised-ML (ϵ-ML) are provided. Simulation results show that the proposed receivers provide as good performance as the corresponding ones operating with perfect knowledge of the frequency offset, and close to that operating with perfect channel knowledge.

Contents

List of Figures

List of Tables

Acknowledgements

I would especially like to thank my supervisor Dr. Yuriy Zakharov for providing me with the opportunity to learn more about joint channel and frequency estimation amongst excellent staff and colleagues in the communications research group. I am sincerely grateful to him for his constant support, encouragement, and guidance throughout all the stages of this work. He has been actively interested in my work, has always been available for advice and I have learned an incredible amount over my MSc and PhD research periods. His motivation, enthusiasm, precision, patience and vast knowledge in the field of signal processing have greatly benefited me.

I also give my thanks to the committee members Dr. Rodrigo de Lamare and Dr Des McLernon for the time they dedicated to this thesis and the valuable comments and suggestions they offered to improve the contents of it.

I would also like to thank all my colleagues in the Communication Research Group for being my surrogate family during the period of my study and for all their advice and help.

Finally, I would like to dedicate this thesis to my parents and sisters, as it is their unconditional love, continuous understanding, endless encouragement, tremendous support and extraordinary patience that have enabled me to continually progress in my academic studies.

Declaration

Some of the research presented in this thesis has resulted in some publications. These publications are listed at the end of Chapter 1.

All work presented in this thesis as original is so, to the best knowledge of the author. References and acknowledgements to other researchers have been given as appropriate.

Chapter 1

Introduction

Contents

The main purpose of this work is to investigate data-aided frequency offset estimators in wireless communications for signals propagated through additive white Gaussian noise (AWGN) channels and slow fading multipath channels, and based on this investigation, to propose joint channel and frequency offset estimators for frequency-flat time-variant and doubly-selective fading channels to be used in developed iterative turbo receivers. The joint estimation would allow higher accuracy with respect to techniques dealing separately with these two problems. We first explore and compare the performance in terms of accuracy and complexity of advanced frequency estimators that has been recently proposed in the literature for the AWGN channels, and present the joint channel and frequency offset estimation together with the corresponding Cramer-Rao lower bounds (CRLB)s. Then, we investigate frequency offset estimators, based on the Bayesian and maximum likelihood (ML) approaches, for time-invariant frequency-selective channels and present

joint channel and frequency offset estimators together with the corresponding CRLBs. After that, we propose joint channel and frequency offset estimators for frequency-flat time-variant fading channels, based on basis expansion models (BEM)s of the fading process, and compare the performance and robustness of the estimators for different BEMs. Then, we propose a joint channel and frequency offset estimator for doubly-selective fading channels. Finally, we develop iterative turbo receivers for frequency-flat time-variant fading channels which jointly perform channel and frequency offset estimation together with data detection and decoding, where soft information generated in the turbo decoder is used to improve the quality of detection in the subsequent iterations.

1.1 Motivation and Problem Statement

Modern digital RF (radio frequency) communication systems are able to operate very close to theoretical performance limits. This fact has enabled everyday technologies, such as cellular telephony and digital television, as well as more exotic applications such as secure military communications and deep-space links with robotic probes. However, many of these systems depend on coherent detection, which requires that the phase of the received signal to be known. In practice, a wireless receiver will not have prior knowledge of the phase of the received RF signal, therefore the receiver must derive the phase of the signal from careful measurement of the signal's parameters. The process of estimating and compensating for the phase is called carrier synchronization or carrier recovery.

An important part of carrier synchronization is compensating for carrier frequency offset. A frequency offset results in a time-varying phase shift. The offset is caused by mismatches between transmitter and receiver oscillators and by Doppler effects. In a typical wireless communication system, the signal to be transmitted is upconverted to a carrier frequency prior to transmission. The receiver is expected to tune to the same carrier frequency for downconverting the signal to baseband, prior to demodulation. However, due to device impairments, the carrier frequency of the receiver f_{cr} may not be the same as the carrier frequency of the transmitter f_{ct}. When this happens, the received baseband signal, instead of being centered at DC (0Hz), will be centered at a frequency f_0, where $f_0 = f_{ct} - f_{cr}$. This frequency offset f_0 in the frequency domain corresponds to an

exponential multiplier in the time domain. Ignoring noise, fading and multipath (that is discussed later in the thesis), the baseband time domain representation of the received signal is

$$r(t) = e^{j2\pi f_0 t} s(t)\,, \tag{1.1}$$

where $s(t)$ is the transmitted signal.

The carrier frequency offset of a modulated signal is estimated in one of two ways: 1) Infer the frequency offset directly from the transmitted data; 2) Infer the frequency from pilot symbols (also sometimes called training symbols, or sync words), which are known a priori by the receiver, and which are inserted into the stream of data symbols. Option 1) is called non data aided (NDA) or decision directed (DD) estimation, depending on whether a preliminary decision on the data symbol is incorporated into the estimate (DD) or not (NDA). Option 2) is known as data aided (DA) estimation.

NDA and DD estimation is the most efficient approach because no additional signal bandwidth is required for aiding synchronization. Nonetheless, NDA and DD estimation performs poorly for low SNR conditions, or for highly distorted signals. In contrast, DA estimation is more tolerant of degraded signal conditions. The downside of DA estimation is that the pilot symbols are non-information bearing, and hence increase the bandwidth overhead of the signal. Yet, DA estimation is widely used in modern communication systems due to its performance advantages, and it is the application studied in this thesis.

1.2 Overview

In wireless communication systems, where reliable transmission techniques at high data rates is a requirement, an appropriate signal detection in the receiver can only be achieved by using highly efficient synchronization techniques in which joint channel and frequency offset estimation is performed. Known data symbols called the pilot symbols is a practical method used to provide the receiver with the required information about the channel [1,2]. For time-invariant channels, the pilot symbols can be sent in a burst mode as preambles, postambles, or midambles. However, for time-variant channels, pilot symbols are usually inserted periodically within the data block in a process known as pilot symbol aided

modulation (PSAM) [3, 4] to keep up with the channel variations.

The periodogram maximiser ML frequency estimator possesses the optimum performance, but also involves impractical complexity. Practical frequency estimators approximating the ML estimator are classified as correlation-based [5–12] and periodogram-based frequency estimators [13–19].

The correlation-based frequency estimators, such as the estimators of Fitz [5], and Luise and Reggiannini (L&R) [6], can exhibit a comparable performance to that of the ML estimator. However, both estimators possess a limited frequency estimation range Ψ. This Ψ is inversely proportional to the number of input samples N and cannot be changed to suit a certain channel requirement. This prevents the estimators from being used for scenarios where a wide frequency estimation range is required. It also limits the usage for relatively large N. In addition, these estimators use nonlinear operations and possess a high computational load. We consider the following correlation-based frequency estimators. A frequency estimator that relies on the phase of the correlation sample at a single lag (L), referred to as the SL estimator, that was proposed in [7]. In [8], an estimator was presented relying on unweighted linear combination of the phase differences of L lags correlation samples, referred to as the B&S estimator. A weighted average phase differences estimator was presented in [9], referred to as the M&M estimator. Depending on the small error assumption, a simplified estimator for the AWGN channel can be derived from the one proposed in [10] based on the nonlinear least-squares (NLS), referred to as the SNLS estimator. An approximated NLS estimator was proposed in [11], referred to as the ANLS estimator, based on the summation-by-parts rule. An improved estimator was proposed in [12] based on the weighted normalised autocorrelation linear predictor, referred to as WNALP.

The periodogram-based frequency estimators use coarse and fine search for the periodogram peak [13]. Usually, the coarse search is an M-point fast Fourier transform (FFT), or discrete Fourier transform (DFT), where $M \geq N$. Some estimators use $M = N$ which allows efficient implementation. However, this requires more complicated methods to be used in the fine search and can affect the accuracy of the estimator. The linear interpolation frequency estimator [14] uses $M = N$ and exploits a three-point linear interpolation fine search. Although the coarse search is computationally efficient, the fine

search requires nonlinear operations to achieve a certain accuracy, which results in an increase of the complexity. This estimator has an f_0-dependent performance that can cause the threshold signal to noise ratio (SNR), *i.e.* the SNR below which the estimation error starts diverging from the CRLB, to be significantly higher than that of the ML estimator. Other methods can be used in the fine search, such as the three/five-point interpolation techniques [15], and Newton's method for locating the root of an equation [16]. In spite of the efficient coarse search, the fine search uses more sophisticated nonlinear techniques, which makes it difficult for practical implementation. We consider the following periodogram-based frequency estimators. A popular estimator of this type is the dichotomous search of the periodogram peak (DS) [17]. This estimator exploits FFT/DFT of the size $M \approx 1.5N$ for the coarse search, and then refines the estimate over Q iterations of searching within binary partitions in the neighbourhood of the initial peak. This estimator relies entirely on linear operations and is perfectly convenient for real-time implementation. An important modified dichotomous search (MDS) estimator was proposed in [18], which attains the CRLB without the need for zero-padding the processed samples, allowing a reduction in the complexity to be achieved. An improved dichotomous search (IDS) estimator was proposed in [19] exploiting a new initialisation scheme in an attempt to accelerate the convergence so that to allow reducing the number of iterations in the fine search and also without the need to zero-padding. A robust hybrid of periodogram-based and correlation-based estimator (grouped here with the periodogram-based estimators) was proposed in [20] and is referred to as MLAF.

Performance analysis is obtained in terms of accuracy and complexity of the mentioned advanced frequency estimators, where the performance is compared for different application scenarios. Based on that, the DS estimator is found to be the best practical choice.

In wireless communication systems, the waves traveling from the transmitter to the receiver get reflected, scattered, diffracted, or refracted due to the surrounding objects and the media property [21]. This creates multiple propagation paths, where the received signal is a sum of many copies of the transmitted signal with different delays and attenuations [22]. As a result, the channel possesses a randomly time-variant impulse response and becomes a fading channel that requires statistical treatment [23, 24]. In this case, the performance of the single-branch receiver is poor due to the SNR reduction, and diversity

reception is used to improve that performance [25, 26]. Depending on the fading rate of the channel compared to the baseband signal variations, the channels can be classified as fast fading or slow fading channels. In the fast fading channels, the channel impulse response changes rapidly within the symbol interval [23]. This implies more complicated models to represent these channels as in [27, 28], and requires special techniques for estimation as described in [29, 30]. However in the slow fading channels, the channel can be simply assumed static (time-invariant) during the observation interval [23].

Most frequency estimators for time-invariant frequency-selective channels in the literature are based on the correlations of the received signal due to the simplicity in the implementation. The estimator in [25] is an extension to the multipath channels with diversity reception of the correlation-based algorithm for the nonfading channels proposed in [6]. However, it has a narrow frequency acquisition range and poor performance at low SNRs. This is a common case in the correlation-based estimators [31–33].

Joint estimators of channel and frequency offset exploiting multipath diversity is considered for the time-invariant channels. This diversity is shown to improve the estimation performance in a similar way that the detection performance in multipath channels is improved by the RAKE receiver [22]. Two joint estimators are studied. The first follows the Bayesian approach and can be used when certain prior statistical knowledge about the channel is available. The other follows the maximum likelihood approach when these channel properties are not available. For practical implementation, both estimators employ the DS frequency estimation. Therefore, and without increasing the complexity, these estimators outperform the correlation-based algorithms and possess a wide frequency acquisition range.

The joint channel and frequency offset estimation becomes challenging when dealing with time-variant channels, where in addition to the additive noise, the transmitted signal is corrupted with a random multiplicative distortion [23]. This makes the channel and frequency offset estimation complicated, and so, traditional techniques have dealt separately with these two problems. Various frequency offset estimators for frequency-flat time-variant fading channels have been proposed in the literature. However most of these estimators are correlation-based [7, 8, 10, 11, 34, 35], and so, their performance is inferior to that of the optimal ML estimator and/or they possess a limited frequency acquisition

range. The estimator in [34] is based on weighted linear regression for the phase of the sample correlation function, however the covariance matrix of the phase estimation is assumed to be known. In [35], a modification was presented to allow the operability in a wider acquisition range, and in this case the covariance matrix is estimated. However, an assumption was made for the fading correlation. No such assumption was made in [8], where two estimators were proposed. The first is based on unweighted version of the method of [35] and the second is based on a nonlinear least-squares (NLS) approach. Similar NLS technique was derived in [10] based on the multiple lags correlation function. Several channel estimators for frequency-flat time-variant channels were proposed in [4, 36–42]. The BEM has been efficiently used for channel estimation [36, 38–43]. However, these estimators yield a severe degradation in the performance at the presence of a frequency offset. This problem can be resolved using joint channel and frequency offset estimation, which to the best of our knowledge, has not been well addressed in the literature and the main aim here is to fill that gap.

We focus on estimating the channel which contains both, the multiplicative distortion and frequency offset. This channel is all what the receiver needs in practical applications, where there is no need for spending much complexity on explicit estimators for its individual components. The goal here is twofold. Firstly, we propose interpolation-based practical frequency offset estimators based on the dichotomous search technique, involving a two stage [13] search of the generalised periodogram peak [44], an FFT-based coarse search [45] and dichotomous fine search [17]. The estimators achieve superior performance compared to that of the correlation-based estimators, and possess a wide frequency acquisition range. Secondly, we propose algorithms that estimate the channel jointly with the frequency offset. The estimation is based on approximating the time-variant fading process by a BEM and employ the DS frequency estimation technique. This leads to a mathematical model that offers a simple (reduced dimensionality) processing in addition to a high-accuracy performance over the wide frequency offset range. The novel joint estimators are derived based on two approaches. The first is the Bayesian approach and can be used when certain prior statistical knowledge about the channel is available. The other is the ML approach and is applicable when the channel statistics are not available.

Simulations for different scenarios in Rayleigh fading channels are used to investigate

the performance of the new estimators. The proposed Bayesian joint estimator is studied based on different BEMs such as Karhunen-Loève (KL), discrete prolate spheroidal (DPS), generalized complex exponential (GCE), and B-spline (BS) functions, where the channel statistics are perfectly or imperfectly known. Based on that, the BS BEM is found to be the best choice in practice.

Accurate channel estimation is challenging in frequency-selective and time-variant fading channels, especially in the presence of a frequency offset. Most of the frequency offset estimators proposed in the literature have been devoted to correlation-based estimation, such as [25, 46] for frequency-selective time-invariant channels and [8, 11, 34] for frequency-flat time-variant fading channels. However, the performance of such estimators is inferior to that of the estimator based on the generalised periodogram [44], and unlike that estimator, they are operable only at high SNRs and/or they possess a limited frequency acquisition range [47, 48]. Periodogram-based joint channel and frequency offset estimation for frequency-flat time-variant fading channels has been considered in [49, 50], where joint estimators exploiting BEM of the channel time variations have been proposed. BEMs have been widely used for frequency-flat time-variant channel estimation [38, 41, 51]. However, these estimators yield a severe degradation in the performance in the presence of a frequency offset. Joint channel and frequency offset estimation for frequency-selective time-invariant channels has been addressed in [52]. For doubly-selective fading channels, BEM-based channel estimation has been considered in [53]. The estimation of doubly-selective fading channels in the presence of a frequency offset for multicarrier systems, based on complex exponential BEM, has been addressed in [54].

We focus on estimating jointly the doubly-selective fading channels and frequency offset by using BS BEM. The proposed estimator is based on representing the fading process by BEMs and employing frequency estimation based on the DS estimator.

By considering the soft information from a soft-input soft-output (SISO) decoder in an iterative channel estimation and data detection, various iterative turbo processing techniques have been widely considered for pilot symbol assisted modulation (PSAM) systems at the receivers. However, most studies have either ignored the possible presence of a frequency offset [55], or assumed time-invariant channels when dealing with the fre-

quency offset [56]. We consider iterative turbo-based receivers for PSAM systems and QAM signals dealing with joint estimation of the time-variant channel and frequency offset together with data detection and decoding, which, to the best of our knowledge, is seldom treated in the literature.

1.3 Contributions

Major contributions in this thesis can be summed up as follows:

- Performance of advanced frequency estimators that have been recently proposed in the literature for signals in the additive white Gaussian noise has been analysed. A fair performance comparison has been obtained of many recent estimators from both classes, correlation-based and periodogram-based estimators, under the same simulation environment and for different application scenarios so that to get a better understanding about the differences, most precisely, in terms of accuracy, complexity, frequency acquisition range, signal to noise ratio (SNR) threshold and the sensitivity of these towards different SNR and frequency scenarios. The dichotomous search estimator, which involves a two stage technique for searching the periodogram peak, an FFT-based coarse search and a dichotomous fine search, has been shown to outperform the other estimators in many scenarios, keeping a high-accuracy performance throughout the wide frequency estimation range and for all considered SNRs. It also relies only on linear operations with a relatively low complexity, which makes it the best choice in many practical scenarios.

- Joint estimation of channel and frequency offset in frequency-selective channels for data-aided scenarios has been studied. The considered estimators exploit the multipath diversity by combining the periodograms of the multipath elements and searching for the maximum of the combined statistic. Two joint estimators have been considered. The first estimator depends on the Bayesian approach and can provide a high-accuracy performance whenever prior statistical characteristics of the channel are known, namely the mean and covariance matrices of the channel parameters and the variance of the AWGN. The second estimator, with a slightly

higher estimation error, is an alternative joint estimator that can operate when these characteristics are unavailable. To reduce the complexity of the frequency offset estimators and attain a high accuracy, the estimators exploit the dichotomous search frequency estimation. These estimators have been extensively investigated for many different application scenarios in Rayleigh fading channels. These estimators have been shown to maintain a high-accuracy performance with an estimation error very close to the CRLB over a wide range of SNR and throughout the wide frequency acquisition range.

- Joint data-aided estimators of channel and frequency offset in time-variant fading channels have been derived, depending on how much knowledge of channel statistics is available, based on basis expansion models (BEM)s of the time variation and the dichotomous search frequency estimation. These estimators are examined for Rayleigh fading channels. They achieve a high accuracy performance over a wide range of signal to noise ratio, for different Doppler frequencies and throughout all the frequency acquisition range.

- The performance of the joint data-aided estimators of channel and frequency offset in time-variant fading channels has been compared using different BEMs such as, Karhunen-Loève (KL), discrete prolate spheroidal (DPS), generalized complex exponential (GCE), and B-spline (BS) functions for different scenarios in Rayleigh fading channels, where the channel statistics are perfectly or imperfectly known. When channel statistics are perfectly known, the KL and DPS BEMs use slightly lower number of basis functions than that of the GCE and BS BEMs to allow achieving the same performance. However, the best reached performance of all the BEM-based estimators is the same. When channel statistics are mismatched, the estimators based on the GCE and BS BEMs are more robust than those based on the KL and DPS BEMs. This makes the BS functions a better choice in practice as it has a sparse matrix that results in a lower complexity than the other basis functions.

- The joint channel and frequency offset estimator has been derived for doubly-selective fading channels. The estimator has been investigated for different scenarios in Rayleigh fading channels, where it maintains a high-accuracy performance over wide SNR, frequency offset and Doppler frequency ranges, which is very close

to that of the Bayesian channel estimator operating with perfect knowledge of the frequency offset.

- Iterative turbo receivers have been developed for time-variant fading channels, depending on how much knowledge of channel statistics is available. The receivers jointly perform channel and frequency offset estimation together with data detection and decoding. Soft information generated in the turbo decoder is used to improve the quality of the detection in the subsequent iterations. The receivers have been shown to provide as good performance as the corresponding ones operating with perfect knowledge of the frequency offset, and is very close to that operating with perfect channel knowledge.

1.4 Thesis Outline

The rest of the report is separated into following chapters, according to the different systems investigated and analyzed.

- Chapter 2: Fundamental Techniques

  In this chapter, fundamental techniques used throughout this thesis are introduced. Different simulators of time-variant channels are first compared and the one whose statistics match to those of the desired reference Clarke's model is applied. The basic principles of BEMs are also described, which are used to approximate the fading channels. Turbo encoder and decoder are also briefly introduced.

- Chapter 3: Joint Estimation of Channel and Frequency Offset in Additive White Gaussian Noise Channels

  In this chapter, a general literature survey of data-aided channel and frequency offset estimators based on the maximum likelihood (ML) principle for signals transmitted through additive white Gaussian noise (AWGN) channels is provided. The CRLBs of the joint estimators are derived. Performance analysis in terms of accuracy and complexity of advanced frequency estimators that has been recently proposed in the literature is performed. The dichotomous-based joint channel and frequency offset estimators are then investigated.

- Chapter 4: Joint Estimation of Channel and Frequency Offset in Frequency-Selective Channels

  This chapter presents the joint data-aided estimation of channel and frequency offset for signals propagated through time-invariant frequency-selective channels. Two joint estimators, Bayesian-based estimator when certain prior statistical knowledge about the channel is known and ML-based estimator when these channel properties are not available, are studied. Both estimators employ an FFT-based coarse search and a dichotomous fine search for the periodogram peak. Extensive simulations for different scenarios are used to investigate the performance of the joint estimators in Rayleigh fading channels.

- Chapter 5: Joint Estimation of Channel and Frequency Offset in Time-Variant Fading Channels

  In this chapter, novel joint data-aided channel and frequency offset estimators are proposed for frequency-flat time-variant fading channels, based on the BEM of the time variation and the dichotomous search frequency estimation technique. Two joint estimators, following the Bayesian and maximum likelihood approaches (depending on the availability of the prior knowledge of the channel statistics), are derived. The performance of the proposed joint estimators is examined for different scenarios in Rayleigh fading channels. The sensitivity of the Bayesian estimator to the knowledge of the Doppler frequency is investigated using different BEMs.

- Chapter 6: Joint Estimation of Channel and Frequency Offset in Doubly-Selective Fading Channels

  In this chapter, the proposed joint data-aided channel and frequency offset estimators are upgraded to be applicable for doubly-selective fading channels. The considered estimator follows the Bayesian approach and is based on the B-spline model representation of the fading process and the dichotomous search frequency estimation technique. This joint estimator is examined for different scenarios in Rayleigh fading channels and compared to the Bayesian channel estimator operating with perfect knowledge of the frequency offset.

- Chapter 7: Iterative Turbo Receivers in Time-Variant Fading Channels

  Iterative turbo receivers are developed in this chapter for time-variant fading channels which jointly perform channel and frequency offset estimation together with

data detection and decoding. Three versions of the joint estimator, the Bayesian, the maximum likelihood and the regularised-maximum likelihood are presented depending on how much knowledge of channel statistics is available. The estimation and detection are based on the basis expansion model of the fading time variations and use the dichotomous search frequency estimation technique. Soft information generated in the turbo decoder is used to improve the quality of detection in the subsequent iterations. The performance of the developed receivers is investigated and compared to that of the corresponding ones operating with perfect knowledge of the frequency offset and also to that of the one operating with perfect channel knowledge.

1.5 Notation

In this thesis, we use capital and small bold fonts to denote matrices and vectors, i.e., $\mathbf{A}$ and $\mathbf{a}$, respectively. Elements of the matrix and vector are denoted as $A_{m,n} = [\mathbf{A}]_{m,n}$ and $a_m = [\mathbf{a}]_m$. The symbol j is an imaginary unit $j = \sqrt{-1}$. We denote $\Re\{\cdot\}$ and $\Im\{\cdot\}$ as the real and imaginary components of a complex number, respectively; $(\cdot)^*$ denotes complex conjugate; $\mathbf{I}_Q$ denotes an $Q \times Q$ identity matrix; $(\cdot)^T$ and $(\cdot)^H$ denote matrix transpose and Hermitian transpose, respectively. $\otimes$ denotes the Kronecker product. $\lceil\cdot\rceil$ denotes the smallest integer. $E\{\cdot\}$ denotes the statistical expectation operator and tr$\{\cdot\}$ denotes the trace operator.

1.6 Publication List

Conference Papers [49, 50, 57–62]

[1] R. N. Khal and Y. V. Zakharov, “Iterative receivers with joint channel and frequency offset estimation in time-variant fading channels,” in *Proc. IEEE ISWCS’10*, York, UK, Sep. 2010, pp. 844–848.

[2] R. N. Khal, "Comparison of accuracy and complexity of advanced frequency estimators," in *Proc. IEEE ISWCS'10*, York, UK, Sep. 2010, pp. 490–495.

[3] J. Zhang, R. N. Khal, and Y. V. Zakharov, "Sensitivity of channel estimation using B-splines to mismatched Doppler frequency," in *Proc. IEEE ISWCS'10*, York, UK, Sep. 2010, pp. 946–950.

[4] J. Zhang, Y. V. Zakharov, and R. N. Khal, "Optimum detection in spatially uncorrelated SIMO Rayleigh fast fading channels with imperfect channel estimation," in *Proc. IEEE ISWCS'10*, York, UK, Sep. 2010, pp. 476–479.

[5] R. N. Khal, Y. V. Zakharov, and J. Zhang, "B-spline based joint channel and frequency offset estimation in doubly-selective fading channels," in *Proc. IEEE ICASSP'10*, Dallas, Texas, USA, Mar. 2010, pp. 3214–3217.

[6] R. N. Khal, J. Zhang, and Y. V. Zakharov, "Robustness of joint Bayesian frequency offset and channel estimation based on basis expansion models," in *Proc. 43rd Asilomar Conf. ACSSC'09*, Pacific Grove, California, USA, Nov. 2009, pp. 957–961.

[7] J. Zhang, Y. V. Zakharov, and R. N. Khal, "Optimal detection for STBC MIMO systems in spatially correlated Rayleigh fast fading channels with imperfect channel estimation," in *Proc. 43rd Asilomar Conf. ACSSC'09*, Pacific Grove, California, USA, Nov. 2009, pp. 1387–1391.

[8] R. N. Khal, Y. V. Zakharov, and J. Zhang, "Joint channel and frequency offset estimators for frequency-flat fast fading channels," in *Proc. 42nd Asilomar Conf. ACSSC'08*, Pacific Grove, California, USA, Oct. 2008, pp. 423–427.

1.7 Awards

[1] Kathleen Mary Stott Prize for excellence in scientific research, The University of York, Department of Electronics, York, UK, Jul. 2010.

Chapter 2

Fundamental Techniques

Contents

2.1 Introduction

In this chapter, fundamental techniques used throughout this thesis are introduced. First, time-variant fading channel models are studied in Section 2.2. Then in Section 2.3, basis expansion models (BEM)s are presented. Finally, a brief description of turbo coding is provided in Section 2.4.

2.2 Time-Variant Fading Channel Models

In this thesis, we investigate joint channel and frequency offset estimation and signal detection in time-variant Rayleigh fading channels. Before that, we should first model and simulate the fading channel accurately. This section introduces a simulator of time-variant Rayleigh fading channels, which is used in the subsequent chapters.

Rayleigh fading is most applicable when there is no dominant propagation along a line of sight between the transmitter and receiver. Rayleigh fading is a reasonable model when there are many objects in the environment that scatter the radio signal before it arrives at the receiver. The central limit theorem holds that, if there is sufficiently much scatter, the channel impulse response will be well-modeled as a Gaussian process irrespective of the distribution of the individual components. If there is no dominant component to the scatter, then such a process will have zero mean and phase evenly distributed between 0 and 2π radians. The envelope of the channel response will therefore be Rayleigh distributed.

Clarke's model [63] and its simplified model by Jakes [64] have been widely used to simulate time-variant Rayleigh fading channels. Although the simplicity of the original Jakes' model makes it popular, there are two deficiencies that can not be ignored [65]: the original Jakes' model is a deterministic model and it is difficult to generate multiple independent fading channels, such as frequency-selective (multipath) fading and MIMO channels. Various modifications [66–69] and improvements [65, 70, 71] have been reported for generating multiple uncorrelated fading waveforms needed for modeling frequency selective fading and MIMO channels, such as Inverse Discrete Fourier Transform (IDFT) [72] and the autoregressive approach [73]. It is pointed in [74] that Jakes' simulator is not wide-sense stationary when averaged across the physical ensemble of fading channels. In [74], an improved simulator, named Pop-Beaulieu simulator, is applied to remove this stationarity problem by introducing random phase shifts in the low-frequency oscillators. However, it is shown that the Pop-Beaulieu simulator has deficiencies in some of its high-order statistics [71].

Based on the Pop-Beaulieu simulator, novel sum-of-sinusoids statistical simulation models with a small number of sinusoids are proposed for Rayleigh fading channels in [65, 71]. These modified models improve the original Jakes' model by introducing ran-

dom path gain, random initial phase and random Doppler frequency for sinusoids within these models [71]. The high-order statistical properties of these novel models, such as the autocorrelations and cross-correlations of the quadrature components, the autocorrelation of the complex envelop, and the probability density functions (PDFs) of the fading envelop, asymptotically approach the desired ones as the number of sinusoids approaches infinity [65, 71].

In this section, we introduce the reference Clarke's model mathematically and analyze the deficiencies of the Jakes' model and the Pop-Beaulieu model. Then, we introduce a modified model proposed in [65, 71] which provides good convergence of the probability density functions of the envelope, the level crossing rate, the average fading duration, and the autocorrelation of the squared fading envelope, even when the number of sinusoids is as small as 8 [71]. This modified model is used to generate multiple independent time-variant channels in this thesis.

2.2.1 Original Clarke's Model

According to Clarke, the fading process of a frequency-flat Rayleigh fading channel is given by [63, 75]

$$g(nT_s) = E_0 \sum_{k=1}^{K_0} C_k \exp\left[j(2\pi f_D T_s n \cos\alpha_k + \phi_k)\right] , \tag{2.1}$$

where E_0 is the normalising factor, K_0 is the number of scatterers, C_k, α_k and ϕ_k are, respectively, the random path gain, angle of incoming wave and initial phase associated with the kth scatterer, f_D is the maximum Doppler frequency occurring when $\alpha_k = 0$, and $f_D T_s$ is the normalised maximum Doppler frequency.

The Doppler effect, named after Austrian physicist Christian Doppler who proposed it, is the change in frequency of a wave for an observer moving relative to the source of the wave.

The Doppler frequency of the kth scatterer is [75]

$$f_k = f_D \cos\alpha_k \, ; \qquad f_D = \frac{\upsilon}{\lambda} , \qquad \lambda = \frac{c}{f} , \tag{2.2}$$

where υ is the receiver's velocity relative to the transmitter, λ is the wavelength of the incident wave, c is the speed of the wave (3×10^8 m/s for electromagnetic waves traveling through air or vacuum) and f is the frequency of the wave.

Assuming that C_k has a real value, (2.1) can be split into inphase and quadrature components as

$$g(nT_s) = g_i(nT_s) + jg_q(nT_s)\,; \tag{2.3a}$$

$$g_i(nT_s) = E_0 \sum_{k=1}^{K_0} C_k \cos(2\pi f_D T_s n \cos\alpha_k + \phi_k)\,, \tag{2.3b}$$

$$g_q(nT_s) = E_0 \sum_{k=1}^{K_0} C_k \sin(2\pi f_D T_s n \cos\alpha_k + \phi_k)\,. \tag{2.3c}$$

For large K_0 , the central limit theorem allows $g_i(nT_s)$ and $g_q(nT_s)$ to be approximated as Gaussian random processes [22]. Adopting Clarke's two-dimensional isotropic scattering model, and assuming that α_k and ϕ_k are independent and uniformly distributed over $[-\pi, \pi]$, each of these processes has a zero-mean value [24, 63]

$$\mu_0 = \mu_{g_i} = \mu_{g_q} = \mathrm{E}\{g_q(nT_s)\} = 0\,, \tag{2.4}$$

and a variance of [24, 63]

$$\sigma_0^2 = \sigma_{g_i}^2 = \sigma_{g_q}^2 = \mathrm{var}\{g_q(nT_s)\} = \frac{E_0^2}{2} \sum_{k=1}^{K_0} \mathrm{E}\left\{C_k^2\right\}\,. \tag{2.5}$$

Therefore, the fading process $g(nT_s)$ has zero mean ($\mu_y = 0$), variance $2\sigma_0^2$, and some second-order statistics as autocorrelation and cross-correlation functions of [63, 75]

$$R_{g_i g_i}(u) = R_{g_q g_q}(u) = \sigma_0^2 J_0(2\pi f_D T_s u)\,, \tag{2.6a}$$

$$R_{g_i g_q}(u) = R_{g_q g_i}(u) = 0\,, \tag{2.6b}$$

$$R_{gg}(u) = 2\sigma_0^2 J_0(2\pi f_D T_s u)\,, \tag{2.6c}$$

$$R_{|g|^2|g|^2}(u) = 4\sigma_0^4 + 4\sigma_0^4 J_0^2(2\pi f_D T_s u) - \frac{4\sigma_0^4 J_0^2(2\pi f_D T_s u)}{K_0}\,, \tag{2.6d}$$

where $J_0(\cdot)$ is the zero-order Bessel function of the first kind [76]. The fading envelope, $|g(nT_s)|$, has Rayleigh distribution and its PDF is given by [75]

$$p_{|g|}(x) = \frac{x}{\sigma_0^2} \exp\left[-\frac{x^2}{2\sigma_0^2}\right]\,, \quad x \geq 0\,, \tag{2.7}$$

whereas the phase, $\Theta_g(t)$, has uniform distribution and its PDF is given by

$$p_{\Theta_g}(\theta_g) = \frac{1}{2\pi}\,, \quad \theta_g \in [-\pi, \pi]\,. \tag{2.8}$$

2.2.2 Jakes' Model

Jakes [64] derived his simulation model for Rayleigh fading channels based on Clarke's model in (2.1) by selecting

$$C_k = \frac{1}{\sqrt{K_0}}\,, \tag{2.9a}$$

$$\alpha_k = \frac{2\pi k}{K_0}\,, \tag{2.9b}$$

$$\phi_k = 0\,, \quad k = 1, 2, \ldots, K_0\,, \tag{2.9c}$$

so that the normalised fading process of this model is given by [64]

$$g(nT_s) = g_i(nT_s) + j g_q(nT_s)\,; \tag{2.10a}$$

$$g_i(nT_s) = \frac{2}{\sqrt{K_0}} \sum_{k=0}^{K} a_k \cos(2\pi f_k n T_s)\,, \tag{2.10b}$$

$$g_q(nT_s) = \frac{2}{\sqrt{K_0}} \sum_{k=0}^{K} b_k \cos(2\pi f_k n T_s)\,; \tag{2.10c}$$

$$K_0 = 4K + 2\,, \tag{2.10d}$$

$$a_k = \begin{cases} \sqrt{2}\cos\beta_0\,, & k = 0\,, \\ 2\cos\beta_k\,, & k = 1, 2, \ldots, K\,, \end{cases} \tag{2.10e}$$

$$b_k = \begin{cases} \sqrt{2}\sin\beta_0\,, & k = 0\,, \\ 2\sin\beta_k\,, & k = 1, 2, \ldots, K\,, \end{cases} \tag{2.10f}$$

$$\beta_k = \begin{cases} \frac{\pi}{4}\,, & k = 0\,, \\ \frac{\pi k}{K}\,, & k = 1, 2, \ldots, K\,, \end{cases} \tag{2.10g}$$

$$f_k = \begin{cases} f_D\,, & k = 0\,, \\ f_D \cos\frac{2\pi k}{K_0}\,, & k = 1, 2, \ldots, K\,. \end{cases} \tag{2.10h}$$

The simplifying parameters selected as (2.9) make the inphase and quadrature components correlated [77], and the simulation model deterministic [28] and wide-sense non-stationary [78]. Therefore, various modifications of Jakes' simulator have been proposed, such as in [28, 78–83].

2.2.3 Modified Simulation Model

A modified simulation model was proposed in [81] and corrected in [83], which resolves the disadvantages of Jakes' model by reintroducing the randomness for the variables C_k, α_k, and ϕ_k. The normalised fading process of the improved simulator proposed in [81] is given by

$$g(nT_s) = g_i(nT_s) + jg_q(nT_s)\,; \tag{2.11a}$$

$$g_i(nT_s) = \sqrt{\frac{2}{K}}E_0 \sum_{k=1}^{K} \cos(\beta_k)\cos(2\pi f_D T_s n \cos\alpha_k + \phi_k)\,, \tag{2.11b}$$

$$g_q(nT_s) = \sqrt{\frac{2}{K}}E_0 \sum_{k=1}^{K} \sin(\beta_k)\sin(2\pi f_D T_s n \cos\alpha_k + \phi_k)\,; \tag{2.11c}$$

$$\alpha_k = \frac{2\pi k - \pi + \theta}{4K}\,, \quad k = 1, 2, \ldots, K\,, \tag{2.11d}$$

where θ, β_k and ϕ_k are independent random variables that are uniformly distributed over $[-\pi, \pi]$.

In [81], the value of ϕ_k was incorrectly chosen to be the same (*i.e.* ϕ) for all k. However, this mistake was acknowledged and the value was corrected to become ϕ_k in [83], which is the version we follow here.

The computational efficiency and statistical correlation functions of this modified model are better than those of Jakes' model [81]. The second-order statistics of the modified model match the desired ones and are independent of the number of sinusoids K [81]. The autocorrelation function of the squared envelope (*i.e.* a fourth-order statistic) asymptotically approaches the desired one as K increases, and converging fast, reaching a good approximation with as small K as 8.

Noting that the autocorrelation and autocovariance functions are identical for the Rayleigh fading process and $\sigma_0^2 = E_0^2/2$, the elements of the $N \times N$ covariance matrix $\mathbf{R}_g$ of the fading process are obtained from (2.6c) as

$$[\mathbf{R}_g]_{u\,v} = R_{gg}(u - v) = E_0^2 J_0(2\pi f_D T_s(u - v))\,, \quad u, v = 1, \ldots, N\,. \tag{2.12}$$

The modified model in (2.11), represented in matrix form by the $N \times 1$ column vector $\mathbf{g}$, is used throughout the thesis to simulate the time-variant fading processes.

2.3 Basis Expansion Models

Accurate estimation of the fading process $g(nT_s)$ in (2.11) requires complicated techniques such as the Wiener filtering [4, 37]. A simpler solution can be obtained based on approximating $g(nT_s)$ using the basis expansion model [36, 38]. This approximation simplifies the time-variant fading model and converts it into a linear combination of several basis functions as

$$\tilde{g}(nT_s) = \sum_{m=1}^{M} a_m B(nT_s, m)\,, \tag{2.13}$$

where $B(nT_s, m)$ are the M known basis functions and a_m are unknown expansion coefficients. In matrix form, it can be written as

$$\tilde{\mathbf{g}} = \mathbf{B}\mathbf{a}\,, \tag{2.14}$$

where $\mathbf{B}$ is an $N \times M$ matrix with elements $B(nT_s, m)$ and $\mathbf{a}$ is an $M \times 1$ vector of expansion coefficients a_m. Thus, the problem of estimating N-dimensional time-variant fading process $g(nT_s)$ is transformed into a lower dimensional problem of estimating only M time-invariant expansion coefficients a_m, where usually $M << N$.

The BEM-based approach has been widely used due to its low complexity and high accuracy. Different basis functions can be used in the BEM such as complex exponential [38, 40, 54], polynomial [39], generalised complex exponential [84, 85], Karhunen-Loève [85–87], discrete prolate spheroidal [41, 88–90], and B-splines [42, 51, 91]. The last four BEMs are most often considered in applications to channel estimation.

2.3.1 Karhunen-Loeve Functions

Karhunen-Loève (KL) functions [87] are a set of orthogonal functions that exploits the fading covariance matrix $\mathbf{R}_g$. This allows the KL-BEM to provide the best approximation of the fading process, assuming the perfect knowledge of $\mathbf{R}_g$. The $N \times N$ matrix $\mathbf{U}$ of eigenvectors of $\mathbf{R}_g$ is obtained first as

$$\mathbf{R}_g\mathbf{U} = \mathbf{U}\boldsymbol{\Upsilon}\,, \tag{2.15}$$

where $\boldsymbol{\Upsilon}$ is the $N \times N$ diagonal matrix of eigenvalues. Then the basis function matrix $\mathbf{B}$ is formed by the M eigenvectors (columns of $\mathbf{U}$) corresponding to the M maximum eigenvalues (diagonal elements of $\boldsymbol{\Upsilon}$).

2.3.2 Discrete Prolate Spheroidal Functions

The use of the KL BEM results in a low modeling error [86, 87]. However, the fading covariance matrix is not always available at the receiver. Alternatively, a BEM based on discrete prolate spheroidal (DPS) functions was proposed in [41]. The DPS BEM corresponds to the discrete KL BEM with a rectangular spectrum [41]. The DPS basis functions are bandlimited to the Doppler frequency $[-f_D T_s, f_D T_s]$ and simultaneously most concentrated in the certain time interval of length M [92]. DPS sequences are widely used for channel estimation both in time and frequency domains [41, 90, 93].

The DPS functions are orthogonal functions that are generated exploiting the Doppler frequency [41]. First, a matrix $\mathbf{D}$ is generated as

$$[\mathbf{D}]_{u\,v} = \frac{\sin\left(2\pi f_D T_s\,(u-v)\right)}{\pi\,(u-v)}\,, \quad u, v = 1, \ldots, N\,. \tag{2.16}$$

Then, $\mathbf{B}$ is formed from M eigenvectors of $\mathbf{D}$ corresponding to the M maximum eigenvalues.

2.3.3 Generalised Complex Exponential Functions

Generalized complex exponential (GCE) functions [84] are a modified version of the complex exponential (CE) functions [38], for which the period of the basis functions is extended longer than the observation interval N, and are given by

$$B(nT_s, m) = e^{j\frac{2\pi n T_s}{\xi N}\left(m-1-\frac{M-1}{2}\right)}\,, \tag{2.17}$$

where $\xi > 1$, and here, we will be using $\xi = 2$. The CE basis functions are generated in the same way, but using $\xi = 1$. This extension in the period helps in decreasing the model approximation error. These basis functions do not exploit any statistical information of the channel.

2.3.4 B-Spline Functions

B-spline (BS) functions [42] do not require any prior channel statistics. The BS functions of order η are symmetrical, bell-shaped functions that are given by [94]

$$B_\eta(x) = \frac{1}{\eta!}\sum_{i=0}^{\eta+1}(-1)^i\binom{\eta+1}{i}\left(\frac{x}{PT_s}+\frac{\eta+1}{2}-i\right)_+^\eta , \tag{2.18}$$

where

$$P = \frac{N-1}{M-\eta}, \tag{2.19}$$

PT_s is the sampling interval separating two adjacent B-spline functions, and $x_+ = \max\{0, x\}$. In this case, $B(nT_s, m) = B_\eta\left(nT_s - (m - \frac{\eta+1}{2})PT_s\right)$. The matrix $\mathbf{B}$ of the BS functions is a sparse matrix that only contains $\eta + 1$ nonzero elements in each row, which makes it attractive for implementation. The accuracy and complexity of the BS-BEM approximation depends on the spline degree η. In many situations, the cubic B-spline ($\eta = 3$) provides the best trade-off between complexity and accuracy [94]. We use the cubic B-spline in the simulation below whenever $M \geq 4$, and for $1 \leq M \leq 3$ we use $\eta = M - 1$.

As shown above, the KL and DPS BEMs can approximate the time-variant fading channel with small modeling error but require the statistics of fading and have to suffer extra error caused by the mismatched estimation of these statistics. Although the GCE and BS BEMs do not require the knowledge of the statistical information of fading, they introduce higher modeling errors than the KL and DPS BEMs. The performance and robustness of estimators using the different BEMs are compared later in Chapter 5, so that to use the one which can provide the most robust performance to approximate the fading process.

2.4 Turbo Coding

A new class of error correction codes named turbo codes were first introduced by a group of researchers (Berrou, Glavieux and Thitimajshima) in 1993 at the International Conference on Communications [95]. These codes were shown to achieve a significant gain

in power efficiency over other coding methods existed at the time and allowed to the first time to approach the Shannon capacity limit within only 0.7 dB. This remarkable achievement ends the conventional thought that the Shannon limit can only be approached using extraordinarily long codes with exceptionally complex decoding processes [96]. As one of the most powerful error correction codes, turbo codes have been developed rapidly and attracted substantial attention in wireless communication community [97–103].

Turbo codes are based on two fundamental concepts, concatenated coding and iterative decoding, the latter of which is the core of the turbo principle and is responsible in the outstanding performance of turbo codes. The turbo codes are used in Chapter 7 of this thesis. A brief discussion of the structure of the turbo encoder and decoder is given together with the differences between the main turbo decoding algorithms. Interested readers can find more detailed description of turbo coding in [104–106].

2.4.1 Turbo Encoding

The structure of the turbo encoder as seen in Figure 2.1 can be analysed from its name, parallel concatenated recursive systematic convolutional (RSC) code. The encoder has two concatenated RSC encoders and an interleaver in between. The RSC codes apply a feedback loop (recursive part) and set one of the outputs equal to the input data (systematic part) unlike non-systematic convolutional (NSC) codes. Figure 2.2 shows the structure of RSC encoder while Figure 2.3 shows the corresponding NSC encoder. The polynomial generation of the feedback and output connectivity in the RSC encoder are 7, 5 in octal.

Description of working principles of turbo encoder is as follows. Firstly, a data sequence of length N, $\mathbf{d} = [d[1], \ldots, d[N]]$, is encoded by the first RSC encoder, where the output is a length N coded sequence $\mathbf{x}_p^1 = [x_p^1[1], \ldots, x_p^1[N]]$. Then, the second RSC encoder encodes an interleaved data sequence to generate another coded sequence $\mathbf{x}_p^2 = [x_p^2[1], \ldots, x_p^2[N]]$ of length N. Finally, the turbo coded sequence is generated by multiplexing $\mathbf{d}$, $\mathbf{x}_p^1$ and $\mathbf{x}_p^2$. This results in a code rate of $1/3$ without puncturing. Similarly, higher code rates can be obtained by applying a puncturing scheme.

The interleaver, as a device, reorders the input data sequence, while a deinterleaver

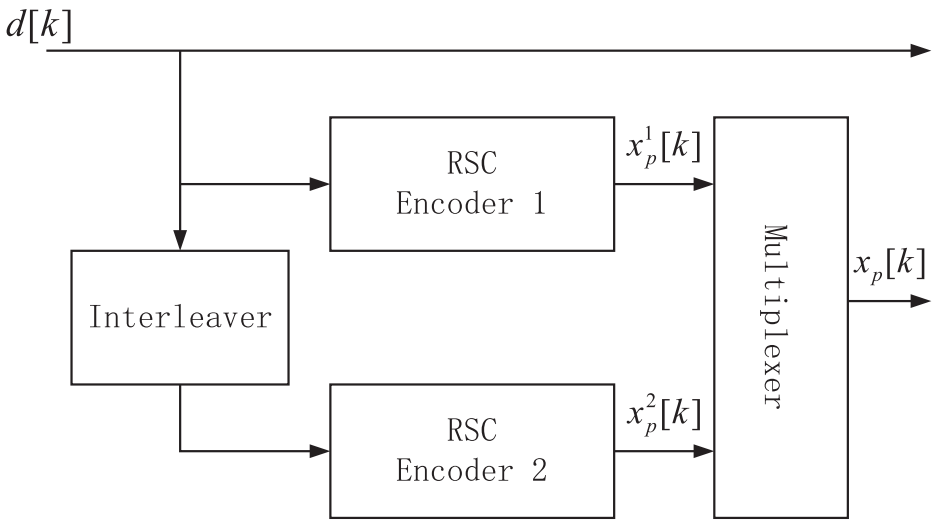

Figure 2.1: Structure of a turbo encoder.

(used in the decoder) recovers the original order of that data sequence. The joint influence of the interleaver and RSC encoder mostly lead to a high code weight composite codeword. This is critical to the performance of turbo codes [107]. A number of interleavers can be used in the turbo encoders such as pseudo-random [108], block [109], and s-random interleavers [110–113]. The s-random interleaver is used in this thesis due to its superior performance [105]. The output pattern of this interleaver is randomly generated, so that any two input bits within a distance of s bits are separated after interleaving by at least s bits.

2.4.2 Turbo Decoding

Figure 2.4 demonstrates the turbo decoder for the encoder in Figure 2.1. Similarly to that used in the encoder, two RSC decoders are linked by an deinterleaver/interleaver.

The turbo decoder works iteratively where in each iteration the two RSC decoders exchange the decoded information in order to assist one another. Received signals $y[k] = (y_d[k], y_p^1[k], y_p^2[k])$ from the demodulator are demultiplexed to sequences $y_d[k]$, $y_p^1[k]$ and $y_p^2[k]$, respectively, where $y_d[k]$ corresponds to the received systematic codes, $y_p^1[k]$ corresponds to the received 1st parity bits, and $y_p^2[k]$ corresponds to the received 2nd parity bits. The first RSC decoder applies $y_d[k]$ and $y_p^1[k]$ as input sequences and the

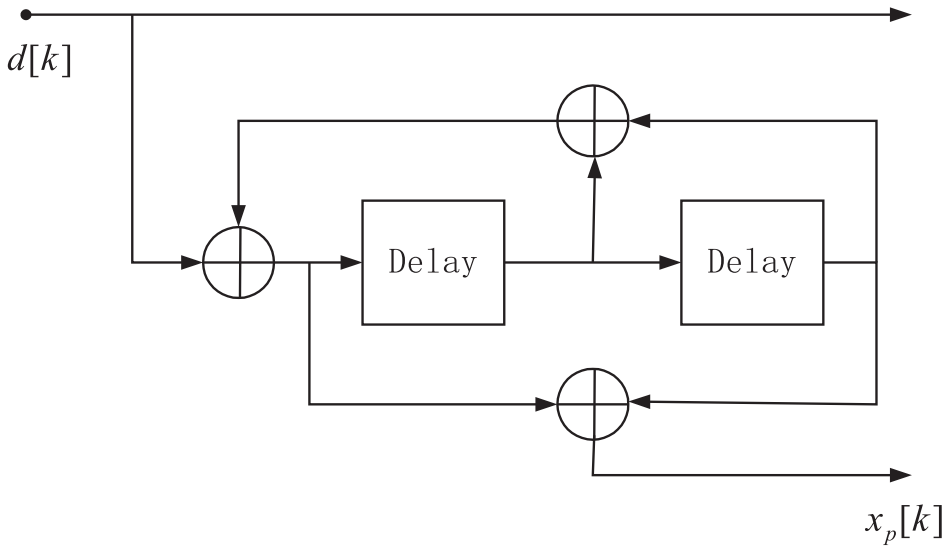

Figure 2.2: Example of a recursive systematic convolutional (RSC) encoder.

second RSC decoder applies $y_d[k]$ and $y_p^2[k]$. Inputs of corresponding decoder are set to zeros at the punctured positions when the parity bits of a given RSC encoder are punctured before transmission. For the initial iteration, the first RSC decoder takes only $y_d[k]$ and $y_p^1[k]$ to generate soft information of the data bits, $L_{E,1}(\bar{d}[k])$. The second RSC decoder can then perform decoding using the soft information of $L_{E,1}(\bar{d}[k])$ and $L_{ap,1}(d[k])$ from the first RSC decoder, in addition to the received $y_d[k]$ and $y_p^2[k]$. The second decoder output is another soft decoding information $L_{E,2}(\bar{d}[k])$, which is deinterleaved to generate $L_{ap,2}(d[k])$ and fed back to the first RSC decoder. During the following iterations, the first RSC decoder takes $L_{ap,2}(d[k])$ from the second RSC decoder in the previous iteration as additional information to $y_d[k]$ and $y_p^1[k]$, to generate $L_{E,1}(\bar{d}[k])$. As the number of iterations increases, the performance of the turbo decoder improves. However, the improvement start later to decrease as the number of iterations increases. This process continues iteratively until the decoders's estimates of the original data bits converge. As a settlement between performance and complexity, eight iterations are commonly used [96]. At the end, the output *a posteriori* information $L(\bar{d}[k])$ of a data bit $d[k]$ delivered from the second RSC decoder is deinterleaved and used for the final hard decision.

Every RSC decoder decodes use its input received signals ($y_d[k]$ and $y_p^i[k], i = 1, 2$) and the *a priori* information ($L_{ap,i}(d[k]), i = 1, 2$) from the other RSC decoder to perform decoding, and provides the extrinsic information $L_{E,i}(\bar{d}[k])$ for the other decoder. Note that the extrinsic information is only exchanged between decoders as intermediate infor-

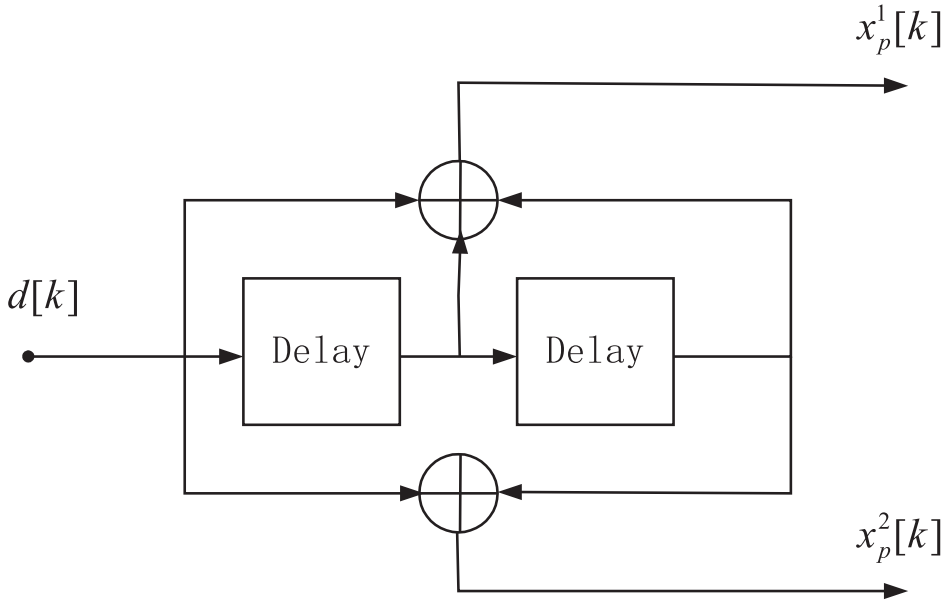

Figure 2.3: Example of a non-systematic convolutional (NSC) encoder.

mation during the decoding process. The turbo decoder is called soft-input soft-output decoder due to the exchange of soft information between both RSC decoders for which it accepts soft *a priori* information $L_{ap,i}(d[k])$ at one of its inputs from the previous decoding process and generates soft information $L_{E,i}(\bar{d}[k])$. Soft information means that besides decoded bits, the associated probability that each bit has been decoded correctly is also provided, usually in the form of log-likelihood ratio (LLR). This indicates that the decoder yields not only the coded bits but also how reliable they are. As its name implies, the LLR is the logarithm of the ratio of two probabilities in the case of binary transmission, e.g., the output *a posteriori* information ($L(\bar{d}[k])$) is generally given by

$$L(\bar{d}[k]) = \log \frac{P(d[k] = +1|\mathbf{y})}{P(d[k] = -1|\mathbf{y})}, \tag{2.20}$$

where the numerator and denominator are probabilities of the transmitted bit $d[k] = +1$ and $d[k] = -1$ conditioned on the received sequence $\mathbf{y}$. Based on (2.20), the more positive the value of $L(\bar{d}[k])$ is, the more reliably the transmitted bit was '1', or the more negative the value of $L(\bar{d}[k])$ is, the more likely '0' was transmitted.

In the turbo decoder shown in Figure 2.4, the output $L(\bar{d}[k])$, *a posteriori* information of an information bit $d[k]$, is given by

$$L(\bar{d}[k]) = L(\tilde{d}[k]) + L_{ap}(d[k]) + L_E(\bar{d}[k]) \quad , \tag{2.21}$$

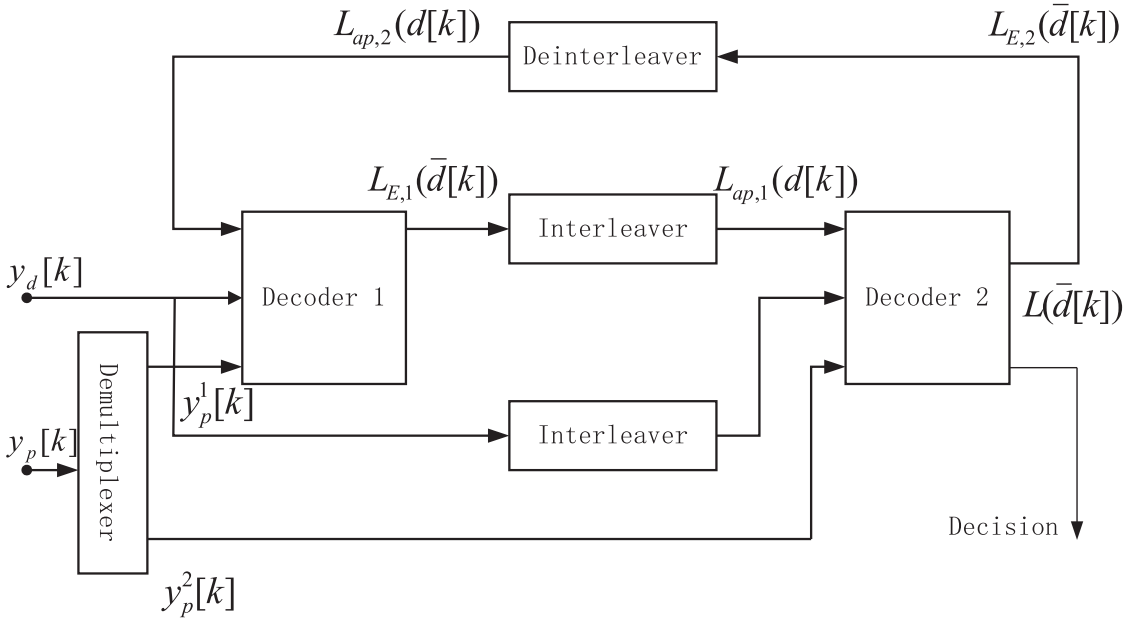

Figure 2.4: Structure of a turbo decoder.

where $L(\tilde{d}[k])$ is the channel information, $L_{ap}(d[k])$ is the *a priori* information and $L_E(\bar{d}[k])$ is the extrinsic information.

The channel information $L(\tilde{d}[k])$ can be extracted directly from $y[k]$ which are the received signals of $d[k]$. Supposing that $d[k]$ are transmitted with E_s transmitted energy per symbol, over an AWGN channel, the received signal is

$$y[k] = a \cdot d[k] + n[k] \quad , \tag{2.22}$$

where n_k denotes an AWGN with a variance of σ_n^2, and a is the fading amplitude in a fading channel or a constant value in an AWGN channel. For such a model, the channel information is given by [96]

$$\begin{aligned} L(\tilde{d}[k]) &= \log \frac{\exp\left(-\frac{E_s}{2\sigma_n^2}(y[k]-a)^2\right)}{\exp\left(-\frac{E_s}{2\sigma_n^2}(y[k]+a)^2\right)} \\ &= \log\left(\exp\left(\frac{2aE_s}{\sigma_n^2}y[k]\right)\right) \\ &= L_c \cdot y[k], \end{aligned} \tag{2.23}$$

where $L_c = 2aE_s/\sigma_n^2$ is the channel reliability factor, which reflects the reliability of estimating the transmitted signal from the received signal. For example, L_c will be large

if SNR in the channel is high, and we can estimate the transmitted signal from the received signal correctly with a high probability. In such a case, the received signal will impact heavily on the final output *a posteriori* LLR.

The *a priori* information $L_{ap}(d[k])$ used here is the deinterleaved extrinsic information from the other RSC decoder.

The extrinsic information $L_E(\bar{d}[k])$ is the information that decoder exploits from the whole received sequence and *a priori* information, but excludes these of the bits which are currently being decoded in this iteration. It is only the extrinsic information that the decoders exchange between each other since the same information should not be used more than once at each decoding step.

Taking all these three types of information above into account, the turbo decoder delivers the *a posteriori* information of data bits. The final decision of the decoding is based on the *a posteriori* information of data bits.

There are three typical decoding algorithms applied widely, the maximum *a Posteriori* (MAP), max-log-MAP and log-MAP algorithms [95, 107, 114–117].

The maximum *a Posteriori* (MAP) algorithm was firstly proposed by Bahl, Cocke, Jelinek and Raviv in [107] and modified by Berrou, Glavieuv and Thitmajshima in [95]. Compared with the conventional maximum likelihood sequence estimation (MLSE) algorithm which can be efficiently implemented by the Viterbi algorithm [118], the MAP algorithm is a symbol-by-symbol detection algorithm based on maximum *a posteriori* information. It is optimal in the sense of minimizing the probability of a symbol error by taking *a priori* information of the coded bits into account and providing soft information about estimated bits. The performance of the MAP and MLSE algorithms would be the same when there is no *a priori* information to be exploited. However, when *a priori* information is available, for example, in the soft-input soft-output turbo decoder exchanging the extrinsic information between two RSC decoders, the MAP algorithm will outperform the conventional MLSE one [95].

Although the MAP algorithm is the optimal decoding scheme, it is too complicated to be realized for implementation since the exact representation of probabilities used in

the MAP algorithm requires a high dynamic range [96]. Moreover, there are many non-linear functions and numerous multiplications proposed in the scheme [96]. Working in the logarithmic domain instead of the linear domain for the probability used in the MAP algorithm and invoking the approximation

$$\ln(e^{x_1} + \ldots + e^{x_n}) \approx \max_{i \in 1,2\ldots,n} x_i, \tag{2.24}$$

the max-log-MAP algorithm reduces the complexity significantly. However, it is obvious that the max-log-MAP algorithm is suboptimal since only a part of information is exploited due to the approximation.

This approximation can be avoided by applying the Jacobian logarithm to calculate $x = \ln(e^{x_1} + \ldots + e^{x_n})$. The Jacobian logarithm [119, 120] is given by

$$\begin{aligned} \ln(e^{x_1} + e^{x_2}) &= \max(x_1, x_2) + \ln(1 + e^{-|x_1 - x_2|}) \\ &= \max(x_1, x_2) + f_c(|x_1 - x_2|) \\ &= g_c(x_1, x_2), \end{aligned} \tag{2.25}$$

where $f_c(|x_1 - x_2|)$ can be regarded as a correction term. Robertson, Hoeher and Villebrun in [115] proposed a method to show how to use the Jacobian logarithm to calculate $\ln(e^{x_1} + \ldots + e^{x_n})$ accurately. They supposed $x = \ln(e^{x_1} + \ldots + e^{x_{n-1}})$ is known. Then, they obtained

$$\begin{aligned} \ln(e^{x_1} + \ldots + e^{x_n}) &= \ln(e^{x} + e^{x_n}) \\ &= \max(x, x_n) + f_c(|x - x_n|). \end{aligned} \tag{2.26}$$

This method is referred to as the log-MAP algorithm [115]. It was also shown that the correction term $f_c(|x_1 - x_2|)$ can be implemented efficiently by a one-dimension look-up table to avoid real time computation, moreover, only a few values are needed for the table. By applying the Jacobian logarithm, the log-MAP algorithm retains the optimality of the original MAP algorithm, while preserves the computational simplicity of the max-log-MAP algorithm, and so, is used here in the thesis. Interested readers can find more details about the MAP, max-log-MAP and log-MAP algorithms in [114, 116, 117].

2.5 Conclusions

Fundamental techniques have been presented in this chapter, such as the models of the time-variant channels, BEMs and Turbo coding, which are used throughout this thesis. After briefly introducing the optimal Clarke's model and the deficiencies of Jakes' model, a recently modified model has been presented. This modified model resolves the correlated, deterministic and nonstationary problems of the Jakes' model using a small number of sinusoids and is adopted in this thesis to simulate the time-variant fading channels.

The BEMs have been widely used to approximate the time-variant fading channels, due to the low complexity and high accuracy it offer. The most widely used BEMs, which are KL, DSP, GCE and BS, have been introduced. The KL functions are generated based on the fading covariance matrix, which allows the best approximation. The DPS functions require the knowledge of the Doppler frequency. No such channel statistics are required to generate the GCE and BS functions. The KL and DPS BEMs can achieve a smaller modeling error compared to that of the GCE and BS BEMs provided the perfect knowledge of the channel statistics. However, the KL and DPS BEMs suffer from an extra error in practice caused by the mismatched estimation of these statistics. This is discussed in more details in Chapter 5 where the performance and robustness of estimators using different BEMs are compared and the best practical choice is decided.

Finally, the turbo encoder and decoder with different decoding algorithms, such as the MAP, max-log-MAP and log-MAP algorithms have been presented. The advantages and disadvantages of each decoding algorithm have been described. The log-MAP decoding algorithm has been adopted to realise the decoding schemes in this thesis as it retains the optimality of the MAP algorithm, while preserves the computational simplicity of the less accurate max-log-MAP algorithm.

Chapter 3

Joint Estimation of Channel and Frequency Offset in Additive White Gaussian Noise Channels

Contents

This chapter offers a general literature survey of data-aided channel and frequency offset estimators based on the maximum likelihood (ML) principle for signals transmitted through additive white Gaussian noise (AWGN) channels. The CRLBs of the joint estimators will be derived and fundamental techniques, used throughout this thesis will be introduced. A performance analysis of advanced frequency estimators that have been recently proposed in the literature is provided. A fair performance comparison is obtained for those estimators under the same simulation environment and for different application scenarios so that to get a better understanding about the differences, most precisely, in

terms of accuracy, complexity, frequency acquisition range, signal to noise ratio (SNR) threshold and the sensitivity of these towards different SNR and frequency offset scenarios.

3.1 Introduction

In digital communication systems, where reliable transmission techniques at high data rates is a requirement, an appropriate signal detection in the receiver can only be achieved by using highly efficient synchronization techniques. Known data symbols called the pilot symbols is a practical method used to provide the receiver with the required information about the channel [1, 2]. In the data-aided systems, these pilot symbols are often inserted within the data stream, either periodically or in a burst mode, during the modulation in the transmitter which helps to perform accurate joint channel and frequency offset estimation in the receiver [1, 2].

The periodogram maximiser ML frequency estimator possesses the optimum performance, but also involves impractical complexity. Practical frequency estimators approximating the ML estimator are classified as correlation-based [5–12] or periodogram-based frequency estimators [13–19].

The correlation-based frequency estimators, such as the estimators of Fitz [5], and Luise and Reggiannini (L&R) [6], can exhibit a comparable performance to that of the ML estimator. However, both estimators possess a limited frequency estimation range Ψ. This Ψ is inversely proportional to the number of input samples N and cannot be changed to suit a certain channel requirement. This prevents the estimators to be used for scenarios where a wide frequency estimation range is required. It also limits the usage for relatively large N. In addition, these estimators use nonlinear operations and possess a high computational load.

In our simulation we consider the following correlation-based frequency estimators. A frequency estimator that relies on the phase of the correlation sample at a single lag (L), referred to as the SL estimator, was proposed in [7]. In [8], an estimator was presented relying on unweighted linear combination of the phase differences of L lags correlation

samples, referred to as the B&S estimator. A weighted average phase differences estimator was presented in [9], referred to as the M&M estimator. Depending on the small error assumption, a simplified estimator for the AWGN channel can be derived from the one proposed in [10] based on the nonlinear least-squares (NLS), referred to as the SNLS estimator. An approximated NLS estimator was proposed in [11], referred to as the ANLS estimator, based on the summation-by-parts rule. An improved estimator was proposed in [12] based on the weighted normalised autocorrelation linear predictor, referred to as WNALP.

The periodogram-based frequency estimators use coarse and fine search for the periodogram peak [13]. Usually, the coarse search is an N_{FFT}-point FFT (or DFT), where $N_{FFT} \geq N$. Some estimators use $N_{FFT} = N$ which allows efficient implementation. However, this requires more complicated methods to be used in the fine search and can affect the accuracy of the estimator. The linear interpolation frequency estimator [14] uses $N_{FFT} = N$ and exploits a three-point linear interpolation fine search. Although the coarse search is computationally efficient, the fine search requires nonlinear operations to achieve a certain accuracy, which results in an increase of the complexity. This estimator has an $f_0 T_s$-dependent performance that can cause the threshold SNR (SNR_{th}), *i.e.* the SNR below which the estimation error starts diverging from the CRLB, to be significantly higher than that of the ML estimator. Other methods can be used in the fine search, such as the three/five-point interpolation techniques [15], and Newton's method for locating the root of an equation [16]. In spite of the efficient coarse search, the fine search uses more sophisticated nonlinear techniques, which makes it difficult for practical implementation.

In our simulation we consider the following periodogram-based frequency estimators. A popular estimator of this type is the dichotomous search of the periodogram peak (DS) [17]. This estimator exploits FFT/DFT of the size $N_{FFT} \approx 1.5N$ for the coarse search, and then refines the estimate over Q iterations of searching within binary partitions in the neighbourhood of the initial peak. This estimator relies entirely on linear operations and is perfectly convenient for real-time implementation. An important modified dichotomous search (MDS) estimator was proposed in [18], which attains the CRLB without the need to perform zero-pad the processed samples and allowing a reduction in the complexity required. An improved dichotomous search (IDS) estimator was proposed in [19] exploiting a new initialisation scheme in an attempt to accelerate the

convergence so that to allow reducing the number of iterations in the fine search and also without the need to perform zero-padding. A robust hybrid of periodogram-based and correlation-based estimator (grouped here with the periodogram-based estimators) was proposed in [20] and is referred to as MLAF.

A performance analysis is conducted in terms of accuracy and complexity of the mentioned advanced frequency estimators, where the performance is compared for different application scenarios, in which some of unknown characteristics are revealed to the first time for some popular estimators. The primary aim is to get a better understanding for which scenarios a certain estimator obtains its best performance, and also to check some of the claimed improvements of several recent estimators.

This chapter is organised as follows. In Section 3.2, the signal and channel models are presented. The maximum likelihood joint estimators are derived in Section 3.3. In Section 3.4, the Cramer-Rao Lower Bounds (CRLB)s are derived for the different ML estimators. Section 3.5 presents a quick literature survey of practical frequency offset estimators. Simulation results and a performance analysis are given in Section 3.6, and Section 3.7 concludes the chapter.

3.2 Signal and Channel Models

It is convenient to start with constructing a certain mathematical model for the received signal in which the most important characteristics of the channel are reflected. It is assumed for the scenarios discussed in this chapter that the considered signal is a known (pilot) signal transmitted through a deterministic (nonfading) single-path channel and corrupted with complex additive white Gaussian noise (AWGN). A unit amplitude PSK modulated pilot block is considered to be transmitted using a unit-energy Nyquist pulse shape $p(t)$. After frequency downconverting (*i.e.* multiplying by $e^{-j2\pi f_{cr}t}$), the complex-baseband representation of the received signal corresponding to the N symbols is

$$r_0(t) = Ae^{j(2\pi f_0 t+\phi)} \sum_{k=0}^{N-1} s(kT_s)p(t-kT_s) + w(t)\,, \tag{3.1}$$

where f_0 and ϕ are the carrier frequency-offset and phase, respectively, T_s is the symbol period and $w(t)$ is a complex-valued, zero-mean, white Gaussian random process.

Then a matched filter is used. The output of this filter matched to the pulse shape $p(t)$ is

$$r(t) = Ae^{j\phi} \sum_{k=0}^{N-1} s(nT_s) e^{j2\pi f_0 t} p(t - kT_s) * p(-t) + w(t) * p(-t)\,. \tag{3.2}$$

If the frequency offset is sufficiently small, then [1]

$$e^{j2\pi f_0 t} p(t - kT_s) \approx e^{j2\pi f_0 T_s k} p(t - kT_s)\,. \tag{3.3}$$

Then, the matched filter output is expressed as

$$r(t) \approx Ae^{j\phi} \sum_{k=0}^{N-1} s(kT_s) e^{j2\pi f_0 T_s k} R(t - kT_s) + z(t) \tag{3.4}$$

where $R(\tau)$ is the pulse shape autocorrelation function

$$R(\tau) = \int_{-\infty}^{\infty} p(t)p(t - \tau)dt\,, \tag{3.5}$$

and $z(t) = w(t) * p(-t)$.

Sampling is then used to get the discrete-time sequence. The output of the matched filter is sampled at $t = nT_s$ to produce

$$r(nT_s) \approx Ae^{j\phi} \sum_{k=0}^{N-1} s(kT_s) e^{j2\pi f_0 T_s k} R(nT_s - kT_s) + z(nT_s) \tag{3.6}$$

$$= Ae^{j\phi} e^{j2\pi f_0 T_s n} s(nT_s) + z(nT_s)\,, \qquad n = 0, 1, \ldots, N-1\,, \tag{3.7}$$

where the last equality follows from the Nyquist no-ISI property of the pulse shape.

Such a situation is configured in Figure 3.1.

For this scenario, the received signal and channel models, respectively, can be expressed as

$$r(nT_s) = s(nT_s)h(nT_s) + z(nT_s)\,; \tag{3.8a}$$

$$h(nT_s) = Ae^{j(2\pi f_0 T_s n + \phi)}\,, \qquad n = 0, 1, \ldots, N-1\,, \tag{3.8b}$$

where

$s(nT_s)$ is the transmitted nth pilot symbol;

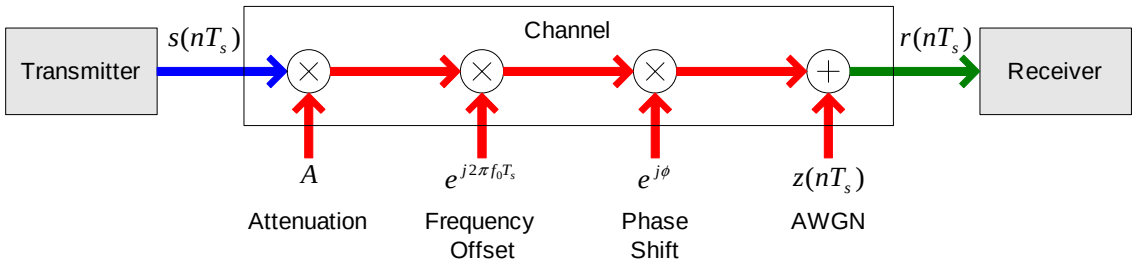

Figure 3.1: Configuration of the channel effects on signals transmitted through AWGN channels.

$z(nT_s)$ is the complex-valued AWGN nth sample with zero mean and variance σ^2;

A is the unknown positive real attenuation to be estimated;

ϕ is the unknown phase shift to be estimated; usually, the attenuation and phase shift are expressed together as a complex scalar $a = Ae^{j\phi}$ termed as the channel parameter;

f_0 is the unknown frequency offset to be estimated;

$f_0 T_s \in \Psi$ is the normalised frequency offset;

$\Psi = [-\psi/2, \psi/2]$ is the normalised frequency acquisition range;

ψ can maximally be 1 for wide acquisition range;

T_s is the interval separating two successive pilot symbols (symbol interval);

N is the number of pilot symbols.

The received signal model can be written in matrix form as

$$\mathbf{r} = \boldsymbol{\mu}(\boldsymbol{\chi}) + \mathbf{z} = \mathbf{S}\mathbf{h}(\boldsymbol{\chi}) + \mathbf{z} = \mathbf{S}\boldsymbol{\lambda}_{f_0 T_s} A e^{j\phi} + \mathbf{z}\,, \tag{3.9}$$

where

$\mathbf{r}$ is an $N \times 1$ column vector with elements $r(nT_s)$;

$n = 0, 1, \ldots, N-1$;

$\boldsymbol{\mu}(\boldsymbol{\chi})$ is an $N \times 1$ column vector of the mean of $\mathbf{r}$;

$\boldsymbol{\chi}$ is a 3×1 column vector $[A \;\; f_0 T_s \;\; \phi]^T$ of the real parameters to be estimated;

$\mathbf{z}$ is an $N \times 1$ column vector of the AWGN with covariance matrix $\mathbf{R}_z = \sigma^2 \mathbf{I}_N$ and elements $z(nT_s)$;

$\mathbf{I}_N$ is an $N \times N$ identity matrix;

$\mathbf{S}$ is an $N \times N$ diagonal matrix of diag$\{s(nT_s)\}$;

$\mathbf{h}(\boldsymbol{\chi})$ is an $N \times 1$ column vector with elements $h(nT_s)$;

$\boldsymbol{\lambda}_{f_0 T_s}$ is an $N \times 1$ column vector with elements $e^{j2\pi f_0 T_s n}$.

3.3 Maximum Likelihood Joint Estimation

The most practical and commonly used method for joint estimation that has been extensively introduced in the literature is the one relying on the maximum likelihood (ML) principle, for which the parameters A, f_0T_s and ϕ required to be estimated are regarded as unknown deterministic constants that maximise the likelihood function [121]. This function is the unconditional probability density function (PDF) of the received signal considered as a function of the unknown parameters after replacing $\mathbf{r}$ by the observed samples [122]. This ML estimation problem was solved by Rife and Boorstyn in [13].

The received signal in the considered scenario has an unconditional PDF of [121]

$$p(\mathbf{r};\boldsymbol{\chi}) = \frac{1}{\pi^N |\mathbf{R}_z|} \exp\left[-(\mathbf{r}-\boldsymbol{\mu}(\boldsymbol{\chi}))^H \mathbf{R}_z^{-1} (\mathbf{r}-\boldsymbol{\mu}(\boldsymbol{\chi}))\right]$$
$$p(\mathbf{r};A,f_0T_s,\phi) = \frac{1}{\pi^N\sigma^{2N}} \exp\left[-\frac{1}{\sigma^2}\left(\mathbf{r}-\mathbf{S}\boldsymbol{\lambda}_{f_0T_s}Ae^{j\phi}\right)^H \left(\mathbf{r}-\mathbf{S}\boldsymbol{\lambda}_{f_0T_s}Ae^{j\phi}\right)\right], \quad (3.10)$$

where $|\mathbf{X}|$ denotes the determinant of matrix $\mathbf{X}$ and $[\cdot]^H$ denotes the matrix conjugate transpose.

3.3.1 Frequency Offset Estimator

The likelihood function has to be maximised to find the ML joint estimator, or equivalently, the function

$$J(a,fT_s) = [\mathbf{r}-\mathbf{S}\boldsymbol{\lambda}_{fT_s}a]^H [\mathbf{r}-\mathbf{S}\boldsymbol{\lambda}_{fT_s}a] \quad (3.11)$$

needs to be minimised [121]. It is easier to start differentiating $J(a,fT_s)$ with respect to a, which leads to [121]

$$\frac{\partial J(a,fT_s)}{\partial a} = -\left[\boldsymbol{\lambda}_{fT_s}^H \mathbf{S}^H (\mathbf{r}-\mathbf{S}\boldsymbol{\lambda}_{fT_s}a)\right]^*, \quad (3.12)$$

where $[\cdot]^*$ denotes the complex conjugate. Setting this equal to zero yields the ML estimator of a for a certain fT_s as [121]

$$\hat{a} = \frac{\boldsymbol{\lambda}_{fT_s}^H \mathbf{S}^H \mathbf{r}}{\boldsymbol{\lambda}_{fT_s}^H \mathbf{S}^H \mathbf{S}\boldsymbol{\lambda}_{fT_s}} = \frac{\boldsymbol{\lambda}_{fT_s}^H \mathbf{S}^H \mathbf{r}}{\mathrm{tr}\{\mathbf{S}^H\mathbf{S}\}}, \quad (3.13)$$

where tr$\{\cdot\}$ denotes the matrix trace. For the sake of simplicity and without loss of generality, $s(nT_s)$ can be assumed to be normalised PSK pilot symbols with a unit amplitude, so that tr $\left\{\mathbf{S}^H\mathbf{S}\right\} = N$. Substituting (3.13) into (3.11) yields [121]

$$\begin{aligned} J(\hat{a}, fT_s) &= \mathbf{r}^H\left(\mathbf{r} - \mathbf{S}\boldsymbol{\lambda}_{fT_s}\hat{a}\right) = \mathbf{r}^H\mathbf{r} - \frac{1}{N}\mathbf{r}^H\mathbf{S}\boldsymbol{\lambda}_{fT_s}\boldsymbol{\lambda}_{fT_s}^H\mathbf{S}^H\mathbf{r} \\ &= \mathbf{r}^H\mathbf{r} - \frac{1}{N}\left|\boldsymbol{\lambda}_{fT_s}^H\mathbf{S}^H\mathbf{r}\right|^2, \end{aligned} \tag{3.14}$$

which is minimised by maximising

$$I_{fT_s} = \left|\boldsymbol{\lambda}_{fT_s}^H\mathbf{S}^H\mathbf{r}\right|^2 \tag{3.15}$$

with respect to fT_s over the frequency acquisition range. This function is known as the periodogram [123], so that the ML frequency offset (MLF) estimator is the periodogram maximiser as has been shown in [13, 45] and is given by

$$\widehat{f_0T_s}_{ML} = \arg\max_{fT_s\in\Psi}\{I_{fT_s}\} = \arg\max_{fT_s\in\Psi}\left\{\left|\sum_{n=0}^{N-1} r(nT_s)s^*(nT_s)e^{-j2\pi fT_s n}\right|^2\right\}. \tag{3.16}$$

This can be done using a DFT or the efficient computation of it using an FFT algorithm of size N_{FFT} of the function $r(nT_s)s^*(nT_s)$, denoted as $\mathcal{FFT}\{r(nT_s)s^*(nT_s), N_{FFT}\}$, over a grid of frequencies fT_s covering the frequency acquisition range. The frequency acquisition range $\Psi = [-\psi/2, \psi/2]$ can either be considered wide (maximally when $\psi = 1$) or narrow (when $\psi << 1$). The narrow frequency acquisition range allows improvement of the frequency estimator performance for low SNR values and reduction in the complexity as detailed in [47, 124]. In this thesis, no constraints are assumed upon the frequency offset, and unless otherwise specified, a wide frequency acquisition range where $\psi = 1$ is considered.

3.3.2 Attenuation Estimator

The ML attenuation (MLA) estimator can be obtained from (3.13) at $\widehat{f_0T_s}$ as

$$\hat{A}_{ML} = \left|\hat{a}_{\widehat{f_0T_s}_{ML}}\right| = \frac{1}{N}\left|\sum_{n=0}^{N-1} r(nT_s)s^*(nT_s)e^{-j2\pi\widehat{f_0T_s}_{ML}n}\right|. \tag{3.17}$$

3.3.3 Phase Estimator

The ML phase (MLP) estimator is also produced from (3.13) at $\widehat{f_0 T_s}$ as

$$\hat{\phi}_{ML} = \arg\left\{\hat{a}_{\widehat{f_0 T_s}_{ML}}\right\} = \arg\left\{\sum_{n=0}^{N-1} r(nT_s)s^*(nT_s)e^{-j2\pi\widehat{f_0 T_s}_{ML}n}\right\}. \tag{3.18}$$

3.3.4 Channel Estimator

In wireless communication systems, the three parameters A, $f_0 T_s$, and ϕ are usually estimated jointly to obtain the channel estimate $\mathbf{h}(\boldsymbol{\chi})$. The ML joint channel and frequency offset (MLJ) estimate is given by

$$\hat{h}_{ML}(nT_s) = \hat{A}_{ML}e^{j(2\pi\widehat{f_0 T_s}_{ML}n+\hat{\phi}_{ML})}, \quad n = 0, 1, \ldots, N-1, \tag{3.19}$$

which is employed by the receiver for detecting the unknown transmitted data.

3.4 Cramer-Rao Lower Bound

The Cramer-Rao lower bound (CRLB) is the lower limit that the variance of any unbiased estimator can reach [121]. The vector CRLB for the real parameter vector $\boldsymbol{\chi}$ is obtained using the Fisher information matrix $\mathbf{I}(\boldsymbol{\chi})$ that is derived as [121]

$$\begin{aligned}
[\mathbf{I}(\boldsymbol{\chi})]_{u\,v} &= 2\Re\left\{\frac{\partial\boldsymbol{\mu}^H(\boldsymbol{\chi})}{\partial\chi_u}\,\mathbf{R}_z^{-1}\,\frac{\partial\boldsymbol{\mu}(\boldsymbol{\chi})}{\partial\chi_v}\right\} \\
&= \frac{2}{\sigma^2}\Re\left\{\sum_{n=0}^{N-1}\frac{\partial s^*(nT_s)h^*(nT_s)}{\partial\chi_u}\,\frac{\partial s(nT_s)h(nT_s)}{\partial\chi_v}\right\} \\
&= \frac{2}{\sigma^2}\Re\left\{\sum_{n=0}^{N-1}\frac{\partial h^*(nT_s)}{\partial\chi_u}\,\frac{\partial h(nT_s)}{\partial\chi_v}\right\},
\end{aligned} \tag{3.20}$$

where $[\mathbf{X}]_{i\,j}$ denotes the (i,j)th element of matrix $\mathbf{X}$, $\Re\{\cdot\}$ denotes the real component of a complex number, and $s^*(nT_s)s(nT_s) = 1$ for $n = 0, 1, \ldots, N-1$ as assumed previously. The CRLB of the considered parameters was derived by Rife and Boorstyn in [13]. The

partial derivatives are obtained as [121]

$$\frac{\partial h(nT_s)}{\partial A} = e^{j(2\pi f_0 T_s n+\phi)}\,, \tag{3.21a}$$

$$\frac{\partial h(nT_s)}{\partial f_0 T_s} = j2\pi n A e^{j(2\pi f_0 T_s n+\phi)}\,, \tag{3.21b}$$

$$\frac{\partial h(nT_s)}{\partial \phi} = jA e^{j(2\pi f_0 T_s n+\phi)}\,. \tag{3.21c}$$

Substituting this into (3.20) produces [121]

$$\begin{aligned}\mathbf{I}(\boldsymbol{\chi}) &= \frac{2}{\sigma^2}\begin{bmatrix} N & 0 & 0 \\ 0 & (2\pi)^2A^2\sum_{n=0}^{N-1} n^2 & 2\pi A^2\sum_{n=0}^{N-1} n \\ 0 & 2\pi A^2\sum_{n=0}^{N-1} n & A^2N \end{bmatrix} \\ &= \frac{2}{\sigma^2}\begin{bmatrix} N & 0 & 0 \\ 0 & \frac{(2\pi)^2A^2N(N-1)(2N-1)}{6} & \pi A^2N(N-1) \\ 0 & \pi A^2N(N-1) & A^2N \end{bmatrix}\,, \end{aligned} \tag{3.22}$$

where the following identities have been used [125]

$$\sum_{n=0}^{N-1} n = \frac{N(N-1)}{2}\,, \tag{3.23a}$$

$$\sum_{n=0}^{N-1} n^2 = \frac{N(N-1)(2N-1)}{6}\,. \tag{3.23b}$$

The inverse of this matrix is [121]

$$\mathbf{I}^{-1}(\boldsymbol{\chi}) = \frac{\sigma^2}{2}\begin{bmatrix} \frac{1}{N} & 0 & 0 \\ 0 & \frac{12}{(2\pi)^2A^2N(N^2-1)} & -\frac{6}{2\pi A^2N(N+1)} \\ 0 & -\frac{6}{2\pi A^2N(N+1)} & \frac{2(2N-1)}{A^2N(N+1)} \end{bmatrix}\,. \tag{3.24}$$

Therefore, the CRLBs of the estimated attenuation (CRLBA), frequency offset (CRLBF) and phase (CRLBP) are given by [121]

$$\sigma^2_{CR_A} = \frac{\sigma^2}{2N}\,, \tag{3.25}$$

$$\sigma^2_{CR_{f_0T_s}} = \frac{6}{4\pi^2\rho N(N^2-1)}\,, \tag{3.26}$$

$$\sigma^2_{CR_\phi} = \frac{2N-1}{\rho N(N+1)}\,, \tag{3.27}$$

where ρ is the signal to noise ratio (SNR) that is defined as

$$\rho = \frac{\boldsymbol{\mu}^H(\boldsymbol{\chi})\boldsymbol{\mu}(\boldsymbol{\chi})}{\mathrm{E}\left\{\mathbf{z}^H\mathbf{z}\right\}} = \frac{A^2\mathrm{tr}\left\{\mathbf{S}^H\mathbf{S}\right\}}{N\sigma^2} = \frac{A^2}{\sigma^2}\,, \tag{3.28}$$

where $\mathrm{E}\{\cdot\}$ denotes the expectation.

For the joint channel and frequency offset estimate, which is a function of the three estimated parameters, the vector CRLB representing the minimum variances of the N elements of the estimated channel $\hat{h}(nT_s)$ is given by the diagonal elements of the covariance matrix [121]

$$\mathbf{R}_{\hat{\mathbf{h}}} = \frac{\partial \mathbf{h}(\boldsymbol{\chi})}{\partial \boldsymbol{\chi}} \mathbf{I}^{-1}(\boldsymbol{\chi}) \frac{\partial \mathbf{h}^H(\boldsymbol{\chi})}{\partial \boldsymbol{\chi}}, \tag{3.29}$$

where

$$\begin{aligned}
\frac{\partial \mathbf{h}(\boldsymbol{\chi})}{\partial \boldsymbol{\chi}} &= \begin{bmatrix} \frac{\partial h(0)}{\partial A} & \frac{\partial h(0)}{\partial f_0 T_s} & \frac{\partial h(0)}{\partial \phi} \\ \frac{\partial h(T_s)}{\partial A} & \frac{\partial h(T_s)}{\partial f_0 T_s} & \frac{\partial h(T_s)}{\partial \phi} \\ \vdots & \vdots & \vdots \\ \frac{\partial h((N-1)T_s)}{\partial A} & \frac{\partial h((N-1)T_s)}{\partial f_0 T_s} & \frac{\partial h((N-1)T_s)}{\partial \phi} \end{bmatrix} \\
&= \begin{bmatrix} \frac{\partial A e^{j\phi}}{\partial A} & \frac{\partial A e^{j\phi}}{\partial f_0 T_s} & \frac{\partial A e^{j\phi}}{\partial \phi} \\ \frac{\partial A e^{j(2\pi f_0 T_s+\phi)}}{\partial A} & \frac{\partial A e^{j(2\pi f_0 T_s+\phi)}}{\partial f_0 T_s} & \frac{\partial A e^{j(2\pi f_0 T_s+\phi)}}{\partial \phi} \\ \vdots & \vdots & \vdots \\ \frac{\partial A e^{j(2\pi f_0 T_s(N-1)+\phi)}}{\partial A} & \frac{\partial A e^{j(2\pi f_0 T_s(N-1)+\phi)}}{\partial f_0 T_s} & \frac{\partial A e^{j(2\pi f_0 T_s(N-1)+\phi)}}{\partial \phi} \end{bmatrix} \\
&= \begin{bmatrix} e^{j\phi} & 0 & jAe^{j\phi} \\ e^{j(2\pi f_0 T_s+\phi)} & j2\pi A e^{j(2\pi f_0 T_s+\phi)} & jAe^{j(2\pi f_0 T_s+\phi)} \\ \vdots & \vdots & \vdots \\ e^{j(2\pi f_0 T_s(N-1)+\phi)} & j2\pi A(N-1)e^{j(2\pi f_0 T_s(N-1)+\phi)} & jAe^{j(2\pi f_0 T_s(N-1)+\phi)} \end{bmatrix}.
\end{aligned} \tag{3.30}$$

Therefore, the CRLB of the element $\hat{h}(nT_s)$ is the $(n+1)$th diagonal element of $\mathbf{R}_{\hat{\mathbf{h}}}$ and

is given by

$$\begin{aligned}
\sigma^2_{CR_{h(nT_s)}} &= [\mathbf{R}_{\hat{\mathbf{h}}}]_{n+1\,n+1} \\
&= \frac{\sigma^2}{2}\left[e^{j(2\pi f_0 T_s n+\phi)} \quad j2\pi A n e^{j(2\pi f_0 T_s n+\phi)} \quad jAe^{j(2\pi f_0 T_s n+\phi)}\right] \\
&\quad \times \begin{bmatrix} \frac{1}{N} & 0 & 0 \\ 0 & \frac{12}{(2\pi)^2 A^2 N(N^2-1)} & -\frac{6}{2\pi A^2 N(N+1)} \\ 0 & -\frac{6}{2\pi A^2 N(N+1)} & \frac{2(2N-1)}{A^2 N(N+1)} \end{bmatrix} \begin{bmatrix} e^{-j(2\pi f_0 T_s n+\phi)} \\ -j2\pi A n e^{-j(2\pi f_0 T_s n+\phi)} \\ -jAe^{-j(2\pi f_0 T_s n+\phi)} \end{bmatrix} \\
&= \frac{\sigma^2}{2} e^{j(2\pi f_0 T_s n+\phi)} \begin{bmatrix} 1 & j2\pi A n & jA \end{bmatrix} \begin{bmatrix} \frac{1}{N} \\ -j\left(\frac{12n}{2\pi AN(N^2-1)} - \frac{6}{2\pi AN(N+1)}\right) \\ -j\left(-\frac{6n}{AN(N+1)} + \frac{2(2N-1)}{AN(N+1)}\right) \end{bmatrix} \\
&\quad \times e^{-j(2\pi f_0 T_s n+\phi)} \\
&= \frac{\sigma^2}{2}\left[\frac{1}{N} + \left(\frac{12n^2}{N(N^2-1)} - \frac{6n}{N(N+1)}\right) + \left(-\frac{6n}{N(N+1)} + \frac{2(2N-1)}{N(N+1)}\right)\right] \\
&= \frac{\sigma^2}{2}\left(\frac{1}{N} + \frac{12n^2}{N(N^2-1)} - \frac{12n}{N(N+1)} + \frac{2(2N-1)}{N(N+1)}\right), \qquad (3.31)
\end{aligned}$$

where $n = 0, 1, \ldots, N-1$.

Finally, the average CRLB of the joint channel and frequency offset estimation (CRLBJ) is given by

$$\begin{aligned}
\sigma^2_{CR_h} &= \frac{\sum_{n=0}^{N-1} \sigma^2_{CR_{h(nT_s)}}}{\sum_{n=0}^{N-1} |h(nT_s)|^2} = \frac{\sigma^2}{2NA^2} \sum_{n=0}^{N-1}\left(\frac{1}{N} + \frac{12n^2}{N(N^2-1)} - \frac{12n}{N(N+1)} + \frac{2(2N-1)}{N(N+1)}\right) \\
&= \frac{1}{2\rho N}\left(1 + \frac{12\sum_{n=0}^{N-1} n^2}{N(N^2-1)} - \frac{12\sum_{n=0}^{N-1} n}{N(N+1)} + \frac{2(2N-1)}{N+1}\right) \\
&= \frac{1}{2\rho N}\left(1 + \frac{2(2N-1)}{N+1} - \frac{6(N-1)}{N+1} + \frac{2(2N-1)}{N+1}\right) \\
&= \frac{1}{2\rho N}\left(\frac{N+1+4N-2-6N+6+4N-2}{N+1}\right) \\
&= \frac{1}{2\rho N}\left(\frac{3N+3}{N+1}\right) \\
&= \frac{3}{2\rho N}, \qquad (3.32)
\end{aligned}$$

where the equalities in (3.23) have been used.

3.5 Literature Survey of Practical Frequency Offset Estimators

It can be noticed that most of the complexity of the joint channel estimator is consumed by the frequency offset estimation part during the evaluation of the periodogram samples in (3.15) using an FFT of size N_{FFT}. For getting an accurate frequency estimate with an error that attains the CRLB using the direct FFT application alone, a high number of periodogram samples, much more than that of the input samples $r(nT_s)s^*(nT_s)$, is required. This implies zero-padding the input samples up to a relatively large size of FFT that has to be [126]

$$N_{FFT} > \frac{1}{\sigma_{CR_{f_0T_s}}} . \tag{3.33}$$

Therefore, the periodogram maximiser ML frequency estimator possesses too much complexity for any practical real-time implementation, and many practical algorithms approximating the ML estimator have been considered in the literature. These estimators are classified as correlation-based frequency estimators and interpolation-based frequency estimators [47].

The correlation-based frequency estimators, such as the estimators of Fitz [5], and Luise and Reggiannini [6], can exhibit a comparable performance to that of the ML estimator. However, both estimators possess a limited frequency acquisition range Ψ. This Ψ is inversely proportional to the number of considered samples N and cannot be changed to suit a certain channel requirement. This prevents the estimators from being used for scenarios where a wide frequency acquisition range is required. It also limits the usage for relatively large N. In addition, these estimators use nonlinear operations and possess a high computational load.

The interpolation-based frequency estimators employ two stages of searching for the periodogram peak, first a coarse search stage, followed by a fine search one [13]. The coarse search stage is based typically on an FFT of a relatively short size (compared to that used in the ML estimator). In this stage, an initial estimation of the frequency offset is determined, which corresponds to the location of the maximum sample of the obtained periodogram. This involves less complexity compared to that for the ML estimator. Then diverse techniques can be used in the fine search stage to refine this estimation by inter-

polating a better value within the neighborhood of the initial value obtained in the coarse search stage. Usually, the coarse search stage is an N-point FFT, which allows efficient implementation. However, this requires more complicated methods to be used in the fine search stage and can affect the accuracy of the estimator. Several methods have been presented over the years beginning with Palmer's suggestion of the FFT coarse search estimator [45], and Rife and Boorstyn [13] proposal of the secant method in the fine search refining the FFT coarse search. Abatzoglou [16] has presented an estimator based on Newton's method for locating the root of an equation in the fine search stage. Other estimators based on three-point interpolation, and five-point interpolation for fine search have been described by Quinn [14, 127] and Macleod [15]. In spite of the efficient coarse search, the fine search uses more sophisticated nonlinear techniques, which makes it difficult for practical implementation. The linear interpolation (LI) frequency estimator [14] exploits N-point FFT-based coarse search and three-point linear interpolation fine search. Although the coarse search is computationally efficient, the fine search requires nonlinear operations to achieve a certain accuracy, which results in an increase of the complexity. In addition, the LI estimator has an f_0-dependent performance that can cause the threshold SNR (SNR_{th}) to be significantly higher than that of the ML estimator.

Zakharov and Tozer [17] have proposed the dichotomous search (DS) estimator that performs three-point interpolation exploiting DFT-based iterations. This estimator relies entirely on linear operations that involves efficient real multiply and accumulate (MAC) operations and is perfectly convenient for real-time implementation. The same authors and Baronkin [47] have presented later a group of combined DFT-based estimators utilising three-point interpolation depending on one or more techniques of parabolic interpolation, dichotomous search and two-rate spectral estimation. This was to reduce the complexity and make it even more desirable for the real-time implementation. Aboutanios [18] has suggested a modified dichotomous search estimator with less complexity (in general) compared to the original dichotomous search and still involving only the efficient linear operations. However, some accuracy deteriorations occurs around the SNR_{th} for certain successive limited frequency intervals at the midway between two DFT frequencies. Furthermore, for certain application scenarios with relatively low N and narrow Ψ, the original DS estimator requires less complexity by using the DFT. More detailed study comparing the performance and complexity of these estimators can be found in [124].

After obtaining the frequency offset estimate $\widehat{f_0 T_s}$, the attenuation, phase, and joint channel and frequency offset estimates, respectively, are given by

$$\hat{A} = \left| \hat{a}_{\widehat{f_0 T_s}} \right| = \frac{1}{N} \left| \sum_{n=0}^{N-1} r(nT_s) s^*(nT_s) e^{-j2\pi \widehat{f_0 T_s} n} \right| , \tag{3.34}$$

$$\hat{\phi} = \arg \left\{ \hat{a}_{\widehat{f_0 T_s}} \right\} = \arg \left\{ \sum_{n=0}^{N-1} r(nT_s) s^*(nT_s) e^{-j2\pi \widehat{f_0 T_s} n} \right\} . \tag{3.35}$$

$$\hat{h}(nT_s) = \hat{A} e^{j(2\pi \widehat{f_0 T_s} n + \hat{\phi})} , \quad n = 0, 1, \ldots, N-1 . \tag{3.36}$$

3.5.1 Correlation-Based Frequency Estimators

The correlation-based frequency estimators, such as the estimators of Fitz [5], and Luise and Reggiannini [6], can exhibit a comparable performance to that of the ML estimator. Both estimators possess a limited frequency acquisition range Ψ. This Ψ is inversely proportional to the number of input samples N and cannot be changed to suit a certain channel requirement. This prevents the estimators to be used for scenarios where a wide frequency acquisition range is required. It also limits the usage for relatively large N. In addition, these estimators use nonlinear operations and possess a high computational load. In general, this type of estimators rely on the normalized correlation samples

$$R_x(mT_s) = \frac{1}{N-m} \sum_{n=m}^{N-1} x(nT_s) x^*(nT_s - mT_s) , \tag{3.37}$$

their phases

$$\varphi(mT_s) = \arg \{ R_x(mT_s) \} , \tag{3.38}$$

and/or their phase differences

$$\Delta\varphi(mT_s) = \arg \{ R_x(mT_s) R_x^*(mT_s - T_s) \} , \tag{3.39}$$

where $x(nT_s) = r(nT_s) s^*(nT_s)$. The following correlation-based estimators are considered in this work.

Single Lag Frequency Estimator

A frequency estimator based on a single lag was proposed in [7] (referred to as the SL estimator) and is given by

$$\widehat{f_0 T_s} = \frac{\varphi(LT_s)}{2\pi L}\,, \tag{3.40}$$

with an estimation range limited to $\pm 3/4N$.

Besson and Stoica Frequency Estimator

An estimator was presented in [8] (referred to as the B&S estimator) and is given by

$$\widehat{f_0 T_s} = \frac{1}{2\pi L}\sum_{m=1}^{L}\Delta\varphi(mT_s)\,, \tag{3.41}$$

with the full estimation range (up to $\pm 1/2$).

Mengali and Morelli Frequency Estimator

A weighted average phase difference estimator was presented in [9] (referred to as the M&M estimator) and is given by

$$\widehat{f_0 T_s} = \frac{1}{2\pi}\sum_{m=1}^{L} w(m)\Delta\varphi(mT_s)\,, \tag{3.42}$$

where $w(m)$ is given by

$$w(m) = \frac{3\left[(N-m)(N-m+1) - L(N-L)\right]}{L\left(4L^2 - 6LN + 3N^2 - 1\right)}\,, \tag{3.43}$$

with the full estimation range.

Simplified Nonlinear Least-Squares Frequency Estimator

A simplified estimator was proposed in [10] for the time-variant fading channels based on the nonlinear least-squares (referred to as the SNLS estimator) and is given by

$$\widehat{f_0 T_s} = \frac{\sum_{m=1}^{L} m\left|R_x(mT_s)\right|^2\varphi(mT_s)}{2\pi\sum_{m=1}^{L} m^2\left|R_x(mT_s)\right|^2}\,. \tag{3.44}$$

For the AWGN channel, and knowing that in this case $|R_x(mT_s)|$ is constant, the SNLS estimator can be derived as

$$\widehat{f_0T_s} = \frac{\sum_{m=1}^{L} m\varphi(mT_s)}{2\pi \sum_{m=1}^{L} m^2}\,, \tag{3.45}$$

where

$$\sum_{m=1}^{L} m^2 = \frac{L(L+1)(2L+1)}{6}\,. \tag{3.46}$$

Therefore, the SNLS for the AWGN is given by

$$\widehat{f_0T_s} = \frac{3}{\pi L(L+1)(2L+1)} \sum_{m=1}^{L} m\varphi(mT_s)\,. \tag{3.47}$$

with an estimation range limited to $\pm 1/N$.

Approximated Nonlinear Least-Squares Frequency Estimator

An approximated NLS estimator was proposed in [11] (referred to as the ANLS estimator), with the full estimation range, and is given by

$$\widehat{f_0T_s} = \frac{3\sum_{m=1}^{L}\left[L(L+1) - m(m-1)\right]\Delta\varphi(mT_s)}{2\pi L(L+1)(2L+1)}\,. \tag{3.48}$$

Weighted Normalised Autocorrelation Linear Predictor Frequency Estimator

An improved estimator was proposed in [12] based on the weighted normalised autocorrelation linear predictor (referred to as WNALP), and also with the full estimation range, which is given by

$$\widehat{f_0T_s} = \arg\left\{\sum_{m=1}^{L} w(m)\bar{R}_x(mT_s)\bar{R}_x^*(mT_s - T_s)\right\}\,, \tag{3.49}$$

where $\bar{R}_x(mT_s) = R_x(mT_s)/\left|R_x(mT_s)\right|$ is the autocorrelation normalised by its amplitude and $w(m)$ is given by (3.43).

3.5.2 Periodogram-Based Frequency Estimators

The periodogram-based frequency estimators use coarse and fine search for the periodogram peak [13] and possess the full estimation range. Usually, the coarse search is an N_{FFT}-point fast Fourier transform (FFT), or discrete Fourier transform (DFT), where $N_{FFT} \geq N$. Some estimators use $N_{FFT} = N$ which allows efficient implementation. However, this requires more complicated methods to be used in the fine search and can affect the accuracy of the estimator. The linear interpolation frequency estimator [14] uses $N_{FFT} = N$ and exploits three-point linear interpolation fine search. Although the coarse search is computationally efficient, the fine search requires nonlinear operations to achieve a certain accuracy, which results in an increase of the complexity. This estimator has an f_0T_s-dependent performance that can cause the threshold SNR to be significantly higher than that of the ML estimator. Other methods can be used in the fine search, such as the three/five-point interpolation techniques [15], and Newton's method for locating the root of an equation [16]. In spite of the efficient coarse search, the fine search uses more sophisticated nonlinear techniques, which makes it difficult for practical implementation.

Dichotomous Search Frequency Estimator

A popular estimator of this type is the dichotomous search of the periodogram peak (DS) [17]. This estimator exploits FFT/DFT of the size $N_{FFT} \approx 1.5N$ for the coarse search, and then refines the estimate over Q iterations of searching within binary partitions in the neighbourhood of the initial peak. This estimator relies entirely on linear operations and is perfectly convenient for real-time implementation. In the coarse search, an FFT/DFT of the signal $r(nT_s)s^*(nT_s)$ with a frequency step $\Delta fT_s = 1/N_{FFT}$ is used to obtain W_{fT_s} over the frequencies $f_kT_s = k\Delta fT_s$, where $k = -K, \ldots, -1, 0, 1, \ldots, K$ and $K = \psi/(2\Delta fT_s)$. Periodogram samples $Y_{fT_s} = |W_{fT_s}|^2$ are then determined and an initial (coarse-search) frequency estimate $f_pT_s = \arg\max_{fT_s \in \Psi} \{Y_{fT_s}\}$ is found. The maximum periodogram sample $Y_2 = Y_{f_pT_s}$ together with its two adjacent samples, $Y_1 = Y_{f_{p-1}T_s}$ and $Y_3 = Y_{f_{p+1}T_s}$ are then located. In the fine search, f_pT_s is refined by exploiting Q dichotomous iterations for which the following steps are repeated:

- $\Delta f T_s = \Delta f T_s / 2$.
- If $Y_3 < Y_1$
  then $Y_3 = Y_2$ and $f_p T_s = f_p T_s - \Delta f T_s$,
  else $Y_1 = Y_2$ and $f_p T_s = f_p T_s + \Delta f T_s$.
- $Y_2 = \left| \sum_{n=0}^{N-1} r(nT_s) s^*(nT_s) e^{-j2\pi f_p T_s n} \right|^2$.

At the end of all iterations, the final DS frequency offset (DSF) estimate is $\widehat{f_0 T_s}_{DS} = f_m T_s$. For optimum performance, the number of iterations Q should be high enough so that the final frequency step $\Delta f T_{sf}$ gets below the minimum value of the frequency CRLB ($\sigma_{CR_{f_0 T_s \min}}$) in the SNR range of interest. This corresponds to the value of the CRLB at the end of that range (taken here at 30 dB). Mathematically speaking, the final frequency step that becomes $\Delta f T_{sf} = \Delta f T_s / 2^Q = \psi / (K 2^{Q+1})$ is required to be $\Delta f T_{sf} < \sigma_{CR_{f_0 T_s \min}}$, and accordingly, Q has to satisfy [47]

$$Q > \log_2 \left(\frac{\Delta f T_s}{\sigma_{CR_{f_0 T_s \min}}} \right) \quad \text{or} \quad Q > \log_2 \left(\frac{\psi}{K \sigma_{CR_{f_0 T_s \min}}} \right) - 1 \,. \tag{3.50}$$

Modified Dichotomous Search Frequency Estimator

An important modified dichotomous search (MDS) estimator was proposed in [18], which attains the CRLB without the need to zero-padding the processed samples and allowing a reduction in the complexity to be achieved. The coarse search of the MDS estimator is the same as that for the DS estimator except for $N_{FFT} = N$. In the fine search, the algorithm performs the following initialisation steps:

- $\Delta f T_s = 0.75 \Delta f T_s$.
- If $Y_3 > Y_1$
  then $Y_1 = \left| \sum_{n=0}^{N-1} r(nT_s) s^*(nT_s) e^{-j2\pi n (f_p T_s - \frac{2}{3}\Delta f T_s)} \right|^2$
  and $f_p T_s = f_p T_s + \frac{1}{3} \Delta f T_s$,
  else $Y_3 = \left| \sum_{n=0}^{N-1} r(nT_s) s^*(nT_s) e^{-j2\pi n (f_p T_s + \frac{2}{3}\Delta f T_s)} \right|^2$
  and $f_p T_s = f_p T_s - \frac{1}{3} \Delta f T_s$.

Then, the following steps are repeated for Q iterations:

- $Y_2 = \left|\sum_{n=0}^{N-1} r(nT_s)s^*(nT_s)e^{-j2\pi n f_p T_s}\right|^2$.
- $\Delta f T_s = \Delta f T_s/2$.
- If $Y_3 > Y_1$
  then $Y_1 = Y_2$ and $f_p T_s = f_p T_s + \Delta f T_s$,
  else $Y_3 = Y_2$ and $f_p T_s = f_p T_s - \Delta f T_s$.

At the end of all iterations, the final frequency estimate is $\widehat{f_0 T_s} = f_p T_s$.

Improved Dichotomous Search Frequency Estimator

An improved dichotomous search (IDS) estimator was proposed in [19] exploiting a new initialisation scheme in an attempt to accelerate the convergence so that to allow reducing the number of iterations in the fine search and also without the need to zero-padding. The initial (coarse-search) frequency estimate is determined as $f_p T_s = \arg \max_{f T_s \in \Psi} \{|W_{f T_s}|\}$. In the fine search, the algorithm performs the following initialisation steps:

- $\lambda = \frac{|W_{f_{p+1}T_s}| - |W_{f_{p-1}T_s}|}{|W_{f_{p+1}T_s}| + |W_{f_{p-1}T_s}| - 2|W_{f_p T_s}|\cos(\frac{\pi N}{M})}$.
- $f_p T_s = f_p T_s + \lambda \Delta f T_s$.
- $c = \min\{0.5,\, 2\sigma_{f_0 T_s}\}$ and $\Delta f T_s = c \Delta f T_s$.
- $Y_1 = \left|\sum_{n=0}^{N-1} r(nT_s)s^*(nT_s)e^{-j2\pi n(f_p T_s - \Delta f T_s)}\right|^2$.
- $Y_2 = \left|\sum_{n=0}^{N-1} r(nT_s)s^*(nT_s)e^{-j2\pi n(f_p T_s)}\right|^2$.
- $Y_3 = \left|\sum_{n=0}^{N-1} r(nT_s)s^*(nT_s)e^{-j2\pi n(f_p T_s + \Delta f T_s)}\right|^2$.

Then, Q dichotomous iterations are performed as with the DS estimator and at the end of all iterations $\widehat{f_0 T_s} = f_p T_s$. However, the way c is presented in [19] and given above does not allow the estimator to perform properly in all scenarios. Besides, it involves nonlinear operations and significant complexity to estimate the SNR. This problem can be resolved by choosing $c = 0.5$, which is used in the complexity and simulation analysis below.

Main Lobe Autocorrelation Function Frequency Estimator

A robust hybrid of periodogram-based and correlation-based estimator (grouped in this thesis with the periodogram-based estimators) was proposed in [20] and is referred to as MLAF. The coarse search is similar to that of the DS estimator but with much more zero-padding, where $N_{FFT} = 4N$ is required to obtain an initial frequency estimate f_pT_s. In the fine search, a refining frequency is obtained by exploiting the maximum periodogram sample and its 8 adjacent samples as $f_rT_s = \frac{1}{2\pi} \arg\left\{\sum_{k=-4}^{4} Y_{f_{p+k}T_s} e^{j2\pi\Delta f T_s}\right\}$. The frequency estimate is then calculated as $\widehat{f_0T_s} = f_pT_s + f_rT_s$.

3.6 Simulation Results and Performance Analysis

A binary sequence transmitted through a deterministic (nonfading) single-path channel and corrupted with a complex AWGN is implemented. The simulated received signal and channel are according to (3.8). The performance of the frequency estimators is analysed first. Then, the performance of the dichotomous search-based frequency, attenuation, phase, and joint channel estimators are investigated.

3.6.1 Performance Analysis of the Frequency Estimators

A complex exponential signal of length $N = 26$ in the AWGN channels is considered in the simulation. The mean square error (MSE) of the frequency estimate in each simulation trial is calculated as

$$f_0T_s\text{-MSE} = \left(f_0T_s - \widehat{f_0T_s}\right)^2, \tag{3.51}$$

and then averaged over $10\,000$ simulation trials. The following parameters are used: $L = N/2$ for M&M, SNLS, ANLS and WNALP, $L = 2N/3$ for SL and B&S, $N_{FFT} = 1.5N$ for DS, $N_{FFT} = N$ for MDS and IDS, and $N_{FFT} = 4N$ for MLAF.

Figure 3.2 shows the SNR-dependent performance of the considered estimators compared to the CRLB for $f_0T_s = 0.025$. This low frequency was chosen to guarantee that the

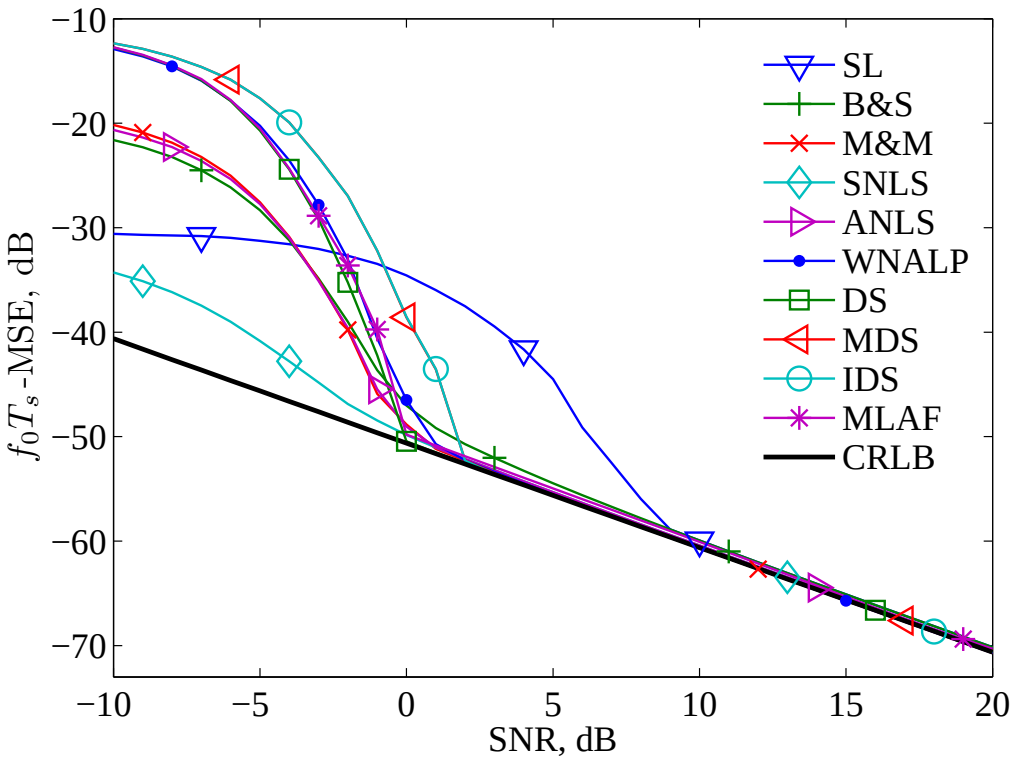

Figure 3.2: f_0T_s-MSE of the frequency estimators for AWGN channels as a function of SNR for a small frequency offset; $N = 26$, $f_0T_s = 0.025$ and $Q = 8$ for DS, MDS and IDS.

narrowest frequency estimation range of the estimators (which is $\psi = 3/2N$ for SL estimator) is not exceeded. All estimators attain the CRLB at high SNRs. At very low SNRs, the SNLS and SL estimators can be seen with a relatively lower f_0T_s-MSE, which is due to the limited frequency estimation range of those estimators. However, the SL estimator possesses the poorest performance in general, with a high SNR threshold (*i.e.* the SNR below which the estimation error starts diverging from the CRLB) of about 10 dB. Among the other estimators with the full frequency estimation range, the DS and MLAF estimators possess the lowest SNR threshold of 0 dB. The SNR threshold is 1 dB for the ANLS, M&M and WNALP estimators and 2 dB for the MDS and IDS estimators. The diverging rate of the f_0T_s-MSE of the WNALP estimator from the CRLB below SNR threshold is comparable to that of the periodogram-based estimators; however, the f_0T_s-MSE of the BS, M&M and ANLS correlation-based estimators possesses a slower diverging rate.

The f_0T_s-dependent performance for SNR $= 4$ dB is shown in Figure 3.3. The WNALP correlation-based estimator and all the periodogram-based estimators are shown

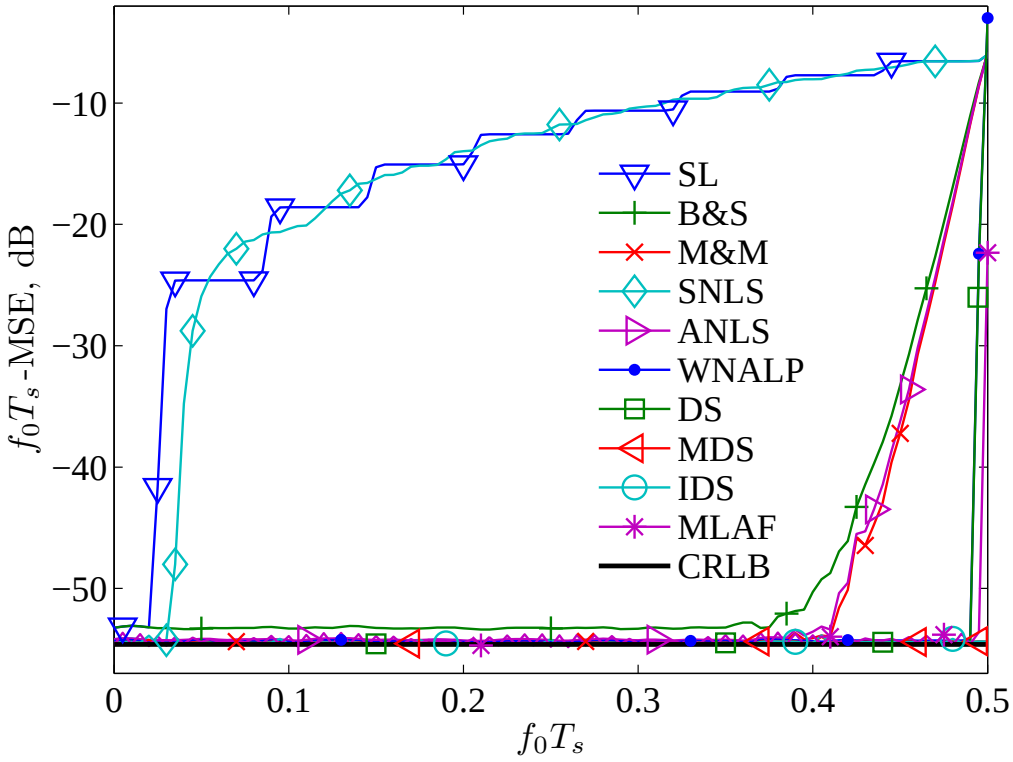

Figure 3.3: f_0T_s-MSE of the frequency estimators for AWGN channels as a function of f_0T_s; $N = 26$, SNR $= 4$ dB and $Q = 8$ for DS, MDS and IDS.

to possess the full frequency estimation range, unlike the other correlation-based estimators, for which the practical range is narrower than the theoretical one. The f_0T_s-MSE of the B&S, M&M and ANLS estimators are shown to start diverging from the CRLB for $f_0T_s > 0.41$. This explains the relatively lower f_0T_s-MSE of the B&S, M&M and ANLS estimators than that of the periodogram-based estimators for SNRs below SNR threshold shown in Figure 3.2.

Simulation results reveal that apart from the WNALP estimator, and unlike the periodogram-based estimators, the performance of the considered correlation-based estimators at low SNRs becomes poorer with the increase of f_0T_s. They even suffer from a frequency-dependent SNR threshold. This can be seen in Figure 3.4, where the SNR-dependent performance is studied again but now for $f_0T_s = 0.41$, which is still within the practical frequency estimation range of the B&S, M&M and ANLS estimators shown in Figure 3.3. Here, the SL and ANLS estimators can no longer operate as the considered frequency is outside their frequency estimation ranges. A significant degradation in the performance of the B&S, M&M and ANLS estimators can be seen for low SNRs,

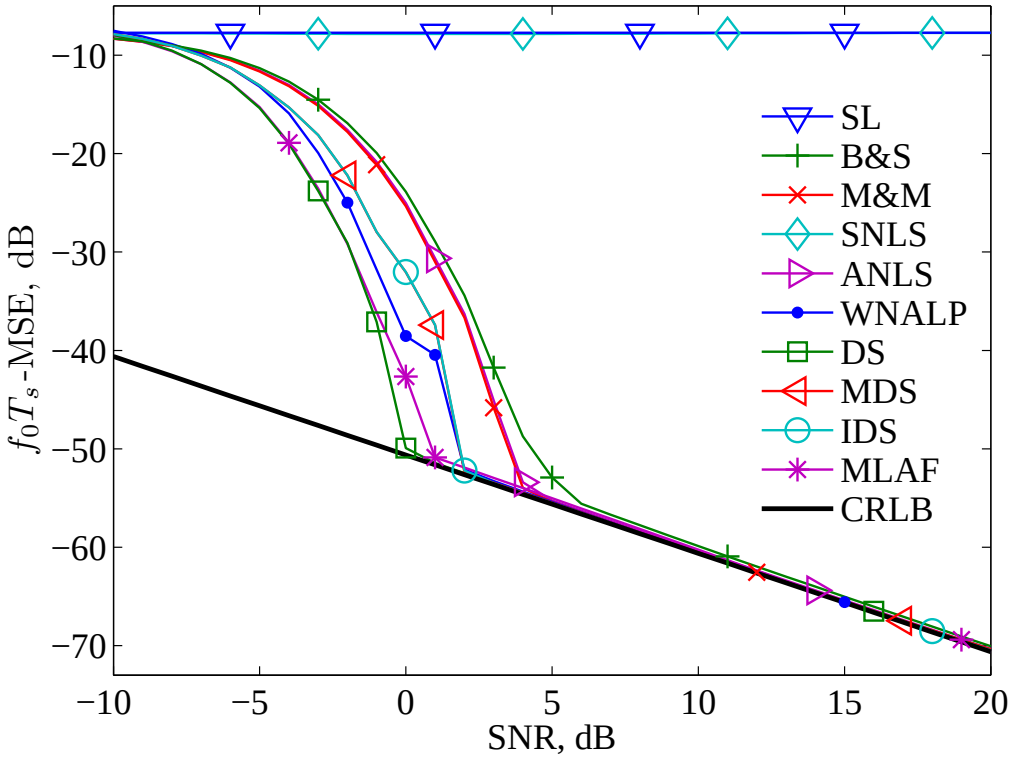

Figure 3.4: f_0T_s-MSE of the frequency estimators for AWGN channels as a function of SNR for a large frequency offset; $N = 26$, $f_0T_s = 0.41$ and $Q = 8$ for DS, MDS and IDS.

where the SNR threshold increases by about 3 dB compared with that of the results in Figure 3.3. Meanwhile, the performance of the WNALP and all the periodogram-based estimators is not significantly changed, and those estimators now outperform the other correlation-based estimators. The DS estimator is seen to possess the best performance with SNR threshold of 0 dB and the MLAF estimator is slightly behind with an SNR threshold of 1 dB.

More attention is next paid to investigate the performance of the periodogram-based estimators and check/challenge the claimed advantages of the recently proposed estimators. Figure 3.5 shows the SNR-dependent performance for $Q = 5$, 6 and 10. Although the fine search of the MLAF estimator is not iterative, it is added for comparison reasons. It can be seen that Q can be chosen depending on the SNR range of interest. As Q increases, the SNR coverage range increases for DS, MDS and IDS estimators in the same way. The claim in [19] that the IDS estimator with $Q = 5$ obtains a similar estimate to that of the DS and MDS estimators with $Q = 10$ is not true.

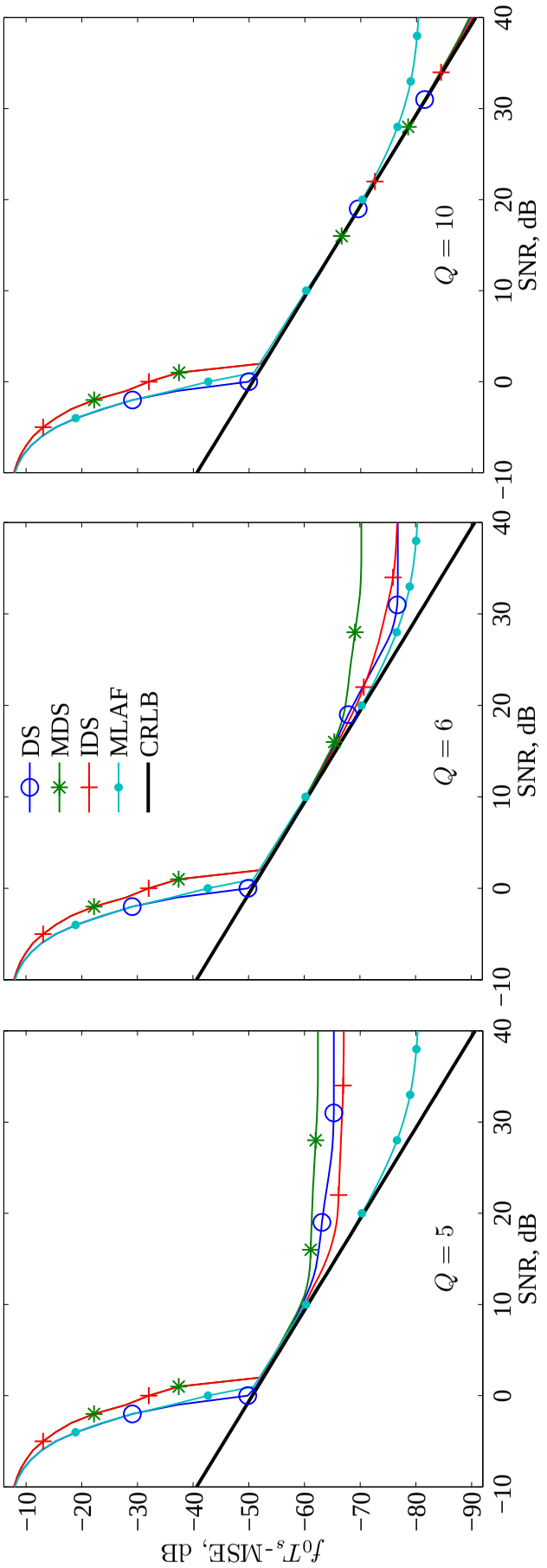

Figure 3.5: f_0T_s-MSE of the periodogram-based frequency estimators for AWGN channels as a function of SNR for different Q; $N = 26$ and $f_0T_s = 0.41$.

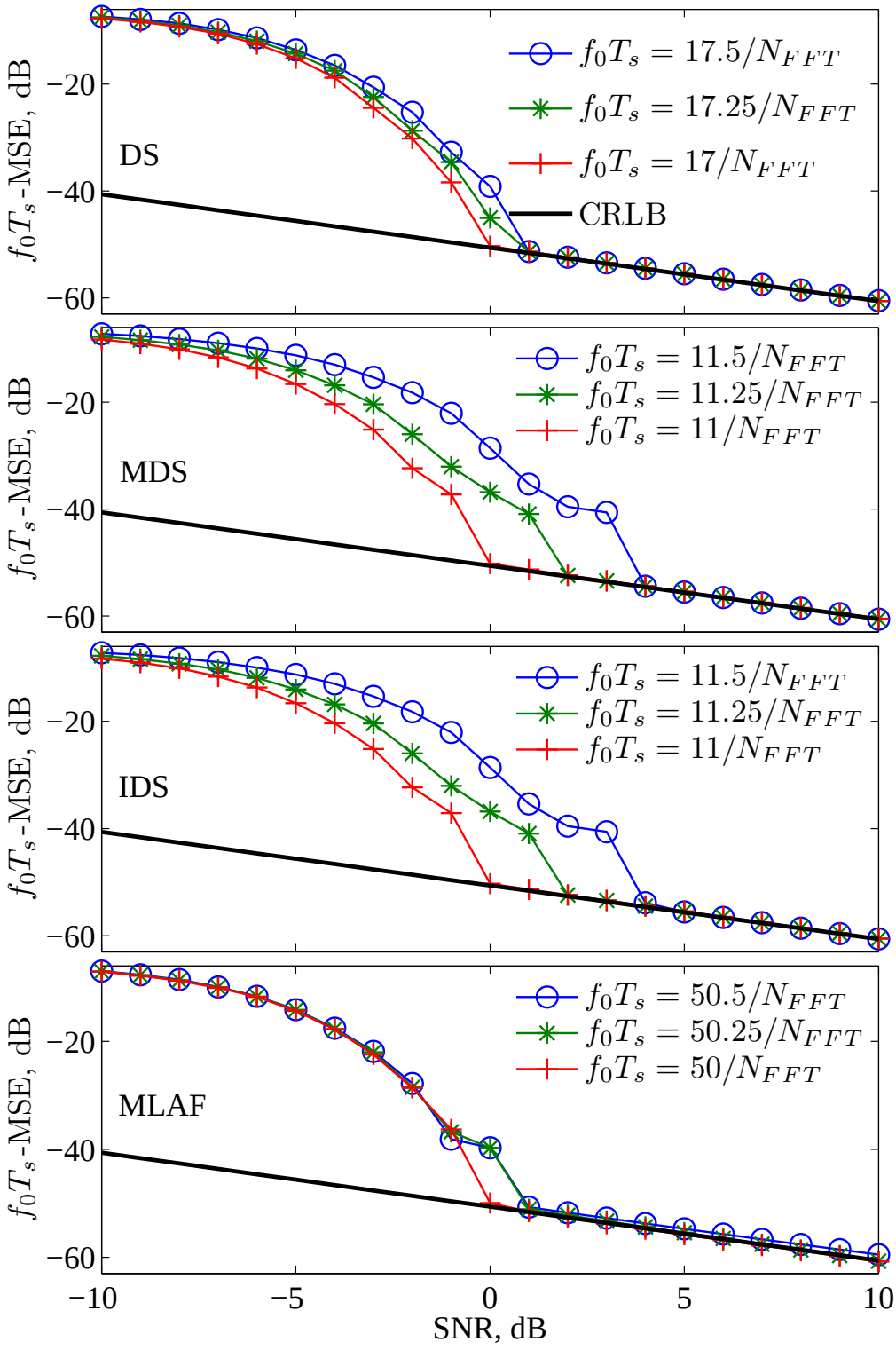

Figure 3.6: f_0T_s-MSE of the periodogram-based frequency estimators for AWGN channels as a function of SNR in the low range for different f_0T_s within one high coarse FFT frequency bin; $N = 26$ and $Q = 10$ for DS, MDS and IDS.

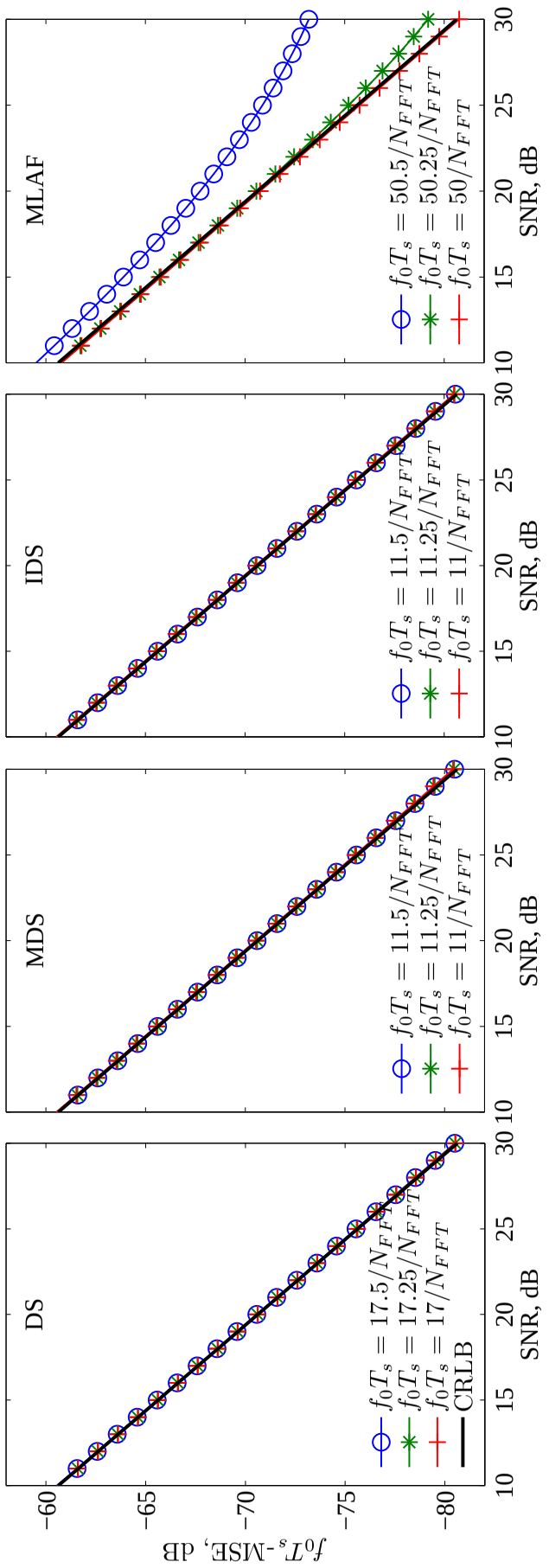

Figure 3.7: f_0T_s-MSE of the periodogram-based frequency estimators for AWGN channels as a function of SNR in the high range for different f_0T_s within one high coarse FFT frequency bin; $N = 26$ and $Q = 10$ for DS, MDS and IDS.

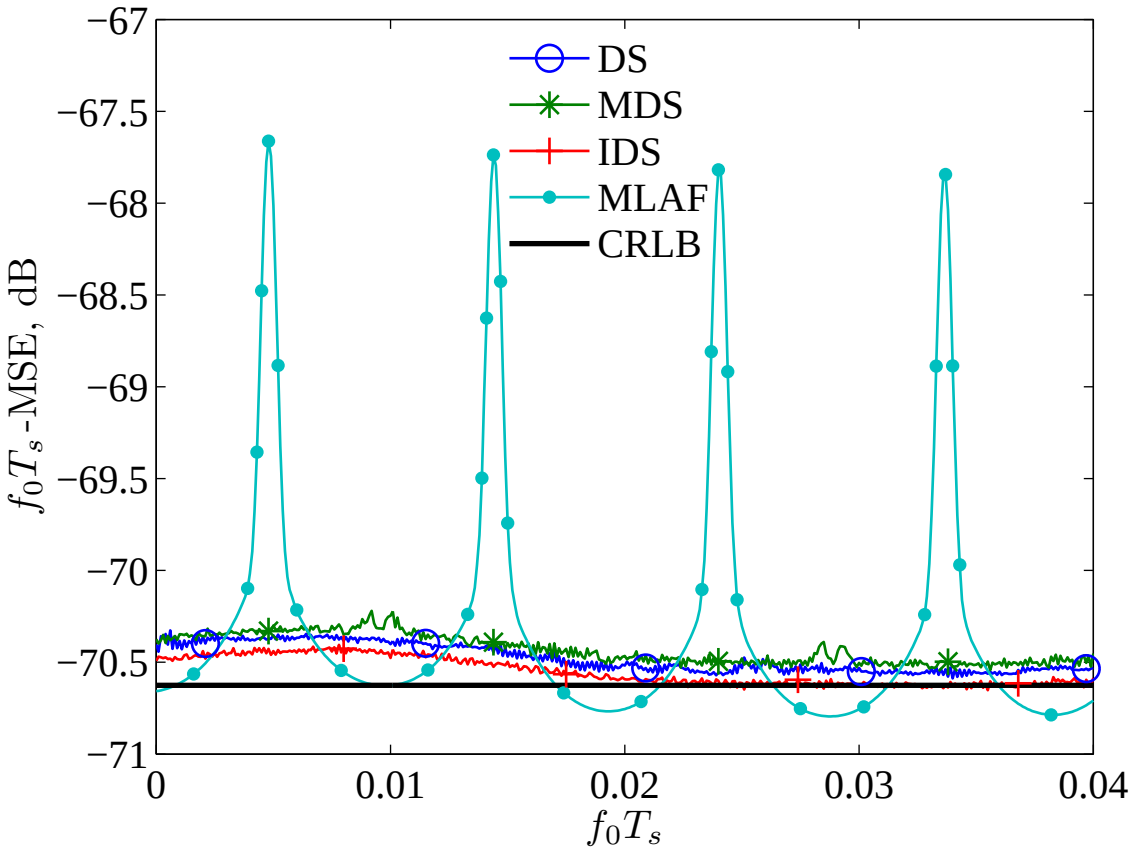

Figure 3.8: f_0T_s-MSE of the periodogram-based frequency estimators for AWGN channels as a function of f_0T_s within the first coarse FFT frequency bin of the MDS estimator for a high SNR; $N = 26$, SNR $= 20$ dB and $Q = 8$ for DS, MDS and IDS.

The performance is then examined for different frequencies within a frequency bin of the course FFT. The SNR-dependent performance for different frequencies within a high frequency bin is shown for low SNR range in Figure 3.6 and for high SNR range in Figure 3.7. The MDS and IDS estimators possess an f_0T_s-dependent SNR threshold, which becomes higher by 4 dB at the bin-centre frequency than that at the bin-edge frequency as shown in Figure 3.6. The DS and MLAF estimators are less sensitive to frequency change with only 1 dB difference in threshold SNR. However, unlike the other estimators, a significant performance degradation of the MLAF estimator can be seen in Figure 3.7 at the bin-centre frequency.

Figure 3.8 investigates the f_0T_s-MSE (at SNR $= 20$ dB) against f_0T_s within a few low frequency bins. The DS, MDS and IDS provide a consistent high-accuracy performance throughout the considered range, whereas a performance degradation of the MLAF estimator is seen at frequencies close to the bin centres. Interestingly, the error of the MLAF

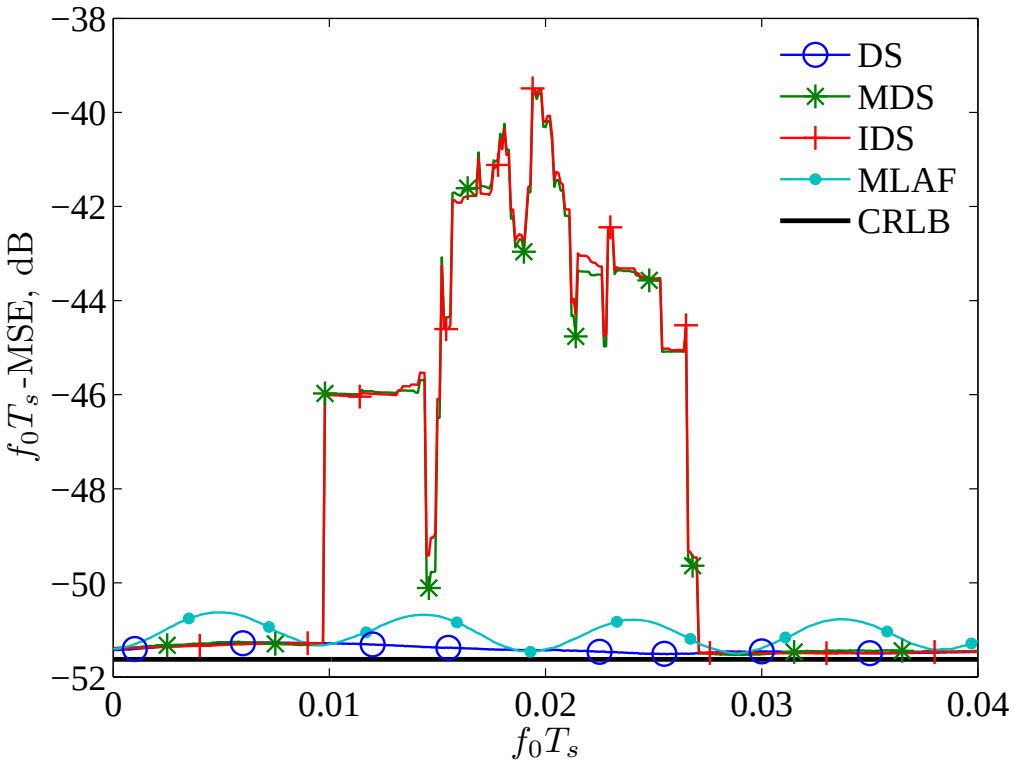

Figure 3.9: f_0T_s-MSE of the periodogram-based frequency estimators for AWGN channels as a function of f_0T_s within the first coarse FFT frequency bin of the MDS estimator for a high SNR; $N = 26$, SNR $= 1$ dB and $Q = 8$ for DS, MDS and IDS.

sometimes is below the CRLB, which is likely to be due to the discrete nature of the larger FFT where the frequency under analysis happens to fall very close to the edge of the bin.

For SNR $= 1$ dB, a significant performance degradation of the MDS and IDS estimators can be seen in Figure 3.9 in the middle of a bin. The MLAF possesses little f_0T_s-MSE fluctuation and the DS estimators is seen to have the lowest (almost constant) f_0T_s-MSE.

The computational complexity of the estimators considered in the simulation and their frequency estimation range are summarised in Table 3.1. For the correlation-based estimators, the SL estimator possesses the lowest complexity but also the worst performance. Then comes the SNLS but it only operates for narrow frequency estimation range. Although the WNALP estimator has the best performance in this group, it possesses the highest complexity with many nonlinear operations. The M&M and SNLS estimators involve similar complexity and performance. They are less complex than the B&S estimator and outperform it. Among the periodogram-based estimators, the IDS estimator

Table 3.1: Computational Complexity and Frequency Estimation Range of the Estimators for AWGN Channels Considered in the Simulation.

Estimator	FFT/DFT	Complex Multiplications	Complex Additions	Nonlinear operations	Estimation Range
SL	—	$N-L$	$N-L-1$	1	$[-\frac{3}{4N}\ \frac{3}{4N})$
B&S	—	$L(2N-L+1)/2$	$L(2N-L-3)/2$	L	$[-\frac{1}{2},\ \frac{1}{2})$
M&M	—	$L(2N-L+1)/2$	$L(2N-L-3)/2$	L	$[-\frac{1}{2},\ \frac{1}{2})$
SNLS	—	$L(2N-L-1)/2$	$L(2N-L-3)/2$	L	$[-\frac{1}{N},\ \frac{1}{N})$
ANLS	—	$L(2N-L+1)/2$	$L(2N-L-3)/2$	L	$[-\frac{1}{2},\ \frac{1}{2})$
WNALP	—	$L(2N-L+1)/2$	$L(2N-L-3)/2$	$2L+1$	$[-\frac{1}{2},\ \frac{1}{2})$
DS	$1.5N$-point	$(Q-1)(N-1)$	$(Q-1)(N-1)$	—	$[-\frac{1}{2},\ \frac{1}{2})$
MDS	N-point	$Q(N-1)$	$Q(N-1)$	—	$[-\frac{1}{2},\ \frac{1}{2})$
IDS	N-point	$(Q+2)(N-1)$	$(Q+2)(N-1)$	$N+4$	$[-\frac{1}{2},\ \frac{1}{2})$
MLAF	$4N$-point	9	8	1	$[-\frac{1}{2},\ \frac{1}{2})$

Table 3.2: Estimators and Bounds for AWGN Channels Considered in the Simulation.

Algorithm		CRLB	ML estimator	DS estimator
Parameter	$\chi_1 = A$	σ_{CR_A} in (3.25)	$\hat{A}_{ML}$ in (3.17)	$\hat{A}_{DS}$ in (3.34)
	$\chi_2 = f_0 T_s$	$\sigma_{CR_{f_0T_s}}$ in (3.26)	$\widehat{f_0 T_s}_{ML}$ in (3.16)	$\widehat{f_0 T_s}_{DS}$ in Section 3.5.2
	$\chi_3 = \phi$	σ_{CR_ϕ} in (3.27)	$\hat{\phi}_{ML}$ in (3.18)	$\hat{\phi}_{DS}$ in (3.35)
	$h(nT_s)$	σ_{CR_h} in (3.32)	$\hat{h}_{ML}(nT_s)$ in (3.19)	$\hat{h}_{DS}(nT_s)$ in (3.36)

has the highest complexity. The MLAF also possesses a high complexity and involves a nonlinear operation. The MDS has slightly less complexity than the DS estimator. Both the estimators do not involve any nonlinear operations and are less complex than the correlation-based M&M and SNLS estimators. However, the DS estimator outperforms the MDS one, and can be less complex in some scenarios when the frequency estimation range is narrow and only a few DFTs are needed in the coarse search.

In conclusion, The DS estimator outperforms the other estimators in many scenarios. It has a high-accuracy performance throughout the wide frequency estimation range and over a wide range of SNRs. This estimator also possesses a relatively low complexity involving only linear operations which makes it the best choice in practice, as so, is used here throughout the thesis.

3.6.2 Performance Analysis of Dichotomous Search-Based Estimators

The performance of the dichotomous search-based estimators is investigated and compared against the reference CRLBs according to Table 3.2 over an SNR range up to 30 dB, which is considered below in the simulations according to (3.28) as $\rho = A^2/\sigma^2$.

Computer simulations are used to estimate the square root of the mean square error

(RMSE) of the parameter χ_i and the joint channel estimations, respectively, as

$$\chi_i\text{-RMSE} = \sqrt{\frac{1}{N_t}\sum_{t=1}^{N_t}\left(\chi_i - \hat{\chi}_{i_t}\right)^2}\,; \qquad i = 1, 2, 3\,, \tag{3.52a}$$

$$\mathbf{h}\text{-RMSE} = \sqrt{\frac{1}{N_t}\sum_{t=1}^{N_t}\frac{\sum_{n=0}^{N-1}\left|h(nT_s) - \hat{h}_t(nT_s)\right|^2}{\sum_{n=0}^{N-1}\left|h(nT_s)\right|^2}}\,, \tag{3.52b}$$

over a number of $N_t = 10\,000$ simulation trials, where $\hat{\chi}_{i_t}$ and $\hat{h}_t(nT_s)$ are the estimated ith parameter and the nth channel sample, respectively, in the tth simulation trial. The following parameters are used for the simulations: the length of the pilot symbols is $N = 63$, the size of the FFT used in the ML estimator according to (3.33) is $N_{FFT} = 40\,960$, the frequency step used in the coarse search stage of the DS estimator is $\Delta f T_s = 0.01238$, and the number of iterations used in the fine search stage according to (3.50) is $Q = 10$.

Frequency Offset Estimator: Figure 3.10 shows the f_0T_s-RMSE of the DS and the ML frequency offset estimators compared to the CRLB versus SNR in (a) and versus f_0T_s in (b). In Figure 3.10(a), the f_0T_s-RMSE of the estimators as a function of SNR is presented for $f_0T_s = 0.01$. The DS estimator as can be seen exhibits a high-accuracy performance which is very close to that of the ML estimator throughout the SNR range of interest. For both estimators, the f_0T_s-RMSE attains the CRLB for a wide range of SNR. However, there exists a threshold SNR (SNR_{th}) of approximately -3 dB below which the error increases rapidly and diverges from the CRLB. This is a known characteristic of nonlinear estimators [121], and is due to the occurrence of the outliers [13]. The considerable error in this area can be limited by constraining the estimated value to a narrow frequency acquisition range, which also helps reducing the complexity [47,124]. Figure 3.10(b) shows the f_0T_s-RMSE of the estimators as a function of f_0T_s for SNR $= 30$ dB. A consistent and accurate performance can be noticed over all the allowable frequency acquisition range for both DS and ML estimators where the error coincides with the CRLB.

Attenuation Estimator: Figure 3.11 shows the A-RMSE of the considered DS and ML attenuation estimators compared to the CRLB for the same scenarios. Figure 3.11(a) illustrates the A-RMSE as a function of SNR for $f_0T_s = 0.01$. The DS estimator as

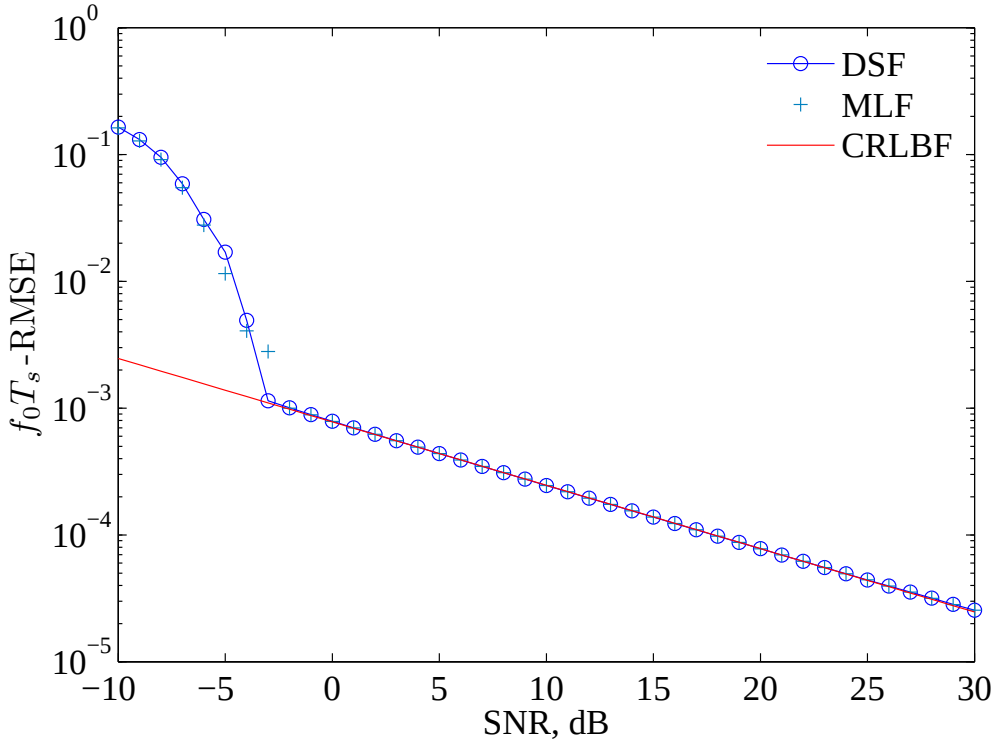

(a)

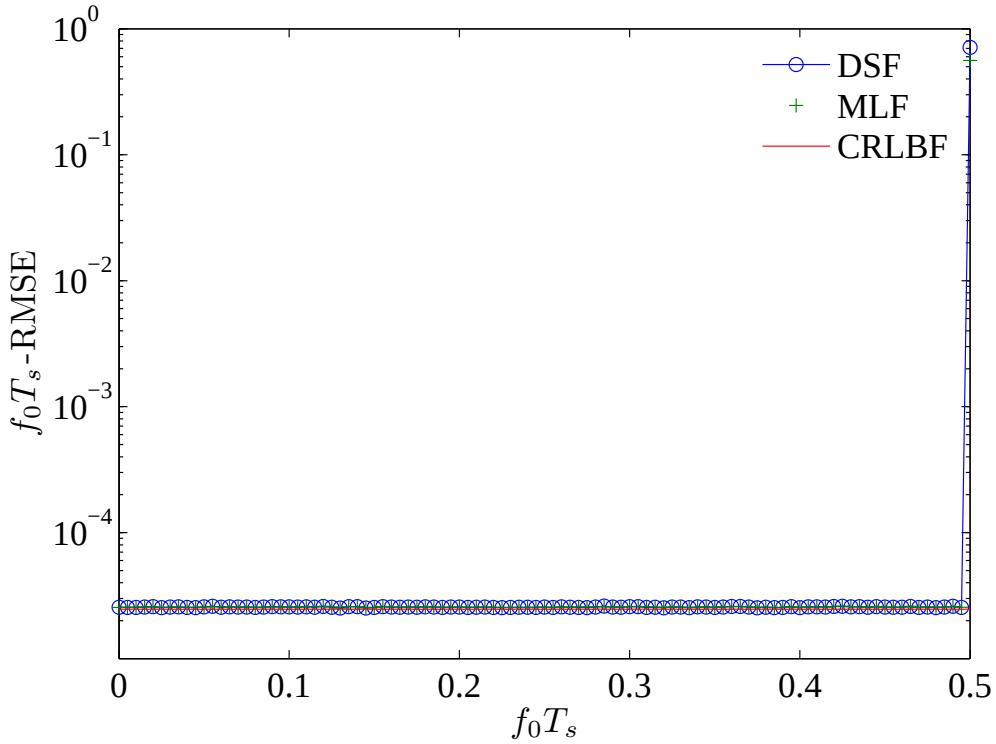

(b)

Figure 3.10: f_0T_s-RMSE of the DS and ML frequency offset estimators for AWGN channels; $N = 63$, $N_{FFT} = 40960$ for ML, $\Delta f T_s = 0.01238$ and $Q = 10$; (a) SNR-dependent performance for $f_0T_s = 0.01$ and (b) f_0T_s-dependent performance for SNR $= 30$ dB.

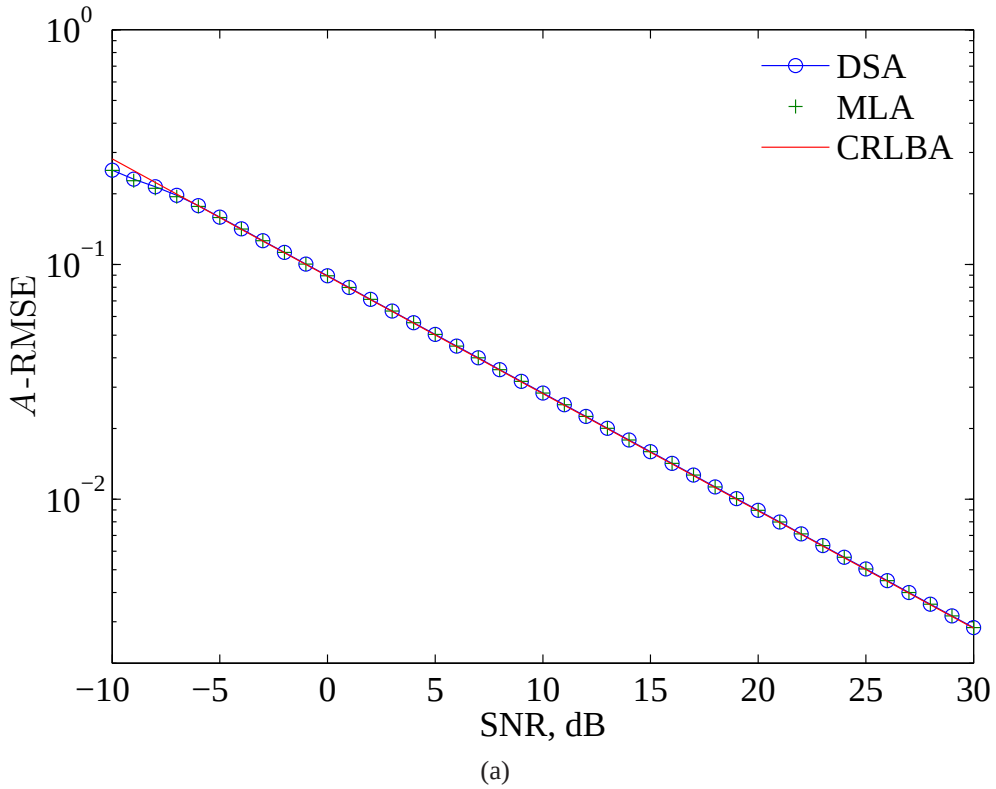

(a)

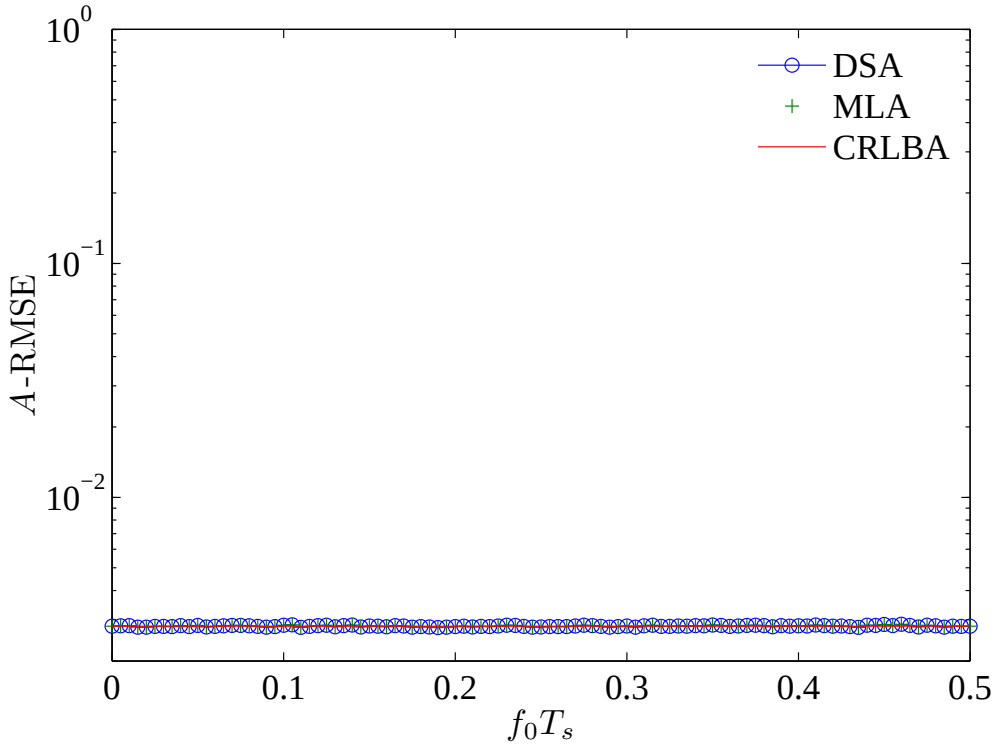

(b)

Figure 3.11: A-RMSE of the DS and ML attenuation estimators for AWGN channels; $N = 63$, $N_{FFT} = 40960$ for ML, $\Delta f T_s = 0.01238$ and $Q = 10$; (a) SNR-dependent performance for $f_0T_s = 0.01$ and (b) f_0T_s-dependent performance for SNR $= 30$ dB.

can be seen exhibits a high-accuracy performance which is very close to that of the ML estimator throughout all the investigated SNR range. In Figure 3.11(b), the A-RMSE is plotted versus f_0T_s for SNR $= 30$ dB. A consistent and accurate performance can also be seen over all the wide frequency acquisition range for both DS and ML estimators and the error coincides with the CRLB.

Phase Estimator: Figure 3.12 shows simulation results concerning the phase estimation error compared to the CRLB for the same scenario. In Figure 3.12(a), the ϕ-RMSE of the estimators is illustrated as a function of SNR. The DS estimator reveals an accurate performance which is very close to that of the ML estimator throughout the SNR range of interest. A threshold SNR can be noticed as for the frequency offset estimators. However, in this case the SNR_{th} is about 1 dB lower. Figure 3.12(b) shows the ϕ-RMSE of the estimators as a function of f_0T_s. It can be seen that the estimation error of both estimators attains the CRLB over all the wide frequency acquisition range, which shows that both estimators possess a wide frequency acquisition range.

Channel Estimator: In Figure 3.13, the $\mathbf{h}$-RMSE of the joint channel and frequency offset estimators compared to the CRLB is illustrated for the same scenario. As can be seen in Figure 3.13(a), a high-accuracy performance of the DS estimator which is identical to that of the ML estimator is achieved over the considered SNR range. Compared to the frequency offset and the phase estimators, the threshold SNR in this case is the lowest ($\text{SNR}_{\text{th}} \approx -6$ dB). The DS estimator, as can be seen in Figure 3.13(b), attains the same ML-like performance throughout the wide frequency acquisition range.

3.7 Conclusions

In this chapter, the maximum likelihood (ML) joint data-aided channel and frequency offset estimation has been studied for signals propagated through AWGN channels. The CRLBs of the joint estimators have been derived and fundamental techniques have been introduced. The ML estimator has optimum performance but impractical complexity. A literature review has been presented for the two main approaches approximating the ML

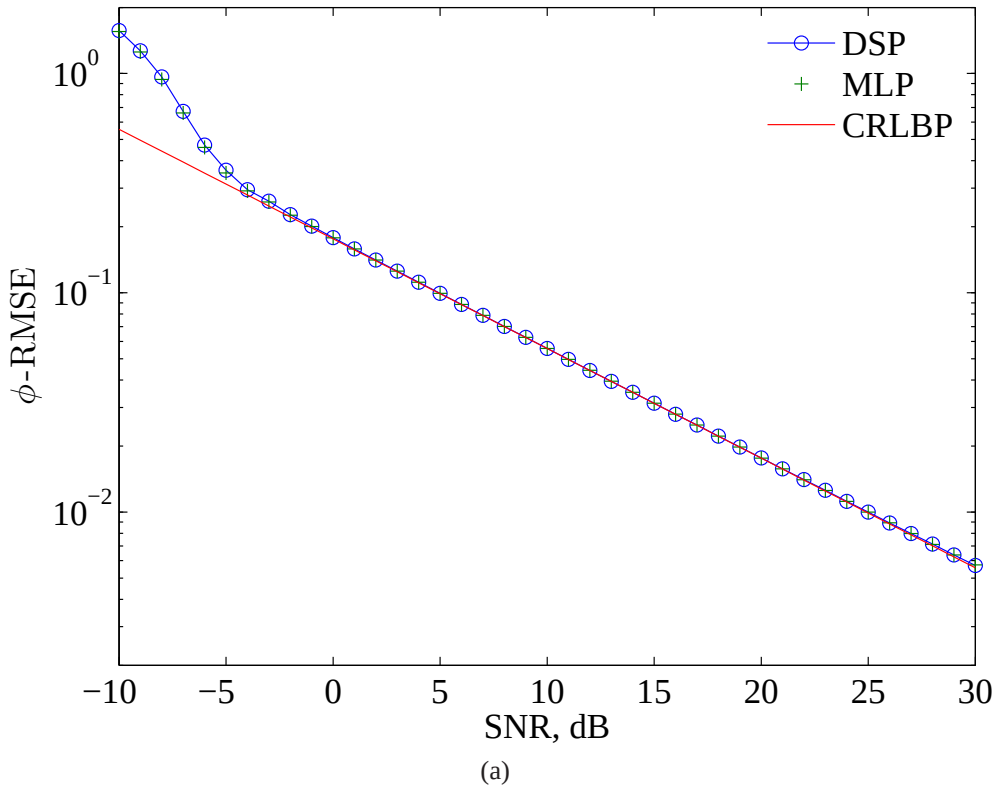

(a)

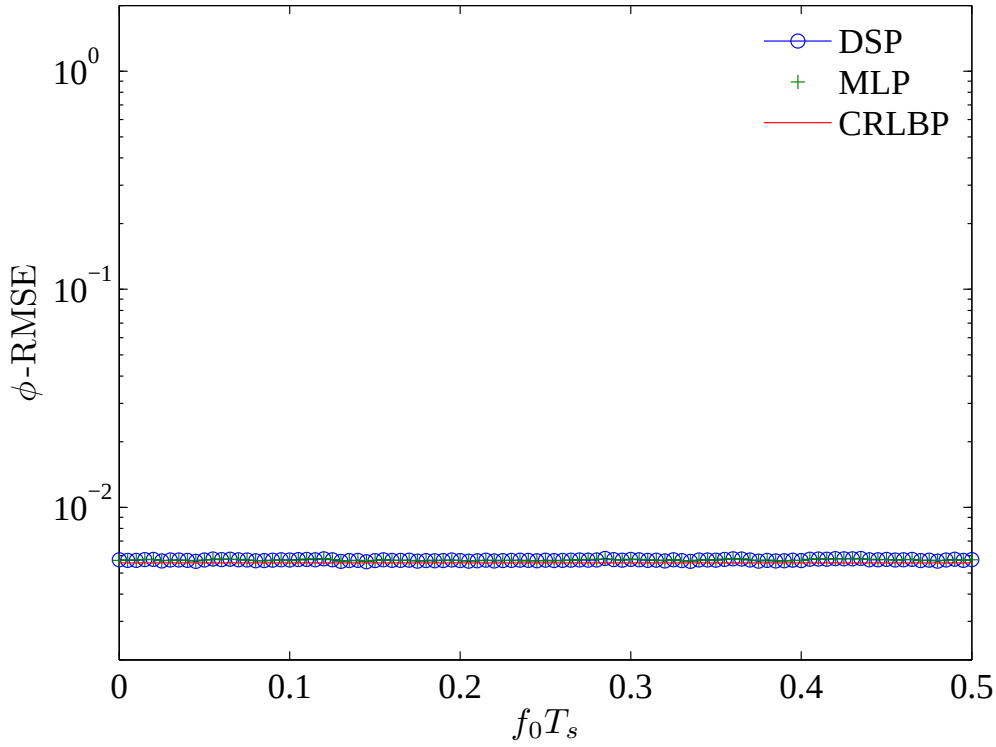

(b)

Figure 3.12: ϕ-RMSE of the DS and ML phase estimators for AWGN channels; $N = 63$, $N_{FFT} = 40960$ for ML, $\Delta f T_s = 0.01238$ and $Q = 10$; (a) SNR-dependent performance for $f_0T_s = 0.01$ and (b) f_0T_s-dependent performance for SNR $= 30$ dB.

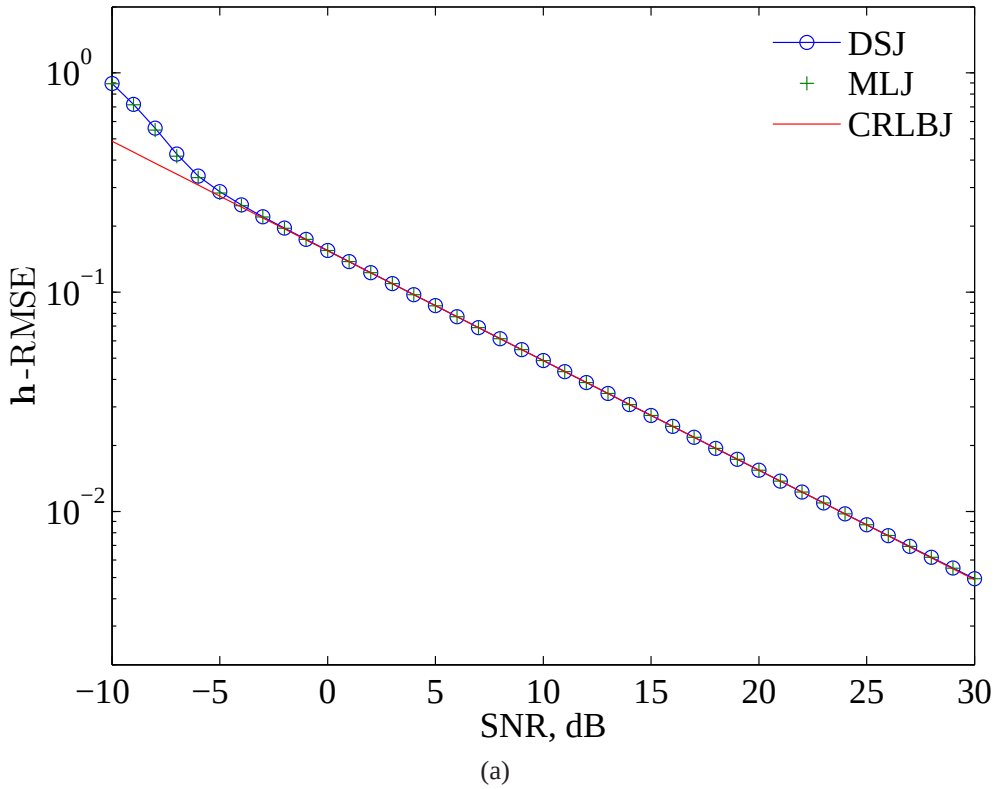

(a)

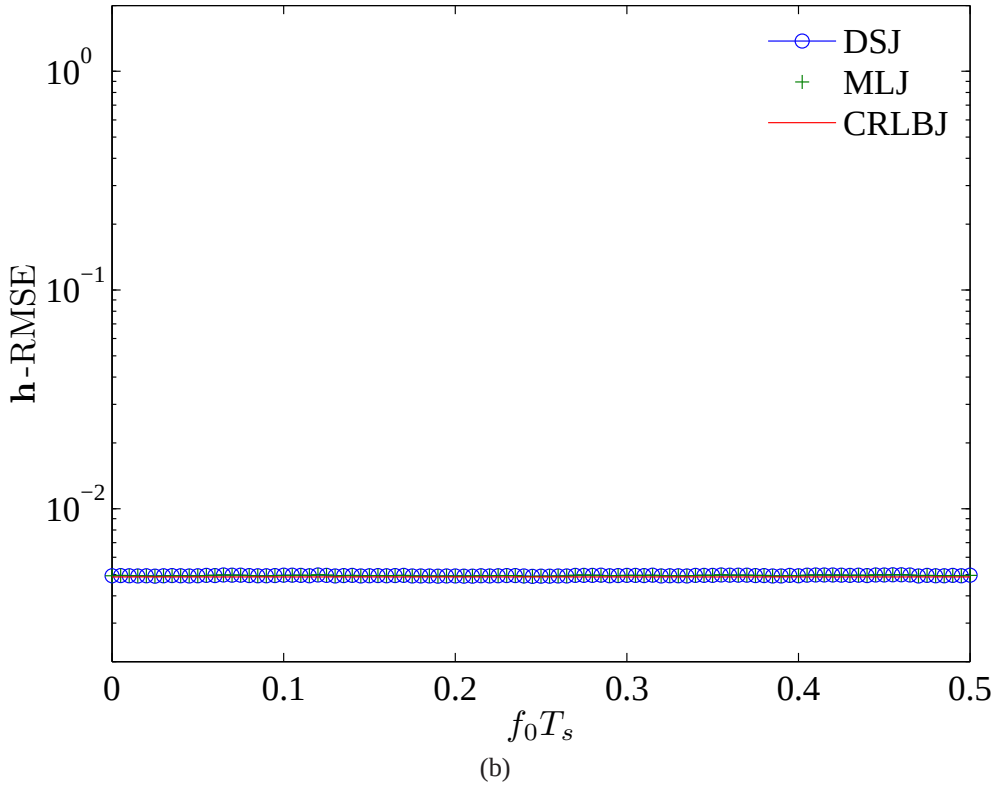

(b)

Figure 3.13: **h**-RMSE of the DS and ML joint estimators for AWGN channels; $N = 63$, $N_{FFT} = 40960$ for ML, $\Delta f T_s = 0.01238$ and $Q = 10$; (a) SNR-dependent performance for $f_0 T_s = 0.01$ and (b) $f_0 T_s$-dependent performance for SNR $= 30$ dB.

estimator, namely, the correlation-based and the periodogram-based estimators, including some recently introduced advanced frequency estimators.

In the first approach, traditional estimators possess good accuracy, however they usually have a high complexity. In addition, these estimators possess a limited frequency acquisition range that depends on number of observed symbols N, and so, might be inapplicable for certain practical scenarios. In the second approach, traditional estimators either exploit complicated nonlinear techniques or have a poor and inconsistent performance that depend on some parameters of the signal.

Performance analysis of recently introduced advanced frequency estimators for signals in the AWGN channels has been presented. The performance of the correlation-based estimators considered, with the exception of the WNALP estimator [12], has been shown to be frequency-sensitive at low SNRs, where the performance degrades and the SNR threshold increases as the frequency increases. Their frequency estimation range is also narrower than that of the WNALP and periodogram-based estimators. However, the WNALP has a relatively high complexity. Among the periodogram-based estimators considered, the IDS [19] and MLAF [20] estimators possess the highest complexity. The performance of both the MDS [18] and IDS estimators is frequency-sensitive at low SNRs, whereas the MLAF estimator possesses a frequency-sensitive performance at high SNRs. The DS estimator [17], exploiting an FFT-based coarse search and dichotomous fine search using three-point interpolation of the periodogram peak and its two adjacent samples, has been shown to outperform the other estimators in many scenarios, keeping a high-accuracy performance throughout the wide frequency estimation range and for all considered SNRs. It also relies only on linear operations with a relatively low complexity, which makes it the best choice in many practical scenarios, and so, is used throughout the thesis.

The dichotomous search algorithm for frequency offset estimation jointly with the channel parameter estimation has been considered. The dichotomous-based joint channel and frequency offset estimator has been investigated for different scenarios. Simulation results have shown a high-accuracy performance of the different parameter and joint channel estimators, which is very close to that of the ML estimator over a wide range of SNR and throughout all the wide frequency acquisition range.

Chapter 4

Joint Estimation of Channel and Frequency Offset in Time-Invariant Frequency-Selective Channels

Contents

In this chapter, the joint data-aided estimation of channel and frequency offset for signals propagated through time-invariant frequency-selective channels is considered. The joint estimation exploits multipath diversity that improves the performance by searching for the maximum of the combined periodograms of the multipath components. Two joint estimators are considered, the first of which is based on the Bayesian approach that can provide a high-accuracy performance when certain prior channel statistical knowledge

is available. The second is based on the ML approach, with a a slightly lower accuracy than that of the Bayesian-based estimator, which can operate in the absence of these channel statistics. The joint estimators exploit the DS frequency estimation technique of the course and fine searching for the maximum of the generalised periodogram. Simulation results for different scenarios in Rayleigh fading channels show that these estimators have a high-accuracy performance with an estimation error very close to the CRLBs over a wide range of SNRs and throughout the wide frequency acquisition range.

4.1 Introduction

In wireless communication systems, the waves traveling from the transmitter to the receiver get reflected, scattered, diffracted, or refracted due to the surrounding objects and the media property [21]. This creates multiple propagation paths, where the received signal is a sum of many copies of the transmitted signal with different delays and attenuations [22]. As a result, the channel possesses a randomly time-variant impulse response and becomes a fading channel that requires statistical treatment [23, 24]. In this case, the performance of the single-branch receiver is poor due to the SNR reduction, and diversity reception is used to improve that performance [25, 26]. Depending on the fading rate of the channel compared to the baseband signal variations, the channels can be classified as fast fading or slow fading channels. In the fast fading channels, the channel impulse response changes rapidly within the symbol interval [23]. This implies more complicated models to represent these channels as in [27, 28], and requires special techniques for estimation as described in [29, 30]. However in the slow fading channels, the channel can be simply assumed static (time-invariant) during the observation interval [23].

Most frequency estimators for time-invariant frequency-selective channels in the literature are based on the correlations of the received signal due to the simplicity in the implementation. The estimator in [25] is an extension to the multipath channels with diversity reception of the correlation-based algorithm for the nonfading channels proposed in [6]. However, it has a narrow frequency acquisition range and poor performance for low SNR range. This is a common case in the correlation-based estimators [31–33]. Significant performance degradation in the single-path scenario have been addressed in many

publications [31, 32], where multipath diversity is not used to improve the performance.

Joint estimators of channel and frequency offset exploiting multipath diversity will be considered in this chapter for the time-invariant channels. This diversity will be shown to improve the estimation performance in a similar way that the detection performance in multipath channels is improved by the RAKE receiver [22]. Two joint estimators are studied. The first follows the Bayesian approach and can be used when certain prior statistical knowledge about the channel is available. The second follows the maximum likelihood approach when these channel properties are not available. For practical implementation, both estimators employ two stages for searching the periodogram peak, the FFT-based coarse search and dichotomous fine search. Without increasing the complexity, these estimators outperform the correlation-based algorithms and possess a wide frequency acquisition range.

Extensive simulation for different conditions is used to investigate the performance of the joint estimators in Rayleigh fading channels. The simulation results show high-accuracy performance of these estimators over a wide range of SNR and f_0T_s with an estimation error very close to the CRLB.

This chapter is organised as follows. Section 4.2 describes the signal and channel models. In Section 4.3, the Bayesian joint estimators are presented and in Section 4.4, the maximum likelihood joint estimators are presented. The Cramer-Rao Lower Bounds (CRLB)s are discussed for the different estimators in Section 4.5. Section 4.6 describes the efficient dichotomous-based implementation. Simulation results and performance analysis are given in Section 4.7, and Section 4.8 concludes the chapter.

4.2 Signal and Channel Models

It is assumed for the scenarios discussed in this chapter that the considered signal is a known (pilot) single transmitted through a time-invariant frequency-selective channel and corrupted with complex AWGN. In the time-invariant channel, the channel parameters required to be estimated can be assumed constant over the observation interval. For such a situation, and after frequency downconverting the received waveform, filtering in

a matched filter and sampling at proper times, the baseband discrete signal and channel models can be represented as [22]

$$r(nT_s) = A(nT_s)e^{j2\pi f_0 T_s n} + z(nT_s)\,; \qquad n = 0, 1, \ldots, N-1\,, \tag{4.1a}$$

$$A(nT_s) = \sum_{m=1}^{M} a_m \varphi_m(nT_s)\,, \qquad \varphi_m(nT_s) = s(nT_s - \tau_m)\,, \tag{4.1b}$$

where

N is the number of the received samples and n is the sample index;

M is the number of paths and m is the path index;

$r(nT_s)$ is the received nth sample;

$A(nT_s)$ is the complex-valued envelope nth sample;

f_0 is the unknown frequency offset to be estimated;

T_s is the symbol interval;

$f_0 T_s$ is the normalised frequency offset;

$z(nT_s)$ is the complex-valued AWGN nth sample with zero mean and variance σ^2;

a_m is the unknown complex-valued mth path amplitude (channel parameter) to be estimated;

$\varphi_m(nT_s)$ is the multipath (delayed) (n, m)th element (basis function) of the transmitted signal;

$s(nT_s)$ is the transmitted nth pilot symbol;

τ_m is the mth path delay.

It is helpful to arrange the received signal in matrix form as

$$\mathbf{r} = \mathbf{\Omega}_{f_0 T_s}\mathbf{a} + \mathbf{z}\,; \qquad \mathbf{\Omega}_{f_0 T_s} = \mathbf{\Lambda}_{f_0 T_s}\mathbf{\Phi}\,, \tag{4.2}$$

where

$\mathbf{r}$ is $N \times 1$ column vector with elements $r(nT_s)$ and $n = 0, 1, \ldots, N-1$;

$\mathbf{\Omega}_{f_0 T_s}$ is $N \times M$ matrix with elements $[\mathbf{\Omega}_{f_0 T_s}]_{nm} = \varphi_m(nT_s)e^{j2\pi f_0 T_s n}$;

$\mathbf{\Lambda}_{f_0 T_s}$ is $N \times N$ diagonal matrix with diagonal elements $e^{j2\pi f_0 T_s n}$;

$\mathbf{\Phi}$ is $N \times M$ basis function matrix with elements $[\mathbf{\Phi}]_{nm} = \varphi_m(nT_s)$;

$\mathbf{a}$ is $M \times 1$ column vector of the channel parameters with elements a_m;

$\mathbf{z}$ is $N \times 1$ column vector of the AWGN with covariance matrix $\mathbf{R}_z = \sigma^2\mathbf{I}_N$ and elements $z(nT_s)$;

$\mathbf{I}_N$ is $N \times N$ identity matrix.

In this case, the task is to estimate the path amplitudes $\{a_m\}_{m=1}^{M}$ that hereafter will be denoted as the channel parameters in addition to the frequency offset f_0T_s. For time-invariant channels, the channel parameters are complex-valued random parameters, but with unchanging values during one observation interval, and f_0T_s is an unknown deterministic parameter.

4.3 Bayesian Joint Estimation

The Bayesian joint estimator as the name implies is derived based on the Bayesian approach in which the parameters $\{a_m\}_{m=1}^{M}$ are assumed to be random variables whose particular realizations are to be estimated [121]. In this case, the joint estimator requires given prior probability density function (PDF) of $\mathbf{a}$, and the received signal has a conditional PDF of [48, 121]

$$p\left(\mathbf{r}|f_0T_s,\mathbf{a}\right)=\frac{1}{\pi^N\sigma^{2N}}\exp\left[-\frac{1}{\sigma^2}\left(\mathbf{r}-\mathbf{\Omega}_{f_0T_s}\mathbf{a}\right)^H\left(\mathbf{r}-\mathbf{\Omega}_{f_0T_s}\mathbf{a}\right)\right]. \tag{4.3}$$

In this section, the channel is assumed to be Rayleigh channel, and so the random channel parameter vector $\mathbf{a}$ has to be zero-mean Gaussian random with normal complex distribution and its prior PDF is

$$p(\mathbf{a})=\frac{1}{\pi^M\left|\mathbf{R}_a\right|}\exp\left[-\mathbf{a}^H\mathbf{R}_a^{-1}\mathbf{a}\right], \tag{4.4}$$

where $\mathbf{R}_a$ is the covariance matrix which is assumed to be known.

4.3.1 Frequency Offset Estimator

The frequency offset f_0T_s is estimated using the same technique as described in [48]. In this case, the channel parameters $\{a_m\}_{m=1}^{M}$ are considered nuisance parameters that can be integrated out of the conditional PDF $p(\mathbf{r}|f_0T_s,\mathbf{a})$ through a Bayesian approach [121]. This is expressed as [48]

$$p\left(\mathbf{r}|f_0T_s\right)=\int p\left(\mathbf{r}|f_0T_s,\mathbf{a}\right)p(\mathbf{a})d\Re\{\mathbf{a}\}d\Im\{\mathbf{a}\}, \tag{4.5}$$

where $\Re\{\cdot\}$ and $\Im\{\cdot\}$ denote the real and imaginary components of a complex function, respectively. In this case, the frequency offset estimator is obtained by maximising the likelihood function $p\left(\mathbf{r}|fT_s\right)$ over the frequency acquisition range as [48, 121]

$$\widehat{f_0T_s}_B = \arg\max_{fT_s\in\Psi}\left\{p\left(\mathbf{r}|fT_s\right)\right\}. \tag{4.6}$$

The likelihood function $p\left(\mathbf{r}|fT_s\right)$ is obtained by solving the integration in (4.5) which gives [48]

$$p\left(\mathbf{r}|fT_s\right) = \frac{e^{-\sigma^{-2}\mathbf{r}^H\mathbf{r}}}{\pi^N\sigma^{2N}}\int\exp\left[2\Re\left\{\sigma^{-2}\mathbf{a}^H\mathbf{W}_{fT_s}\right\} - \sigma^{-2}\mathbf{a}^H\mathbf{\Gamma}\mathbf{a}\right]p(\mathbf{a})d\Re\{\mathbf{a}\}d\Im\{\mathbf{a}\}, \tag{4.7}$$

where

$$\mathbf{\Gamma} = \mathbf{\Phi}^H\mathbf{\Phi} \tag{4.8}$$

is an $M\times M$ correlation matrix [128] of the basis functions with elements

$$\gamma_{u\,v} = \sum_{n=0}^{N-1}\varphi_u^*(nT_s)\varphi_v(nT_s); \qquad u,\,v = 1,\ldots,M, \tag{4.9}$$

and

$$\mathbf{W}_{fT_s} = \mathbf{\Phi}^H\mathbf{\Lambda}_{fT_s}^H\mathbf{r}, \tag{4.10}$$

which can be obtained by

$$W_{fT_s}(m) = \mathcal{FFT}\left\{r(nT_s)\varphi_m^*(nT_s), N_{FFT}\right\}; \qquad m = 1,\ldots,M. \tag{4.11}$$

The PDF in (4.7) as solved in [48] yields

$$p\left(\mathbf{r}|fT_s\right) = \frac{\exp\left[-\sigma^{-2}\mathbf{r}^H\mathbf{r}\right]}{\pi^N\sigma^{2N}\left|\sigma^{-2}\mathbf{R}_a\mathbf{\Gamma}+\mathbf{I}_M\right|}\exp\left[\sigma^{-2}Y_{fT_s}\right], \tag{4.12}$$

where

$$Y_{fT_s} = \mathbf{W}_{fT_s}^H\left(\mathbf{\Gamma}+\sigma^2\mathbf{R}_a^{-1}\right)^{-1}\mathbf{W}_{fT_s} \tag{4.13}$$

and $\mathbf{I}_M$ is the $M\times M$ identity matrix. Now, substituting (4.12) into (4.6) produces

$$\widehat{f_0T_s}_B = \arg\max_{fT_s\in\Psi}\left\{\frac{\exp\left[-\sigma^{-2}\mathbf{r}^H\mathbf{r}\right]}{\pi^N\sigma^{2N}\left|\sigma^{-2}\mathbf{R}_a\mathbf{\Gamma}+\mathbf{I}_M\right|}\exp\left[\sigma^{-2}Y_{fT_s}\right]\right\}. \tag{4.14}$$

Excluding the frequency-independent first factor inside the brackets, and taking the natural logarithm, the Bayesian frequency offset (BF) estimator becomes [48]

$$\widehat{f_0T_s}_B = \arg\max_{fT_s\in\Psi}\left\{Y_{fT_s}\right\} = \arg\max_{fT_s\in\Psi}\left\{\mathbf{W}_{fT_s}^H\left(\mathbf{\Gamma}+\sigma^2\mathbf{R}_a^{-1}\right)^{-1}\mathbf{W}_{fT_s}\right\}, \tag{4.15}$$

where Y_{fT_s} is therefore a generalised periodogram [44] that exploits the multipath diversity by combining the periodograms of the multipath elements.

4.3.2 Channel Estimator

The channel parameters are then jointly estimated exploiting the estimated value of the frequency offset. Now, after obtaining $\widehat{f_0 T_s}_B$ and replacing its value in (4.2), this model becomes linear and can be reformed as

$$\mathbf{r} = \mathbf{\Omega}_{\widehat{f_0 T_s}_B} \mathbf{a} + \mathbf{z}\,, \tag{4.16}$$

where $\mathbf{\Omega}_{\widehat{f_0 T_s}_B}$ is now a known $N \times M$ matrix. This model is the well-known Bayesian general linear model, and the Bayesian channel parameter (BC) estimator is the MMSE estimator given by [121]

$$\hat{\mathbf{a}}_B = \left(\mathbf{\Omega}^H_{\widehat{f_0 T_s}_B} \mathbf{\Omega}_{\widehat{f_0 T_s}_B} + \sigma^2 \mathbf{R}_a^{-1} \right)^{-1} \mathbf{\Omega}^H_{\widehat{f_0 T_s}_B} \mathbf{r}\,. \tag{4.17}$$

Considering (4.8) and (4.10), the BC estimator becomes

$$\hat{\mathbf{a}}_B = \left(\mathbf{\Gamma} + \sigma^2 \mathbf{R}_a^{-1} \right)^{-1} \mathbf{W}_{\widehat{f_0 T_s}_B}\,. \tag{4.18}$$

4.4 Maximum Likelihood Joint Estimation

In Section 4.3, the channel is considered to have Rayleigh fading with a known covariance matrix $\mathbf{R}_a$, and complex AWGN with a known variance σ^2. As can be seen in (4.15) and (4.18), these prior statistical specifications are included in the derived Bayesian joint estimator. However, when dealing with different scenarios where there is no certainty about these statistical properties of the channel and the AWGN, a maximum likelihood joint estimator can be used. For the ML approach, the parameters $\mathbf{a}$ are assumed to be deterministic but unknown parameters which are required to be estimated. In this case, the received signal has an unconditional PDF of [121]

$$p\left(\mathbf{r}; f_0 T_s, \mathbf{a}\right) = \frac{1}{\pi^N \sigma^{2N}} \exp\left[-\frac{1}{\sigma^2} \left(\mathbf{r} - \mathbf{\Omega}_{f_0 T_s} \mathbf{a} \right)^H \left(\mathbf{r} - \mathbf{\Omega}_{f_0 T_s} \mathbf{a} \right) \right]. \tag{4.19}$$

4.4.1 Frequency Offset Estimator

The frequency offset $f_0 T_s$ is estimated using the same technique described in [44]. The ML estimator produces the values of the required parameters that maximise the likelihood

function or minimise the function [121]

$$J(fT_s, \mathbf{a}) = (\mathbf{r} - \mathbf{\Omega}_{fT_s}\mathbf{a})^H(\mathbf{r} - \mathbf{\Omega}_{fT_s}\mathbf{a})\,. \tag{4.20}$$

It is easier first to differentiate $J(fT_s, \mathbf{a})$ with respect to $\mathbf{a}$, which produces [121], [44]

$$\frac{\partial J(fT_s, \mathbf{a})}{\partial \mathbf{a}} = -\left[\mathbf{\Omega}_{fT_s}^H(\mathbf{r} - \mathbf{\Omega}_{fT_s}\mathbf{a})\right]^*\,. \tag{4.21}$$

Now setting it equal to zero yields the ML estimator of $\mathbf{a}$ for a certain fT_s as [121], [44]

$$\hat{\mathbf{a}} = \left(\mathbf{\Omega}_{fT_s}^H\mathbf{\Omega}_{fT_s}\right)^{-1}\mathbf{\Omega}_{fT_s}^H\mathbf{r}\,. \tag{4.22}$$

Substituting this into (4.20) yields [44]

$$J(fT_s, \hat{\mathbf{a}}) = \mathbf{r}^H\mathbf{r} - \mathbf{r}^H\mathbf{\Omega}_{fT_s}\left(\mathbf{\Omega}_{fT_s}^H\mathbf{\Omega}_{fT_s}\right)^{-1}\mathbf{\Omega}_{fT_s}^H\mathbf{r}\,, \tag{4.23}$$

which is minimised by maximising

$$Y_{fT_s} = \mathbf{r}^H\mathbf{\Omega}_{fT_s}\left(\mathbf{\Phi}^H\mathbf{\Phi}\right)^{-1}\mathbf{\Omega}_{fT_s}^H\mathbf{r} \tag{4.24}$$

over the frequency acquisition range. Hence, and recalling $\mathbf{\Gamma}$ and $\mathbf{W}_{fT_s}$ from (4.8) and (4.10), it follows that the ML frequency offset (MLF) estimator is [44]

$$\widehat{f_0T_s}_{ML} = \arg\max_{fT_s\in\Psi}\left\{\mathbf{W}_{fT_s}^H\mathbf{\Gamma}^{-1}\mathbf{W}_{fT_s}\right\}\,. \tag{4.25}$$

4.4.2 Channel Estimator

After getting the estimated value of the frequency offset $\widehat{f_0T_s}_{ML}$, the channel parameters can then be jointly estimated. Substituting $\widehat{f_0T_s}_{ML}$ from (4.25) into (4.22), the ML channel parameter (MLC) estimator is [44]

$$\hat{\mathbf{a}}_{ML} = \mathbf{\Gamma}^{-1}\mathbf{W}_{\widehat{f_0T_s}_{ML}}\,. \tag{4.26}$$

4.5 Cramer-Rao Lower Bound

The variance of any unbiased estimator must be greater than or equal to the CRLB [121]. For unbiased frequency offset estimators operating on the scenarios considered in this

chapter, the CRLB of the estimated frequency offset (CRLBF) has been derived by Baronkin *et al.* [48] and is given by

$$\sigma_{CR_{f_0T_s}} = \sqrt{\frac{\mathrm{tr}\left\{\mathbf{\Gamma R}_a\right\}}{8\pi^2 N\rho \mathrm{tr}\left\{\mathbf{CR}_a\right\}}} = \sqrt{\frac{\sigma^2}{8\pi^2 \mathrm{tr}\left\{\mathbf{CR}_a\right\}}}\,, \tag{4.27}$$

where ρ is the SNR that is defined as

$$\begin{aligned}\rho &= \frac{\mathrm{E}\left\{\left(\mathbf{\Omega}_{f_0T_s}\mathbf{a}\right)^H\left(\mathbf{\Omega}_{f_0T_s}\mathbf{a}\right)\right\}}{\mathrm{E}\left\{\mathbf{z}^H\mathbf{z}\right\}} = \frac{\mathrm{E}\left\{\mathbf{a}^H\mathbf{\Phi}^H\mathbf{\Lambda}^H_{f_0T_s}\mathbf{\Lambda}_{f_0T_s}\mathbf{\Phi a}\right\}}{N\sigma^2} \\ &= \frac{\mathrm{E}\left\{\mathbf{a}^H\mathbf{\Gamma a}\right\}}{N\sigma^2} = \frac{\mathrm{tr}\left\{\mathbf{\Gamma R}_a\right\}}{N\sigma^2}\,,\end{aligned} \tag{4.28}$$

and

$$\mathbf{C} = \mathbf{\Phi}^H\mathbf{T}\left[\mathbf{I}_N - \mathbf{\Phi\Gamma}^{-1}\mathbf{\Phi}^H\right]\mathbf{T\Phi}\,; \quad \mathbf{T} = \mathrm{diag}\{n\}\,, \quad n = 0, 1, \ldots, N-1\,. \tag{4.29}$$

For the estimators of the channel parameters, the vector CRLB representing the minimum variances of the M elements of $\{\hat{a}_m\}_{m=1}^M$ based on the Bayesian and the maximum likelihood approaches, respectively, are given by the diagonal elements of the covariance matrices [121]

$$\mathbf{R}_{\hat{\mathbf{a}}B} = \left(\sigma^{-2}\mathbf{\Gamma} + \mathbf{R}_a^{-1}\right)^{-1}\,, \tag{4.30}$$

$$\mathbf{R}_{\hat{\mathbf{a}}ML} = \sigma^2\mathbf{\Gamma}^{-1}\,. \tag{4.31}$$

The average CRLBs of the Bayesian estimated channel parameters ($\mathrm{CRLBC_B}$) and the ML estimated channel parameters ($\mathrm{CRLBC_{ML}}$) are hence given by

$$\sigma_{CR_{aB}} = \sqrt{\frac{\mathrm{tr}\left\{\left(\sigma^{-2}\mathbf{\Gamma} + \mathbf{R}_a^{-1}\right)^{-1}\right\}}{\mathrm{tr}\{\mathbf{R}_a\}}}\,, \tag{4.32}$$

$$\sigma_{CR_{aML}} = \sqrt{\frac{\sigma^2\mathrm{tr}\left\{\mathbf{\Gamma}^{-1}\right\}}{\mathrm{tr}\{\mathbf{R}_a\}}}\,. \tag{4.33}$$

These CRLBs will be used in the simulation-based analysis of the considered estimators for multipath slow fading Rayleigh channels to provide a reference level against which the performance of these estimators can be compared.

4.6 Efficient Dichotomous-Based Implementation

A considerable reduction in the complexity, and without deterioration in the accuracy can be obtained using the dichotomous search frequency estimator. This technique has been proposed in [17] and studied in Section 3.5.2 for AWGN channels. For time-invariant frequency-selective channels, the DS frequency estimation algorithm has been presented in [44, 48]. It consists of two stages of FFT-based coarse search and dichotomous fine search and its implementation for the joint channel and frequency offset estimation based on the Bayesian and the maximum likelihood approaches is described hereafter to follow.

For practical simulation of the dichotomous search technique and according to the proposed joint estimators in (4.15), (4.18), (4.25) and (4.26), the best way for implementation is as follows. First, the $M \times M$ known deterministic matrix $\mathbf{G}$ is precomputed as

$$\mathbf{G} = \begin{cases} \left(\mathbf{\Phi}^H \mathbf{\Phi} + \sigma^2 \mathbf{R}_a^{-1}\right)^{-1} , & \text{Bayesian approach} , \\ \left(\mathbf{\Phi}^H \mathbf{\Phi}\right)^{-1} , & \text{ML approach} . \end{cases} \tag{4.34}$$

Next, the following FFTs are calculated

$$W_{fT_s}(m) = \mathcal{FFT}\{r(nT_s)\varphi_m^*(nT_s), N_{FFT}\} ; \quad m = 1, \ldots, M , \tag{4.35}$$

where $N_{FFT} \approx 4N$ [44,48,124]. Then, the generalised periodogram samples are obtained over a grid of frequencies separated by $\Delta f T_s = 1/N_{FFT}$ and covering the frequency acquisition range as

$$Y_{fT_s} = \sum_{u=1}^{M} \sum_{v=1}^{M} [\mathbf{G}]_{u\,v}\, W_{fT_s}^*(u) W_{fT_s}(v) , \tag{4.36}$$

and the initial coarse-search frequency estimate is

$$f_p T_s = \arg \max_{fT_s \in \Psi} \{Y_{fT_s}\} , \tag{4.37}$$

which is passed to the fine search together with the periodogram peak $Y_2 = Y_{f_p T_s}$ and its two adjacent samples $Y_1 = Y_{f_{p-1} T_s}$ and $Y_3 = Y_{f_{p+1} T_s}$.

In the fine search stage, the initial frequency estimate $f_p T_s$ is refined exploiting Q dichotomous iterations of DFT-based three-point interpolation of Y_1, Y_2 and Y_3. Each iteration repeats the following steps [17]:

- $\Delta f T_s = \Delta f T_s / 2$.
- If $Y_3 < Y_1$ then $Y_3 = Y_2$ and $f_p T_s = f_p T_s - \Delta f T_s$, else $Y_1 = Y_2$ and $f_p T_s = f_p T_s + \Delta f T_s$.
- $W_{f_p T_s}(m) = \sum_{n=0}^{N-1} r(nT_s) \varphi_m^*(nT_s) e^{-j2\pi f_p T_s n}$, where $m = 1, \ldots, M$.
- $Y_2 = \sum_{u=1}^{M} \sum_{v=1}^{M} [\mathbf{G}]_{u\,v} W_{f_p T_s}^*(u) W_{f_p T_s}(v)$.

At the end of all iterations, the frequency offset estimator is $\widehat{f_0 T_s} = f_p T_s$. For optimum performance, the number of iterations Q should be high enough so that the final frequency step in the fine search gets below the minimum value of the frequency CRLB ($\sigma_{CR_{f_0 T_s \min}}$) in the SNR range of interest. Accordingly, Q has to satisfy (3.50).

Finally, the values of $\left\{W_{f_p T_s}(m)\right\}_{m=1}^{M}$ from the last iteration are used to estimate the $M \times 1$ column vector of the channel parameters as

$$\hat{\mathbf{a}} = \mathbf{G}\mathbf{W}_{f_p T_s} . \tag{4.38}$$

4.7 Simulation Results and Performance Analysis

A binary sequence transmitted through a time-invariant frequency-selective Rayleigh channel and corrupted with a complex AWGN is implemented according to (4.1). The performance of the dichotomous search joint Bayesian and ML estimators is investigated and compared against the reference CRLBs over an SNR range up to 30 dB, which is considered below in the simulation according to (4.28) as $\rho = \text{tr}\left\{\mathbf{\Gamma R}_a\right\} / N\sigma^2$.

Computer simulations are used to estimate the square root of the mean square error (RMSE) of the frequency offset $f_0 T_s$ and the channel parameters $\{a_m\}_{m=1}^{M}$ estimates,

respectively, as

$$f_0T_s\text{-RMSE} = \sqrt{\frac{1}{N_t}\sum_{t=1}^{N_t}\left(f_0T_s - \widehat{f_0T_s}_t\right)^2}, \tag{4.39a}$$

$$\mathbf{a}\text{-RMSE} = \sqrt{\frac{1}{N_t}\sum_{t=1}^{N_t}\frac{\sum_{m=1}^{M}\left|a_m - \hat{a}_{m_t}\right|^2}{\sum_{m=1}^{M}|a_m|^2}}, \tag{4.39b}$$

over a number of $N_t = 10\,000$ simulation trials, where $\widehat{f_0T_s}_t$ and $\hat{a}_{m_t}$ are the estimated frequency offset and the mth channel parameter, respectively, in the tth simulation trial. The following parameters are used for the simulations: the length of the pilot symbols is $N_p = 63$, the size of the FFT used in the coarse search stage of the dichotomous estimator is $N_{FFT} = 256$, and the number of iterations used in the fine search stage is $Q = 8$. Regular path delays are considered with $\tau_m = (m-1)T_s$, where $m = 1, \ldots, M$. However, to explore the performance difference between the Bayesian and maximum likelihood approaches, a delay uncertainty of $M = 18$ is assumed. In this case, uncorrelated zero-mean Gaussian channel parameters are generated for each trial with variances

$$\sigma_m^2 = \begin{cases} 1\,, & m = 1, \ldots, M_r\,, \\ 10^{-7}\,, & m = M_r + 1, \ldots, M\,, \end{cases} \tag{4.40}$$

where M_r is the number of real paths that is considered to be $M_r = 1,\ 2,\ 4$, or 9. The size of the observed received signal block is $N = N_p + M - 1 = 80$.

Estimation of the Frequency Offset: Figure 4.1 shows the f_0T_s-RMSE, as a function of SNR in (a) and as a function of f_0T_s in (b), for the Bayesian and ML frequency offset estimators compared to the CRLB for $M_r = 9$. In Figure 4.1(a), the f_0T_s-RMSE of the estimators versus SNR is presented for $f_0T_s = 0.01$. The Bayesian estimator as can be seen exhibits a high-accuracy performance with an estimation error attaining the CRLB throughout the investigated SNR range above $\text{SNR}_{\text{th}} \approx 1$ dB. For the ML estimator, the f_0T_s-RMSE is very close to the CRLB for a wide range of SNR, with a slightly higher level than that for the Bayesian estimator. However, the threshold SNR ($\text{SNR}_{\text{th}} \approx 3$ dB) is about 2 dB higher than that of the B estimator. This small difference is expected and corresponds to the absence of the prior channel statistics in the ML approach. Most

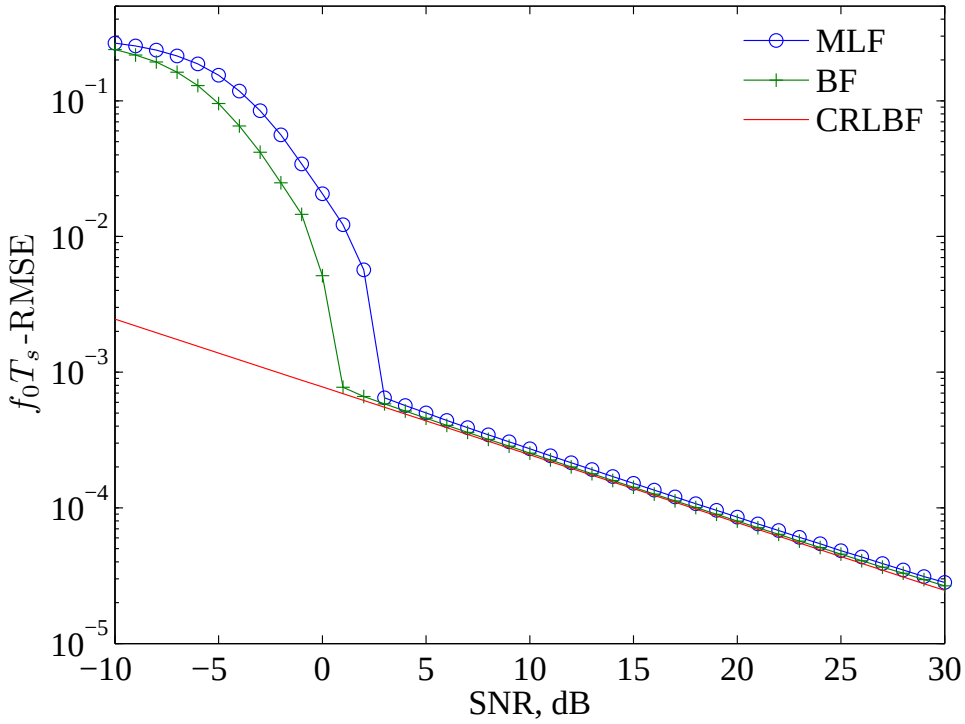

(a)

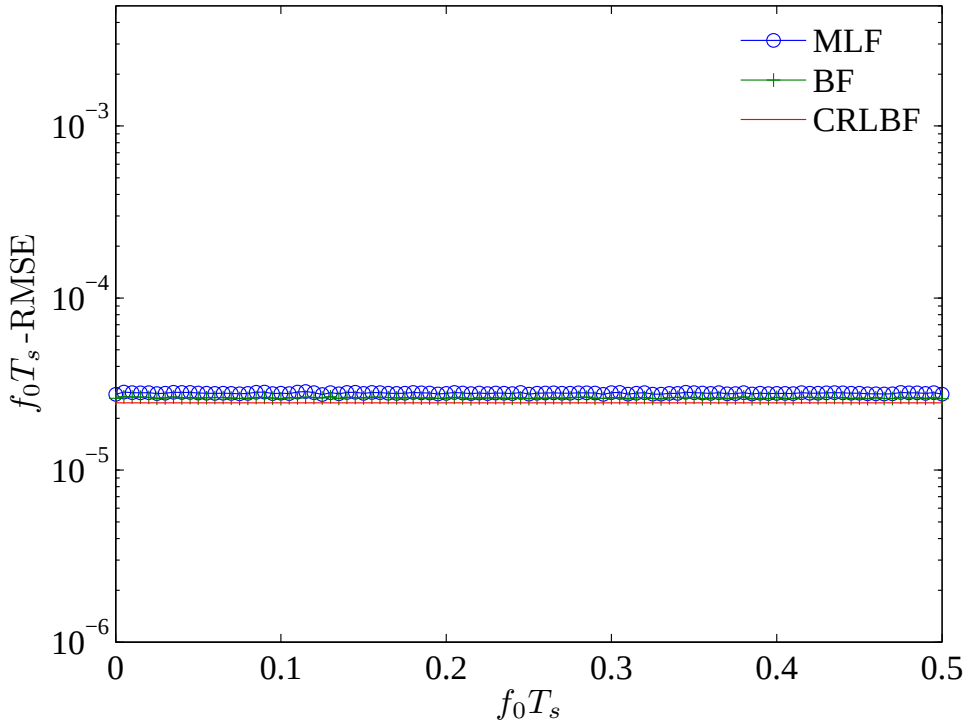

(b)

Figure 4.1: f_0T_s-RMSE of the frequency offset estimators for time-invariant frequency-selective channels; $N_p = 63$, $f_0T_s = 0.01$, $M = 18$, $M_r = 9$, $N_{FFT} = 256$ and $Q = 8$; (a) SNR-dependent performance for $f_0T_s = 0.01$ and (b) f_0T_s-dependent performance for SNR $= 30$ dB.

importantly, this is due to the lack of the path delay knowledge. Figure 4.1(b) shows the f_0T_s-RMSE of the estimators versus f_0T_s for SNR $= 30$ dB. It can be noticed that the high-accuracy performance of both estimators is independent of f_0T_s. This shows that both estimators possess a wide frequency acquisition range.

Estimation of the Channel Parameters: Figure 4.2 shows simulation results concerning the channel parameter estimation error compared to the CRLB for the same scenario. Figure 4.2(a) illustrates the SNR-dependent performance for $f_0T_s = 0.01$. It can be noticed that the Bayesian estimator outperforms the ML estimator, which is also reflected through the level difference between the two CRLBs. This is due to the use of the prior information of $\mathbf{R}_a$ and σ^2 that characterises the Bayesian approach. However, both estimators exhibit a high-accuracy performance with an $\mathbf{a}$-RMSE being very close to the CRLB throughout the SNR range of interest. In Figure 4.2(b), the $\mathbf{a}$-RMSE of the estimators as a function of f_0T_s is shown for SNR $= 30$ dB. The $\mathbf{a}$-RMSE is constant and very close to the CRLB for both estimators over all the wide frequency acquisition range.

SNR-Dependent Performance for Different M_r: Simulation results shown in Figure 4.3 analyse the performance of the frequency offset estimators, Bayesian in (a) and ML in (b), with respect to the number of real paths M_r compared to the CRLB and for $f_0T_s = 0.01$. For both estimators, a relatively poor performance can be noticed for the single-path channel ($M_r = 1$), where the f_0T_s-RMSE does not attain the CRLB even for the high SNR range. An initial increase of the number of real paths to $M_r = 2$ is shown to lead to a substantial improvement of the accuracy, where the f_0T_s-RMSE attains the CRLB for high SNR range. A further increase of M_r allows an additional accuracy improvement, but this improvement is not as significant as in the initial case. For example, increasing the real paths for the Bayesian estimator from $M_r = 4$ to $M_r = 9$ is shown in Figure 4.3(a) to result in a decrease of the SNR_{th} by only 3 dB compared to the 12 dB reduction caused by the initial increase of the real paths to $M_r = 2$. This phenomenon is similar to that encountered in the RAKE receivers, where the diversity reception in fading channels leads to an improvement in the bit error rate performance [22]. It can be seen in Figure 4.3 that the SNR_{th}s corresponding to different M_r values for the ML estimator are higher in general than those for the Bayesian estimator. This is the penalty for the

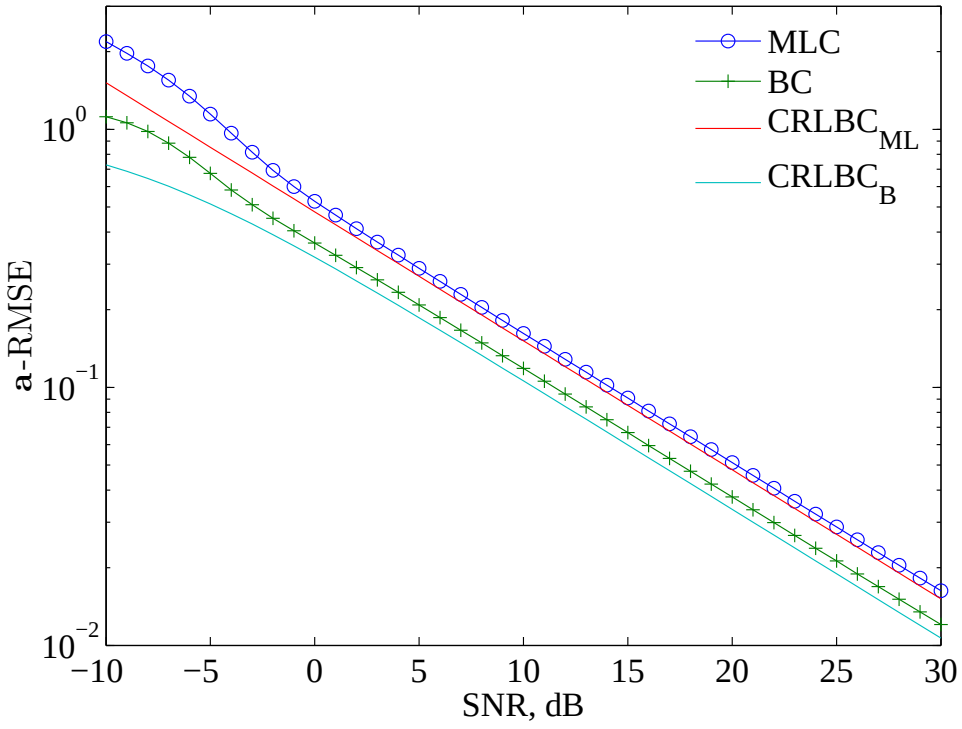

(a)

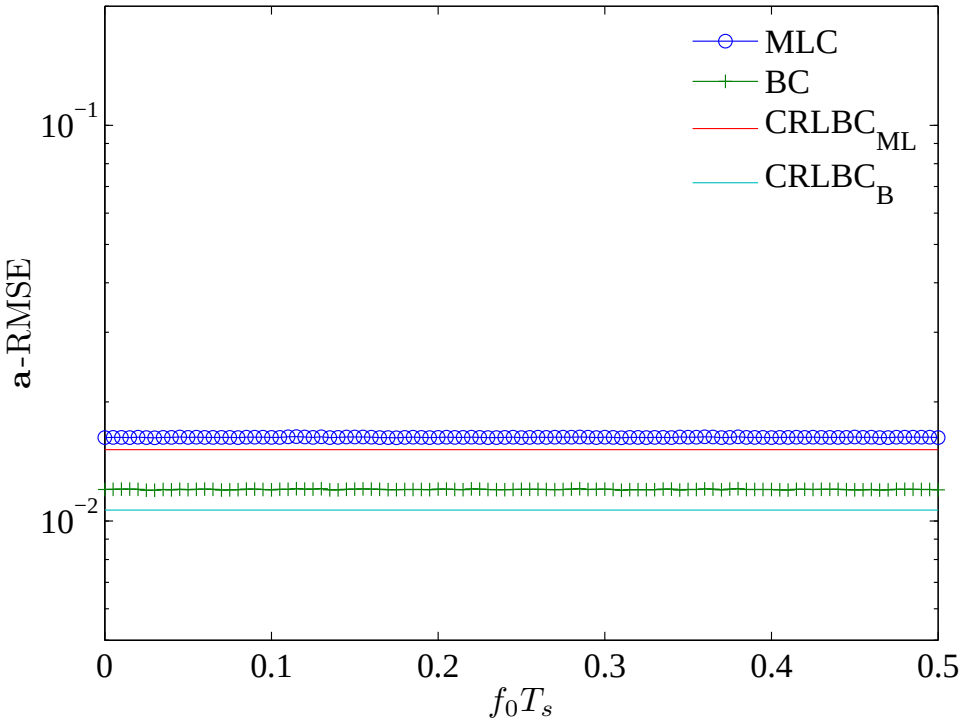

(b)

Figure 4.2: $\mathbf{a}$-RMSE of the channel parameter estimators for time-invariant frequency-selective channels; $N_p = 63$, $f_0T_s = 0.01$, $M = 18$, $M_r = 9$, $N_{FFT} = 256$ and $Q = 8$; (a) SNR-dependent performance for $f_0T_s = 0.01$ and (b) f_0T_s-dependent performance for SNR $= 30$ dB.

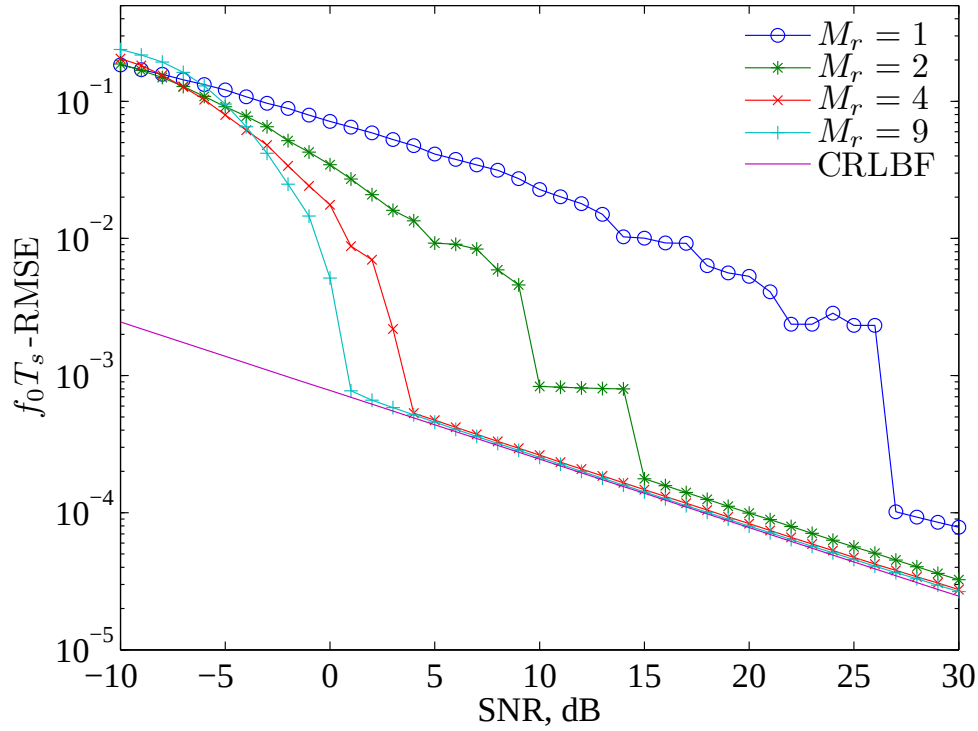

(a)

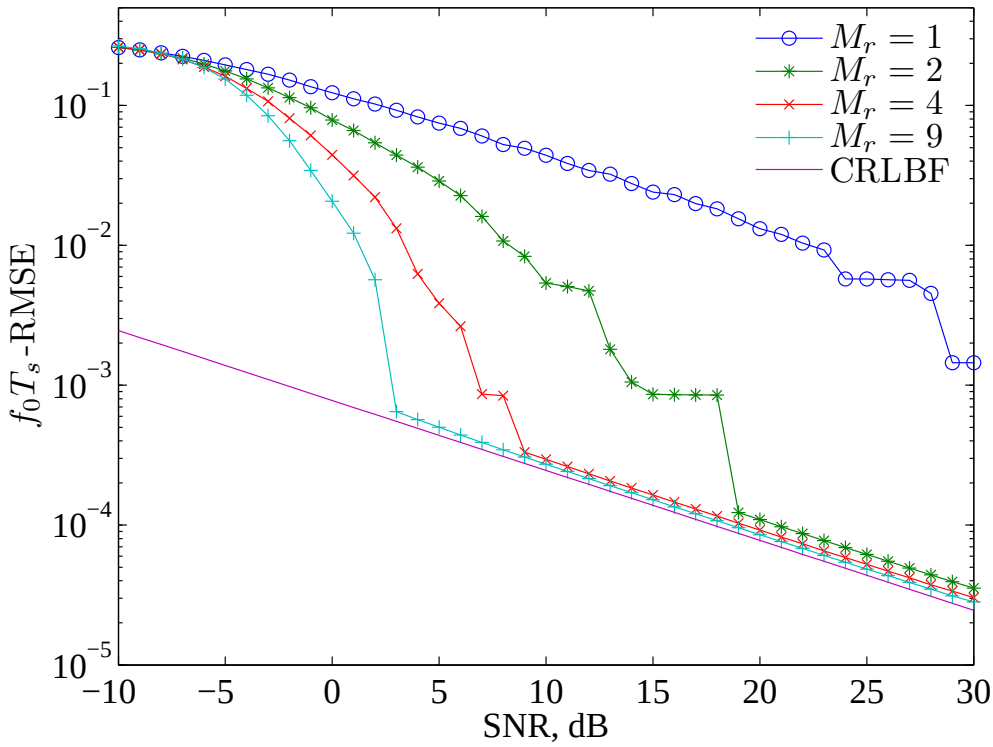

(b)

Figure 4.3: f_0T_s-RMSE of the frequency offset estimators for time-invariant frequency-selective channels for different numbers of real paths; $N_p = 63$, $f_0T_s = 0.01$, $M = 18$, $N_{FFT} = 256$ and $Q = 8$; (a) Bayesian estimator and (b) ML estimator.

capability to operate in the absence of timing information.

4.8 Conclusions

In this chapter, the joint data-aided estimation of the channel and frequency offset has been studied for signals propagated through time-invariant frequency-selective channels. The considered frequency offset estimators exploit the multipath diversity by combining the periodograms of the multipath elements and searching for the maximum of the combined statistic. The CRLBs have been presented for these estimators.

Two joint estimators have been studied. The first joint estimator depends on the Bayesian approach and can provide a high-accuracy performance whenever prior statistical characteristics of the channel are known, namely the mean and covariance matrices of the channel parameters and the variance of the AWGN. The second estimator, with a slightly higher estimation error, is an alternative joint estimator that can operate when these characteristics are unavailable. To reduce the complexity of the frequency offset estimators and attain a high accuracy, the estimators exploit a two stage technique for searching the periodogram peak, an FFT-based coarse search and a dichotomous fine search.

These estimators have been extensively investigated for many different application scenarios in Rayleigh fading channels. The simulation results have demonstrated high-accuracy performance of these estimators with an estimation error very close to the CRLB over a wide range of SNR and throughout the wide frequency acquisition range.

Chapter 5

Joint Estimation of Channel and Frequency Offset in Frequency-Flat Time-Variant Fading Channels

Contents

In this chapter, new joint data-aided channel and frequency offset estimators are proposed for frequency-flat time-variant fading channels. The proposed estimators are based on the basis expansion model of the fading process and the dichotomous search frequency estimation technique. The first estimator relies on the Bayesian approach and

exploits prior channel statistics to provide a high performance. The second estimator follows the maximum likelihood approach, and with a slightly lower accuracy, can operate when the prior statistics are unknown. The performance of the proposed joint estimators is examined for different scenarios in Rayleigh fading channels. The sensitivity of the Bayesian estimator is investigated using such BEMs as Karhunen-Loève (KL), discrete prolate spheroidal (DPS), generalized complex exponential (GCE), and B-spline (BS) functions to the knowledge of the Doppler frequency.

5.1 Introduction

Efficient channel and frequency offset estimation is a crucial task in wireless communication systems, where reliable transmission at high data rates is required. Transmitting pilot symbols is a practical method used to provide the receiver with the required information about the channel [1, 2]. For time-invariant (TI) channels, the pilot symbols can be sent in a burst mode as preambles, postambles, or midambles. However, for time-variant channels, pilot symbols are usually inserted periodically within the data block in a process known as pilot symbol aided modulation (PSAM) [3, 4] to keep up with the channel variations.

The joint channel and frequency offset estimation becomes challenging when dealing with time-variant channels, where in addition to the additive noise, the transmitted signal is corrupted with a random multiplicative distortion [23]. This makes the channel and frequency offset estimation complicated, and so, traditional techniques have dealt separately with these two problems.

Various frequency offset estimators for frequency-flat time-variant fading channels have been proposed in the literature. However most of these estimators are correlation-based [7, 8, 10, 11, 34, 35], and so, their performance is inferior to that of the optimal maximum likelihood (ML) estimator and/or they possess a limited frequency acquisition range. The estimator in [34] is based on weighted linear regression for the phase of the sample correlation function, however the covariance matrix of the phase estimation is assumed to be known. In [35], a modification was presented to allow the operability in a

wider acquisition range, and in this case the covariance matrix is estimated. However, an assumption was made regarding the form of the fading correlation. No such assumption was made in [8], where two estimators were proposed. The first is based on unweighted version of the method of [35] and the second is based on a nonlinear least-squares (NLS) approach. Similar NLS technique was derived in [10] based on the multiple lags correlation function.

Several channel estimators for frequency-flat time-variant channels were proposed in [4, 36–42] and the basis expansion model (BEM) has been efficiently used for the channel estimation [36, 38–43]. However, these estimators yield a severe degradation in the performance at the presence of a frequency offset. This problem can be resolved using joint channel and frequency offset estimation, which to the best of our knowledge, has not been well addressed in the literature and the main aim here is to fill that gap. The joint channel and frequency offset estimation would allow a higher accuracy performance, compared to the techniques dealing separately with these two problems.

We focus on estimating the channel which contains both, the multiplicative distortion and frequency offset. This channel is all what the receiver needs in practical applications, where there is no need for spending much complexity on explicit estimators for its individual components.

The goal of this chapter is twofold. Firstly, we propose interpolation-based practical frequency offset estimators based on the dichotomous search technique, involving two stage [13] search of the generalised periodogram peak [44], a fast Fourier transform (FFT)-based coarse search [45] and dichotomous fine search [17], which achieve superior performance compared to that of the correlation-based estimators, and possess a wide frequency acquisition range. Secondly, we propose algorithms that estimate the channel jointly with the frequency offset. The estimation is based on approximating the time-variant fading process by a BEM and employ the dichotomous search frequency estimation technique. The use of BEMs leads to a mathematical model that offers a simple (reduced dimensionality) processing in addition to a high-accuracy performance over the wide frequency offset range. The novel joint estimators are derived based on two approaches. The first is the Bayesian approach and can be used when certain prior statistical knowledge about the channel is available. The other is the ML approach and is applicable

when the channel statistics are not available.

Simulation for different scenarios in Rayleigh fading channels is used to investigate the performance of the new estimators. This is done using the improved Rayleigh fading simulator in [83]. The proposed Bayesian joint estimator is studied based on different BEMs such as the Karhunen-Loève (KL), discrete prolate spheroidal (DPS), generalized complex exponential (GCE), and B-spline (BS) functions, where the channel statistics are perfectly or imperfectly known. When channel statistics are perfectly known, simulation results show that the KL and DPS BEMs use a fewer number of basis functions than that of the GCE and BS BEMs to allow achieving the same performance. However, the best reached performance of all the BEM-based estimators is the same. When channel statistics are mismatched, results show that the estimators based on the GCE and BS BEMs are more robust than those based on the KL and DPS BEMs. This makes the BS functions a better choice in practice as it has a sparse matrix that results in a lower complexity than the other basis functions. For the proposed BS-based Bayesian and ML estimators, results show that the proposed frequency offset estimators outperform known correlation-based estimators for different examined scenarios. In addition, the proposed joint estimators significantly outperform the conventional channel estimator that does not account for the frequency offset, and achieve a very close accuracy to that of the ideal channel estimator operating with perfect knowledge of the frequency offset.

This chapter is organised as follows. Section 5.2 describes signal and channel models. The basis expansion models are presented in Section 5.3. Sections 5.4 and 5.5 illustrate the derivation of the proposed joint Bayesian and maximum likelihood estimators, respectively. Efficient implementation of the estimators using the dichotomous search algorithm is presented in Section 5.6. Simulation results using different BEMs are discussed in Section 5.7 and using B-splines are discussed in Section 5.8. Finally, Section 5.9 contains conclusions.

5.2 Signal and Channel Models

We consider a known (pilot) signal transmitted through frequency-nonselective (flat) time-variant Rayleigh channel and corrupted with complex additive white Gaussian noise (AWGN). For such a scenario, the baseband discrete received signal and channel models, respectively, after frequency downconverting, filtering in a matched filter and sampling at proper times, can be expressed in time domain as [22]

$$r(nT_s) = s(nT_s)h(nT_s) + z(nT_s)\,; \tag{5.1a}$$

$$h(nT_s) = g(nT_s)e^{j2\pi f_0 T_s n}\,, \quad n = 0, 1, \ldots, N-1\,, \tag{5.1b}$$

where $s(nT_s)$ is the transmitted pilot signal, $z(nT_s)$ is the complex-valued AWGN with zero mean and variance σ^2, $g(nT_s)$ is the fading process, f_0 is the frequency offset, f_0T_s is the normalised frequency offset (for simplicity, it will be termed as the frequency offset), T_s is the symbol interval and N is the number of the considered pilot symbols.

The fading process $g(nT_s)$ is modeled as a complex Gaussian process with zero mean and covariance matrix with elements [24, 63, 64]

$$[\mathbf{R}_g]_{u\,v} = R_g(u-v) = J_0(2\pi f_D T_s(u-v))\,, \quad u,\, v = 1, \ldots, N\,, \tag{5.2}$$

where $R_g(\cdot)$ is the autocorrelation function of $g(nT_s)$, $J_0(\cdot)$ is the zero-order Bessel function of the first kind, f_D is the Doppler frequency and f_DT_s is the normalised Doppler frequency (for simplicity, it will be termed as the Doppler frequency).

The received signal and channel models, respectively, in matrix form can be written as

$$\mathbf{r} = \mathbf{S}\mathbf{h} + \mathbf{z}\,, \tag{5.3a}$$

$$\mathbf{h} = \mathbf{\Lambda}_{f_0T_s}\mathbf{g}\,, \tag{5.3b}$$

where $\mathbf{r}$, $\mathbf{h}$, $\mathbf{g}$ and $\mathbf{z}$ are $N \times 1$ column vectors with elements $r(nT_s)$, $h(nT_s)$, $g(nT_s)$ and $z(nT_s)$, respectively, $\mathbf{S}$ and $\mathbf{\Lambda}_{f_0T_s}$ are $N \times N$ diagonal matrices of diag$\{s(nT_s)\}$ and diag$\left\{e^{j2\pi f_0 T_s n}\right\}$, respectively, and $n = 0, 1, \ldots, N-1$.

5.3 Basis Expansion Models

Accurate estimation of the fading process $g(nT_s)$ in (5.1b) requires complicated techniques such as the Wiener filtering [4, 37]. A simpler solution is based on approximating $g(nT_s)$ using the basis expansion model [36, 38]. This approximation simplifies the time-variant fading model and converts it into a linear combination of several basis functions as

$$\tilde{g}(nT_s) = \sum_{m=1}^{M} a_m B(nT_s, m)\,, \tag{5.4}$$

where $B(nT_s, m)$ are the M known basis functions and a_m are unknown expansion coefficients. In matrix form, it can be written as

$$\tilde{\mathbf{g}} = \mathbf{B}\mathbf{a}\,, \tag{5.5}$$

where $\mathbf{B}$ is an $N \times M$ matrix with elements $B(nT_s, m)$ and $\mathbf{a}$ is an $M \times 1$ vector of expansion coefficients a_m. Thus, the problem of estimating N-dimensional time-variant fading process $g(nT_s)$ is transformed into a lower dimensional problem of estimating only M time-invariant expansion coefficients a_m, where usually $M << N$. Therefore, the vector of unknown parameters includes the expansion coefficients $\{a_m\}_{m=1}^{M}$ and the frequency offset f_0T_s.

The resulting approximated received signal model will be shown to have a similar form to that of the slow fading multipath Rayleigh channels discussed in Chapter 4. As a result, two novel joint estimators for the frequency-flat time-variant fading channels are proposed in Sections 5.4, 5.5 by expanding the Bayesian and the maximum likelihood approaches that was discussed in Chapter 4 for the time-invariant frequency-selective channels.

Using the basis expansion model (5.5) to represent the channel fading in (5.1), the approximated received signal and channel models, respectively, in matrix form can be written as

$$\tilde{\mathbf{r}} = \mathbf{S}\tilde{\mathbf{h}} + \mathbf{z}\,; \tag{5.6a}$$

$$\tilde{\mathbf{h}} = \mathbf{\Lambda}_{f_0T_s}\mathbf{B}\mathbf{a}\,, \tag{5.6b}$$

where $\tilde{\mathbf{r}}$, $\tilde{\mathbf{h}}$ and $\mathbf{z}$ are $N \times 1$ column vectors with elements $\tilde{r}(nT_s)$, $\tilde{h}(nT_s)$ and $z(nT_s)$, respectively, $\mathbf{S}$ and $\mathbf{\Lambda}_{f_0T_s}$ are $N \times N$ diagonal matrices of diag$\{s(nT_s)\}$ and diag$\{e^{j2\pi f_0T_s n}\}$, respectively, and $n = 0, 1, \ldots, N-1$.

The proposed estimators rely on the fact that the approximation error can be ignored when choosing M high enough, so that the BEM approximation model (5.6) can be used instead of the original received signal model of the fast fading frequency-flat Rayleigh channel represented in (5.1). Therefore, the processed model can be reformed as

$$\mathbf{r} = \mathbf{\Lambda}_{f_0 T_s} \mathbf{\Phi a} + \mathbf{z}\,; \quad \mathbf{\Phi} = \mathbf{SB}\,, \tag{5.7a}$$

$$\mathbf{h} = \mathbf{\Lambda}_{f_0 T_s} \mathbf{Ba}\,, \tag{5.7b}$$

which is of a similar form to that of the time-invariant frequency-selective channel model considered in Chapter 4. This encourages tracking the same way of estimation, and two methods are involved. The first is based on the Bayesian approach that leads to the minimum mean square error (MMSE) joint channel estimation. Whereas, the second is based on the maximum likelihood (ML) approach. The Bayesian joint estimator demonstrates a high-accuracy performance as it incorporates some prior knowledge about the required parameters to be estimated [121]. However, the ML one, and without loosing much of the accuracy, is a good choice when the statistical characteristics of the fading and noise are unknown. The two proposed joint estimators are described below.

The BEM-based approach has been widely used due to its low complexity and high accuracy. In this approach, in addition to the statistical estimation error, the BEM-based estimator suffers from a modeling error. Different basis functions can be used in the BEM such as complex exponential [38, 40], polynomial [39], discrete prolate spheroidal [41], and B-splines [42, 91, 129]. The following four BEMs are most often considered in applications to channel estimation.

5.3.1 KL Functions

KL functions as described in Section 2.3.1 exploit the fading covariance matrix $\mathbf{R}_g$. This allows the KL-BEM to provide the best approximation of the fading process provided the perfect knowledge of $\mathbf{R}_g$. The $N \times N$ matrix $\mathbf{U}$ of eigenvectors of $\mathbf{R}_g$ is obtained first as

$$\mathbf{R}_g \mathbf{U} = \mathbf{U} \mathbf{\Upsilon}\,, \tag{5.8}$$

where $\mathbf{\Upsilon}$ is the $N \times N$ diagonal matrix of eigenvalues. Then the basis function matrix $\mathbf{B}$ is formed by the M eigenvectors (columns of $\mathbf{U}$) corresponding to the M maximum eigenvalues (diagonal elements of $\mathbf{\Upsilon}$).

5.3.2 DPS Functions

DPS functions as mentined in Section 2.3.2 are generated exploiting the Doppler frequency. First, a matrix $\mathbf{D}$ is generated as

$$[\mathbf{D}]_{u\,v} = \frac{\sin\left(2\pi f_D T_s\left(u-v\right)\right)}{\pi\left(u-v\right)}\,, \quad u,v = 1,\ldots,N\,. \tag{5.9}$$

Then, $\mathbf{B}$ is formed from M eigenvectors of $\mathbf{D}$ corresponding to the M maximum eigenvalues.

5.3.3 GCE Functions

GCE functions as discussed in Section 2.3.3 are a modified version of the complex exponential functions for which the period of the basis functions is extended longer than the observation interval, and are given by

$$B(nT_s, m) = e^{j\frac{2\pi n T_s}{\xi N}\left(m-1-\frac{M-1}{2}\right)}\,, \tag{5.10}$$

where $\xi > 1$, and here, we use $\xi = 2$.

5.3.4 BS Functions

BS functions are described in Section 2.3.4 and do not require any prior channel statistics. The BS functions are given by [94]

$$B_\eta(x) = \frac{1}{\eta!}\sum_{i=0}^{\eta+1}(-1)^i\binom{\eta+1}{i}\left(\frac{x}{PT_s}+\frac{\eta+1}{2}-i\right)_+^\eta\,, \tag{5.11}$$

where

$$P = \frac{N-1}{M-\eta}\,, \tag{5.12}$$

PT_s is the sampling interval separating two adjacent B-spline functions, and $x_+ = \max\{0,x\}$. In this case, $B(nT_s,m) = B_\eta\left(nT_s-(m-\frac{\eta+1}{2})PT_s\right)$. The matrix $\mathbf{B}$ of the BS functions is a sparse matrix that only contains $\eta+1$ nonzero elements in each row, which makes it attractive for implementation. The accuracy and complexity of the

BS-BEM approximation depends on the spline degree η. In many situations, the cubic B-spline ($\eta = 3$) provides the best trade-off between complexity and accuracy [94]. We use the cubic B-spline in the simulation below whenever $M \geq 4$, and for $1 \leq M \leq 3$ we use $\eta = M - 1$.

The approximation mean square error is defined as

$$\epsilon^2 = E\left\{ \frac{\sum_{n=0}^{N-1} |g(nT_s) - \tilde{g}(nT_s)|^2}{\sum_{n=0}^{N-1} |g(nT_s)|^2} \right\}. \tag{5.13}$$

As described in [43], this error is inversely affected by the sampling factor γ that is given as

$$\gamma = \frac{1}{f_D T_s P}. \tag{5.14}$$

For a certain Doppler frequency $f_D T_s$, which is assumed here to be known or can be determined, increasing M leads to a decrease in P and an increase in γ, which results in a desired decrease in the error ϵ^2 [43]. However, in Section 5.7, it is shown that depending on $f_D T_s$ and the signal to noise ratio (SNR) range of interest, there is an optimum value of M, denoted as M_O, above which the performance of the B-spline-based joint estimator can not be improved. This is due to the fact that there is a lower bound, the CRLB, on the variance of any unbiased estimator. Therefore, it is essential to use $M = M_O$, so that to prevent getting a low-accuracy performance (when $M < M_O$) or adding some unnecessary extra complexity (when $M > M_O$).

The approximation error depends also on the method used to determine the spline coefficients a_m. Different methods can be used to determine a_m, and in [43], the optimal spline, spline interpolation and local spline approximations with several types of coefficients have been examined.

In the proposed algorithms however, these coefficients are estimated jointly with the frequency offset as described in Sections 5.4, 5.5. The resulting estimation error of that method is comparable to the approximation error of the optimal spline method while a significantly lower complexity is achieved.

5.4 Bayesian Joint Estimator

The Bayesian joint estimator is derived based on the Bayesian approach in which the parameters $\mathbf{a}$ are assumed to be random variables whose particular realizations are to be estimated [121]. In this case, the joint estimator requires given prior probability density functions (PDF) of $\mathbf{a}$, and the received signal has a conditional PDF of [48, 121]

$$p\left(\mathbf{r}|f_0T_s,\mathbf{a}\right)=\frac{1}{\pi^N\sigma^{2N}}\exp\left[-\frac{1}{\sigma^2}\left(\mathbf{r}-\mathbf{\Lambda}_{f_0T_s}\mathbf{\Phi a}\right)^H\left(\mathbf{r}-\mathbf{\Lambda}_{f_0T_s}\mathbf{\Phi a}\right)\right]. \tag{5.15}$$

The random spline coefficient vector $\mathbf{a}$ has to follow the assumed Rayleigh channel properties, and so, it is also zero-mean Gaussian random with normal complex distribution and its prior PDF is

$$p(\mathbf{a})=\frac{1}{\pi^M\left|\mathbf{R}_a\right|}\exp\left[-\mathbf{a}^H\mathbf{R}_a^{-1}\mathbf{a}\right], \tag{5.16}$$

where $\mathbf{R}_a$ is the covariance matrix of $\mathbf{a}$. This matrix can be obtained as described in [129] using the original covariance matrix $\mathbf{R}_g$ of the fading process of the channel, obtained in (5.2). The fading covariance matrix of the approximated fading process has to be equal to that of the original one, and since the fading is Rayleigh (*i.e.* zero-mean), it follows that [129]

$$\mathbf{R}_g=\mathrm{E}\left\{\mathbf{g}\mathbf{g}^H\right\}=\mathrm{E}\left\{\tilde{\mathbf{g}}\tilde{\mathbf{g}}^H\right\}=\mathrm{E}\left\{\mathbf{B}\mathbf{a}\mathbf{a}^H\mathbf{B}^H\right\}=\mathbf{B}\mathbf{R}_a\mathbf{B}^H. \tag{5.17}$$

Multiplying both sides of (5.17) by $\left(\mathbf{B}^H\mathbf{B}\right)^{-1}\mathbf{B}^H$ from the left and $\mathbf{B}\left(\mathbf{B}^H\mathbf{B}\right)^{-1}$ from the right yields [129]

$$\mathbf{R}_a=\left(\mathbf{B}^H\mathbf{B}\right)^{-1}\mathbf{B}^H\mathbf{R}_g\mathbf{B}\left(\mathbf{B}^H\mathbf{B}\right)^{-1}. \tag{5.18}$$

5.4.1 Frequency Offset Estimator

For estimation of the frequency offset f_0T_s, the expansion coefficients a_m are considered to be nuisance parameters that can be integrated out of the conditional PDF $p(\mathbf{r}|f_0T_s,\mathbf{a})$ through Bayesian approach [121]. This is expressed as [48]

$$p\left(\mathbf{r}|fT_s\right)=\int p\left(\mathbf{r}|fT_s,\mathbf{a}\right)p(\mathbf{a})d\Re\{\mathbf{a}\}d\Im\{\mathbf{a}\}. \tag{5.19}$$

The frequency offset estimator is obtained by maximising the likelihood function $p\left(\mathbf{r}|fT_s\right)$ over a grid of frequencies fT_s covering the frequency acquisition range $\Psi = [-\psi/2, \psi/2]$ as [48, 121]

$$\widehat{f_0T_s} = \arg\max_{fT_s\in\Psi}\left\{p\left(\mathbf{r}|fT_s\right)\right\}. \tag{5.20}$$

The frequency acquisition range Ψ can be considered either wide ($\psi = 1$) or narrow ($\psi << 1$).

The likelihood function $p(\mathbf{r}|fT_s)$ is obtained by solving the integration in (5.19) which gives [48]

$$p\left(\mathbf{r}|fT_s\right) = \frac{\exp\left[-\sigma^{-2}\mathbf{r}^H\mathbf{r}\right]}{\pi^N\sigma^{2N}}\int\exp\left[2\Re\left\{\sigma^{-2}\mathbf{a}^H\mathbf{W}_{fT_s}\right\} - \sigma^{-2}\mathbf{a}^H\mathbf{\Gamma}\mathbf{a}\right]p(\mathbf{a})d\Re\{\mathbf{a}\}d\Im\{\mathbf{a}\}, \tag{5.21}$$

where

$$\mathbf{\Gamma} = \mathbf{\Phi}^H\mathbf{\Phi} = \mathbf{B}^H\mathbf{S}^H\mathbf{S}\mathbf{B}, \tag{5.22}$$

$$\mathbf{W}_{fT_s} = \mathbf{\Phi}^H\mathbf{\Lambda}_{fT_s}^H\mathbf{r} = \mathbf{B}^H\mathbf{S}^H\mathbf{\Lambda}_{fT_s}^H\mathbf{r}. \tag{5.23}$$

The PDF in (5.21) yields [48]

$$p\left(\mathbf{r}|fT_s\right) = \frac{\exp\left[-\sigma^{-2}\mathbf{r}^H\mathbf{r}\right]}{\pi^N\sigma^{2N}\left|\sigma^{-2}\mathbf{R}_a\mathbf{\Gamma} + \mathbf{I}_M\right|}\exp\left[\sigma^{-2}Y_{fT_s}\right], \tag{5.24}$$

where

$$Y_{fT_s} = \mathbf{W}_{fT_s}^H\left(\mathbf{\Gamma} + \sigma^2\mathbf{R}_a^{-1}\right)^{-1}\mathbf{W}_{fT_s} \tag{5.25}$$

and $\mathbf{I}_M$ is the $M \times M$ identity matrix. Now, substituting (5.24) into (5.20) produces

$$\widehat{f_0T_s} = \arg\max_{fT_s\in\Psi}\left\{\frac{\exp\left[-\sigma^{-2}\mathbf{r}^H\mathbf{r}\right]}{\pi^N\sigma^{2N}\left|\sigma^{-2}\mathbf{R}_a\mathbf{\Gamma} + \mathbf{I}_M\right|}\exp\left[\sigma^{-2}Y_{fT_s}\right]\right\}. \tag{5.26}$$

Excluding the frequency-independent first factor inside the brackets in (5.26), and taking the natural logarithm, the frequency offset estimator becomes [48]

$$\widehat{f_0T_s} = \arg\max_{fT_s\in\Psi}\left\{Y_{fT_s}\right\}, \tag{5.27}$$

which is a maximiser of the generalised periodogram Y_{fT_s} [44] over the frequency acquisition range. Finally, the Bayesian frequency offset (BF) estimator is given by

$$\widehat{f_0T_s} = \arg\max_{fT_s\in\Psi}\left\{\mathbf{W}_{fT_s}^H\left(\mathbf{\Gamma} + \sigma^2\mathbf{R}_a^{-1}\right)^{-1}\mathbf{W}_{fT_s}\right\} \tag{5.28a}$$

$$= \arg\max_{fT_s\in\Psi}\left\{\mathbf{r}^H\mathbf{\Lambda}_{fT_s}\mathbf{S}\mathbf{B}\left(\mathbf{B}^H\mathbf{S}^H\mathbf{S}\mathbf{B} + \sigma^2\mathbf{R}_a^{-1}\right)^{-1}\mathbf{B}^H\mathbf{S}^H\mathbf{\Lambda}_{fT_s}^H\mathbf{r}\right\}. \tag{5.28b}$$

5.4.2 Channel Estimator

The channel is then jointly estimated exploiting the estimated value of the frequency offset. Replacing the frequency offset in (5.7a) by the estimated value $\widehat{f_0 T_{sB}}$, this model becomes linear and can be reformed as

$$\mathbf{r} = \mathbf{\Omega}\mathbf{a} + \mathbf{z}\,; \qquad \mathbf{\Omega} = \mathbf{\Lambda}_{\widehat{f_0 T_{sB}}}\mathbf{\Phi}\,, \tag{5.29}$$

where, after determining $\widehat{f_0 T_{sB}}$, $\mathbf{\Omega}$ is a known $N \times M$ matrix. Hence, the MMSE estimator of the spline coefficients $\mathbf{a}$ is [121]

$$\hat{\mathbf{a}}_B = \left(\mathbf{\Omega}^H\mathbf{\Omega} + \sigma^2\mathbf{R}_a^{-1}\right)^{-1}\mathbf{\Omega}^H\mathbf{r}\,. \tag{5.30}$$

Substituting the value of $\mathbf{\Omega}$ from (5.29) into (5.30), and considering (5.22) and (5.23), the estimator becomes

$$\hat{\mathbf{a}}_B = \left(\mathbf{\Gamma} + \sigma^2\mathbf{R}_a^{-1}\right)^{-1}\mathbf{W}_{\widehat{f_0 T_{sB}}}\,. \tag{5.31}$$

Finally, the Bayesian joint channel and frequency offset (BJ) estimator is obtained by substituting (5.31) into (5.6b) as

$$\hat{\mathbf{h}} = \mathbf{\Lambda}_{\widehat{f_0 T_{sB}}}\mathbf{B}\left(\mathbf{\Gamma} + \sigma^2\mathbf{R}_a^{-1}\right)^{-1}\mathbf{W}_{\widehat{f_0 T_{sB}}} \tag{5.32a}$$

$$= \mathbf{\Lambda}_{\widehat{f_0 T_{sB}}}\mathbf{B}\left(\mathbf{B}^H\mathbf{S}^H\mathbf{S}\mathbf{B} + \sigma^2\mathbf{R}_a^{-1}\right)^{-1}\mathbf{B}^H\mathbf{S}^H\mathbf{\Lambda}^H_{\widehat{f_0 T_{sB}}}\mathbf{r}\,. \tag{5.32b}$$

5.5 Maximum Likelihood Joint Estimation

So far, the fast fading frequency-flat channel is considered to have Rayleigh fading with a known covariance matrix $\mathbf{R}_g$ (*i.e.* a known $\mathbf{R}_a$), and AWGN with a known variance σ^2. As can be seen in (5.28) and (5.32), these prior statistical specifications are included in the derived Bayesian joint estimator. However, when dealing with different scenarios where there is no certainty about these statistical properties of the fading and the AWGN, the classical ML joint estimation approach can be used. For the ML approach, the coefficients $\mathbf{a}$ are assumed to be deterministic but unknown parameters which are required to be estimated. In this case, the received signal has an unconditional PDF of [121]

$$p\left(\mathbf{r}; f_0 T_s, \mathbf{a}\right) = \frac{1}{\pi^N \sigma^{2N}} \exp\left[-\frac{1}{\sigma^2}\left(\mathbf{r} - \mathbf{\Lambda}_{f_0 T_s}\mathbf{\Phi}\mathbf{a}\right)^H\left(\mathbf{r} - \mathbf{\Lambda}_{f_0 T_s}\mathbf{\Phi}\mathbf{a}\right)\right]\,. \tag{5.33}$$

5.5.1 Frequency Offset Estimator

The frequency offset f_0T_s is estimated using the same technique as described in [44] and detailed in Section 4.4.1. The ML frequency offset (MLF) estimator is the maximiser of the generalised periodogram

$$Y_{fT_s} = \mathbf{r}^H \mathbf{\Lambda}_{fT_s} \mathbf{\Phi} \left(\mathbf{\Phi}^H \mathbf{\Phi} \right)^{-1} \mathbf{\Phi}^H \mathbf{\Lambda}_{fT_s}^H \mathbf{r} \tag{5.34}$$

over the frequency acquisition range and is given by

$$\widehat{f_0T_s} = \arg \max_{fT_s \in \Psi} \left\{ \mathbf{W}_{fT_s}^H \mathbf{\Gamma}^{-1} \mathbf{W}_{fT_s} \right\} \tag{5.35a}$$

$$= \arg \max_{fT_s \in \Psi} \left\{ \mathbf{r}^H \mathbf{\Lambda}_{fT_s} \mathbf{SB} \left(\mathbf{B}^H \mathbf{S}^H \mathbf{SB} \right)^{-1} \mathbf{B}^H \mathbf{S}^H \mathbf{\Lambda}_{fT_s}^H \mathbf{r} \right\} . \tag{5.35b}$$

5.5.2 Channel Estimator

After getting the estimated value of the frequency offset $\widehat{f_0T_{sML}}$, the channel can then be jointly estimated. As shown in Section 4.4.2, the coefficients $\mathbf{a}$ are estimated as [44]

$$\hat{\mathbf{a}}_{ML} = \mathbf{\Gamma}^{-1} \mathbf{W}_{\widehat{f_0T_{sML}}} , \tag{5.36}$$

and finally from (5.6b) the ML joint channel and frequency offset (MLJ) estimator follows as

$$\hat{\mathbf{h}} = \mathbf{\Lambda}_{\widehat{f_0T_{sML}}} \mathbf{B} \mathbf{\Gamma}^{-1} \mathbf{W}_{\widehat{f_0T_{sML}}} \tag{5.37a}$$

$$= \mathbf{\Lambda}_{\widehat{f_0T_{sML}}} \mathbf{B} \left(\mathbf{B}^H \mathbf{S}^H \mathbf{SB} \right)^{-1} \mathbf{B}^H \mathbf{S}^H \mathbf{\Lambda}_{\widehat{f_0T_{sML}}}^H \mathbf{r} . \tag{5.37b}$$

5.6 Efficient Dichotomous-based Implementation

For real-time implementation, the DS technique can lead to a high-accuracy performance with a considerable decrease in complexity.

According to the proposed joint estimators in (5.28), (5.32), (5.35) and (5.37), the best way for implementation based on the DS technique is summarised in Table 5.1.

Table 5.1: Dichotomous Search Algorithms for the Proposed Joint Channel and Frequency Offset Estimators for Frequency-Selective Time-Variant Fading Channels.

Compute	$\mathbf{G} = \begin{cases} \left(\mathbf{B}^H\mathbf{S}^H\mathbf{S}\mathbf{B} + \sigma^2\mathbf{R}_a^{-1}\right)^{-1}, & \text{Bayesian approach} \\ \left(\mathbf{B}^H\mathbf{S}^H\mathbf{S}\mathbf{B}\right)^{-1}, & \text{ML approach} \end{cases}$
Calculate	$W_{fT_s}(m) = \mathcal{FFT}\{r(nT_s)s^*(nT_s)B^*(nT_s,\, m), N_{FFT}\}\,; \quad m = 1, \ldots, M$
Determine	$Y_{fT_s} = \sum_{u=1}^{M}\sum_{v=1}^{M} [\mathbf{G}]_{u\,v}\, W^*_{fT_s}(u) W_{fT_s}(v)$
Find	$f_pT_s = \arg\max_{fT_s \in \Psi} \{Y_{fT_s}\}$
Locate	$Y_1 = Y_{f_{p-1}T_s}\,, \quad Y_2 = Y_{f_pT_s}\,, \quad Y_3 = Y_{f_{p+1}T_s}$
For Q iterations do	
	$\Delta fT_s = \Delta fT_s/2$
	If $Y_3 < Y_1$ then $Y_3 = Y_2$ and $f_pT_s = f_pT_s - \Delta fT_s$,
	else $Y_1 = Y_2$ and $f_pT_s = f_pT_s + \Delta fT_s$
	$W_{f_pT_s}(m) = \sum_{n=0}^{N-1} r(nT_s)s^*(nT_s)B^*(nT_s,\, m)e^{-j2\pi f_pT_s n}\,; \quad m = 1, \ldots, M$
	$Y_2 = \sum_{u=1}^{M}\sum_{v=1}^{M} [\mathbf{G}]_{u\,v}\, W^*_{f_pT_s}(u) W_{f_pT_s}(v)$
Finally	$\widehat{f_0T_s} = f_pT_s\,, \qquad \widehat{\mathbf{h}} = \mathbf{\Lambda}_{f_pT_s}\mathbf{B}\mathbf{G}\mathbf{W}_{f_pT_s}$

5.7 Simulation Results and Performance Comparison for different BEMs

A binary sequence transmitted through a time-variant Rayleigh fading channel and corrupted with a complex AWGN is implemented. The received signal and channel models in (5.1) are simulated using the modified version of Jakes' model [64] that was proposed in [81] and corrected in [83]. However, we assume in the estimation process that the received signal and channel models are based on the BEM as in (5.7), and so, the results contain the model mismatching error.

The SNR below is calculated as

$$\text{SNR} = \frac{\text{E}\left\{\left(\mathbf{\Lambda}_{f_0T_s}\mathbf{S}\mathbf{g}\right)^H\left(\mathbf{\Lambda}_{f_0T_s}\mathbf{S}\mathbf{g}\right)\right\}}{\text{E}\left\{\mathbf{z}^H\mathbf{z}\right\}} = \frac{\text{tr}\left\{\mathbf{S}^H\mathbf{S}\mathbf{R}_g\right\}}{N\sigma_z^2}\,, \tag{5.38}$$

where the following matrices manipulation has been used

$$\left(\mathbf{A}\mathbf{B}\right)^H = \mathbf{B}^H\mathbf{A}^H\,. \tag{5.39}$$

The mean square error (MSE) of the joint channel and frequency offset estimation is calculated as

$$\mathbf{h}\text{-MSE} = \frac{1}{N_t}\sum_{t=1}^{N_t}\frac{\sum_{n=0}^{N-1}\left|h(nT_s)-\hat{h}_t(nT_s)\right|^2}{\sum_{n=0}^{N-1}\left|h(nT_s)\right|^2}, \tag{5.40}$$

over a number of $N_t = 10\,000$ simulation trials, where $\hat{h}_i(nT_s)$ is the nth estimated channel sample in the tth simulation trial. We use a binary pseudo-random transmitted sequence of length $N = 128$, the frequency offset is $f_0T_s = 0.0123$, the size of the FFT in the coarse search is $N_{FFT} = N = 128$, the number of dichotomous iterations is $Q = 5$, and the frequency acquisition range is wide ($\psi = 1$).

As seen in (5.32), the joint Bayesian BEM-based estimators employ prior information about the Doppler frequency due to the dependence of $\mathbf{R}_a$ (and $\mathbf{B}$ for the KL and DPS BEMs) on f_DT_s. The performance of the joint BEM-based estimators is studied first for the case of the perfect knowledge of the Doppler frequency. Then, the performance of different BEMs is compared in two scenarios of the mismatched Doppler frequency. The estimators with perfect knowledge of the Doppler frequency are termed as perfect, the others are termed as mismatched.

5.7.1 Perfect Doppler Estimation

Here we assume that the receiver knows the exact value of the Doppler frequency. Figure 5.1 shows the M-dependent $\mathbf{h}$-MSE performance for the BEM-based dichotomous joint Bayesian estimators in slow ($f_DT_s = 0.005$), moderate ($f_DT_s = 0.02$), and fast ($f_DT_s = 0.05$) fading channels, where SNR $= 30$ dB. It can be seen that for any BEM, there exists a threshold M (M_{th}), below which $\mathbf{h}$-MSE increases rapidly. This is due to a high modeling error for such a low M. The $\mathbf{h}$-MSE stays almost constant for $M > M_{\text{th}}$. The exploitation of the fading covariance matrix (in $\mathbf{R}_a$) and the noise variance σ_z^2 in the Bayesian estimators prevents degradation in the performance for high M. For a higher f_DT_s, the estimator requires a higher M_{th} to achieve its best performance. The M_{th} for the KL and DPS BEMs is lower than that for the GCE and BS BEMs. This is due to exploitation of prior statistical information of the channel when generating KL and DPS basis functions. However, the best achieved performance, for $M > M_{\text{th}}$, is the same for all BEMs.

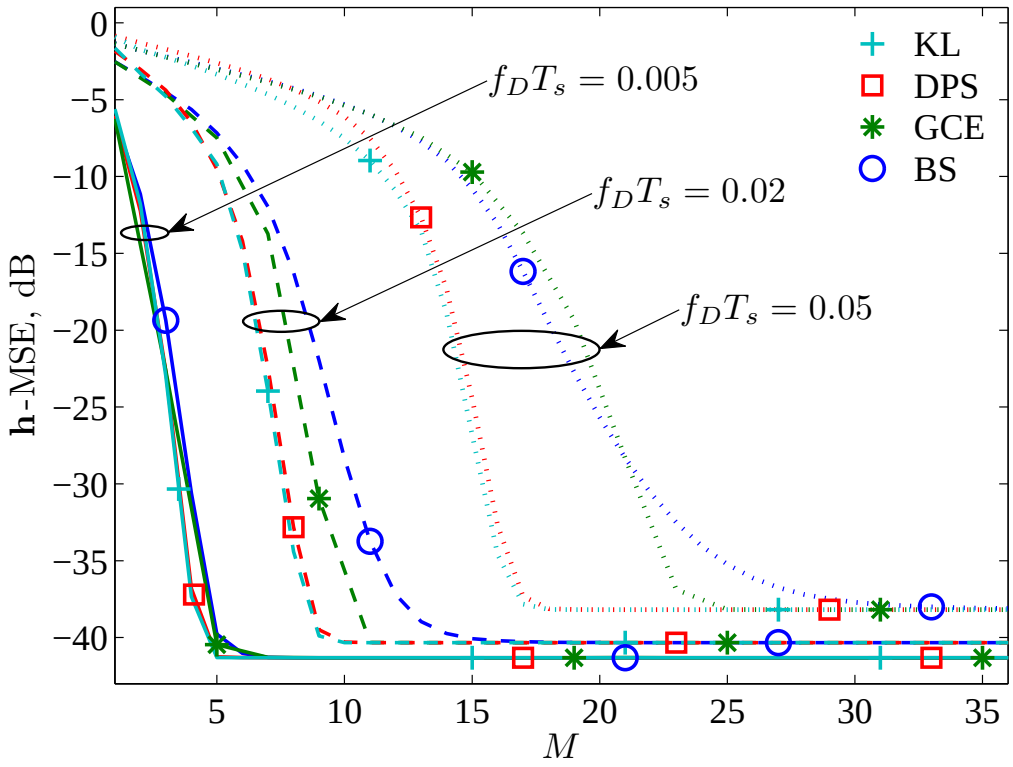

Figure 5.1: $\mathbf{h}$-MSE of the Bayesian joint estimators for frequency-flat time-variant fading channels as a function of M *vs* f_DT_s for perfect knowledge of the Doppler frequency; $N = 128$, $f_0T_s = 0.0123$, $N_{FFT} = 128$, $Q = 5$ and SNR $= 30$ dB.

In real life scenarios however, it is difficult for the receiver to obtain the exact value of the Doppler frequency, which means that there will be a mismatch between the real Doppler frequency f_DT_s and the corresponding value used in the estimator, which is termed as $\widehat{f_DT_s}$.

5.7.2 Mismatched Doppler Estimation

We consider two possible scenarios for choosing $\widehat{f_DT_s}$. The first is to use a value, which corresponds to a maximum speed difference between two communication terminals. The second is to estimate the real Doppler frequency.

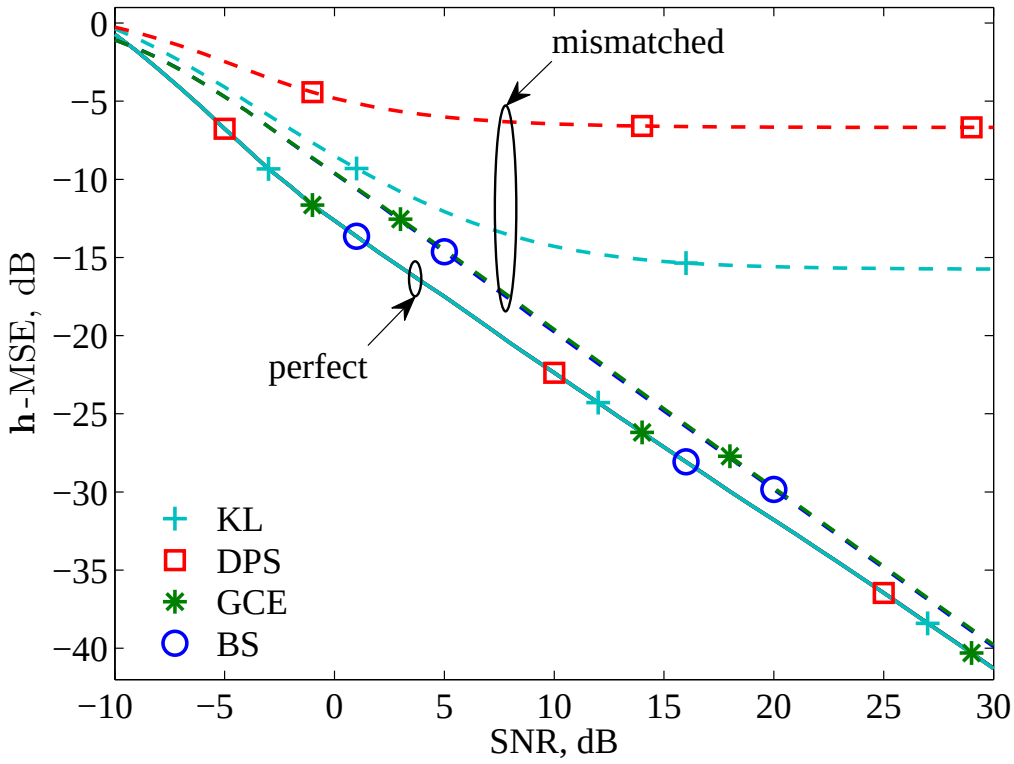

Figure 5.2: $\mathbf{h}$-MSE of the Bayesian joint estimators for frequency-flat time-variant fading channels as a function of SNR for the mismatched Doppler frequency; $N = 128$, $f_0 T_s = 0.0123$, $N_{FFT} = 128$, $Q = 5$, $f_D T_s = 0.005$ and $M = 7$; perfect: $\widehat{f_D T_s} = f_D T_s$ and mismatched: $\widehat{f_D T_s} = 0.05$.

Significantly Overestimated Doppler Frequency

Here we consider that the receiver assumes a fixed Doppler frequency, such as $\widehat{f_D T_s} = 0.05$. Figure 5.2 shows the $\mathbf{h}$-MSE performance of the joint estimators for $f_D T_s = 0.005$ and $M = 7$. For the perfect estimators, all BEMs allow achieving the same $\mathbf{h}$-MSE performance. For the mismatched estimators, the ones using the GCE and BS BEMs are seen to be less sensitive to the mismatched Doppler frequency than those using the KL and DPS BEMs. The $\mathbf{h}$-MSE of the mismatched GCE and BS-based estimators is close to that of the perfect estimators, whereas the KL and DPS-based estimators suffer from a significantly higher $\mathbf{h}$-MSE with the DPS-based one being the worst. This is due to the fact that the basis matrix $\mathbf{B}$ for the KL and DPS functions depends on the Doppler frequency, whereas for the GCE and BS, it is independent of the Doppler frequency.

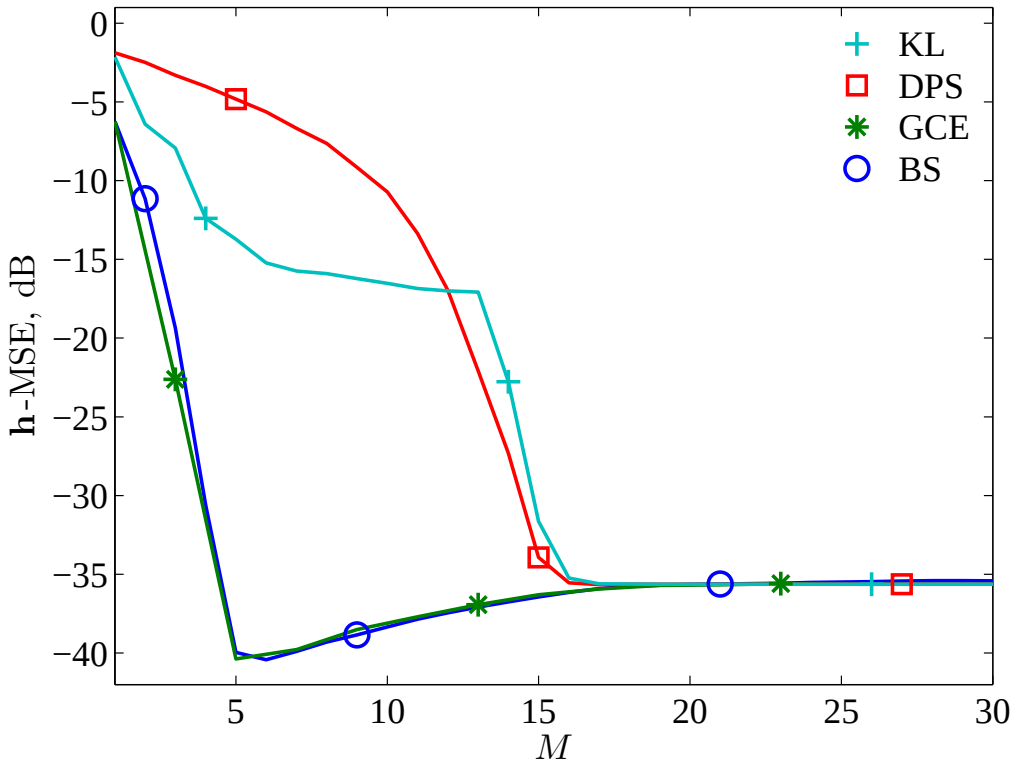

Figure 5.3: $\mathbf{h}$-MSE of the Bayesian joint estimators for frequency-flat time-variant fading channels as a function of M for the mismatched Doppler frequency; $N = 128$, $f_0T_s = 0.0123$, $N_{FFT} = 128$, $Q = 5$, SNR $= 30$ dB, $f_DT_s = 0.005$ and $\widehat{f_DT_s} = 0.05$.

A better understanding of such mismatched estimators can be obtained from the M-dependent performance in Figure 5.3 for SNR $= 30$ dB. Unlike the case with the perfect estimators (as shown in Figure 5.1), the GCE and BS BEMs now allow achieving a better performance and using a significantly smaller M than the KL and DPS BEMs. This can also be seen in Figure 5.4. With $M = 5$, the GCE and BS-based mismatched estimators achieve a high-accuracy performance, which is very close to that of the perfect estimators. The performance of the KL and DPS-based mismatched estimators using $M = 17$ is better than that using $M = 7$ (see Figure 5.2), however it is still inferior to that of the GCE and BS-based mismatched estimators with $M = 5$.

Estimated Doppler Frequency

Here we assume that the receiver estimates the Doppler frequency f_DT_s that is considered to be random and uniformly distributed between 0 and 0.02. The estimated value $\widehat{f_DT_s}$ is

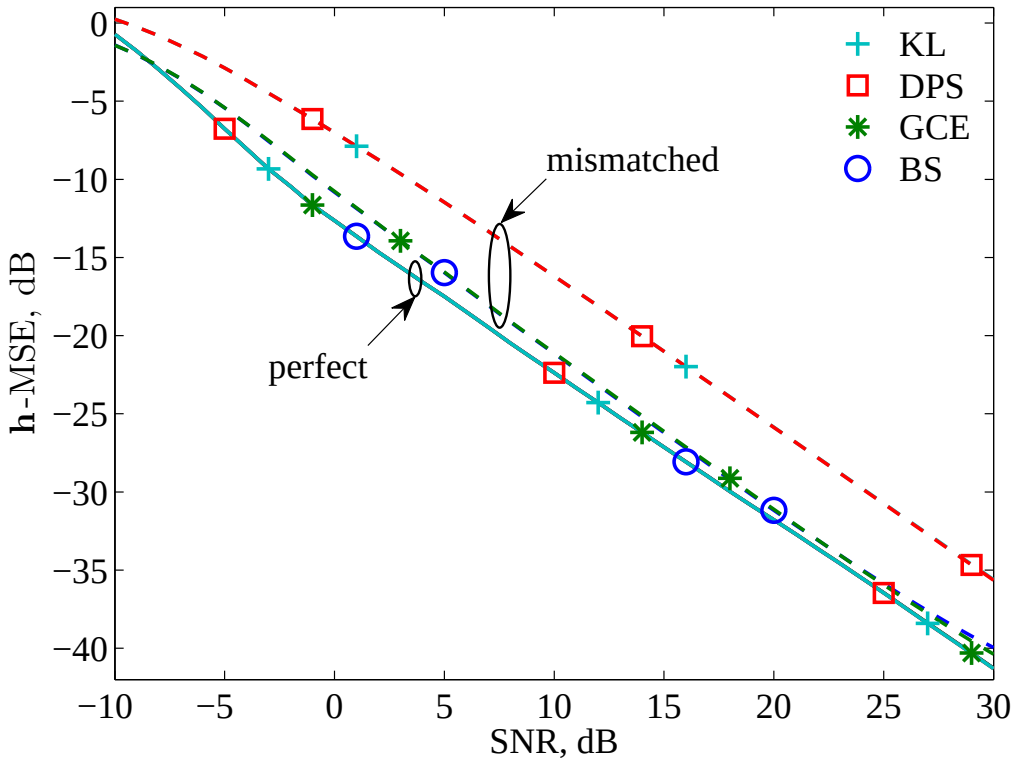

Figure 5.4: $\mathbf{h}$-MSE of the Bayesian joint estimators for frequency-flat time-variant fading channels as a function of SNR for the mismatched Doppler frequency; $N = 128$, $f_0 T_s = 0.0123$, $N_{FFT} = 128$, $Q = 5$ and $f_D T_s = 0.005$; perfect: $\widehat{f_D T_s} = f_D T_s$ and $M = 7$, and mismatched: $\widehat{f_D T_s} = 0.05$, $M = 5$ for GCE & BS, and $M = 17$ for KL & DPS.

considered as random and normally distributed with mean $f_D T_s$ and variance 16×10^{-6}. The $\mathbf{h}$-MSE performance of such estimators is shown in Figure 5.5. We use $M = 16$ that guarantees a best performance for $f_D T_s$ up to 0.02 as expected from Figure 5.1. The results show that the GCE and BS BEMs allow achieving a significantly better performance compared to that of the KL and DPS-based estimators. The performance of the DPS-based mismatched estimator is the poorest.

Finally, the $\mathbf{h}$-MSE performance of the mismatched estimators against M is examined in Figure 5.6. The results show that the GCE and BS BEMs allow achieving a similar performance, which is significantly better than that of the estimators using the KL and DPS BEMs.

It is seen that the GCE and BS BEMs are a good choice in practical scenarios, due to their low sensitivity to the mismatched Doppler frequency. Unlike the case with the GCE,

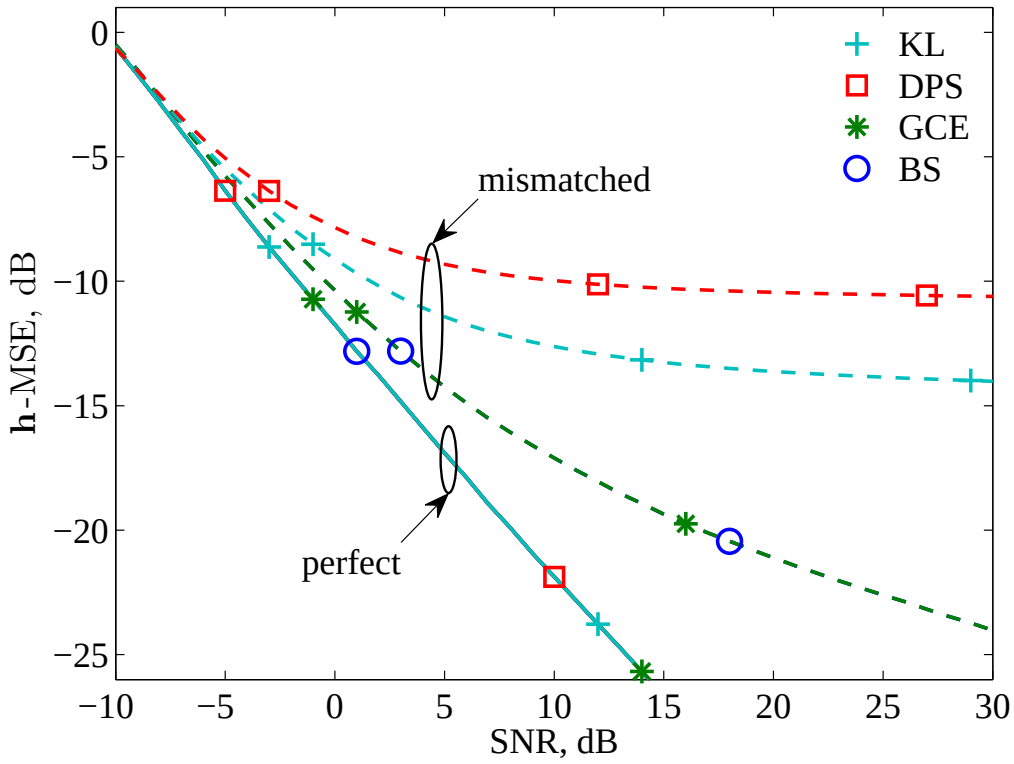

Figure 5.5: $\mathbf{h}$-MSE of the Bayesian joint estimators for frequency-flat time-variant fading channels as a function of SNR for the mismatched Doppler frequency; $N = 128$, $f_0 T_s = 0.0123$, $N_{FFT} = 128$, $Q = 5$, $f_D T_s \sim \mathcal{U}(0,\, 0.02)$ and $M = 16$; perfect: $\widehat{f_D T_s} = f_D T_s$ and mismatched: $\widehat{f_D T_s} \sim \mathcal{N}(f_D T_s,\, 16 \times 10^{-6})$.

the basis matrix $\mathbf{B}$ for the BS BEM is a sparse matrix, which results in a low complexity of the estimator and makes the BS a good choice in practice.

Therefore, the B-spline functions are used as a BEM throughout this thesis and the BS-based estimators are examined in details below.

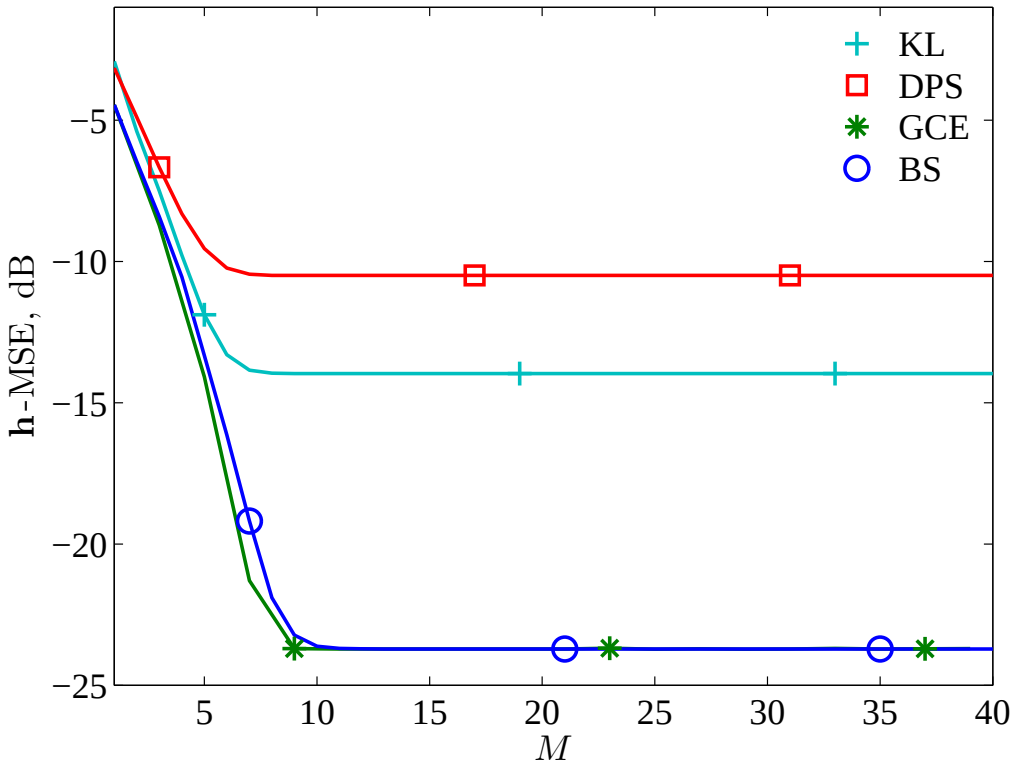

Figure 5.6: **h**-MSE of the Bayesian joint estimators for frequency-flat time-variant fading channels as a function of M for the mismatched Doppler frequency; $N = 128$, $f_0T_s = 0.0123$, $N_{FFT} = 128$, $Q = 5$, SNR $= 30$ dB, $f_DT_s \sim \mathcal{U}(0, 0.02)$ and $\widehat{f_DT_s} \sim \mathcal{N}(f_DT_s, 16 \times 10^{-6})$.

5.8 Simulation Results and Performance Analysis of Estimators using B-Spline BEM

The square root of the mean square error (RMSE) of the frequency offset and channel estimates, respectively, are calculated as

$$f_0T_s\text{-RMSE} = \sqrt{\frac{1}{N_t}\sum_{i=1}^{N_t}\left(f_0T_s - \widehat{f_0T_{si}}\right)^2}, \tag{5.41a}$$

$$\mathbf{h}\text{-RMSE} = \sqrt{\frac{1}{N_t}\sum_{i=1}^{N_t}\frac{\sum_{n=0}^{N-1}\left|h(nT_s) - \hat{h}_i(nT_s)\right|^2}{\sum_{n=0}^{N-1}\left|h(nT_s)\right|^2}}, \tag{5.41b}$$

over $N_t = 10\,000$ simulation trials, where $\widehat{f_0T_{si}}$ and $\hat{h}_i(nT_s)$ are frequency and channel estimates obtained in the ith simulation trial.

Table 5.2: Estimators for Frequency-Selective Time-Variant Fading Channels Considered in the Simulation.

Estimator	Algorithm	Frequency	Channel	Equation
Frequency	BF	Deterministic	Unknown Random	(5.28)
	MLF	Deterministic	Unknown Deterministic	(5.35)
	RMLF	Deterministic	Known	(5.43)
Channel	BC	Ignored	Random	(5.42)
	BJ	Deterministic	Random	(5.32)
	MLJ	Deterministic	Deterministic	(5.37)
	RBC	Known	Random	(5.32)

A binary pseudo-random sequence of length N is generated as the pilot signal, the size of the FFT in the coarse search stage is N_{FFT}, and the frequency acquisition range, unless otherwise specified, is wide ($\psi = 1$).

The proposed joint channel and frequency offset estimators are compared with a reference Bayesian channel estimator, denoted as RBC, where the frequency offset is considered to be known (or zero). This estimator is given as in (5.32) but with $\widehat{f_0 T_s}$ being replaced with $f_0 T_s$. Another estimator is introduced for comparison, the Bayesian channel estimator, denoted as BC, which ignores the frequency offset of the channel and is derived as

$$\hat{\mathbf{h}} = \mathbf{B}\left(\mathbf{B}^H\mathbf{S}^H\mathbf{S}\mathbf{B} + \sigma^2\mathbf{R}_a^{-1}\right)^{-1}\mathbf{B}^H\mathbf{S}^H\mathbf{r}\,. \tag{5.42}$$

In addition, the frequency estimators are compared with a reference ML frequency estimator, denoted as RMLF, where the fading process of the channel is considered to be known. This is the well-known ML frequency estimator that is given as [13]

$$\widehat{f_0 T_s} = \arg\max_{fT_s\in\Psi}\left|\sum_{n=0}^{N-1} s^*(nT_s)g^*(nT_s)r(nT_s)e^{-j2\pi fT_s n}\right|^2 . \tag{5.43}$$

The frequency estimation is an intermediate stage for the joint channel estimation and so its accuracy is not as significant as that of the final total channel estimation (that contains both the fading and the frequency offset). However the frequency estimation study is

added to gain insight about the proposed algorithms. Table 5.2 summarises the properties of the different estimators considered in the simulation.

To start with, it is of significant importance to learn how to select the key parameters, Q and M so as to get the best performance of the proposed algorithms within the minimum complexity. For that reason, the reference estimators RMLF and RBC are examined first as they have the maximum accuracy and their RMSE can serve as lower bounds for the proposed estimators.

Figure 5.7 shows the SNR-dependent RMSE of (a) the RMLF estimator with different Q and (b) the RBC estimator with different M. As can be seen in Figure 5.7(a), for each SNR in the low range below 20 dB, the f_0T_s-RMSE reaches the same level for all Q values, and the increase in Q does not affect the accuracy in this range. For the highest SNR of 60 dB, the f_0T_s-RMSE reaches the minimum value only for $Q = 14$. For the other values of Q, there is a Q-dependent maximum SNR, denoted as SNR_{max}, above which the f_0T_s-RMSE diverges above that for the $Q = 14$. Increasing the value of Q leads to an increase in the SNR_{max}. These results reveal that according to the SNR_{max} implied by the channel, the value of Q needs to be adjusted to an optimum value Q_O that assures a high-accuracy performance over all the considered SNR range. The criterion for selecting Q_O is as follows.

- For the given SNR_{max}, the minimum required f_0T_s-RMSE (f_0T_s-RMSE_{min}) is determined from the f_0T_s-RMLF estimator's plot for $Q = 14$ in Figure 5.7(a), which is of a comparable level to that of the CRLB at that point.
- For that error, the required Q_O is the one that makes the final frequency step after all the iterations in the dichotomous fine search stage below f_0T_s-RMSE_{min}. Hence

$$\begin{aligned} &\frac{1}{N_{FFT}2^{Q_O}} < (f_0T_s\text{-RMSE}_{\text{min}}) \\ &\Rightarrow \quad Q_O > \log_2\left(\frac{1}{N_{FFT}\,(f_0T_s\text{-RMSE}_{\text{min}})}\right). \end{aligned} \tag{5.44}$$

This criterion is followed later on in the simulation results examining the proposed BJ and MLJ estimators (and the corresponding BF and MLF estimators), where SNR_{max} is assumed to be 30 dB, and for this case $Q_O = 8$.

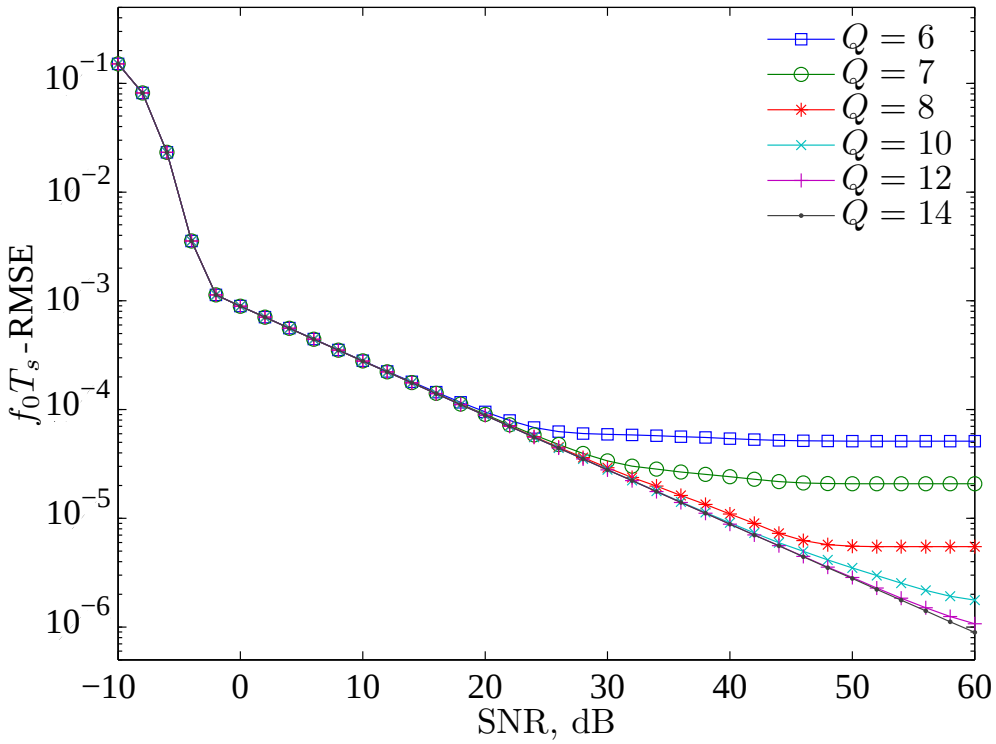

(a)

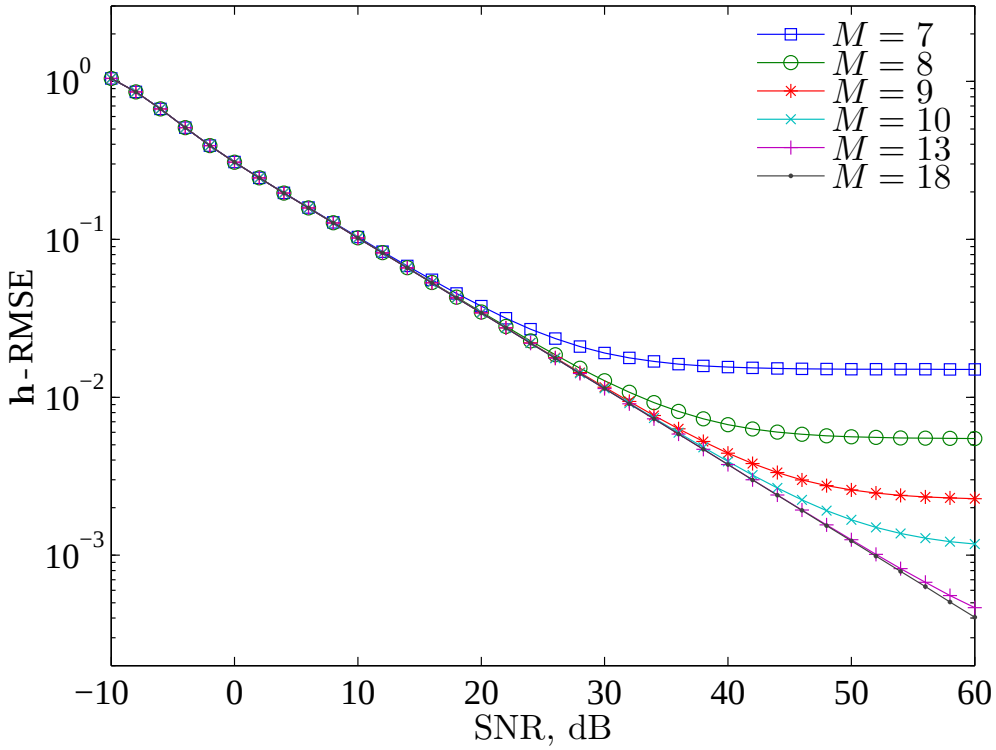

(b)

Figure 5.7: RMSE of the reference estimators for frequency-flat time-variant fading channels as a function of SNR; $N = 64$, $N_{FFT} = 256$, $f_0T_s = 0.01$ and $f_DT_s = 0.02$; (a) RMLF with $M = 18$ and different Q, and (b) RBC with $Q = 14$ and different M.

The same attribute is applied regarding the required value of M in the RBC estimator for getting the best accuracy over a certain SNR range. This can be seen in Figure 5.7(b), where the SNR_{max} defining the range of the best reached accuracy is directly related to M. For $\text{SNR}_{\text{max}} = 60$ dB, the required M_O is 18, whereas for a lower SNR_{max}, a lower value of M_O is sufficient. The value of M_O depends as well on the known $f_D T_s$. Therefore, the best way to obtain the value of M_O is according to the following criterion.

- For the given SNR_{max}, the $\mathbf{h}$-RMSE_{min} is determined from the RBC estimator's plot for $M = 18$ in Figure 5.7(b).
- For that error, γ is determined from the relationship between the approximation error and the sampling factor given for the optimal splines in [43].
- For that γ, P is determined from (5.14) according to the given $f_D T_s$.
- For that P, the required M_O is determined from (5.12) according to the given N and T_s.

For the simulation examining the proposed BJ and MLJ estimators that is followed later on, SNR_{max} is assumed to be 30 dB, and the desired M_O depends on the given $f_D T_s$ according to the above criterion and is determined such that the sampling factor $\gamma = (M-3)/f_D T_s(N-1)$ is approximately 5 for the BJ estimator, and 4 for the MLJ estimator (*e.g.* for $f_D T_s = 0.02$, $M_O = 9$ for the BJ estimator and $M_O = 8$ for the MLJ estimator).

It is worth mentioning that the simulation results described above in Figure 5.7(b) were carried out first for $Q = 14$ so as to concentrate the attention on the influence of changing M without being affected by a low Q. Then, the simulations were repeated for the optimum values Q_O deducted from Figure 5.7(a) according to the best reached SNR range for a certain M obtained in the first time. Identical results to that shown in Figure 5.7(b) have been obtained. The same was done with the simulations in Figure 5.7(a), starting with $M = 18$ for all Q values, then repeating with the optimum M_O.

Figure 5.8 shows the SNR-dependent $f_0 T_s$-RMSE of the considered frequency estimators (mentioned in Table 5.2) for Doppler frequencies $f_D T_s = 0.01, 0.02, 0.03$ ($M = 6, 9, 12$ for the BF estimator, and $M = 6, 8, 11$ for the RMLF and MLF estimators). It can be seen that the $f_0 T_s$-RMSE of the BF estimator is considerably higher

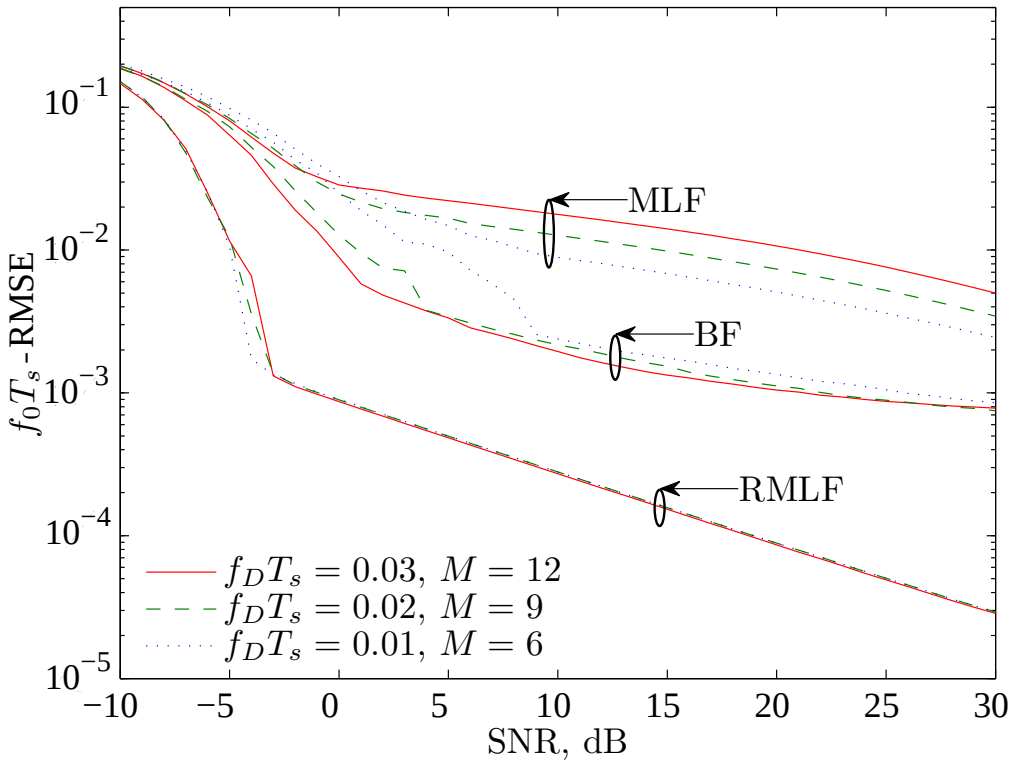

Figure 5.8: f_0T_s-RMSE of the proposed BS-based frequency offset estimators for frequency-flat time-variant fading channels as a function of SNR for different values of f_DT_s (and M); $N = 64$, $N_{FFT} = 256$, $f_0T_s = 0.01$ and $Q = 8$.

than that of the RMLF estimator over all the considered SNR range. In addition, the threshold SNR (SNR_{th}) below which the f_0T_s-RMSE increases more rapidly, is becoming higher for lower f_DT_s. The f_0T_s-RMSE above the SNR_{th} is approximately the same for the different f_DT_s, with slightly higher levels for $f_DT_s = 0.01$. The performance is even poorer for the MLF estimator. It can be noticed that below the SNR_{th}, the f_0T_s-RMSE is approximately the same for the different f_DT_s, and with slightly higher SNR_{th} for lower f_DT_s. However, the f_0T_s-RMSE differs significantly above the SNR_{th} and is higher for higher f_DT_s.

The poor frequency offset estimation is expected and due to the effect of the Doppler frequency in the time-variant fading channels. In practical scenarios, the final joint channel estimation $\hat{\mathbf{h}}$ (that contains the fading process and the frequency offset) is of more significant importance for the receivers. Therefore, and as far as it is concerned in the proposed joint channel estimator, there is no need to employ more complicated techniques for getting an accurate individual estimate of f_0T_s.

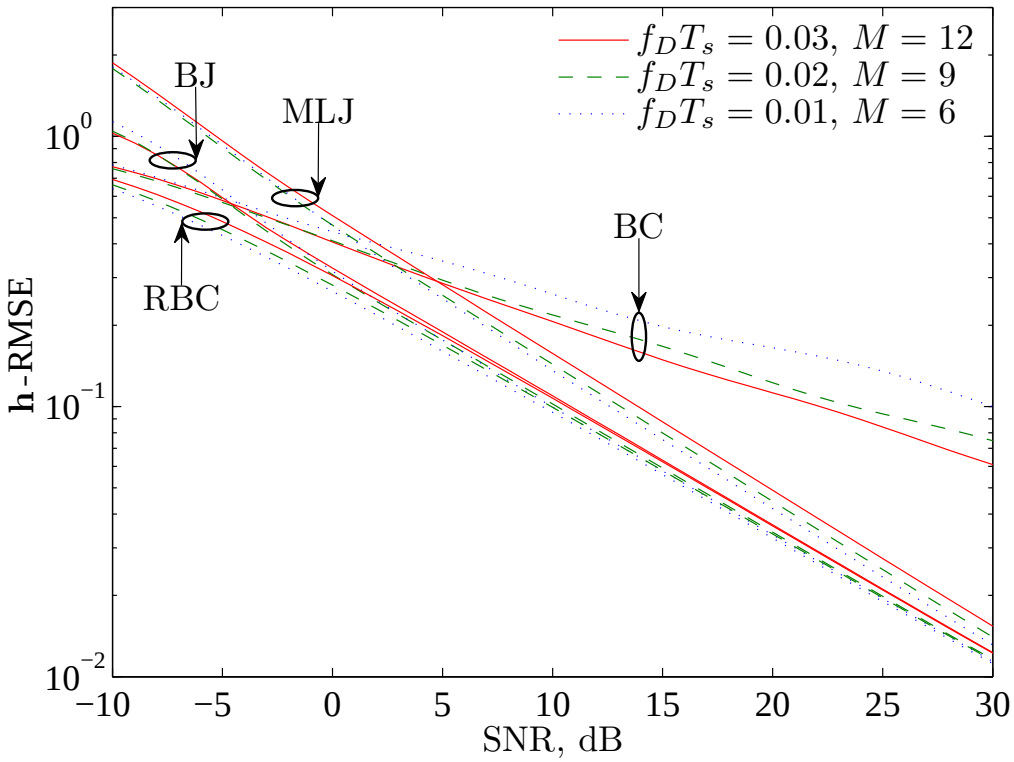

Figure 5.9: $\mathbf{h}$-RMSE of the proposed BS-based joint estimators for frequency-flat time-variant fading channels as a function of SNR for different values of f_DT_s (and M); $N = 64$, $N_{FFT} = 256$, $f_0T_s = 0.01$ and $Q = 8$.

Figure 5.9 shows the SNR-dependent $\mathbf{h}$-RMSE of the considered channel estimators for Doppler frequencies $f_DT_s = 0.01, 0.02, 0.03$ ($M = 6, 9, 12$ for the RBC and BJ estimators, $M = 6, 8, 11$ for the MLJ estimator, and $M = 7, 9, 11$ for the BC estimator). It can be seen that the $\mathbf{h}$-RMSE of the proposed BJ estimator is very close to that of the (ideal) RBC estimator throughout the considered range of SNRs above 0 dB. A slight shift can be noticed between $\mathbf{h}$-RMSE plots that correspond to different f_DT_s, similarly to that of the RBC estimator. But in general, a high-accuracy performance is obtained for all values of f_DT_s. The same behavior can be seen for the proposed MLJ estimator, except for the small loss in the accuracy that is more noticeable at low SNRs. This is due to the absence of the prior information of $\mathbf{R}_a$ and σ^2. For the BC estimator, a poor performance in general can be seen, with $\mathbf{h}$-RMSE that increases for lower f_DT_s. This shows the inappropriateness of such estimators and gives an idea about the improvement offered by considering the frequency offset for the new joint estimators.

Figure 5.10 shows the f_0T_s-dependent $\mathbf{h}$-RMSE for different f_DT_s (and M values as

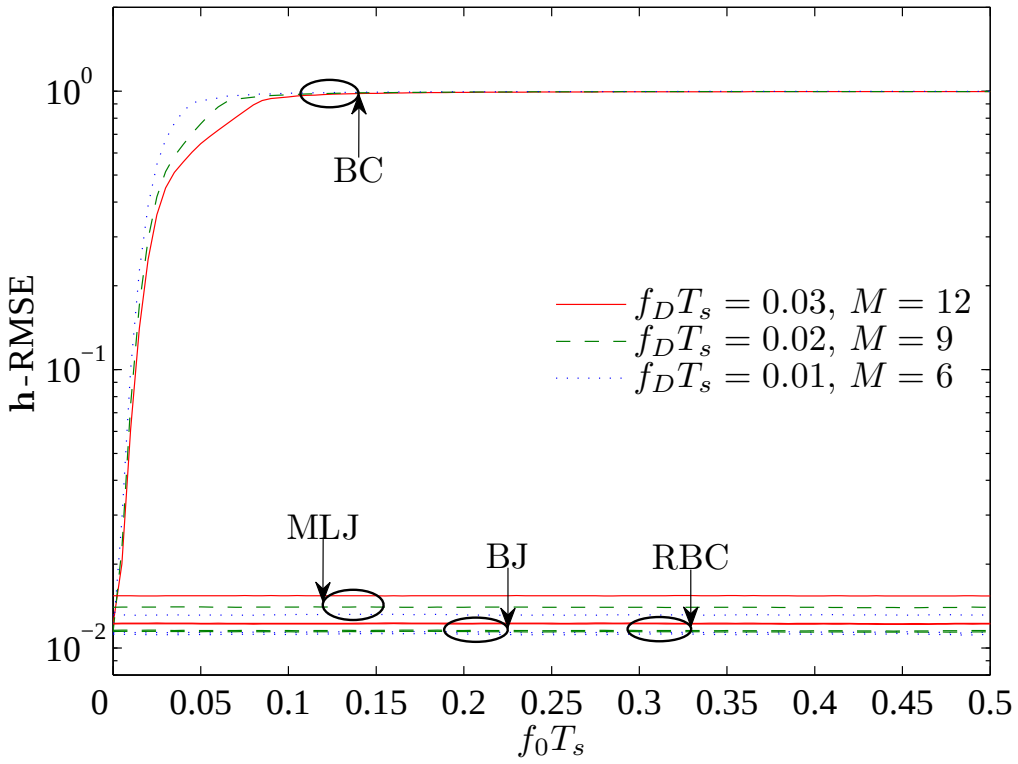

Figure 5.10: **h**-RMSE of the proposed BS-based joint estimators for frequency-flat time-variant fading channels as a function of f_0T_s for different values of f_DT_s (and M); $N = 64$, $N_{FFT} = 256$, $Q = 8$ and SNR $= 30$ dB.

mentioned above). It can be seen that for the proposed BJ estimator, a high-accuracy performance in general is obtained for all the values of f_DT_s and throughout the entire wide f_0T_s range, where the **h**-RMSE is constant and almost the same as that of the (ideal) RBC estimator. This is true as well for the proposed MLJ estimator with the **h**-RMSE plots being slightly upward shifted by the same amount over all the f_0T_s range and for all the f_DT_s values. However, the **h**-RMSE of the BC estimator increases rapidly diverging from that of the RBC estimator at the beginning of the f_0T_s range. This expresses a poor and impractical performance even with a low frequency offset.

Figure 5.11 shows the f_DT_s-dependent **h**-RMSE for different frequency offsets f_0T_s, $M = 16$ for the RBC, BJ and BC estimators, and $M = 12$ for the MLJ estimator. For the proposed BJ estimator, a high-accuracy performance can be seen with the **h**-RMSE having the same level for all the f_0T_s values and practically coincides with that of the (ideal) RBC estimator over all the considered f_DT_s range. The **h**-RMSE level however can be seen slightly increasing when f_DT_s increases. For the proposed MLJ estimator,

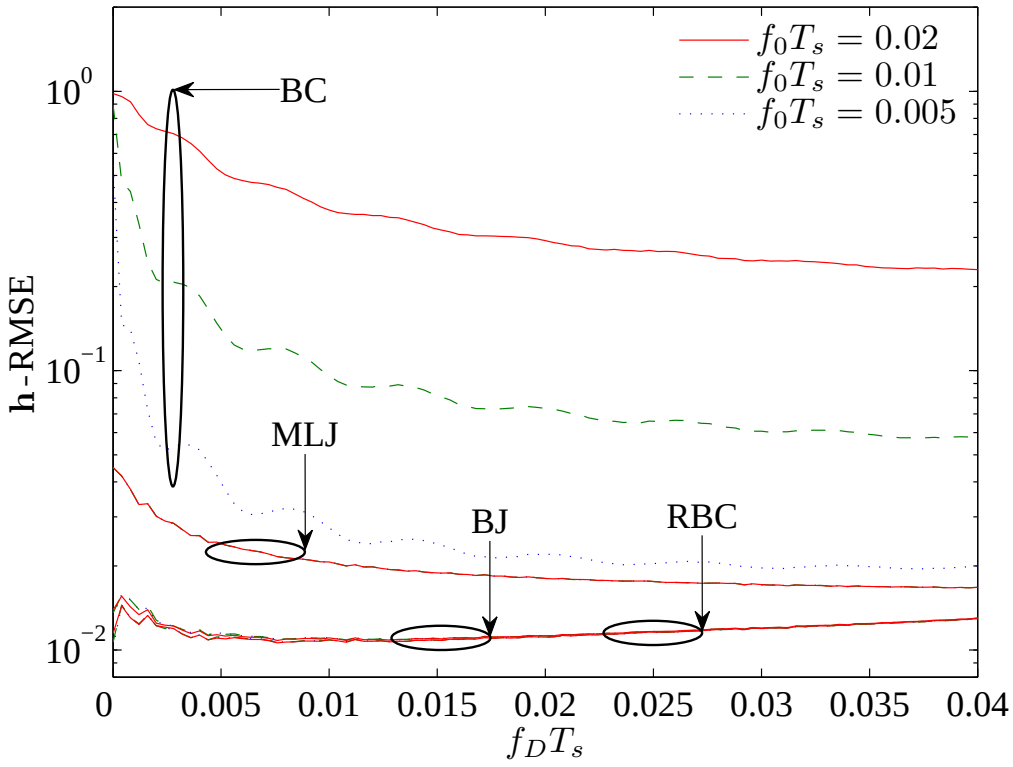

Figure 5.11: $\mathbf{h}$-RMSE of the proposed BS-based joint estimators for frequency-flat time-variant fading channels as a function of f_DT_s for different values of f_0T_s; $N = 64$, $N_{FFT} = 256$, $Q = 8$ and SNR $= 30$ dB.

the $\mathbf{h}$-RMSE is the same for all the f_0T_s values but with higher level than that of the RBC estimator. This additional error decreases slowly with the increase in f_DT_s. However, the $\mathbf{h}$-RMSE of the BC estimator is varied significantly with f_0T_s. This error can approach that of the MLJ estimator for only the low frequency offset of 0.005 and high f_DT_s. Apart from that, a significant error is obtained.

5.8.1 Performance Analysis of Frequency Offset Estimators

The performance of the proposed BF and MLF estimators depends on the parameters N_{FFT}, Q and M. Simulation results (not shown here) reveal that the minimum required value of N_{FFT} to achieve an accurate frequency offset estimation is $4N$, which is in agreement with [44, 48]. The optimal value of Q depends on the maximum SNR, and for a range of interest up to 30 dB, we use $Q = 8$. These values are used in the simulation.

However, the optimal value of M is not the same in the two proposed estimators, and it depends on SNR and $f_D T_s$. We investigate the performance of these estimators for different values of M, SNR and $f_D T_s$ to get a better understanding of the optimal value of M to be used for each estimator.

Figure 5.12 shows the M-dependent $f_0 T_s$-RMSE of the proposed frequency offset estimators for different $f_D T_s$. We use cubic ($\eta = 3$) splines for $M > 3$, and zero-order ($\eta = 0$), linear ($\eta = 1$) and parabolic ($\eta = 2$) splines for $M = 1$, 2 and 3, respectively. The $f_0 T_s$-RMSE of both estimators decreases as M increases. This is due to the decrease of the model mismatching error [43]. However, for the MLF estimator, the $f_0 T_s$-RMSE reaches a minimum at a certain optimal M and increases with further increase of M. The MLF estimator is more sensitive to the choice of M for a lower $f_D T_s$ and a lower SNR. On the other hand, the $f_0 T_s$-RMSE of the BF estimator continues to decrease before reaching a floor level at a certain threshold M. Thus, the exploitation of the fading covariance matrix $\mathbf{R}_g$ and the noise variance σ^2 in the BF estimator allows achieving a higher-accuracy performance compared to that of the MLF estimator. In both estimators, a greater value of optimal/threshold M is required as SNR or $f_D T_s$ increases, where the threshold M of the BF estimator is always greater than the optimal M of the MLF estimator.

Figure 5.13 shows the $f_D T_s$-dependent $f_0 T_s$-RMSE of the estimators for different M. For the BF estimator, a high-accuracy performance is achieved for all Doppler frequencies up to a certain value (depending on M), above which the $f_0 T_s$-RMSE increases rapidly. Apart from the very low Doppler frequencies, the increase in the minimum $f_0 T_s$-RMSE of the BF estimator is hardly noticeable as $f_D T_s$ increases. However, the MLF estimator achieves its best performance for a certain $f_D T_s$-range (depending on M), where the $f_0 T_s$-RMSE increases rapidly outside that range. This range becomes wider for higher Doppler frequencies.

It is seen that the optimal choice of M depends on SNR and $f_D T_s$. In the following simulation, the performance is investigated for SNR-range up to 30 dB, using one value of M for the entire range. According to Figure 5.12, the threshold M at SNR $= 30$ dB will guarantee a best performance at SNR ≤ 30 dB for the BF estimator. However, for the MLF estimator, since there is a degradation in the performance as M increases higher than

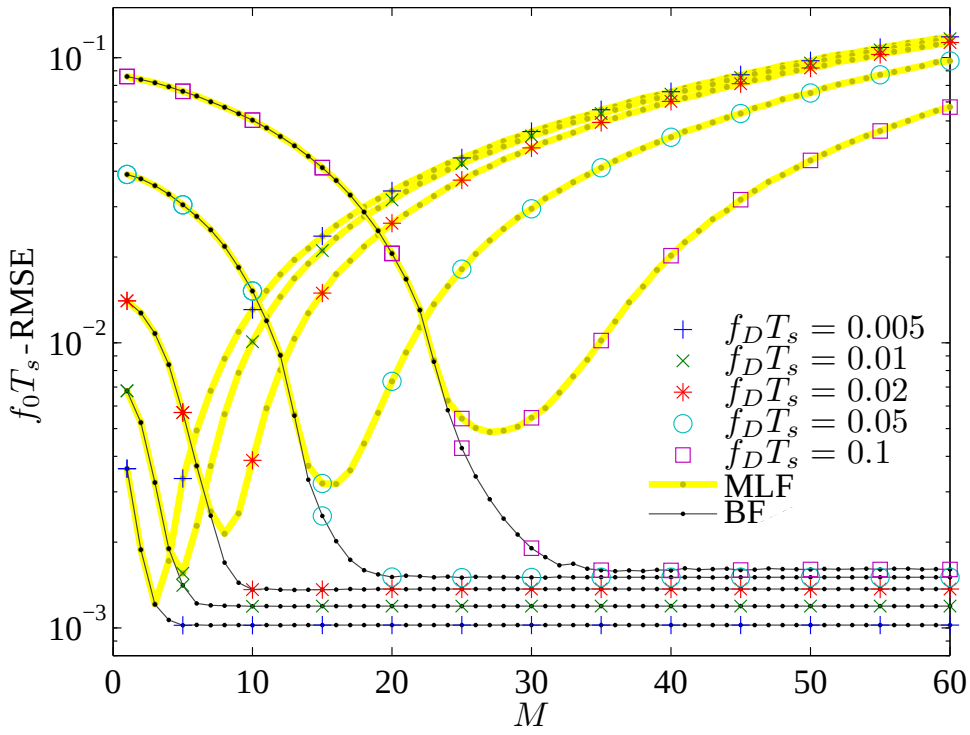

(a)

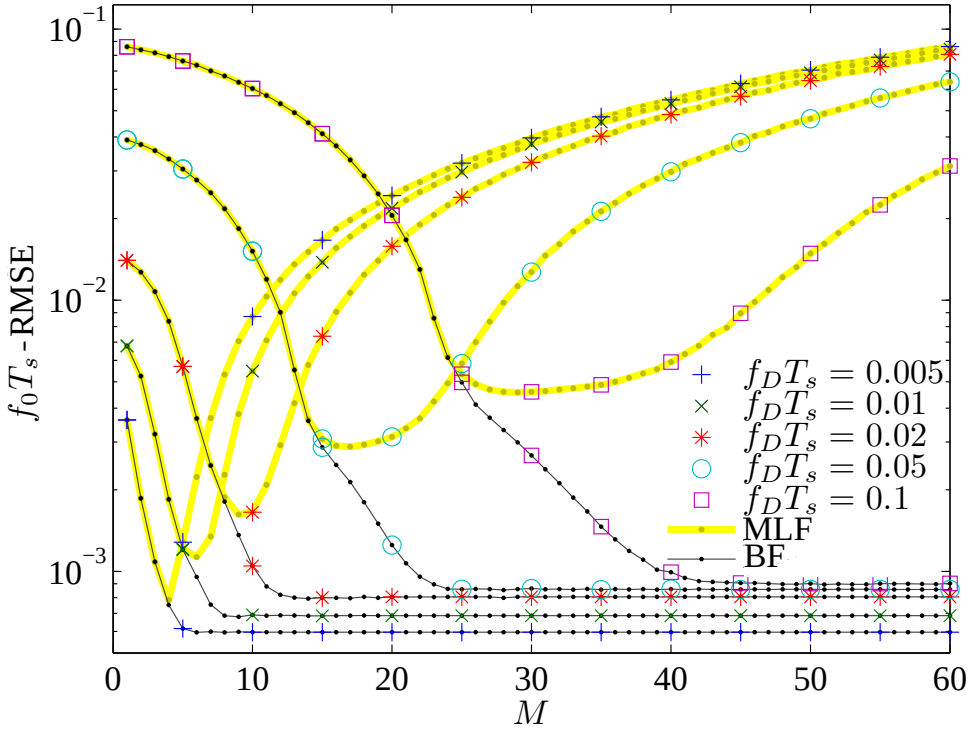

(b)

Figure 5.12: f_0T_s-RMSE of the proposed BS-based frequency offset estimators for frequency-flat time-variant fading channels as a function of M for different values of f_DT_s; $N = 100$, $N_{FFT} = 4N$, $f_0T_s = 0.0123$ and $Q = 8$; (a) SNR $= 15$ dB and (b) SNR $= 30$ dB.

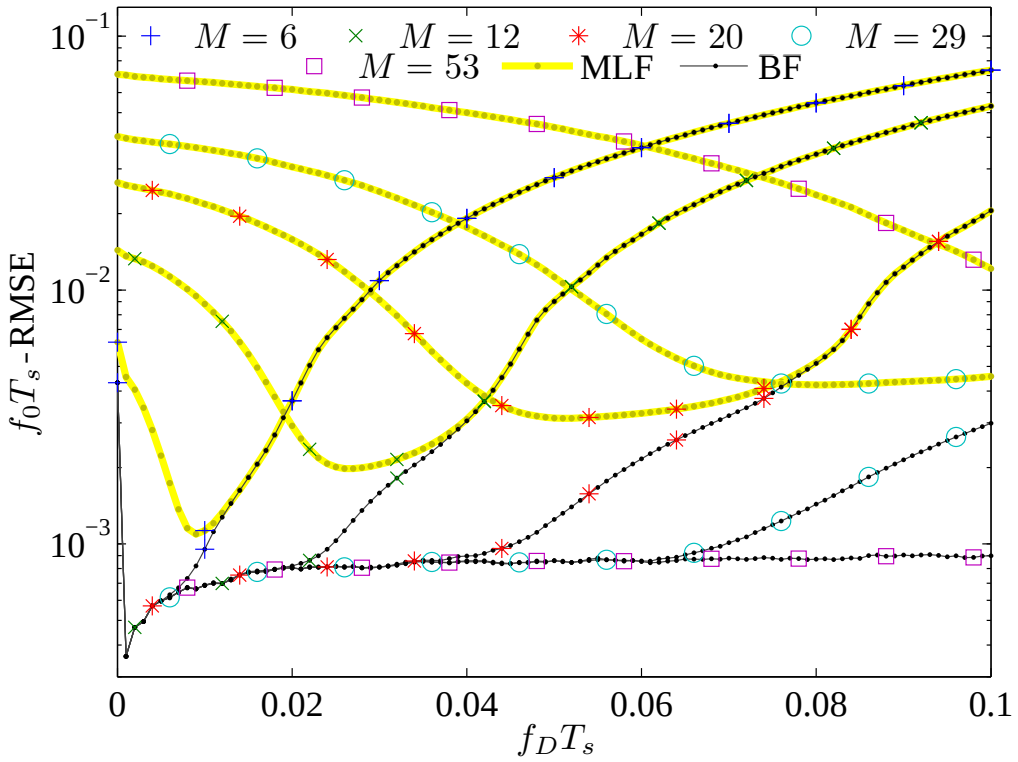

Figure 5.13: f_0T_s-RMSE of the proposed BS-based frequency offset estimators for frequency-flat time-variant fading channels as a function of f_DT_s for different values of M; $N = 100$, $N_{FFT} = 4N$, $f_0T_s = 0.0123$, $Q = 8$ and SNR $= 30$ dB.

the optimal M, using the optimal M at SNR $= 30$ dB will not allow a good performance for lower SNRs. Other simulation results (not presented here) have shown that the optimal M at SNR $= 15$ dB (midrange) provides the best trade off between performance at low and high SNR-range. For that reason, the optimal M of the MLF estimator is chosen such that to achieve the best performance at SNR $= 15$ dB, whereas the threshold M of the BF estimator is chosen such that to achieve the best performance at SNR $= 30$ dB. Simulation results for different values of N (not presented here) have shown that the optimal choice of M can be determined such that the sampling factor $\gamma = 1/(f_DT_sP)$ [43], for SNR-range of interest up to 30 dB, is

$$\gamma = \frac{M-\eta}{f_DT_s(N-1)} \approx \begin{cases} 2.5\,, & \text{for MLF estimator}\,, \\ 5\,, & \text{for BF estimator}\,. \end{cases} \tag{5.45}$$

Now, the performance of the proposed frequency offset estimators is compared with the performance of known frequency offset estimators that rely on the normalized corre-

lation samples

$$R_x(mT_s) = \frac{1}{N-m}\sum_{n=m}^{N-1} x(nT_s)x^*(nT_s - mT_s)\,, \tag{5.46}$$

their phases $\varphi(mT_s) = \arg\{R_x(mT_s)\}$, and/or their phase difference $\Delta\varphi(mT_s) = \varphi(mT_s) - \varphi(mT_s - T_s)$ where $x(nT_s) = r(nT_s)s^*(nT_s)$. In our simulation, we consider the following estimators:

- A frequency estimator proposed in [7] (referred to as the SL estimator) is given by

$$\widehat{F}_0 = \frac{\varphi(LT_s)}{2\pi L}\,. \tag{5.47}$$

- An estimator presented in [8] (referred to as the BS estimator) is given by

$$\widehat{F}_0 = \frac{1}{2\pi L}\sum_{m=1}^{L} \Delta\varphi(mT_s)\,. \tag{5.48}$$

- An estimator in [8] (referred to as the NLS estimator) is given by

$$\widehat{F}_0 = \frac{1}{2}\arg\max_{F\in\Psi} \Re\left\{\sum_{m=0}^{L} R_x^2(mT_s)e^{-j2\pi mF}\right\}\,. \tag{5.49}$$

- A simplified NLS estimator proposed in [10,11] (referred to as the SNLS estimator) is given by

$$\widehat{F}_0 = \frac{\sum_{m=1}^{L} m\left|R_x(mT_s)\right|^2\varphi(mT_s)}{2\pi\sum_{m=1}^{L} m^2\left|R_x(mT_s)\right|^2}\,. \tag{5.50}$$

- To extend the frequency acquisition range of the SNLS estimator, a frequency estimator proposed in [10] (referred to as the SNLSu estimator) is given as in (5.50) but with $\varphi(mT_s)$ being replaced with the unwrapped phase

$$\varphi_u(mT_s) = \varphi_u(mT_s - T_s) + \arctan\left\{\frac{\sin\left(\Delta\varphi(mT_s)\right)}{\cos\left(\Delta\varphi(mT_s)\right)}\right\}, \tag{5.51}$$

  where $\varphi_u(0) = \varphi(0)$.

- An approximated NLS estimator proposed in [11] (referred to as the ANLS estimator) is given by

$$\widehat{F}_0 = \frac{\sum_{m=1}^{L}\left[\sum_{k=m}^{L-1} k\left|R_x(mT_s)\right|^2\right]\Delta\varphi(mT_s)}{2\pi\sum_{m=1}^{L} m^2\left|R_x(mT_s)\right|^2}\,. \tag{5.52}$$

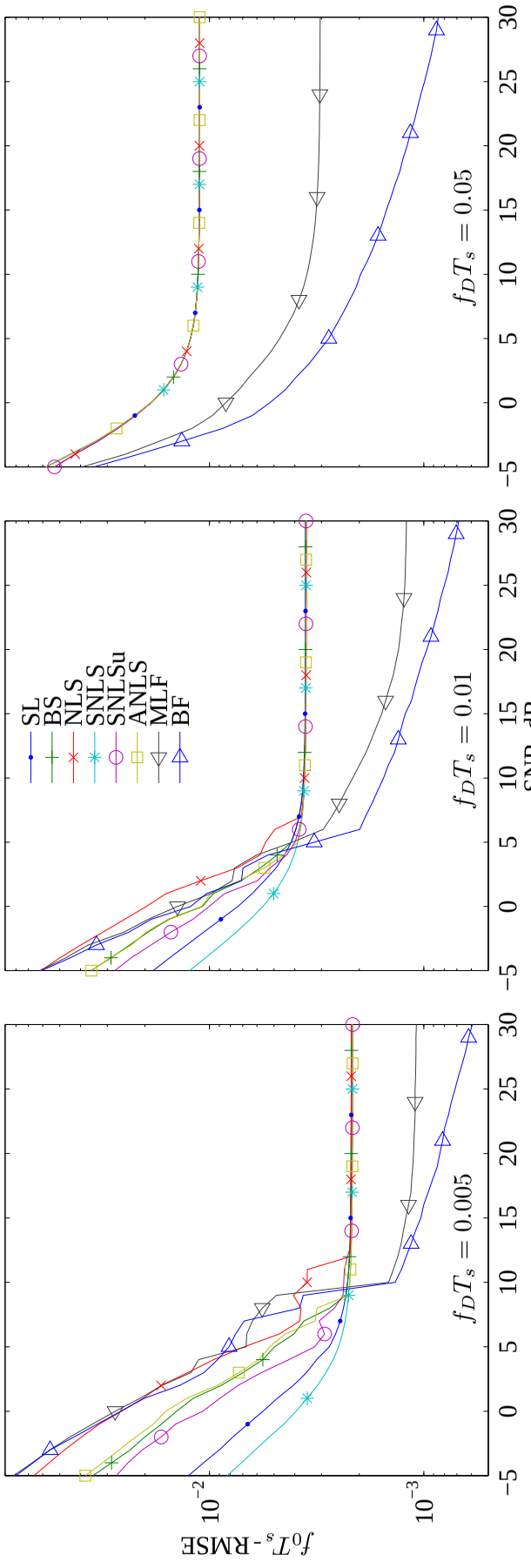

Figure 5.14: f_0T_s-RMSE of the frequency offset estimators for frequency-flat time-variant fading channels as a function of SNR for slow, moderate and fast fading channels; $N = 100$ and $f_0T_s = 0.0123$.

Table 5.3: Optimal Choice of M for the Proposed Frequency Offset Estimators for Frequency-Selective Time-Variant Fading Channels.

	Optimal M	**Threshold M**
$f_D T_s$	**MLF**	**BF**
0.005	3	5
0.01	5	8
0.05	15	28

Table 5.4: Optimal Choice of L for the Correlation-Based Frequency Offset Estimators for Frequency-Selective Time-Variant Fading Channels Considered in the Simulation.

	Optimal L					
$f_D T_s$	**BS**	**SL**	**NLS**	**SNLS**	**SNLSu**	**ANLS**
0.005	9	9	12	9	8	9
0.01	5	5	4	5	5	5
0.05	1	1	1	1	1	1

Figure 5.14 shows the SNR-dependent f_0T_s-RMSE of the frequency offset estimators in the slow ($f_DT_s = 0.005$), moderate ($f_DT_s = 0.01$) and fast ($f_DT_s = 0.05$) fading channels. For the proposed estimators, we use values of M that satisfy (5.45) as recorded in Table 5.3. The optimal choice of L for the correlation-based estimators are summarized in Table 5.4 and obtained according to simulation results not shown here. For all scenarios, there exists a threshold SNR (SNR_{th}) below which the f_0T_s-RMSE increases rapidly. The proposed BF and MLF estimators outperform the correlation-based estimators in all the fading channels at SNR $>$ SNR_{th}. The BF estimator outperforms the MLF estimator. For all estimators, for lower f_DT_s, SNR_{th} is higher and f_0T_s-RMSE at SNR $>$ SNR_{th} is smaller. For SNR $<$ SNR_{th}, the f_0T_s-RMSE depends on the frequency acquisition range [47]. The SL and SNLS estimators possess a narrow (L-dependent) frequency acquisition range of $\psi = 1/L$ [7, 11], which explains the relatively low f_0T_s-RMSE. For the proposed estimators, the SNR_{th} and the f_0T_s-RMSE for SNR $<$ SNR_{th} depend on the frequency acquisition range, and in Figure 5.14, the wide ($\psi = 1$) acquisition range is used.

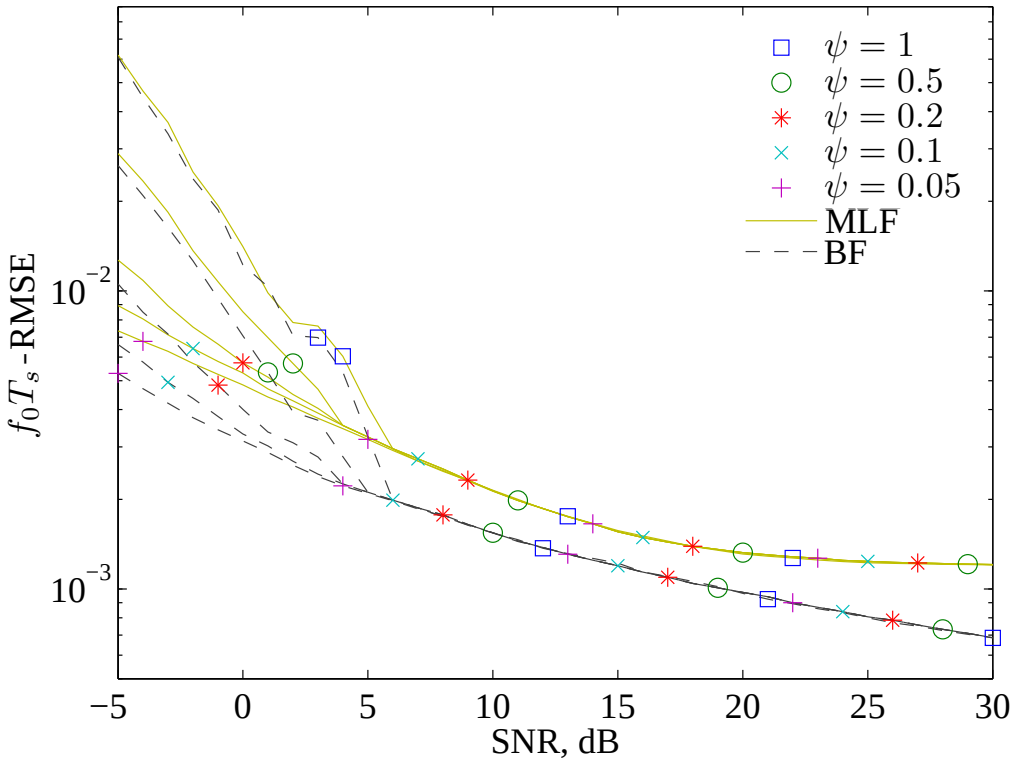

Figure 5.15: f_0T_s-RMSE of the proposed BS-based frequency offset estimators for frequency-flat time-variant fading channels as a function of SNR for different values of ψ; $N = 100$, $N_{FFT} = 4N$, $f_0T_s = 0.0123$, $f_DT_s = 0.01$, $Q = 8$, $M = 5$ for MLF and $M = 8$ for BF.

Figure 5.15 shows the SNR-dependent f_0T_s-RMSE of the proposed frequency offset estimators for different ψ, where $f_0T_s = 0.0123$ and $f_DT_s = 0.01$. It can be seen that using a narrower frequency acquisition range leads to an improvement in the performance at SNR $<$ SNR$_{\text{th}}$. This demonstrates the superiority of the proposed frequency offset estimators over the correlation-based estimators in having an adjustable frequency acquisition range (up to $\psi = 1$).

Figure 5.16 shows the f_0T_s-dependent f_0T_s-RMSE of the frequency offset estimators for $f_DT_s = 0.01$ and SNR $= 10$ dB. The value of L for the correlation-based estimators is selected according to Table 5.4. Both proposed estimators possess the widest frequency acquisition range among the investigated estimators. The theoretical frequency acquisition range is $\psi = 1$ for the BF, MLF, ANLS and BS estimators, $\psi = 0.5$ for the SNLSu and NLS estimators, and $\psi = 1/L = 0.2$ for the SNLS and SL estimators. This can be achieved at high SNRs, whereas for SNR $= 10$ dB, the real frequency acquisition

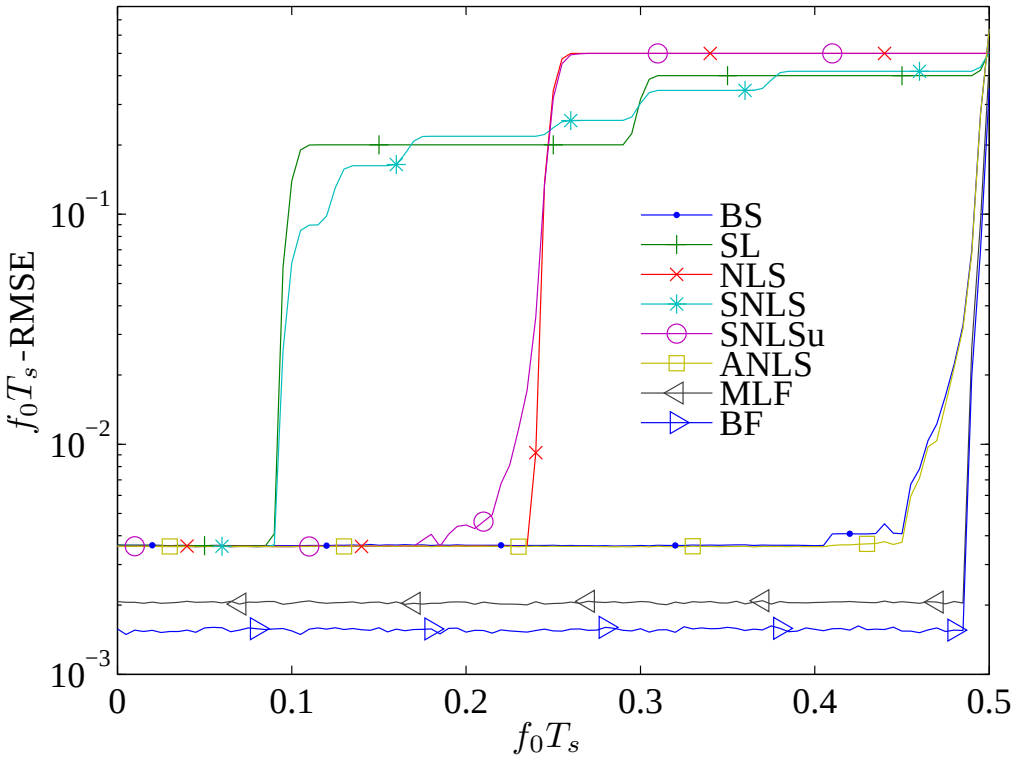

Figure 5.16: f_0T_s-RMSE of the frequency offset estimators for frequency-flat time-variant fading channels as a function of f_0T_s; $N = 100$, $f_DT_s = 0.01$, SNR $= 10$ dB, $M = 4$ for MLF and $M = 6$ for BF.

range of the estimators is slightly lower than the theoretical one. The proposed estimators outperform the correlation-based estimators over all the investigated range of f_0T_s.

5.8.2 Performance Analysis of Joint Channel and Frequency Offset Estimators

The performance of the proposed joint channel and frequency offset estimators is compared with the performance of an ideal reference Bayesian channel (RBC) estimator, where the frequency offset is known. This estimator is given as in (5.32) but with $\widehat{F}_0$ being replaced with f_0T_s. Another estimator is also introduced for comparison, the Bayesian channel (BC) estimator, which ignores the frequency offset and is given by

$$\hat{\mathbf{h}} = \mathbf{B}\left(\mathbf{B}^H\mathbf{S}^H\mathbf{S}\mathbf{B} + \sigma^2\mathbf{R}_a^{-1}\right)^{-1}\mathbf{B}^H\mathbf{S}^H\mathbf{r}\,. \tag{5.53}$$

Table 5.5 summarizes properties of the estimators considered in the simulation.

Table 5.5: Channel Estimators for Frequency-Selective Time-Variant Fading Channels Considered in the Simulation.

Algorithm	**Frequency Offset**	**Channel**	**Equation**
RBC	Known	Random	(5.32)
BC	Ignored	Random	(5.53)
BJ	Deterministic	Random	(5.32)
MLJ	Deterministic	Deterministic	(5.37)

Table 5.6: Optimal Choice of M for the Proposed Estimators for Frequency-Selective Time-Variant Fading Channels at SNR $= 30$ dB.

	Optimal M		**Threshold M**			
$f_D T_s$	**MLF**	**MLJ**	**RBC**	**BC**	**BJ**	**BF**
0.01	6	7	8	10	8	8
0.02	9	11	13	13	13	13
0.03	12	15	18	16	18	18

Figure 5.17 shows the M-dependent $\mathbf{h}$-RMSE of the joint estimators for different $f_D T_s$. The best performance of the MLJ estimator is achieved at an optimal value of M, above which the $\mathbf{h}$-RMSE increases slowly. However, the BJ estimator achieves a better performance for high M values, and the $\mathbf{h}$-RMSE reaches a floor level at a threshold M depending on $f_D T_s$. For a higher $f_D T_s$, the estimators require a higher M.

Figure 5.18 shows the $f_D T_s$-dependent $\mathbf{h}$-RMSE of the joint estimators for different M. For the BJ estimator, an optimal performance can be seen for Doppler frequencies lower than a certain value (depending on M), above which the $\mathbf{h}$-RMSE increases rapidly. Using a greater value of M allows maintaining the optimal performance for a wider range of Doppler frequencies. The optimal performance is seen to cover the Doppler frequencies up to $f_D T_s = 0.1$ using $M = 53$. However for the MLJ estimator, and depending on the value of M, a good performance can be achieved for a certain $f_D T_s$ range, above which the $\mathbf{h}$-RMSE increases rapidly. For a greater value of M, this range becomes wider and

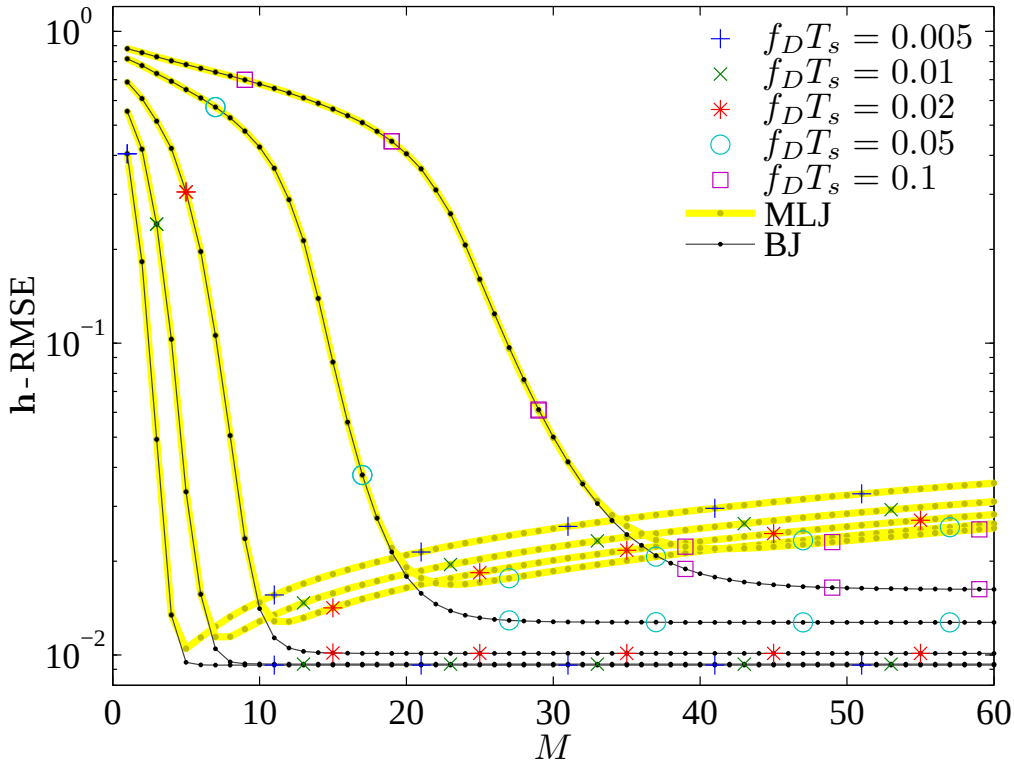

Figure 5.17: $\mathbf{h}$-RMSE of the proposed BS-based joint estimators for frequency-flat time-variant fading channels as a function of M for different values of f_DT_s; $N = 100$, $N_{FFT} = 4N$, $f_0T_s = 0.0123$, $Q = 8$ and SNR $= 30$ dB.

covers higher Doppler frequencies.

Simulation results (not presented here) have shown that the optimal M also depends on SNR and N, and an optimal/threshold value of M throughout an SNR-range of interest up to 30 dB is determined such that the sampling factor is

$$\gamma \approx \begin{cases} 4\,, & \text{for MLJ estimator}\,, \\ 5\,, & \text{for BJ estimator}\,. \end{cases} \tag{5.54}$$

Figure 5.19 shows the SNR-dependent $\mathbf{h}$-RMSE of the channel estimators for different f_DT_s. The value of M for the estimators is selected according to Table 5.6. The $\mathbf{h}$-RMSE of the BJ estimator is very close to that of the (ideal) RBC estimator throughout the SNR-range. For all the values of f_DT_s, a high-accuracy performance in general is obtained. The same behavior can be seen for the proposed MLJ estimator, except for a slight increase of $\mathbf{h}$-RMSE due to the absence of the prior information of $\mathbf{R}_a$ and σ^2. However, the BC

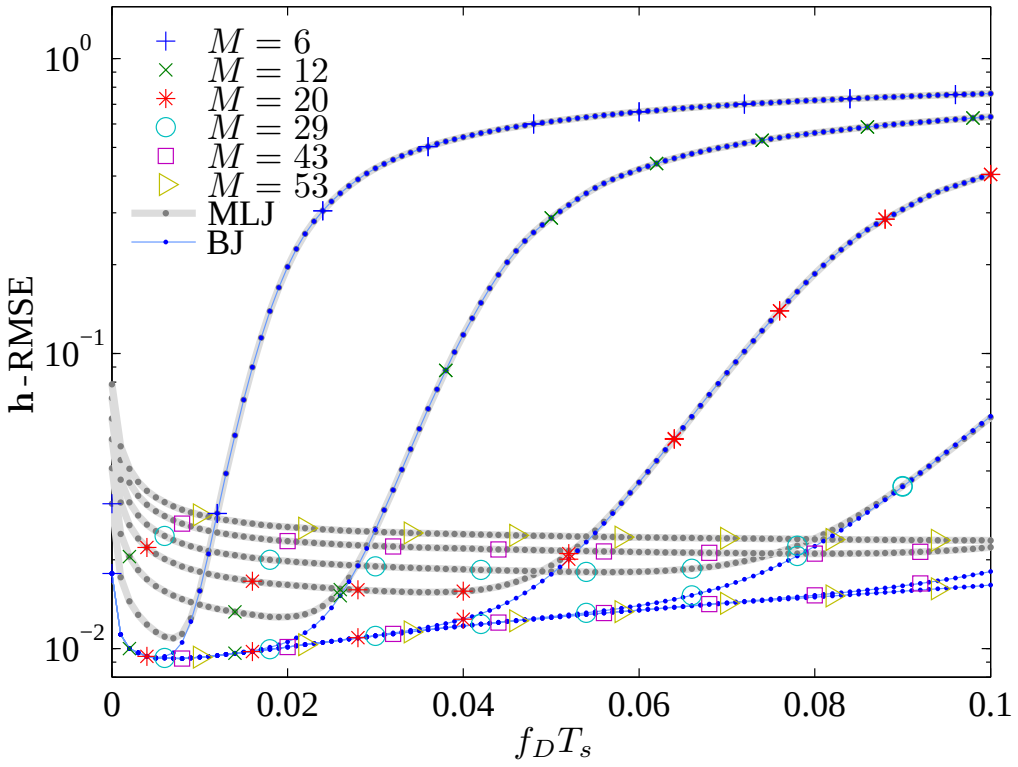

Figure 5.18: **h**-RMSE of the proposed BS-based joint estimators for frequency-flat time-variant fading channels as a function of $f_D T_s$ for different values of M; $N = 100$, $N_{FFT} = 4N$, $f_0 T_s = 0.0123$, $Q = 8$ and SNR $= 30$ dB.

estimator demonstrates a poor performance in all scenarios.

Figure 5.20 shows the $f_0 T_s$-dependent RMSE of the channel estimators in Figure 5.20(a) and the frequency offset estimators in Figure 5.20(b) for different $f_D T_s$. We use the values of M as summarized in Table 5.6. For the BJ estimator and all Doppler frequencies, a high-accuracy performance can be seen throughout the entire wide frequency acquisition range, where the **h**-RMSE is constant and almost the same as that of the (ideal) RBC estimator. The same is seen for the proposed MLJ estimator with the **h**-RMSE plots being slightly upward shifted over all $f_0 T_s$ range and for all the $f_D T_s$ values. However, the **h**-RMSE of the BC estimator increases rapidly diverging from that of the RBC estimator as $f_0 T_s$ increases. This shows a poor performance of such channel estimators, even for low frequency offset values. The proposed frequency offset estimators, as seen in Figure 5.20(b), possess a wide frequency acquisition range ($\psi \approx 1$) for all the examined Doppler frequencies.

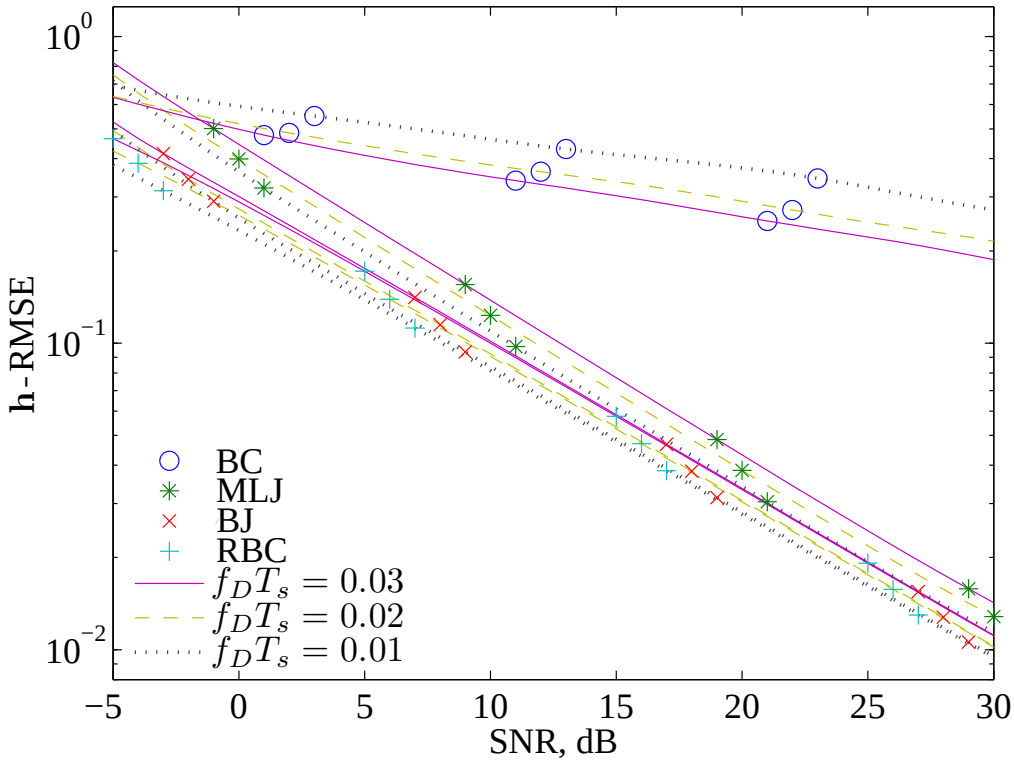

Figure 5.19: $\mathbf{h}$-RMSE of the proposed BS-based joint estimators for frequency-flat time-variant fading channels as a function of SNR for different values of $f_D T_s$; $N = 100$, $N_{FFT} = 4N$, $f_0 T_s = 0.0123$ and $Q = 8$.

Finally, a valuable characteristic of the proposed joint estimators is investigated below. So far in the simulation, we used $N_{FFT} = 4N = 400$ and $Q = 8$, which is a necessity for a high-accuracy frequency offset estimation for SNR up to 30 dB. However, the proposed joint estimators do not require that much accuracy in the frequency offset estimation and can achieve a good performance without zero-padding the processed signal (*i.e.* with $N_{FFT} = N$) and using a few dichotomous iterations. Figure 5.21 shows the $f_0 T_s$-dependent RMSE for different N_{FFT} and Q, where $f_D T_s = 0.01$, SNR $= 30$ dB and $M = 8$. In Figure 5.21(a), the $\mathbf{h}$-RMSE of the BJ estimator is plotted against that of the ideal RBC estimator, whereas Figure 5.21(b) illustrates the $f_0 T_s$-RMSE of the BF estimator. For the BF estimator, a high-accuracy frequency offset estimation performance, as seen in Figure 5.21(b), is only achieved for $N_{FFT} = 400$ and $Q = 8$. Using $N_{FFT} = 100$ and lower Q leads to a significant performance degradation. For the BJ estimator, a performance very close to that of the ideal RBC estimator is achieved for $N_{FFT} = 400$ and $Q = 8$. However, the performance is still very good when using $N_{FFT} = 100$ and $Q = 4$,

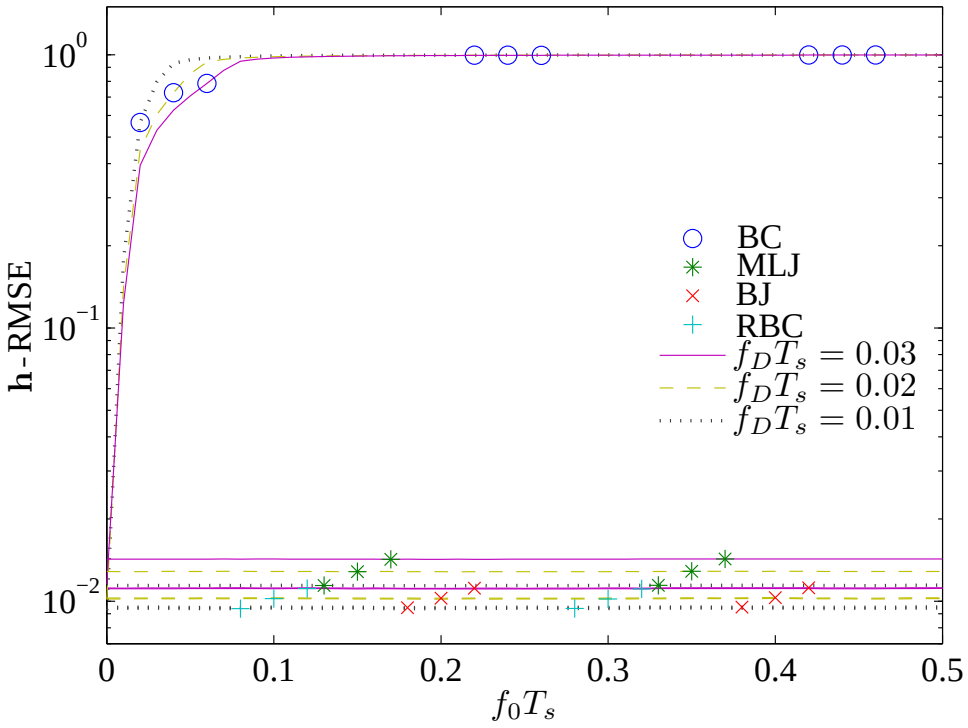

(a)

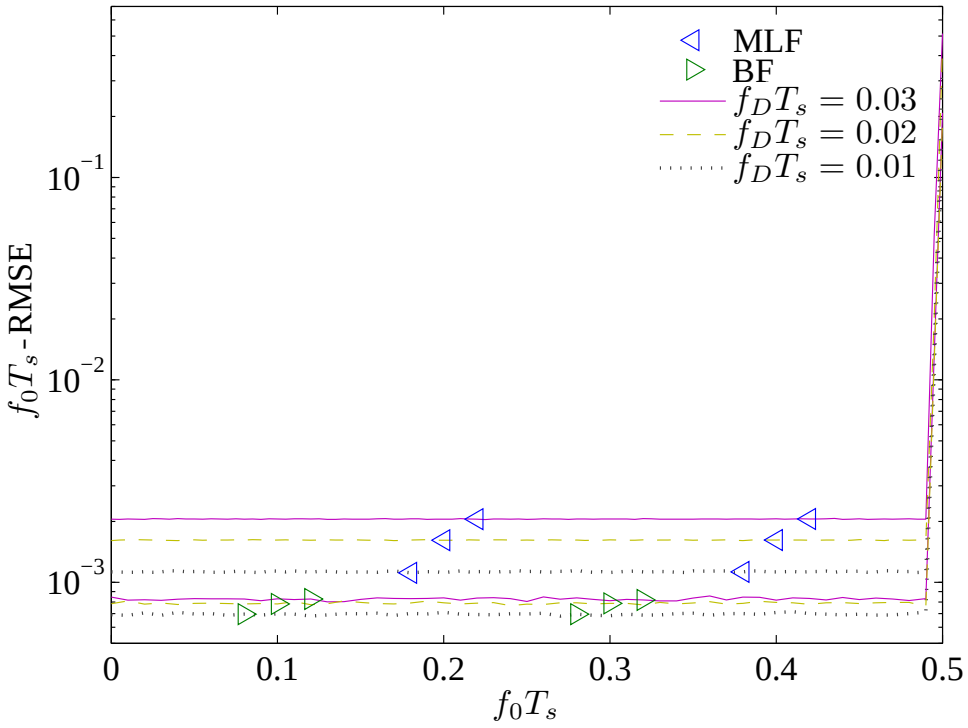

(b)

Figure 5.20: RMSE of the proposed BS-based estimators for frequency-flat time-variant fading channels as a function of f_0T_s for different values of f_DT_s; $N = 100$, $N_{FFT} = 4N$, $Q = 8$ and SNR $= 30$ dB; (a) proposed joint estimators and (b) proposed frequency offset estimators.

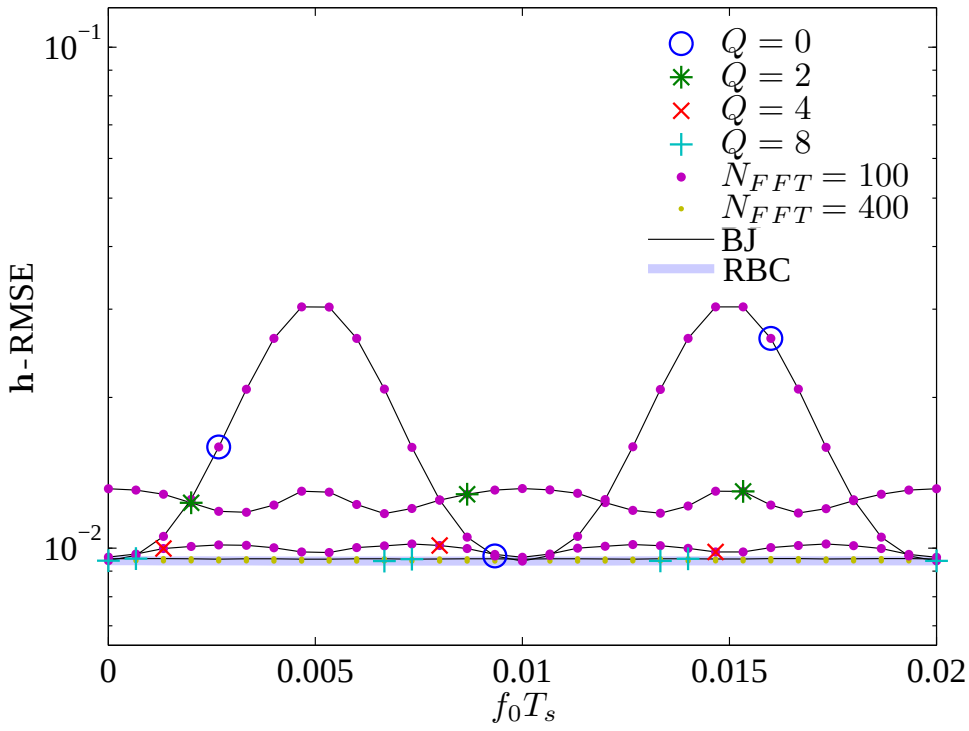

(a)

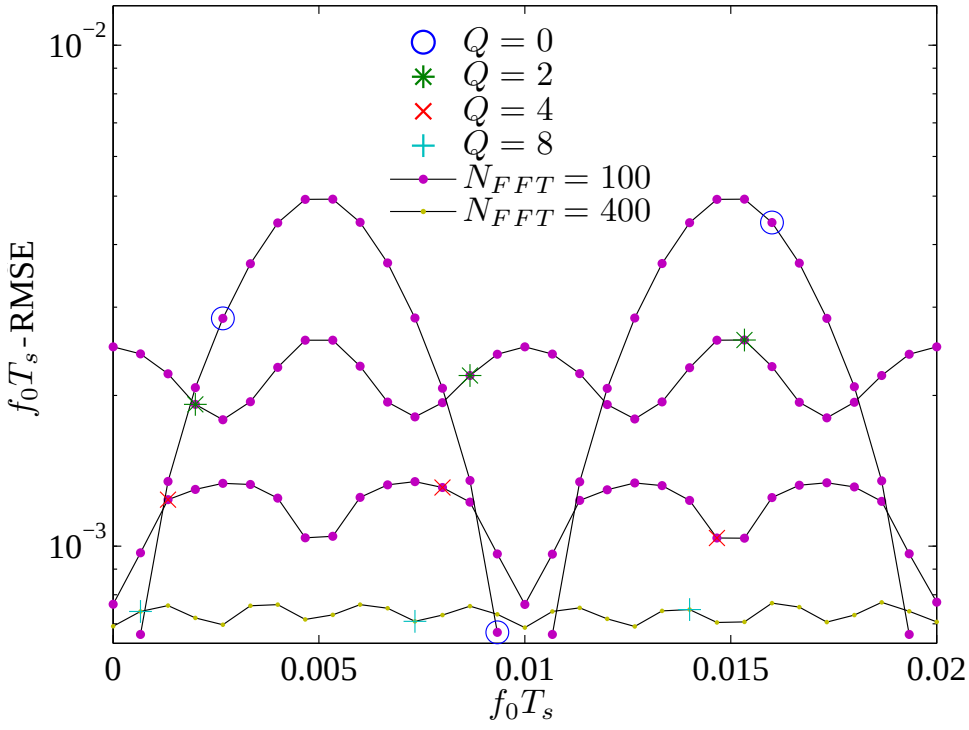

(b)

Figure 5.21: RMSE of the proposed BS-based Bayesian estimators for frequency-flat time-variant fading channels as a function of f_0T_s for different values of N_{FFT} and Q; $N = 100$, $f_DT_s = 0.01$, SNR $= 30$ dB; (a) proposed BJ and ideal RBC estimators, and (b) proposed BF estimator.

where the change in the $\mathbf{h}$-RMSE is hardly noticeable. For $Q = 2$ and $Q = 0$ (coarse search only), the performance degradation of the BJ estimator is less significant than that of the BF estimator. Similar simulation (not shown here) has been carried out for the proposed ML-based estimators. The results have shown that the MLJ estimator achieves a high-accuracy performance when using $N_{FFT} = 100$ and $Q = 3$, which is hardly distinguishable from its performance when using $N_{FFT} = 400$ and $Q = 8$. As a result, the spline-approximation reduces the impact of the frequency offset estimation errors on the joint estimate of the channel. This is the benefit of using the joint channel and frequency offset estimation rather than dealing separately with the two estimation problems.

5.9 Conclusions

In this chapter, novel joint data-aided channel and frequency offset estimators have been proposed for frequency-flat time-variant fading channels. These estimators are based on representing the time-variant fading process using the BEM. This model simplifies the solution and allows the estimators to achieve a high-accuracy performance. To reduce the complexity of the frequency offset estimators, and attain a high accuracy, the new estimators exploit a two stage technique for searching the generalised periodogram peak, an FFT-based coarse search and dichotomous fine search.

The first joint estimator is based on the Bayesian approach and can provide a high-accuracy performance whenever prior statistical characteristics of the channel are known, namely the covariance matrix of the fading and the variance of the AWGN. The second estimator, with a slightly higher estimation error, is an alternative joint estimator that can operate when these characteristics are unavailable.

The proposed Bayesian joint estimator have been studied based on different BEMs such as, Karhunen-Loève (KL), discrete prolate spheroidal (DPS), generalized complex exponential (GCE), and B-spline (BS) functions for different scenarios in Rayleigh fading channels, where the channel statistics are perfectly or imperfectly known. When channel statistics are perfectly known, simulation results have shown that the KL and DPS BEMs use fewer number of basis functions than that of the GCE and BS BEMs to allow achiev-

ing the same performance. However, the best reached performance of all the BEM-based estimators is the same. When channel statistics are mismatched, results have shown that the estimators based on the GCE and BS BEMs are more robust than those based on the KL and DPS BEMs. This makes the BS functions a better choice in practice as it has a sparse matrix that results in a lower complexity than the other basis functions.

The proposed BS-based Bayesian and ML joint estimators have been extensively investigated for different application scenarios in Rayleigh fading channels. Simulation results have shown that the proposed periodogram-based frequency offset estimators clearly outperform known correlation-based estimators. The new estimators have also been shown to possess the widest frequency acquisition range, which can be adjusted according to a priori knowledge of the frequency offset range to improve the accuracy. The proposed joint estimators provide a substantial performance improvement compared to the Bayesian channel estimator that ignores the frequency offset. Both of the proposed estimators have been shown to maintain a high-accuracy performance over wide SNR, f_0T_s and f_DT_s ranges, which is very close to that of the Bayesian channel estimator operating with perfect knowledge of the frequency offset. An explicit criterion for adjusting the parameters N_{FFT}, M and Q to an optimum value has been clarified so that according to the required SNR range and f_DT_s, the maximum accuracy of the frequency and channel estimation is achieved within the minimum complexity. Moreover, the proposed estimation techniques are superior in being able to compensate for the inaccuracy in the frequency offset estimation and capable of achieving a high-accuracy channel estimation performance without zero-padding the processed signal and using a simplified fine search (less number of iterations Q).

Chapter 6

Joint Estimation of Channel and Frequency Offset in Doubly-Selective Fading Channels

Contents

In this Chapter, a joint data-aided channel and frequency offset estimator is proposed for doubly-selective fading channels. The joint estimator is based on the B-spline model for approximating the fading process and the dichotomous search frequency estimation technique. The estimator relies on the Bayesian approach. It is examined for different scenarios in Rayleigh fading channels. Simulation results show that the proposed estimator achieves a high accuracy performance, which is close to that with perfect knowledge of the frequency offset, over a wide range of signal to noise ratios, for different Doppler

frequencies and throughout all the frequency acquisition range.

6.1 Introduction

Accurate channel estimation is very important in communication systems, where reliable transmission is required. This is challenging in frequency-selective and time-variant fading channels, especially in the presence of a frequency offset.

Most of the frequency offset estimators proposed in the literature have been devoted to correlation-based estimation, such as [25, 46] for frequency-selective time-invariant channels and [8, 11, 34] for frequency-flat time-variant fading channels. However, the performance of such estimators is inferior to that of the estimator based on the generalized periodogram [44], and unlike that estimator, they are operable only for high signal to noise ratios (SNR)s and/or they possess a limited frequency acquisition range [47, 48]. Periodogram-based joint channel and frequency offset estimation for frequency-flat time-variant fading channels has been considered in Chapter 5, where joint estimators exploiting basis expansion model (BEM) of the channel time variations have been proposed. BEMs have been widely used for frequency-flat time-variant channel estimation [38, 41, 51]. However, these estimators yield a severe degradation in the performance in the presence of a frequency offset. Joint channel and frequency offset estimation for frequency-selective time-invariant channels has been addressed in [52]. For doubly-selective fading channels, BEM-based channel estimation has been considered in [53]. The estimation of doubly-selective fading channels in the presence of a frequency offset for multicarrier systems, based on complex exponential BEM, has been addressed in [54, 91].

We focus on estimating jointly the doubly-selective fading channels and frequency offset by using B-spline BEM. The joint estimation allows more efficient and higher accuracy performance, compared to techniques dealing separately with these two problems. The proposed estimator is based on representing the fading process by BEMs and employing frequency estimation based on the dichotomous search [17] of the generalized periodogram peak.

Extensive simulations for different conditions are used to investigate the performance of the new estimators. The simulation results show accurate performance of the new estimators for the different examined scenarios.

This chapter is organised as follows. Section 6.2 describes the signal and channel models. In Section 6.3, the basis expansion model is described. Sections 6.4 illustrates the derivation of the proposed joint estimators. An efficient implementation of the estimators using the dichotomous search algorithm is presented in Section 6.5. Simulation results are discussed in Section 6.6. Finally, Section 6.7 contains conclusions.

6.2 Signal and Channel Models

We consider a known (pilot) signal transmitted through a doubly-selective fading channel. The baseband discrete received signal and channel models, respectively, after frequency downconverting, filtering in a matched filter and sampling at proper times, can be expressed as

$$r(nT_s) = \sum_{l=0}^{L-1} s(nT_s - \tau_l) h_l(nT_s) + z(nT_s)\,, \tag{6.1a}$$

$$h_l(nT_s) = g_l(nT_s) e^{j2\pi f_0 T_s n}\,, \quad n = 0, 1, \ldots, N-1\,, \tag{6.1b}$$

where $s(uT_s)$ is the transmitted pilot symbol, the first $L-1$ $\left(\{s(uT_s)\}_{u=-L+1}^{-1}\right)$ of which are the *precursors*, $z(nT_s)$ is the complex-valued additive white Gaussian noise (AWGN) with zero mean and variance σ_n^2, τ_l and $g_l(nT_s)$ are the lth path delay and fading process, respectively, $f_0 T_s$ is the frequency offset and T_s is the symbol interval; L and N are the number of paths and received symbols, respectively.

The paths are assumed to be independent and the fading of each path follows Jakes' model [64]. The covariance matrix of such fading process is given by

$$\mathbf{R}_g = \mathbf{P}_L \otimes \overline{\mathbf{R}}_g\,, \tag{6.2a}$$

$$\left[\,\overline{\mathbf{R}}_g\,\right]_{u\,v} = J_0(2\pi f_D T_s (u-v))\,, \quad u,\, v = 1,\, 2,\, \ldots,\, N\,, \tag{6.2b}$$

where $\mathbf{P}_L = \operatorname{diag}\left\{\sigma_{g_l}^2\right\}_{l=0}^{L-1}$ is the power delay profile, $\sigma_{g_l}^2$ is the variance of the lth path, $J_0(\cdot)$ is the zero-order Bessel function of the first kind, $f_D T_s$ is the Doppler frequency

and $\otimes$ denotes the Kronecker product. The Kronecker product of $\mathbf{A}$ and $\mathbf{B}$, denoted as $\mathbf{A} \otimes \mathbf{B}$, where $\mathbf{A}$ is an $N \times M$ matrix and $\mathbf{B}$ is an $L \times K$ matrix, is defined by

$$\mathbf{A} \otimes \mathbf{B} = \begin{bmatrix} \mathbf{A}_{1\,1}\mathbf{B} & \cdots & \mathbf{A}_{1\,M}\mathbf{B} \\ \vdots & \ddots & \vdots \\ \mathbf{A}_{N\,1}\mathbf{B} & \cdots & \mathbf{A}_{N\,M}\mathbf{B} \end{bmatrix} . \tag{6.3}$$

The received signal and channel models, respectively, in matrix form can be written as

$$\mathbf{r} = \mathbf{S}\mathbf{h} + \mathbf{z} \,, \tag{6.4a}$$

$$\mathbf{h} = \mathbf{\Lambda}_{f_0 T_s}\mathbf{g} \,, \quad \mathbf{\Lambda}_{f_0 T_s} = \mathbf{I}_L \otimes \overline{\mathbf{\Lambda}}_{f_0 T_s} \,, \tag{6.4b}$$

where $\mathbf{r}$ and $\mathbf{z}$ are $N \times 1$ received signal and noise vectors with elements $r(nT_s)$ and $z(nT_s)$, respectively, $\mathbf{S} = [\text{diag}(\mathbf{s}_0), \ldots, \text{diag}(\mathbf{s}_l), \ldots, \text{diag}(\mathbf{s}_{L-1})]$ is an $N \times NL$ pilot matrix, $\mathbf{s}_l$ is a $1 \times N$ vector with elements $s(nT_s - \tau_l)$, $\mathbf{h} = [\mathbf{h}_0^T, \ldots, \mathbf{h}_l^T, \ldots, \mathbf{h}_{L-1}^T]^T$ is an $NL \times 1$ channel response vector, $[\cdot]^T$ denotes the matrix transpose, $\mathbf{h}_l$ is an $N \times 1$ vector with elements $h_l(nT_s)$, $\mathbf{g} = [\mathbf{g}_0^T, \ldots, \mathbf{g}_l^T, \ldots, \mathbf{g}_{L-1}^T]^T$ is an $NL \times 1$ fading process vector, $\mathbf{g}_l$ is an $N \times 1$ vector with elements $g_l(nT_s)$, $\mathbf{I}_L$ is an $L \times L$ identity matrix, and $\overline{\mathbf{\Lambda}}_{F_0} = \text{diag}\left\{e^{j2\pi f_0 T_s n}\right\}$ is the frequency offset matrix.

6.3 Basis Expansion Model

Accurate estimation of the fading processes $g_l(nT_s)$ requires complicated techniques such as the Wiener filtering [4]. A simpler solution can be obtained based on representing $g_l(nT_s)$ using a basis expansion model (BEM) with M basis functions as

$$\tilde{g}_l(nT_s) = \sum_{m=1}^{M} a_l(m) B(nT_s, m) \,, \quad l = 0,\, 1,\, \ldots,\, L-1 \,, \tag{6.5}$$

where $B(nT_s, m)$ are basis functions and $a_l(m)$ are unknown expansion coefficients. In matrix form, it can be written as

$$\tilde{\mathbf{g}} = \mathbf{B}\mathbf{a} \,, \quad \mathbf{B} = \mathbf{I}_L \otimes \overline{\mathbf{B}} \,, \tag{6.6}$$

where $\overline{\mathbf{B}}$ is an $N \times M$ basis function matrix with elements $\{B(nT_s, m)\}$, $\mathbf{a} = [\mathbf{a}_0^T, \ldots, \mathbf{a}_l^T, \ldots, \mathbf{a}_{L-1}^T]^T$ is an $ML \times 1$ expansion coefficient vector and $\mathbf{a}_l$ is an $M \times 1$ vector with elements $\{a_l(m)\}$.

Thus, the estimation problem of the $L \times N$ time-variant fading process $g_l(nT_s)$ is transformed into estimation of the $L \times M$ time-invariant expansion coefficients $a_l(m)$. Usually $M << N$, which makes the BEM-based approach attractive.

Different basis functions can be used in the BEM such as complex exponential [38,54], Karhunen-Loève [87], discrete prolate spheroid- al [41] and B-splines [51]. It is shown in Chapter 5 that the channel estimation based on the B-splines is less sensitive to the accurate knowledge of statistical characteristics of the fading and simpler for implementation than that based on the other BEMs. Therefore, here we use the BS BEM.

The B-splines of order η are symmetrical, bell-shaped functions that are given by [94]

$$B_\eta(x) = \frac{1}{\eta!}\sum_{i=0}^{\eta+1}(-1)^i \binom{\eta+1}{i}\left(\frac{x}{PT_s} + \frac{\eta+1}{2} - i\right)_+^\eta , \tag{6.7}$$

where $P = (N-1)/(M-\eta)$, PT_s is the sampling interval separating two adjacent B-spline functions and $x_+ = \max\{0, x\}$. In this case, elements of the basis function matrix are calculated as $B(nT_s, m) = B_\eta\left(nT_s - (m - \frac{\eta+1}{2})PT_s\right)$. The accuracy and complexity of B-spline approximation depends on the spline degree η. In many situations, the cubic B-spline ($\eta = 3$) provides the best trade-off between complexity and accuracy [94]. We use the cubic B-spline in the simulation below whenever $M \geq 4$. However, other BEMs can also be used in the joint estimator.

6.4 Joint Estimation

The model mismatching error due to the approximation of the fading process can be neglected when choosing M high enough, so that $\mathbf{g}$ can be assumed equal to $\tilde{\mathbf{g}}$; this is a practical assumption as detailed in [38, 41, 43]. Thus, the signal model can be now regarded as

$$\mathbf{r} = \overline{\mathbf{\Lambda}}_{f_0 T_s}\mathbf{\Phi}\mathbf{a} + \mathbf{z}\,; \quad \mathbf{\Phi} = \mathbf{S}\mathbf{B}\,, \tag{6.8a}$$

$$\mathbf{h} = \mathbf{\Lambda}_{f_0 T_s}\mathbf{B}\mathbf{a}\,. \tag{6.8b}$$

The vector $\mathbf{a}$ is assumed to be zero mean Gaussian with *a priori* PDF $p(\mathbf{a}) = \pi^{-M} |\mathbf{R}_a|^{-1} e^{-\mathbf{a}^H \mathbf{R}_a^{-1} \mathbf{a}}$, and $\mathbf{R}_a$ is the covariance matrix of $\mathbf{a}$ that can be obtained as [51]

$$\mathbf{R}_a = \mathbf{P}_L \otimes \overline{\mathbf{R}}_a \,, \quad \overline{\mathbf{R}}_a = \left(\overline{\mathbf{B}}^H \overline{\mathbf{B}}\right)^{-1} \overline{\mathbf{B}}^H \overline{\mathbf{R}}_g \overline{\mathbf{B}} \left(\overline{\mathbf{B}}^H \overline{\mathbf{B}}\right)^{-1} . \tag{6.9}$$

6.4.1 Frequency Offset Estimator

By using the Bayesian approach (as detailed in [48, 49]), we arrive at the following Bayesian frequency (BF) estimator

$$\begin{aligned} \widehat{f_0 T_s} &= \arg \max_{f T_s \in \Psi} \{Y_{f T_s}\} \\ &= \arg \max_{f T_s \in \Psi} \left\{ \mathbf{r}^H \overline{\mathbf{\Lambda}}_{f T_s} \mathbf{S} \mathbf{B} \left(\mathbf{B}^H \mathbf{S}^H \mathbf{S} \mathbf{B} + \sigma_n^2 \mathbf{R}_a^{-1} \right)^{-1} \mathbf{B}^H \mathbf{S}^H \overline{\mathbf{\Lambda}}_{f T_s}^H \mathbf{r} \right\} \end{aligned} \tag{6.10}$$

where

$$Y_{f T_s} = \mathbf{W}_{f T_s}^H \left(\mathbf{\Gamma} + \sigma_n^2 \mathbf{R}_a^{-1} \right)^{-1} \mathbf{W}_{f T_s} \,, \tag{6.11a}$$

$$\mathbf{\Gamma} = \mathbf{\Phi}^H \mathbf{\Phi} = \mathbf{B}^H \mathbf{S}^H \mathbf{S} \mathbf{B} \,, \tag{6.11b}$$

$$\mathbf{W}_{f T_s} = \mathbf{\Phi}^H \overline{\mathbf{\Lambda}}_{f T_s}^H \mathbf{r} = \mathbf{B}^H \mathbf{S}^H \overline{\mathbf{\Lambda}}_{f T_s}^H \mathbf{r} \,, \tag{6.11c}$$

$(\cdot)^H$ denotes the Hermitian transpose, $Y_{f T_s}$ is the generalised periodogram [44, 48], and $\Psi = [-\psi/2, \psi/2]$ is the frequency acquisition range that can be considered either wide ($\psi = 1$) or narrow ($\psi << 1$).

6.4.2 Channel Estimator

After obtaining $\widehat{F}_0$ and substituting it in (6.8), the minimum mean square error (MMSE) estimator of the vector $\mathbf{a}$ is given by

$$\widehat{\mathbf{a}} = \left(\mathbf{\Gamma} + \sigma_n^2 \mathbf{R}_a^{-1} \right)^{-1} \mathbf{W}_{\widehat{f_0 T_s}} \,. \tag{6.12}$$

Finally, the Bayesian joint channel and frequency offset (BJ) estimator is obtained by substituting (6.12) into (6.8b) as

$$\widehat{\mathbf{h}} = \mathbf{\Lambda}_{\widehat{f_0 T_s}} \mathbf{B} \left(\mathbf{B}^H \mathbf{S}^H \mathbf{S} \mathbf{B} + \sigma_n^2 \mathbf{R}_a^{-1} \right)^{-1} \mathbf{B}^H \mathbf{S}^H \overline{\mathbf{\Lambda}}_{\widehat{f_0 T_s}}^H \mathbf{r} \,. \tag{6.13}$$

Table 6.1: Dichotomous Search Algorithm for the Proposed Joint Channel and Frequency Offset Estimator for Doubly-Selective Fading Channels.

Compute	$\mathbf{G} = \left(\mathbf{B}^H\mathbf{S}^H\mathbf{S}\mathbf{B} + \sigma_n^2\mathbf{R}_a^{-1}\right)^{-1}$
Calculate	$D_{fT_s}^{(m)}(l) = \sum_{n=0}^{N-1} r(nT_s)s^*(nT_s - \tau_l)B^*(nT_s, m)e^{-j2\pi fT_s n}$
Rearrange	$\mathbf{W}_{fT_s} = [\mathbf{D}_{fT_s}(0), \ldots, \mathbf{D}_{fT_s}(l), \ldots, \mathbf{D}_{fT_s}(L-1)]^T$
Determine	$Y_{fT_s} = \sum_{u=1}^{ML}\sum_{v=1}^{ML}[\mathbf{G}]_{u\,v}\,W_{fT_s}^*(u)W_{fT_s}(v)$
Find	$f_pT_s = \arg\max_{fT_s\in\Psi}\{Y_{fT_s}\}$
Locate	$Y_1 = Y_{f_{p-1}T_s}\,, \quad Y_2 = Y_{f_pT_s}\,, \quad Y_3 = Y_{f_{p+1}T_s}$
For Q iterations do	
	$\Delta fT_s = \Delta fT_s/2$
	If $Y_3 < Y_1$ then $Y_3 = Y_2$ and $f_pT_s = f_pT_s - \Delta fT_s$,
	else $Y_1 = Y_2$ and $f_pT_s = f_pT_s + \Delta fT_s$
	$D_{f_pT_s}^{(m)}(l) = \sum_{n=0}^{N-1} r(nT_s)s^*(nT_s - \tau_l)B^*(nT_s, m)e^{-j2\pi f_pT_s n}$
	$\mathbf{W}_{f_pT_s} = [\mathbf{D}_{f_pT_s}(0), \ldots, \mathbf{D}_{f_pT_s}(l), \ldots, \mathbf{D}_{f_pT_s}(L-1)]^T$
	$Y_2 = \sum_{u=1}^{ML}\sum_{v=1}^{ML}[\mathbf{G}]_{u\,v}W_{f_pT_s}^*(u)W_{f_pT_s}(v)$
Finally	$\widehat{f_0T_s} = f_pT_s\,, \quad \widehat{\mathbf{h}} = \mathbf{\Lambda}_{f_pT_s}\mathbf{B}\mathbf{G}\mathbf{W}_{f_pT_s}$

6.5 Dichotomous-based Implementation

Most of the complexity in the proposed estimator is consumed by the frequency offset estimation part when calculating $\mathbf{W}_{fT_s}$ in (6.11c) that is used for evaluation of the generalized periodogram Y_{fT_s} in (6.11a). For a coarse evaluation (search), FFT of a size $N_{FFT} \geq N$ (with a frequency step $\Delta fT_s = 1/N_{FFT}$) can be used. For a fine search, we use the dichotomous search [17]. This approach is free of nonlinear operations and well suited for real-time implementation [47]. The proposed estimator is summarised in Table 6.1.

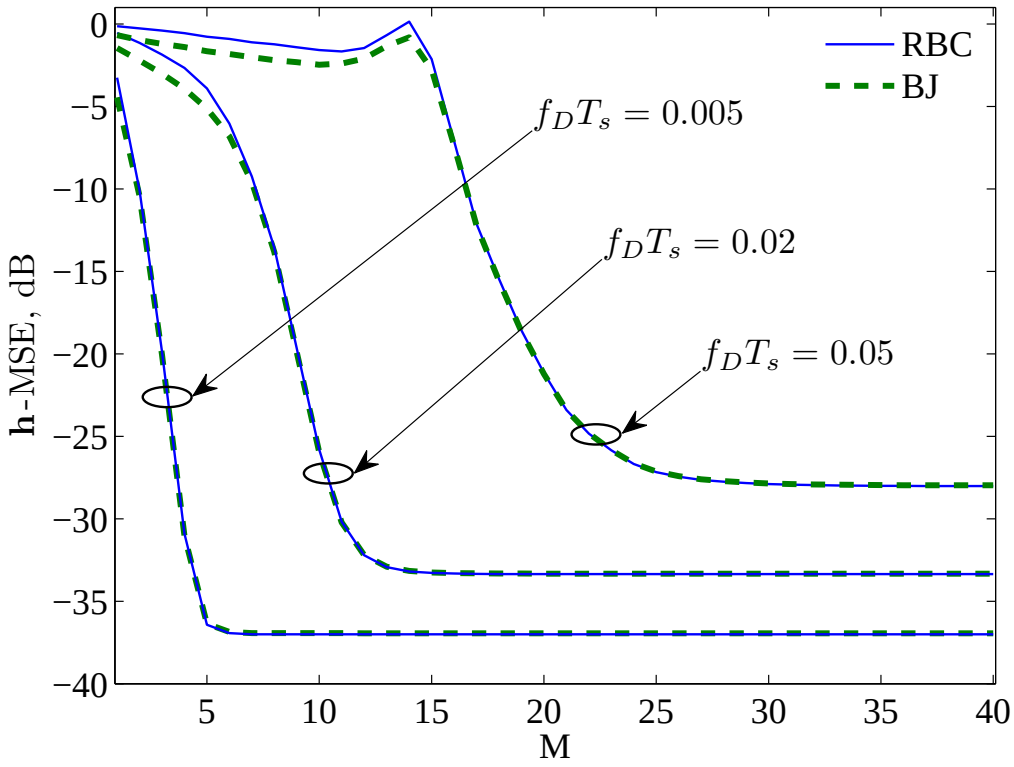

Figure 6.1: $\mathbf{h}$-MSE of the proposed BS-based Bayesian joint estimators for doubly-selective fading channels as a function of M for different values of f_DT_s; $N = 128$, $N_{FFT} = N$, $L = 5$, $f_0T_s = 0.0123$, $Q = 5$ and SNR $= 30$ dB.

6.6 Simulation Results and Performance Analysis

We consider a binary pseudo-random pilot signal and the signal to noise ratio (SNR) is calculated as

$$\text{SNR} = \frac{\text{E}\left\{\left(\overline{\mathbf{\Lambda}}_{f_0T_s}\mathbf{Sg}\right)^H\left(\overline{\mathbf{\Lambda}}_{f_0T_s}\mathbf{Sg}\right)\right\}}{\text{E}\left\{\mathbf{z}^H\mathbf{z}\right\}} = \frac{\epsilon}{\sigma_n^2}\,, \tag{6.14}$$

where $\epsilon = \sum_{l=0}^{L-1}\sigma_{g_l}^2$. The mean square error (MSE) of estimation is averaged over $10\,000$ simulation trials, where the MSE of the frequency offset and channel estimates, respectively, in each simulation trial are calculated as

$$f_0T_s\text{-MSE} = \left(f_0T_s - \widehat{f_0T_s}\right)^2\,, \tag{6.15a}$$

$$\mathbf{h}\text{-MSE} = \frac{\sum_{l=0}^{L-1}\sum_{n=0}^{N-1}\left|h_l(nT_s) - \hat{h}_l(nT_s)\right|^2}{\sum_{l=0}^{L-1}\sum_{n=0}^{N-1}\left|h_l(nT_s)\right|^2}. \tag{6.15b}$$

We consider a random pilot signal of length $N = 128$ transmitted through doubly-

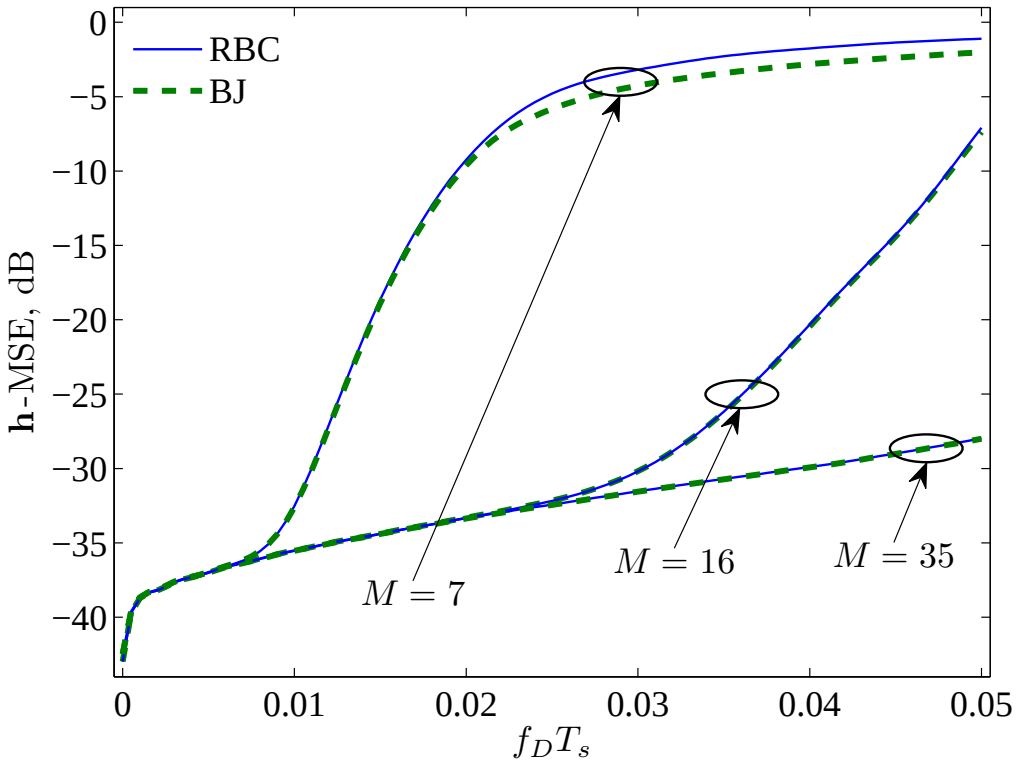

Figure 6.2: **h**-MSE of the proposed BS-based Bayesian joint estimators for doubly-selective fading channels as a function of $f_D T_s$ for different values of M; $N = 128$, $N_{FFT} = N$, $L = 5$, $f_0 T_s = 0.0123$, $Q = 5$ and SNR $= 30$ dB.

selective fading channel that has $L = 5$ paths, with an exponentially decaying power delay profile. The frequency acquisition range is wide ($\psi = 1$). Unless otherwise specified, the size of FFT in the coarse search is $N_{FFT} = N = 128$ and the number of dichotomous iterations in the fine search is $Q = 5$.

The proposed estimator is compared to an ideal reference Bayesian channel (RBC) estimator, where the frequency offset is assumed to be known. This estimator is given as in (6.13) but with $\widehat{f_0 T_s}$ being replaced with $f_0 T_s$.

Figure 6.1 shows the M-dependent **h**-MSE in the slow ($f_D T_s = 0.005$), moderate ($f_D T_s = 0.02$) and fast ($f_D T_s = 0.05$) fading channels. There is a threshold M, below which the error rapidly increases due to a high modeling mismatch error, and above which the error stays almost constant. The exploitation of the fading covariance matrix and the noise variance prevents a degradation in the performance for high M. For a higher $f_D T_s$, the estimator requires a higher M to achieve its best performance. This M can

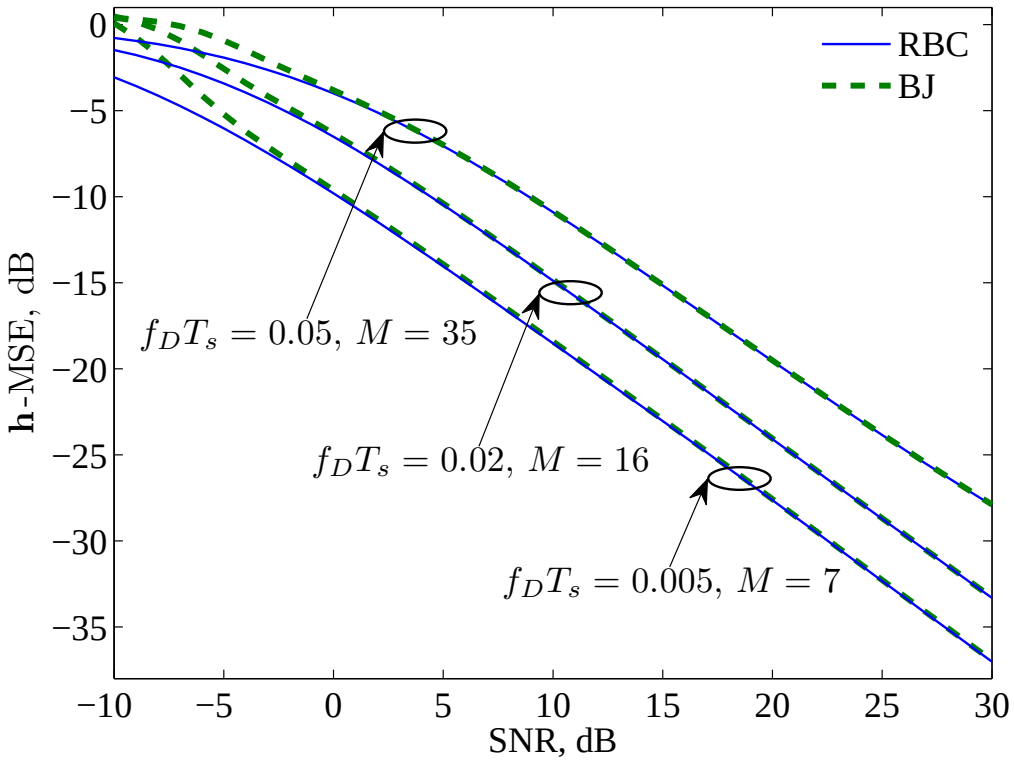

Figure 6.3: $\mathbf{h}$-MSE of the proposed BS-based Bayesian joint estimators for doubly-selective fading channels as a function of SNR for different values of f_DT_s (and M); $N = 128$, $N_{FFT} = N$, $L = 5$, $f_0T_s = 0.0123$ and $Q = 5$.

be determined such that the sampling factor $\gamma = 1/(f_DT_sP)$ is approximately 5, which is defined by approximating properties of B-splines [43]. Figure 6.2 shows the f_DT_s-dependent $\mathbf{h}$-MSE for different M. The best performance is achieved for f_DT_s smaller than a threshold that increases with M. It is seen from Figure 6.1 and Figure 6.2 that the proposed BJ estimator achieves a high accuracy performance which is close to that of the ideal RBC estimator. Thus, the frequency offset (nonlinear) estimation involved in the BJ estimator helps in reducing the modeling mismatch error, even when $f_0T_s = 0$ (according to simulation results not shown here).

Figure 6.3 shows the SNR-dependent $\mathbf{h}$-MSE for different f_DT_s. We notice a threshold SNR, below which the $\mathbf{h}$-MSE of the BJ estimator diverts slightly from that of the RBC estimator. This characteristic appears due to the involvement of the nonlinear frequency estimation and the occurrence of the outliers [13].

Figure 6.4 shows the f_0T_s-dependent MSE performance for different N_{FFT} and Q.

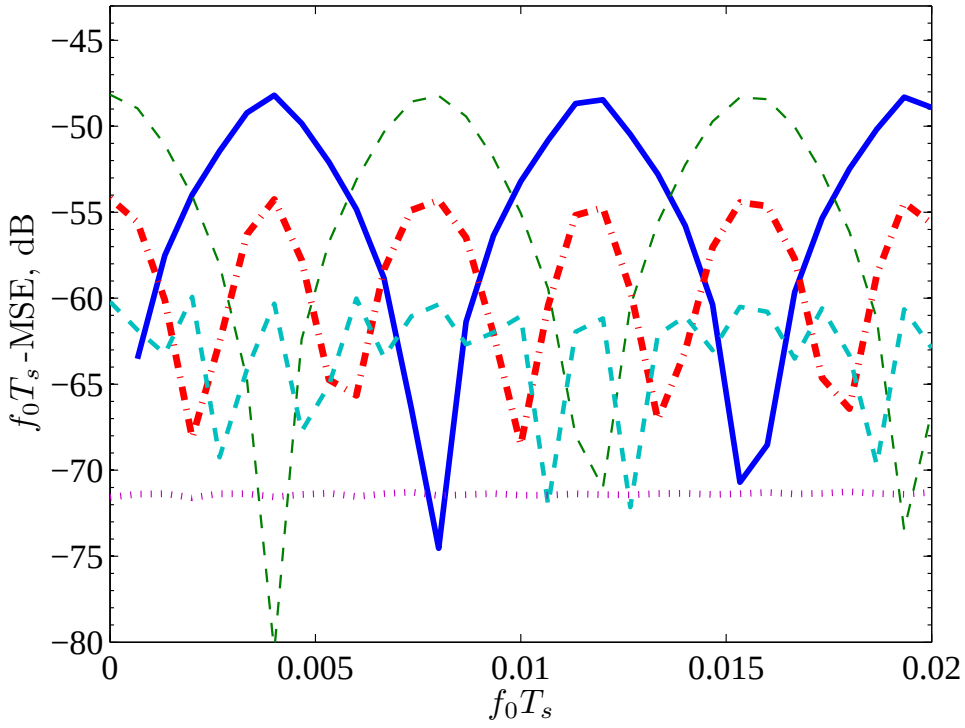

(a)

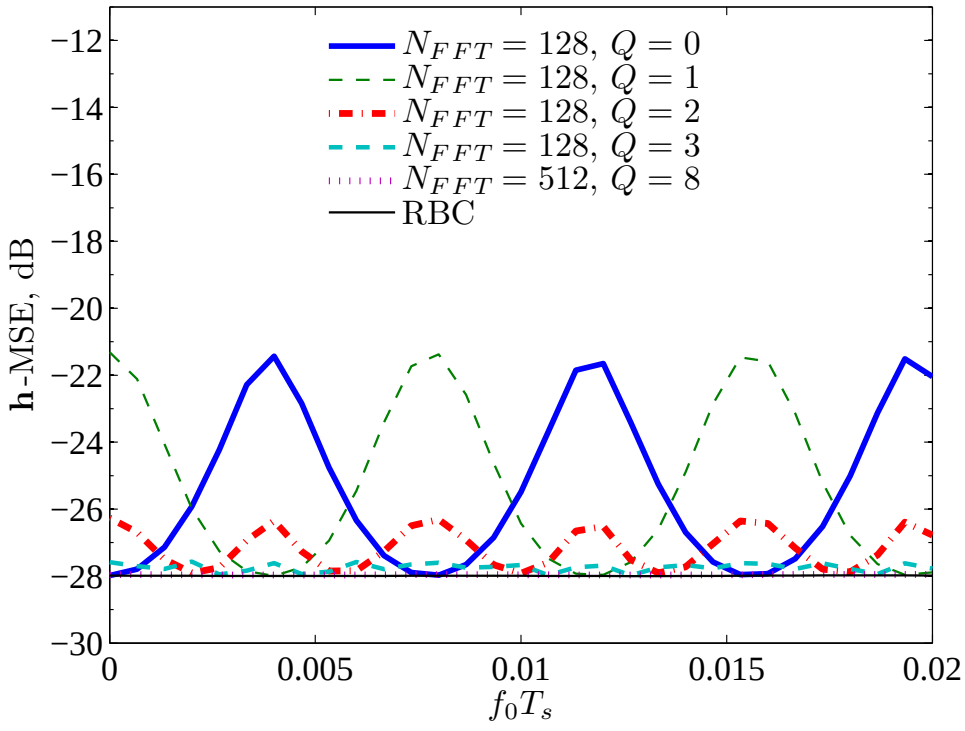

(b)

Figure 6.4: MSE of the proposed BS-based Bayesian estimators in doubly-selective fading channels as a function of f_0T_s for different values of N_{FFT} and Q; $N = 128$, $L = 5$, $f_DT_s = 0.05$, $M = 35$ and SNR $= 30$ dB; (a) proposed BF estimator and (b) proposed BJ and ideal RBC estimators.

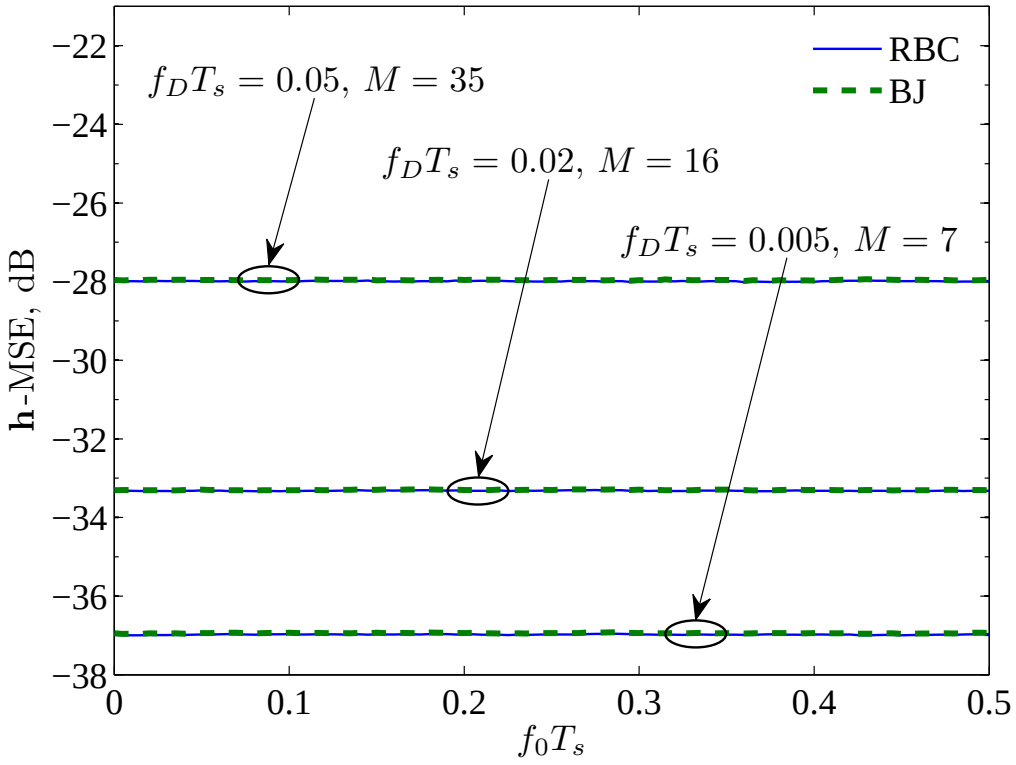

Figure 6.5: $\mathbf{h}$-MSE of the proposed BS-based Bayesian joint estimators for doubly-selective fading channels as a function of f_0T_s for SNR $= 30$ dB and different values of f_DT_s (and M).

For the BF estimator, $N_{FFT} = 4N = 512$ and $Q = 8$ is a necessity for a high-accuracy frequency estimation. However, the BJ estimator does not require that high accuracy in the frequency offset estimation and can achieve a good joint estimation ($\mathbf{h}$-MSE) performance with a significantly lower N_{FFT} (with as small N_{FFT} as $N_{FFT} = N$) and using a few dichotomous iterations. For $f_DT_s = 0.05$, an RBC-like performance is achieved using as small Q as $Q = 3$. Slower fading channels may require a slightly higher Q and other simulation results (not presented here) have shown that $Q = 5$ is the best choice and covers all the f_DT_s. Figure 6.5 shows that the proposed estimator possesses a wide frequency acquisition range for different f_DT_s and using $N_{FFT} = N = 128$ and $Q = 5$.

6.7 Conclusions

A novel joint data-aided channel and frequency offset estimator has been proposed for doubly-selective fading channels. This estimator is based on approximating the fading process using the B-spline model. This model simplifies the solution and allows the estimator to achieve a high accuracy performance. The joint estimator is based on the Bayesian approach and provides a high accuracy performance when some prior statistical characteristics of the channel are known, namely the covariance matrix of the fading and the variance of the AWGN. To reduce the complexity of the frequency offset estimation, a two stage technique is exploited for searching a peak of the generalized periodogram, an FFT-based coarse search and dichotomous fine search. Simulation results for different scenarios in Rayleigh fading channels have shown that the proposed estimator maintains, over wide SNR, frequency offset and Doppler frequency ranges, a high accuracy performance, which is very close to that of the Bayesian channel estimator operating with perfect knowledge of the frequency offset.

Chapter 7

Iterative Turbo Receivers with Joint Channel and Frequency Offset Estimation in Frequency-Flat Time-Variant Fading Channels

Contents

In this chapter, we develop iterative turbo receivers for frequency-flat time-variant fading channels which jointly perform channel and frequency offset estimation together with data detection and decoding. Three versions of the joint estimator, the Bayesian, the maximum likelihood and the regularised-maximum likelihood are presented depending on

how much knowledge of channel statistics is available. The estimation and detection are based on the basis expansion model of the fading time variations and use the dichotomous search frequency estimation technique. Soft information generated in the turbo decoder is used to improve the quality of detection in the subsequent iterations. Simulation results show that the proposed receivers provide as good performance as the corresponding ones operating with perfect knowledge of the frequency offset.

7.1 Introduction

Various frequency offset estimators have been proposed for time-variant channels [8, 11]. However most of these estimators are correlation-based with inferior performance to that of the optimal estimator and/or possess a limited frequency acquisition range [49]. Different estimators of the channel time variations have also been proposed [37, 42], however, the frequency offset is not taken into account in these works. By considering the soft information from a soft-input soft-output (SISO) decoder in an iterative channel estimation and data detection, various iterative turbo processing techniques have been widely considered for pilot symbol assisted modulation (PSAM) systems at the receivers. However, most studies have either ignored the possible presence of a frequency offset [55], or assumed time-invariant channels when dealing with the frequency offset [56]. We consider iterative turbo-based receivers for PSAM systems and QAM signals dealing with joint estimation of the time-variant channel and frequency offset together with data detection and decoding, which, to the best of our knowledge, has not been discussed in the literature.

This chapter is organised as follows. Section 7.2 describes transmission models. Section 7.3 illustrates the joint frequency offset and channel estimators exploited in the receivers. Efficient implementation of the estimators using the dichotomous search algorithm is presented in Section 7.4. Classical receivers with joint estimation are considered in Section 7.5 and iterative turbo-based receivers are proposed in Section 7.6. Simulation results are discussed in Section 7.7. Finally, Section 7.8 contains conclusions.

7.2 Transmission Models

We consider a PSAM system, where a block of N symbols is transmitted through a frequency-flat time-variant fading channel. The transmitted block consists of N_d data symbols and N_p pilot symbols that are inserted periodically between each $T-1$ data symbols. The baseband discrete received signal and channel, respectively, after frequency downconverting, filtering in a matched filter and sampling at proper times, are modeled as

$$r(nT_s) = s(nT_s)h(nT_s) + z(nT_s)\,, \tag{7.1a}$$

$$h(nT_s) = g(nT_s)e^{j2\pi f_0 T_s n}\,, \quad n = 0,\, 1,\, \ldots,\, N-1\,, \tag{7.1b}$$

where $s(nT_s)$ is the transmitted signal, $z(nT_s)$ is the complex-valued additive white Gaussian noise with zero mean and variance σ_z^2, T_s is the symbol interval, f_0T_s is the normalised frequency offset and $g(nT_s)$ is the fading process. We consider a Rayleigh fading process following the Jakes' model [64] with a covariance matrix given by

$$[\mathbf{R}_g]_{u\,v} = \sigma_g^2 J_0(2\pi f_D T_s(u-v))\,, \quad u,\, v = 1,\, \ldots,\, N\,, \tag{7.2}$$

where σ_g^2 is the fading variance, $J_0(\cdot)$ is the zero-order Bessel function of the first kind and f_DT_s is the normalised Doppler frequency.

The received signal and channel models, respectively, can be written in matrix form as

$$\mathbf{r} = \mathbf{S}\mathbf{h} + \mathbf{z}\,, \tag{7.3a}$$

$$\mathbf{h} = \mathbf{\Lambda}_{f_0T_s}\mathbf{g}\,, \tag{7.3b}$$

where $\mathbf{r}$, $\mathbf{h}$, $\mathbf{g}$ and $\mathbf{z}$ are $N \times 1$ column vectors with elements $r(nT_s)$, $h(nT_s)$, $g(nT_s)$ and $z(nT_s)$, respectively, $\mathbf{S} = \text{diag}\{s(nT_s)\}$ and $\mathbf{\Lambda}_{f_0T_s} = \text{diag}\left\{e^{j2\pi f_0 T_s n}\right\}$.

The fading process $g(nT_s)$ can be represented using a basis expansion model [38] with M basis functions as

$$g(nT_s) = \sum_{m=1}^{M} a_m B(nT_s, m)\,, \tag{7.4}$$

where a_m are unknown expansion coefficients and $B(nT_s, m)$ are known basis functions. Thus, the problem of estimating an N-dimensional time-variant fading process $g(nT_s)$

is transformed into a lower dimensional problem of estimating only M time-invariant expansion coefficients a_m, where usually $M << N$.

The processed model in matrix form is given now by

$$\mathbf{r} = \mathbf{\Lambda}_{f_0 T_s} \mathbf{\Phi a} + \mathbf{z}\,, \quad \mathbf{\Phi} = \mathbf{SB}\,, \tag{7.5a}$$

$$\mathbf{h} = \mathbf{\Lambda}_{f_0 T_s} \mathbf{Ba}\,, \tag{7.5b}$$

where $\mathbf{a}$ is $M \times 1$ column vector of expansion coefficients a_m, $\mathbf{B}$ is $N \times M$ matrix with elements $B(nT_s, m)$, $n = 0, 1, \ldots, N-1$ and $m = 1, \ldots, M$.

7.3 Joint Frequency Offset and Channel Estimation

The frequency offset estimator is given by [49]

$$\begin{aligned} \widehat{f_0 T_s} &= \arg \max_{fT_s \in \Psi} \{Y_{fT_s}\} \\ &= \arg \max_{fT_s \in \Psi} \left\{ \mathbf{W}_{fT_s}^H \left(\mathbf{\Gamma} + \mathbf{\Upsilon} \right)^{-1} \mathbf{W}_{fT_s} \right\}\,, \end{aligned} \tag{7.6}$$

where $[\cdot]^H$ denotes the Hermitian transpose, $\Psi = [-\psi/2, \psi/2]$ is the frequency acquisition range, $0 < \psi \leq 1$, Y_{fT_s} is the generalized periodogram [44, 48], $\mathbf{W}_{fT_s} = \mathbf{\Phi}^H \mathbf{\Lambda}_{fT_s}^H \mathbf{r}$, $\mathbf{\Gamma} = \mathbf{\Phi}^H \mathbf{\Phi}$ and $\mathbf{\Upsilon}$ depends on the estimation approach relying on how much knowledge of channel statistics is available. For the Bayesian estimation, $\mathbf{\Upsilon} = \sigma_z^2 \mathbf{R}_a^{-1}$, where $\mathbf{R}_a$ is the $M \times M$ covariance matrix of the expansion coefficients, which can be obtained by [51]

$$\mathbf{R}_a = \left(\mathbf{B}^H \mathbf{B} \right)^{-1} \mathbf{B}^H \mathbf{R}_g \mathbf{B} \left(\mathbf{B}^H \mathbf{B} \right)^{-1}\,. \tag{7.7}$$

This approach provides the best performance and is applicable when σ_z^2 and $\mathbf{R}_g$ are known. In the absence of this prior information, the maximum likelihood estimation can be used with a slight performance degradation, for which $\mathbf{\Upsilon} = \mathbf{O}$, where $\mathbf{O}$ is $M \times M$ zero matrix. A third option is the regularised-maximum likelihood estimation, for which $\mathbf{\Upsilon} = \epsilon \sigma_z^2 \mathbf{I}_M$, where $\mathbf{I}_M$ is $M \times M$ identity matrix and ϵ is a regularising parameter with the best value of σ_g^{-2}. This approach is applicable when σ_z^2 and σ_g^2 are known and provides a performance which is better than that of the maximum likelihood estimator and worse than that of the Bayesian estimator.

The expansion coefficient vector estimator is then given by [49]

$$\hat{\mathbf{a}} = (\mathbf{\Gamma} + \mathbf{\Upsilon})^{-1} \mathbf{W}_{\widehat{f_0 T_s}} \tag{7.8}$$

and the joint channel and frequency offset estimator is obtained as [49]

$$\widehat{\mathbf{h}} = \mathbf{\Lambda}_{\widehat{f_0 T_s}} \mathbf{B} \hat{\mathbf{a}} \,. \tag{7.9}$$

7.4 Efficient Implementation

Complexity in the described estimator is mostly consumed by the frequency offset estimation part for calculating $\mathbf{W}_{fT_s}$. This can be done using fast Fourier transform (FFT) of a size $N_{FFT} >> N$, which however is very complicated. We use a more practical two-stage technique for searching the maximum in (7.6): an FFT of size $N_{FFT} \approx N$ is used in a coarse search with a frequency resolution $\Delta f T_s = 1/N$, then the frequency offset estimate is refined by a dichotomous fine search [17] of a small number of iterations Q.

This approach allows achieving a high-accuracy performance throughout the wide frequency acquisition range and well suited for implementation [47]. The algorithm is summarised in Table 7.1.

7.5 Classical Receivers

The received signal can be split into two parts corresponding to the pilot and data instants, respectively, as $\mathbf{r}_p = \mathbf{S}_p \mathbf{h}_p + \mathbf{z}_p$ and $\mathbf{r}_d = \mathbf{S}_d \mathbf{h}_d + \mathbf{z}_d$, where $\mathbf{S}_p$, $\mathbf{h}_p$ and $\mathbf{z}_p$ correspond to the pilot instants and $\mathbf{S}_d$, $\mathbf{h}_d$ and $\mathbf{z}_d$ correspond to the data instants of $\mathbf{S}$, $\mathbf{h}$ and $\mathbf{z}$, respectively. The fading process as well can be split into two parts corresponding to the pilot and data instants, respectively, as $\mathbf{g}_p = \mathbf{B}_p \mathbf{a}$ and $\mathbf{g}_d = \mathbf{B}_d \mathbf{a}$, where $\mathbf{B}_p$ and $\mathbf{B}_d$ correspond to the pilot and data instants of $\mathbf{B}$, respectively.

Classical receivers can exploit the above estimation scheme using only pilot symbols to obtain $\widehat{f_0 T_s}$ and $\hat{\mathbf{a}}$ according to (7.6) and (7.8), respectively, but with replacing $\mathbf{B}$, $\mathbf{S}$, $\mathbf{r}$

Table 7.1: Dichotomous Search Algorithms for the Proposed Joint Channel and Frequency Offset Estimators in the Iterative Turbo Receivers for Frequency-Selective Time-Variant Fading Channels.

Compute	$\mathbf{G} = \left(\mathbf{B}^H\mathbf{S}^H\mathbf{S}\mathbf{B} + \boldsymbol{\Upsilon}\right)^{-1}$;
	$\boldsymbol{\Upsilon} = \begin{cases} \sigma_z^2\mathbf{R}_a^{-1}, & \text{Bayesian approach} \\ \sigma_g^{-2}\sigma_z^2\mathbf{I}_M, & \epsilon\text{-ML approach} \\ \mathbf{O}, & \text{ML approach} \end{cases}$
Calculate	$W_{fT_s}(m) = \sum_{n=0}^{N-1} r(nT_s)s^*(nT_s)B^*(nT_s, m)e^{-j2\pi fT_s n}$
Determine	$Y_{fT_s} = \sum_{u=1}^{M}\sum_{v=1}^{M}[\mathbf{G}]_{u\,v}\, W^*_{fT_s}(u)W_{fT_s}(v)$
Find	$f_pT_s = \arg\max_{fT_s\in\Psi}\{Y_{fT_s}\}$
Locate	$Y_1 = Y_{f_{p-1}T_s}, \quad Y_2 = Y_{f_pT_s}, \quad Y_3 = Y_{f_{p+1}T_s}$
For Q iterations do	
	$\Delta fT_s = \Delta fT_s/2$
	If $Y_3 < Y_1$ then $Y_3 = Y_2$ and $f_pT_s = f_pT_s - \Delta fT_s$,
	else $Y_1 = Y_2$ and $f_pT_s = f_pT_s + \Delta fT_s$
	$W_{f_pT_s}(m) = \sum_{n=0}^{N-1} r(nT_s)s^*(nT_s)B^*(nT_s, m)e^{-j2\pi f_pT_s n}$
	$Y_2 = \sum_{u=1}^{M}\sum_{v=1}^{M}[\mathbf{G}]_{u\,v}W^*_{f_pT_s}(u)W_{f_pT_s}(v)$
Finally	$\widehat{f_0T_s} = f_pT_s, \quad \hat{\mathbf{a}} = \mathbf{G}\mathbf{W}_{f_pT_s}, \quad \widehat{\mathbf{h}} = \boldsymbol{\Lambda}_{\widehat{f_0T_s}}\mathbf{B}\hat{\mathbf{a}}$

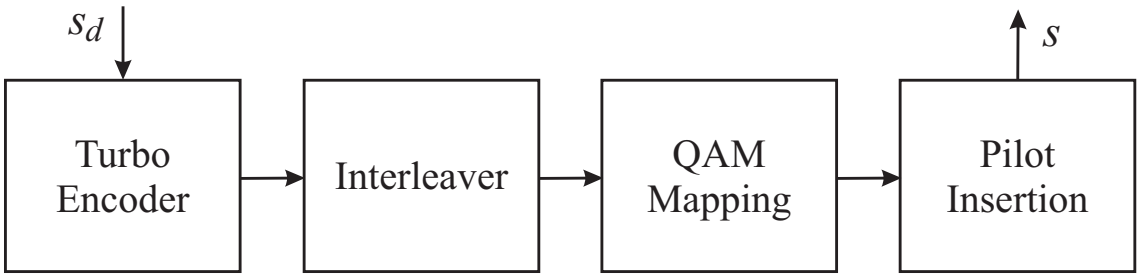

Figure 7.1: Turbo-based transmission system of QAM signals.

with $\mathbf{B}_p$, $\mathbf{S}_p$, $\mathbf{r}_p$. Then $\widehat{\mathbf{h}}$ is determined as in (7.9) and $\widehat{\mathbf{h}}_d$ can be obtained from $\widehat{\mathbf{h}}$ at the data instants. Finally, a minimum Euclidean distance detector is used as

$$\hat{s}_d = \arg\min_{s_d \in \mathcal{A}} \left\{ (\mathbf{r}_d - \mathbf{S}_d \widehat{\mathbf{h}}_d)^H (\mathbf{r}_d - \mathbf{S}_d \widehat{\mathbf{h}}_d) \right\} , \tag{7.10}$$

where $\mathcal{A}$ is the alphabet of all symbols corresponding to the modulation constellation points (we consider 2^K-QAM modulation, where K is the number of bits used to represent each symbol).

7.6 Iterative Receivers

To obtain a significant performance improvement, we develop turbo iterative receivers for QAM modulation systems in which joint channel and frequency offset estimation, detection and decoding are iteratively refined.

The turbo-based transmission system with QAM modulation is shown in Figure 7.1. First, the data bits are encoded by a turbo encoder. Then, the output bits of the turbo encoder are interleaved by a channel interleaver. After that, QAM mapping is performed where the output bits of the channel interleaver are grouped into QAM symbols. Finally, the pilot symbols are inserted periodically between each $T-1$ data symbols.

The proposed turbo-based iterative reception system for QAM modulated signals is shown in Figure 7.2. In the first iteration, pilot-based joint channel and frequency offset estimation is performed in the same way as discussed for the classical receivers considered in Section 7.5. The channel estimates are then passed to an improved detector, which

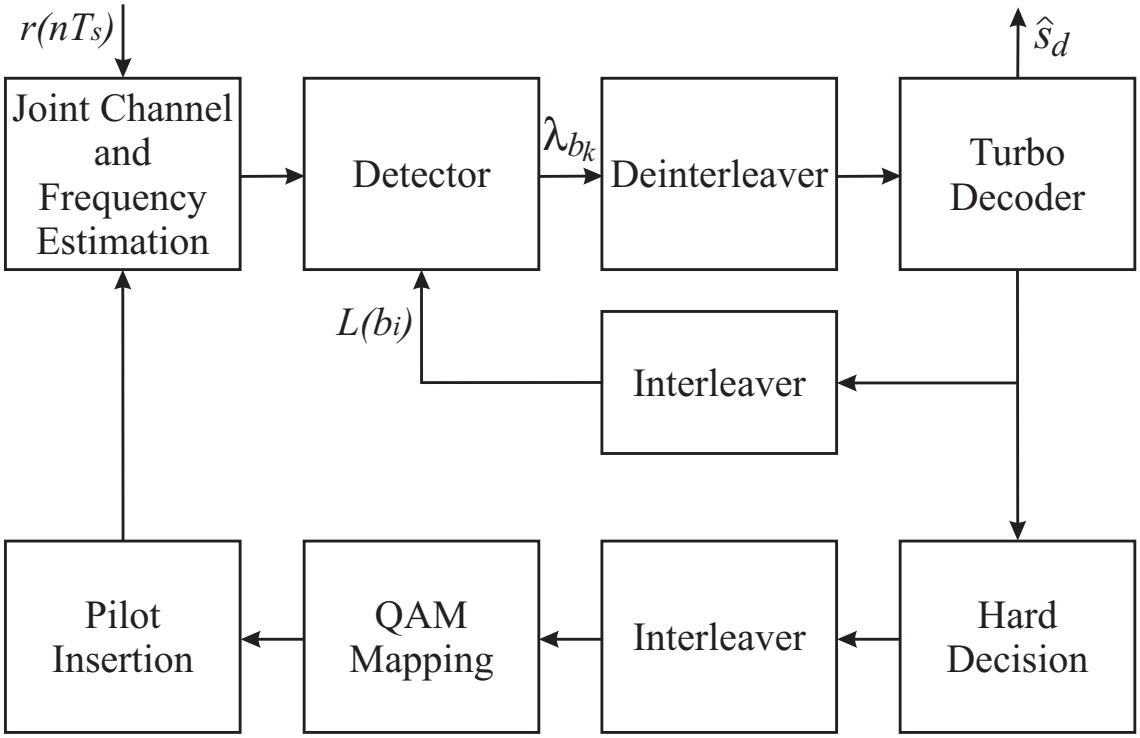

Figure 7.2: Proposed turbo-based iterative reception system of QAM signals.

has the ability in the subsequent iteration to improve the performance by utilising the soft output log-likelihood ratio (LLR) information generated at a soft-input soft-output (SISO) turbo decoder in the current iteration. In the first iteration, there are no *a priori* soft LLR from the decoder yet and the detector generates *a posteriori* soft LLR for every bit $b_k = \pm 1$, $k = 1, \ldots, K$ of a received symbol as

$$\lambda_{b_k} = \ln \sum_{s_d \in \mathcal{A}_k^+} e^{-\delta(s_d)} - \ln \sum_{s_d \in \mathcal{A}_k^-} e^{-\delta(s_d)}, \tag{7.11}$$

where $\mathcal{A}_k^{\pm} = \{s_d \in \mathcal{A} | b_k = \pm 1\}$ and the metric $\delta(s_d)$ is calculated as

$$\delta(s_d) = \sigma_z^{-2} \left| r_d - s_d \hat{h}_d \right|^2 . \tag{7.12}$$

The detector LLRs, λ_{b_k}, are then deinterleaved and passed to a SISO turbo iterative decoder, which generates initial decoded bits and initial soft LLR information. The decoder LLRs are then interleaved to provide *a priori* soft LLR, $L(b_i)$, which is required for the detector in the subsequent iteration. The decoder LLRs (which correspond to all coded bits) are also transformed to binary bits by hard decision. These are treated as initial coded data bits, which are then interleaved, QAM mapped (using Gray code) and have pilot symbols inserted in the same way as in the transmission system. The second iteration

then starts by performing the joint channel and frequency offset estimation, but now based on all pilot and data symbols, and so, more accurate estimates are obtained and passed to the detector. The improved detector then generates *a posteriori* soft LLR as [130]

$$\lambda_{b_k} = \ln \left[\frac{\sum_{s_d \in \mathcal{A}_k^+} e^{-\delta(s_d)} \prod_{i \neq k} P(b_i)}{\sum_{s_d \in \mathcal{A}_k^-} e^{-\delta(s_d)} \prod_{i \neq k} P(b_i)} \right] , \tag{7.13}$$

where $P(b_i)$ is *a priori* probability of a bit b_i and obtained using its *a priori* soft LLR, $L(b_i)$, as [130]

$$P(b_i) = \frac{1}{2} \left[1 + b_i \tanh \left(\frac{1}{2} L(b_i) \right) \right] . \tag{7.14}$$

Hence, the detector LLRs are now refined, which leads to refined decoder LLRs and less error in the decoded bits. The same estimation, detection and decoding reception scheme repeats for a few iterations to obtain a high-accuracy performance.

7.7 Simulation Results

Different basis functions can be used in the BEM such as complex exponential [38], Karhunen-Loève [87], discrete prolate spheroidal [41] and B-splines [51]. It is shown in Chapter 5 that the channel estimation based on B-splines is less sensitive to the accurate knowledge of statistical characteristics of the fading and simpler for implementation than that based on the other BEMs. Therefore, in our simulation, we use B-splines, however, other BEMs can also be used.

The mean square error (MSE) of the frequency offset and channel estimates, respectively, in each simulation trial are calculated as

$$f_0 T_s\text{-MSE} = \left(f_0 T_s - \widehat{f_0 T_s} \right)^2 , \tag{7.15a}$$

$$\mathbf{h}\text{-MSE} = \frac{\sum_{n=0}^{N-1} \left| h(nT_s) - \hat{h}(nT_s) \right|^2}{\sum_{n=0}^{N-1} |h(nT_s)|^2} \tag{7.15b}$$

and then averaged over all trials. We consider a PSAM system for 16-QAM signals transmitted in a time-variant fading channel with a Doppler frequency $f_D T_s = 0.01$ and the total number of symbols is $N = 514$, of which $N_p = 28$ are pilots that are inserted periodically every $T = 19$ symbols. We assume a frequency offset $f_0 T_s = 0.0123$ and a

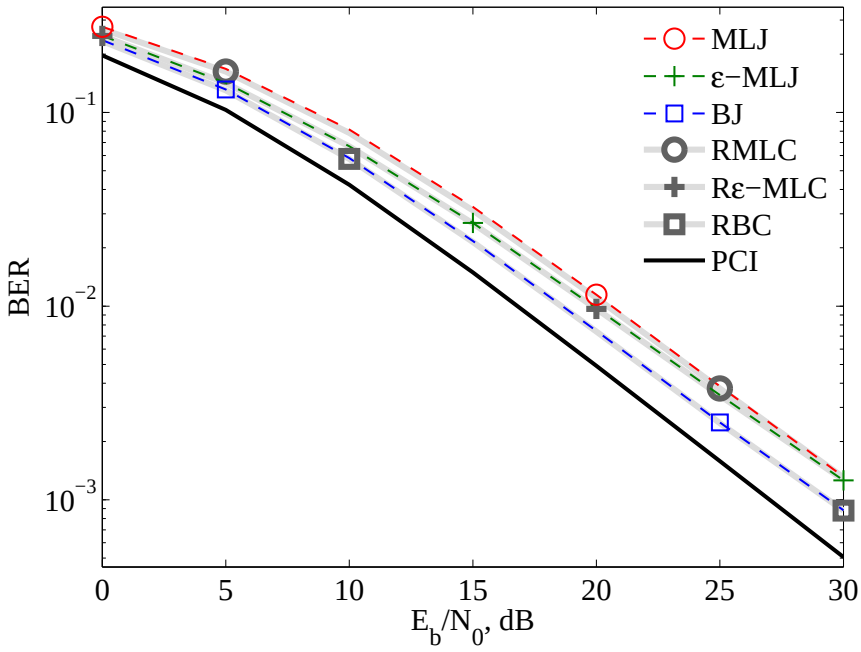

Figure 7.3: BER performance of the classical receivers for 16-QAM signals in frequency-flat time-variant fading channels; $N = 514$, $N_p = 28$, $T = 19$, $f_D T_s = 0.01$, $f_0 T_s = 0.0123$, $M = 23$, $N_{FFT} = 32$ and $Q = 5$.

wide frequency estimation range $\psi = 1$, where the number of dichotomous iterations in the fine search is $Q = 5$.

The BER performance of the developed joint estimation-based receivers is compared to that of the ideal reference channel-based receivers, where the frequency offset is assumed to be known, and also to the one operating with perfect channel information. The considered receivers/estimators are summarised in Table 7.2.

Figure 7.3 shows the BER performance of the classical receivers, where $M = 23$ and $N_{FFT} = 32$. The performance of the joint estimation-based receivers, MLJ, ϵ-MLJ, BJ is as good as that of the ideal reference RMLC, Rϵ-MLC, RBC channel-based receivers that operate with perfect knowledge of $f_0 T_s$ and is close to that of the PCI receiver that operates with perfect channel information. The performance of channel estimation ($\mathbf{h}$-MSE) and frequency offset estimation ($f_0 T_s$-MSE) can be seen in Figure 7.4 and Figure 7.5, respectively. The receivers based on joint estimation provide very close channel estimation performance to that of the corresponding ideal receivers with perfect frequency offset knowledge, and in all cases, the best performance is obtained by the Bayesian-based receiver, which employs more initial knowledge of channel statistics.

Table 7.2: Receivers/Estimators for Frequency-Selective Time-Variant Fading Channels Considered in the Simulation.

	Maximum Likelihood	**Regularised-Maximum Likelihood**	**Bayesian**
Computation	$\boldsymbol{\Upsilon} = \mathbf{O}$	$\boldsymbol{\Upsilon} = \sigma_g^{-2}\sigma_z^2\mathbf{I}_M$	$\boldsymbol{\Upsilon} = \sigma_z^2\mathbf{R}_a^{-1}$
$\widehat{f_0 T_s}$ as in (7.6)	MLF	ϵ-MLF	BF
$\widehat{\mathbf{h}}$ as in (7.9)	MLJ	ϵ-MLJ	BJ
$\widehat{\mathbf{h}}$ as in (7.9); $\widehat{f_0 T_s} = f_0 T_s$	RMLC	Rϵ-MLC	RBC
$\widehat{\mathbf{h}} = \mathbf{h}$			PCI

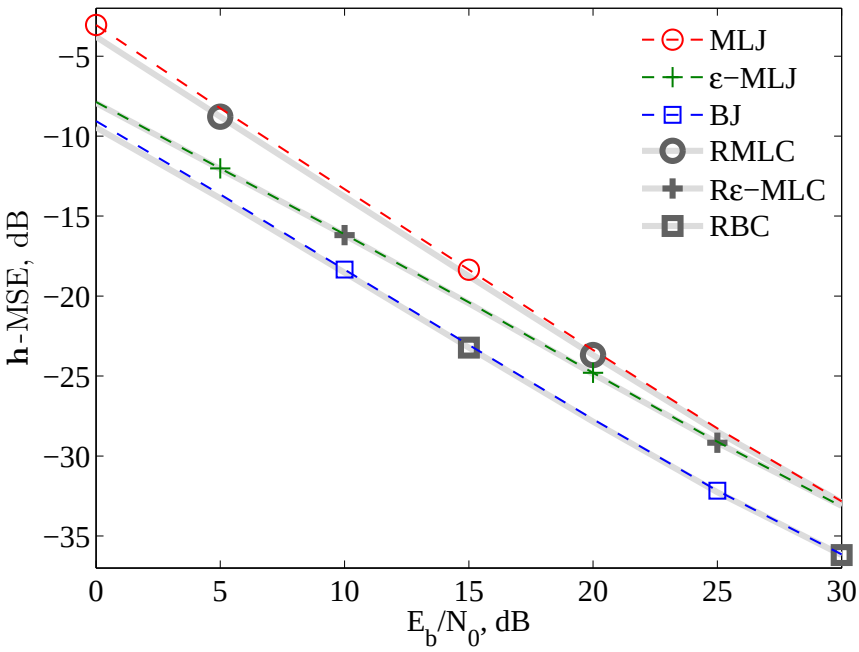

Figure 7.4: $\mathbf{h}$-MSE performance of the classical receivers for 16-QAM signals in frequency-flat time-variant fading channels; $N = 514$, $N_p = 28$, $T = 19$, $f_D T_s = 0.01$, $f_0 T_s = 0.0123$, $M = 23$, $N_{FFT} = 32$ and $Q = 5$.

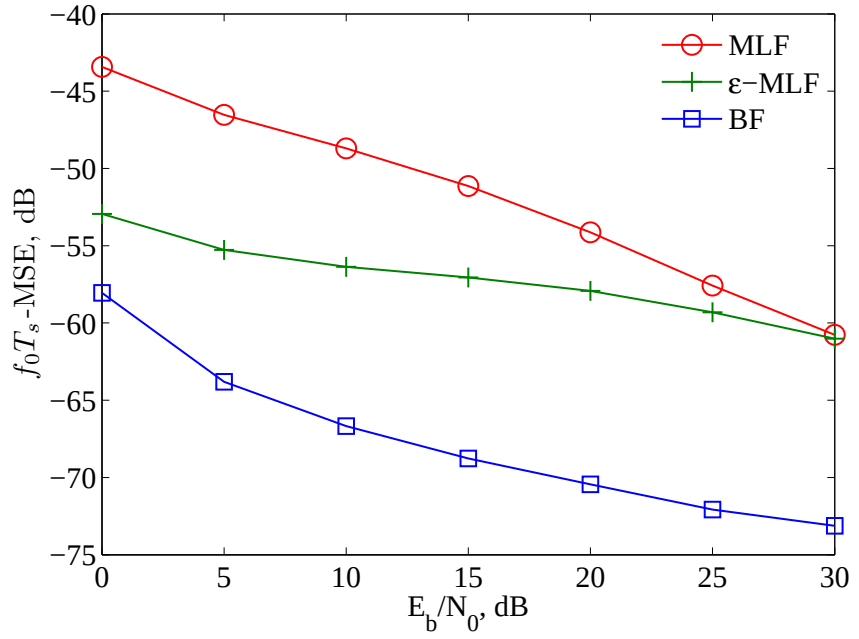

Figure 7.5: $f_0 T_s$-MSE performance of the classical receivers for 16-QAM signals in frequency-flat time-variant fading channels; $N = 514$, $N_p = 28$, $T = 19$, $f_D T_s = 0.01$, $f_0 T_s = 0.0123$, $M = 23$, $N_{FFT} = 32$ and $Q = 5$.

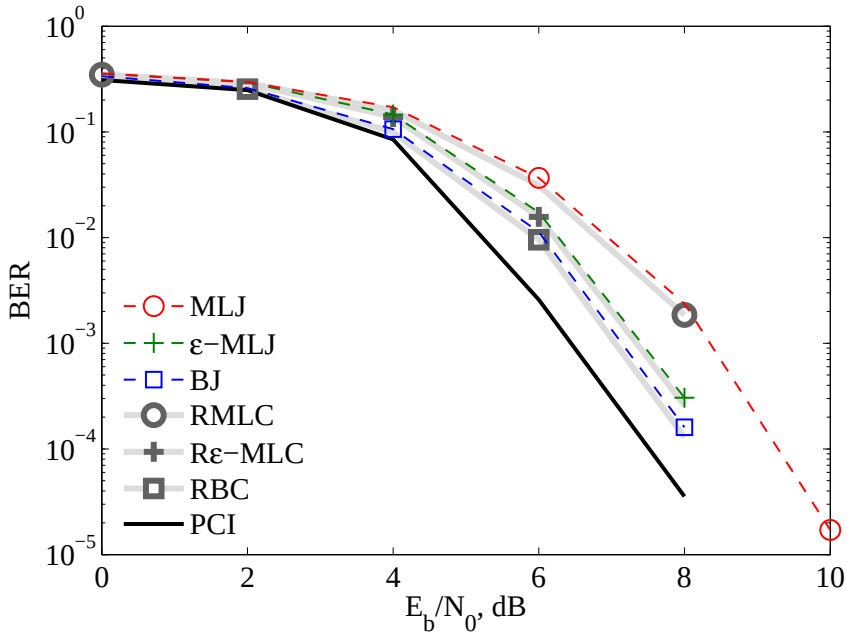

Figure 7.6: BER performance of the developed iterative turbo receivers for 16-QAM signals in frequency-flat time-variant fading channels encoded by a $1/3$ turbo coder with generation polynomial of 13, 15 in octal and obtained after the 4th iteration; $N = 514$, $N_p = 28$, $T = 19$, $f_D T_s = 0.01$, $f_0 T_s = 0.0123$, $M = 17$, $N_{FFT} = N$ and $Q = 5$.

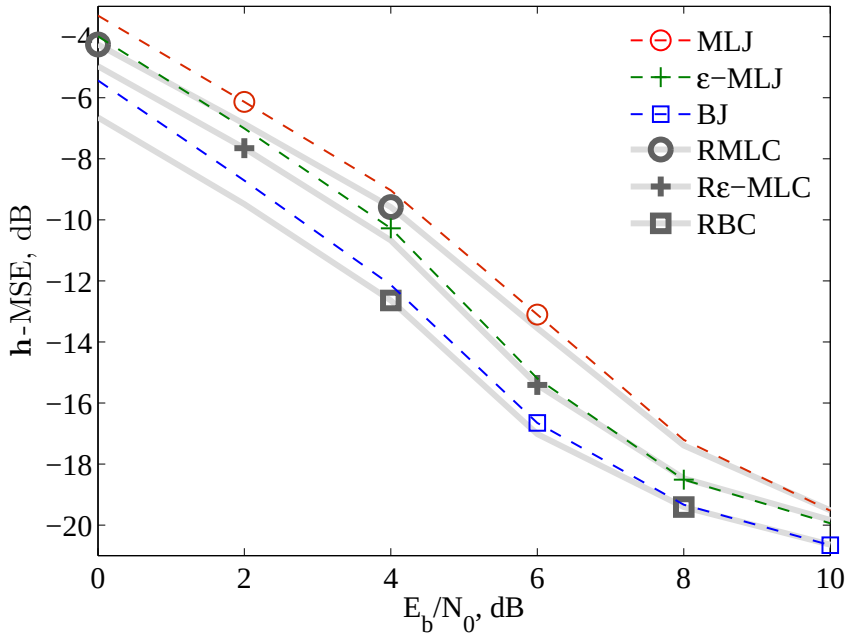

Figure 7.7: $\mathbf{h}$-MSE performance of the developed iterative turbo receivers for 16-QAM signals in frequency-flat time-variant fading channels encoded by a $1/3$ turbo coder with generation polynomial of 13, 15 in octal and obtained after the 4th iteration; $N = 514$, $N_p = 28$, $T = 19$, $f_D T_s = 0.01$, $f_0 T_s = 0.0123$, $M = 17$, $N_{FFT} = N$ and $Q = 5$.

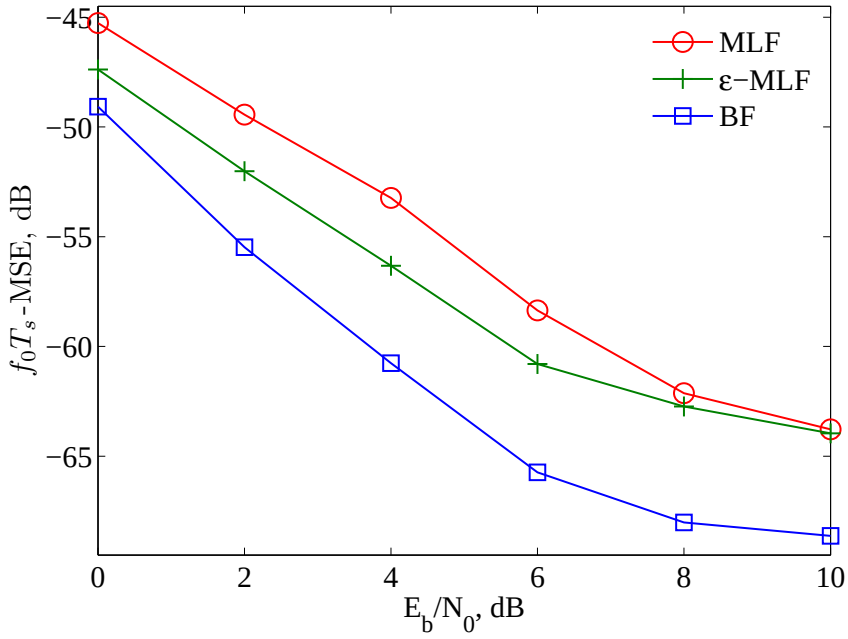

Figure 7.8: f_0T_s-MSE performance of the developed iterative turbo receivers for 16-QAM signals in frequency-flat time-variant fading channels encoded by a $1/3$ turbo coder with generation polynomial of 13, 15 in octal and obtained after the 4th iteration; $N = 514$, $N_p = 28$, $T = 19$, $f_DT_s = 0.01$, $f_0T_s = 0.0123$, $M = 17$, $N_{FFT} = N$ and $Q = 5$.

Figure 7.6, Figure 7.7 and Figure 7.8 show BER, $\mathbf{h}$-MSE and f_0Ts-MSE performance for the proposed iterative receivers/estimators encoded by a $1/3$ turbo coder of which the generation polynomial is 13, 15 in octal and obtained after the 4th iteration, where $M = 17$ and $N_{FFT} = N$. It can be seen that a significant performance improvement over the classical receivers is obtained, and again, the joint estimation-based receivers provide very close performance to that using the ideal reference channel estimators operating with perfect frequency offset knowledge and is close to that of the iterative receiver with perfect channel information.

7.8 Conclusions

We have developed iterative turbo receivers for time-variant fading channels which jointly perform channel and frequency offset estimation together with data detection and decoding. The Bayesian, maximum likelihood and regularised-maximum likelihood estimators

have been presented depending on how much knowledge of channel statistics is available. The estimation and detection are based on the basis expansion model representation of the fading time variations, the B-splines BEM is chosen, and use the dichotomous search frequency estimation technique. Soft information generated in the turbo decoder is used to improve the quality of the detection in the subsequent iterations. Simulation results have shown that the proposed receivers provide as good performance as the corresponding ones operating with perfect knowledge of the frequency offset, and is very close to that operating with perfect channel knowledge.

Chapter 8

Conclusions and Further Work

Contents

This thesis has investigated the joint channel and frequency offset estimation in different scenarios of wireless communications. The joint estimation of the channel and frequency offset in AWGN channels has been investigated and the performance has been compared in terms of accuracy and complexity of advanced frequency estimators that have been recently proposed in the literature and the DS estimator has been found to be the best choice. DS-based joint estimation of channel and frequency offset in time-invariant frequency-selective channels has been studied. A joint channel and frequency offset estimators have been proposed for frequency-flat time-variant fading channels based on different BEMs (such as the KL, DPS, GCE, and BS) of the fading time variations and the DS frequency estimation, where the BS-BEM has been found to be the best choice. Joint channel and frequency offset estimator has been proposed for doubly-selective fading channels based on the BS-BEM representation of the fading process and the DS frequency estimation. Finally, iterative turbo receivers have been developed for frequency-flat time-variant fading channels which jointly perform channel and frequency offset estimation together with data detection and decoding based on the BS-BEM of the fading process and the DS frequency estimation, where soft information generated in the turbo decoder is used to improve the quality of detection in the subsequent iterations.

8.1 Conclusions

A brief introduction of the whole work has been given, and fundamental techniques that have been used throughout the thesis, including simulators of time-variant fading channels, BEMs and turbo codes have been presented.

The maximum likelihood (ML) joint channel and frequency offset estimation has been presented for signals propagated through AWGN channels. The CRLBs of the joint estimators have been given. A literature review has been provided for the two main approaches approximating the ML estimator, namely, the correlation-based and the periodogram-based estimators, including some recently introduced advanced frequency estimators. In the first approach, conventional estimators possess good accuracy, however they normally have a high complexity. These estimators also possess a limited frequency estimation range that depends on the number of observed symbols, and so, might be inapplicable for certain practical scenarios. In the second approach, conventional estimators either exploit complicated nonlinear techniques or have a poor and inconsistent performance that depend on some parameters of the signal. The performance of recently introduced advanced frequency estimators has been studied. With the exception of the WNALP estimator, the performance of the correlation-based estimators considered has been shown to be frequency-sensitive at low SNRs, whereas the frequency increases, the performance degrades and the SNR threshold increases. Their frequency estimation range is also narrower than that of the WNALP and periodogram-based estimators. However, the WNALP has a relatively high complexity. For the periodogram-based estimators considered, the IDS and MLAF estimators possess the highest complexity. At low SNRs, the performance of both the MDS and IDS estimators is frequency-sensitive, whereas at high SNRs, the MLAF estimator possesses a frequency-sensitive performance. The DS estimator, exploiting a two stage technique for searching the periodogram peak, an FFT-based coarse search and dichotomous fine search, has been shown to outperform the other estimators in many scenarios, keeping a high-accuracy performance for all considered SNRs and throughout the wide frequency estimation range. It also relies only on linear operations with a relatively low complexity, which makes it the best choice in many practical scenarios, and so, the DS estimator has been used throughout the thesis. The DS-based joint channel and frequency offset estimator has been investigated for different scenarios.

Results have shown a high-accuracy performance of the joint channel and frequency offset estimators, which is very close to that of the ML estimator throughout all the wide frequency acquisition range and over a wide range of SNR.

The joint estimation of the channel and frequency offset for signals propagated through time-invariant frequency-selective channels has been investigated. The frequency offset estimators utilise the multipath diversity by combining the periodograms of the multipath components and searching for the greatest of the combined statistic. The CRLBs have been presented for these estimators. Two joint estimators, Bayesian-based estimator that can provide a high-accuracy performance whenever prior knowledge of certain channel statistics, namely the covariance matrix of the fading and the variance of the AWGN, is available, and ML-based estimator, with a slightly higher estimation error, that can operate in the absence of these channel statistics, have been studied. To reduce the estimation complexity and keep a high accuracy, the estimators exploit the DS frequency estimation technique of two-stage searching for the generalised periodogram peak. The estimators have been investigated for different application scenarios in Rayleigh fading channels. Results have shown a high-accuracy performance with an estimation error very close to the CRLB throughout the wide frequency acquisition range and over a wide range of SNR.

Novel joint channel and frequency offset estimators have been derived for frequency-flat time-variant fading channels. These estimators rely on representing the time-variant fading process using the BEM, which leads to a simplification in the processing and allows the estimators to achieve a high-accuracy performance. The new estimators use the DS frequency offset estimation technique, which allows a reduction in the complexity, and attaining a high accuracy performance. Two Bayesian-based and ML-based joint estimators have been proposed depending on the availability of the prior knowledge of the channel statistics. The proposed Bayesian joint estimator have been studied based on different BEMs such as, KL, DPS, GCE, and BS functions for different scenarios in Rayleigh fading channels, where the channel statistics are perfectly or imperfectly known. For perfectly known channel statistics, results have shown that the KL and DPS BEMs use fewer basis functions than the GCE and BS BEMs to allow achieving the same performance. However, the best reached performance of all the BEM-based estimators is the same. For mismatched channel statistics, results have shown that the GCE and BS BEMs

are more robust than the KL and DPS BEMs. This makes the BS-BEM a better choice in practice as it has a sparse matrix that results in a lower complexity than the other basis functions, and so, the BS-BEM has been used throughout the thesis. The proposed BS-based Bayesian and ML joint estimators have been investigated for different application scenarios in Rayleigh fading channels. Results have shown that the proposed DS-based frequency offset estimators outperform known correlation-based estimators. The new estimators have also been shown to possess the widest frequency acquisition range, which can be adjusted according to a priori knowledge of the frequency offset range to improve the accuracy for low SNRs. The proposed joint estimators offer a substantial performance improvement compared to the Bayesian channel estimator that ignores the frequency offset. Both proposed estimators have been shown to keep a high-accuracy performance over wide SNR, frequency offset and Doppler frequency ranges, which is very close to that of the Bayesian channel estimator operating with perfect frequency offset knowledge. An explicit criterion for adjusting the estimator parameters has been presented so that according to the required SNR range and the Doppler frequency, the maximum accuracy of the frequency and channel estimation is achieved within the minimum complexity. Moreover, the proposed estimation techniques are superior in being able to compensate for the inaccuracy in the frequency offset estimation and capable of achieving a high-accuracy channel estimation performance even without zero-padding the processed signal and using a simplified fine search.

A novel joint channel and frequency offset estimator has been derived for doubly-selective fading channels. This estimator is based on the the B-spline BEM representation of the fading process that simplifies the solution and allows achieving a high accuracy performance. The joint estimator relies on the Bayesian approach and provides a high accuracy performance when the prior knowledge of the statistical characteristics of the channel is available. The DS frequency estimation technique is used to reduce the complexity of the frequency offset estimation. Simulation results for different scenarios in Rayleigh fading channels have shown that the proposed estimator keeps a high accuracy performance, over wide SNR, frequency offset and Doppler frequency ranges, which is very close to that of the Bayesian channel estimator operating with perfect knowledge of the frequency offset.

Iterative turbo receivers have been developed for time-variant fading channels which

jointly perform channel and frequency offset estimation together with data detection and decoding. Depending on how much knowledge of the channel statistics is available, the Bayesian, maximum likelihood and regularised-maximum likelihood estimators have been presented. The estimation and detection are based on the B-splines BEM representation of the fading time variations and use the DS frequency estimation technique. Soft information generated in the turbo decoder is used to improve the detection performance in the subsequent iterations. Simulation results have shown that the proposed receivers provide as good performance as the corresponding ones operating with perfect knowledge of the frequency offset, and is very close to that operating with perfect channel knowledge.

8.2 Further Work

Some suggestions for further work based on this thesis are given below:

- In this thesis, the performance of the joint channel and frequency offset estimation in frequency-flat time-variant fading channels has been studied for the case of the perfect knowledge of the Doppler frequency using different BEMs in slow, moderate, and fast fading channels. The cubic B-spline is used as it has been reported in the literature to provide the best trade-off between accuracy and complexity in many scenarios. However, a noticeable higher number of cubic B-splines are required for the fast fading channels compared to that of the Karhunen-Loève and discrete prolate spheroidal basis functions for the estimator to achieve its best performance. It is expected that a higher order B-splines is a better choice for the fast fading channels to reduce the required number of basis functions, but further research needs to be done here to compare the performance in terms of accuracy and complexity for that scenario.

- The iterative turbo receivers with joint estimation of channel and frequency offset in frequency-flat time-variant fading channels are considered to operate with perfect knowledge of the Doppler frequency. The sensitivity of the channel estimation to the mismatched Doppler frequency has been investigated in some of our publications, where the performance is found to be very sensitive to underestimation

of the Doppler frequency and has little sensitivity to overestimation, which can be assumed to be applicable for the joint channel and frequency offset estimation as well. Therefore, a good upgrade of the work in this thesis is to derive a practical joint channel, frequency offset and Doppler frequency estimator (with a certain Doppler frequency overestimation to avoid degradation in performance caused by underestimation of the Doppler frequency) and investigate the performance of iterative turbo receivers that use this upgraded joint estimator.

- In this thesis, the joint channel and frequency offset estimators are derived and investigated for the Rayleigh fading channels. It is straightforward to specify the estimators for different types of fading channels, such as the Rician and Nakagami fading channels, by considering the different corresponding PDFs of the fading process, with the presence of a vector of means and a different covariance matrix. Therefore, it will be helpful to extend the joint estimators for such more general fading channels and more research can be done to investigate its performance.

- The iterative turbo receivers with joint estimation of channel and frequency offset in time-variant fading channels are considered in this thesis. Those receivers can be specified in a future research for orthogonal frequency division multiplexing (OFDM) signals in frequency-selective channels, which has been of great interest recently. This can be done by employing pilot tones and perform similar BEM-based processing in the frequency domain.

- In this thesis, the iterative turbo receivers with joint estimation of channel and frequency offset are considered for single-input single-output (SISO) fading channels. In a further research work, those receivers can be extended for the multiple-input multiple-output (MIMO) fading channels, where special techniques concerning multiplexing are required.

Glossary

AWGN	**A**dditional **W**hite **G**aussian **N**oise
BEM	**B**asis **E**xpansion **M**odel
BER	**B**it-**E**rror-**R**ate
BS	**B**-**S**plines
BPSK	**B**inary **P**hase **S**hift **K**eying
CE	**C**omplex **E**xponential
CP	**C**yclic **P**refix
dB	Decibel
DPS	**D**iscrete **P**rolate **S**pheroidal
FEC	**F**orward **E**rror **C**orrection
Hz	**H**ertz
ICI	**I**nter-**C**arrier **I**nterference
ISI	**I**nter-**S**ymbol **I**nterference
IDFT	**I**nverse **D**iscrete **F**ourier **T**ansform
GCE	**G**eneralized **C**omplex **E**xponential
KL	**K**arhunen-**L**oeve
LLR	**L**og-**L**ikelihood **R**atio
MAP	**M**aximum **A** **P**osteriori
MIMO	**M**ultiple-**I**nput **M**ultiple-**O**utput
ML	**M**aximum **L**ikelihood
MLSE	**M**aximum **L**ikelihood **S**equential **E**stimation
MMSE	**M**inimum **M**ean **S**quare **E**rror
MSE	**M**ean **S**quare **E**rror
NSC	**N**on-**S**ystematic **C**onvolutional
OFDM	**O**rthogonal **F**requency **D**ivision **M**ultiplexing

PCI	**P**erfect **C**hannel **I**nformation
PDF	**P**robability **D**ensity **F**unction
PSAM	**P**ilot **S**ymbol **A**ssisted **M**odulation
PSK	**P**hase-**S**hift **K**eying
QAM	**Q**uadrature **A**mplitude **M**odulation
rms	**r**oot-**m**ean-**s**quare
RSC	**R**ecursive **S**ystematic **C**onvolutional
SIHO	**S**oft-**I**nput **H**ard-**O**utput
SISO	**S**oft-**I**nput **S**oft-**O**utput
SISO	**S**ingle-**I**nput **S**ingle-**O**utput
SNR	**S**ignal to **N**oise **R**atio
STBC	**S**pace-**T**ime **B**lock **C**odes
STTC	**S**pace-**T**ime **T**rellis **C**odes
SVD	**S**ingular **V**alue **D**ecomposition

Bibliography

[1] U. Mengali and A. N. D'Andrea, *Synchronization Techniques for Digital Receivers*, Plenum Press, New York, 1997.

[2] H. Meyr, M. Moeneclaey, and S. A. Fechtel, *Digital Communication Receivers: Synchronization, Channel Estimation, and Signal Processing*, Wiley, New York, 1998.

[3] J. H. Lodge and M. L. Moher, "Time diversity for mobile satellite channels using trellis coded modulations", in *Proc. IEEE GLOBECOM'87*, Tokyo, Japan, Nov. 1987, vol. 3.

[4] J. K. Cavers, "An analysis of pilot symbol assisted modulation for Rayleigh fading channels", *IEEE Trans. Veh. Technol.*, vol. 40, no. 4, pp. 686–693, Nov. 1991.

[5] M. P. Fitz, "Further results in the fast estimation of a single frequency", *IEEE Trans. Commun.*, vol. 42, no. 2/3/4, pp. 862–864, February/March/April 1994.

[6] M. Luise and R. Reggiannini, "Carrier frequency recovery in all-digital modems for burst-mode transmissions", *IEEE Trans. Commun.*, vol. 43, no. 2/3/4, pp. 1169–1178, February/March/April 1995.

[7] S. S. Abeysekera, "Performance of pulse-pair method of Doppler estimation", *IEEE Trans. Aerosp. Electron. Syst.*, vol. 34, no. 2, pp. 520–531, Apr. 1998.

[8] O. Besson and P. Stoica, "On frequency offset estimation for flat-fading channels", *IEEE Commun. Lett.*, vol. 5, no. 10, pp. 402–404, October 2001.

[9] U. Mengali and M. Morelli, "Data-aided frequency estimation for burst digital transmission", *IEEE Trans. Commun.*, vol. 45, no. 1, pp. 23–25, January 1997.

[10] P. Ubolkosold, G. F. Tchere, S. Knedlik, and O. Loffeld, "Simple carrier frequency offset estimators in frequency flat-fading channels", in *Proc. IEEE ICC'07*, Glasgow, UK, June 2007, pp. 2671–2675.

[11] P. Ubolkosold, G. F. Tchere, S. Knedlik, and O. Loffeld, "A new closed-form frequency estimator in the presence of fading-induced multiplicative noise", in *Proc. IEEE VTC'08*, Singapore, May 2008, pp. 2912–2616.

[12] A. B. Awoseyila, C. Kasparis, and B. G. Evans, "Improved single frequency estimation with wide acquisition range", *Electron. Lett.*, vol. 44, no. 3, pp. 245–246, Jan. 2008.

[13] D. C. Rife and R. R. Boorstyn, "Single-tone parameter estimation from discrete-time observations", *IEEE Trans. Info. Theory*, vol. IT-20, no. 5, pp. 591–598, September 1974.

[14] B. G. Quinn, "Estimation of frequency, amplitude, and phase from the DFT of a time series", *IEEE Trans. Signal Process.*, vol. 45, no. 3, pp. 814–817, March 1997.

[15] M. D. Macleod, "Fast nearly ML estimation of the parameters of real or complex single tones or resolved multiple tones", *IEEE Trans. Signal Process.*, vol. 46, no. 1, pp. 141–148, January 1998.

[16] T. J. Abatzoglou, "A fast maximum likelihood algorithm for frequency estimation of a sinusoid based on Newton's method", *IEEE Trans. Acoust. Speech Signal Process.*, vol. ASSP-33, no. 1, pp. 77–89, February 1985.

[17] Y. V. Zakharov and T. C. Tozer, "Frequency estimator with dichotomous search of periodogram peak", *Electron. Lett.*, vol. 35, no. 19, pp. 1608–1609, September 1999.

[18] E. Aboutanios, "A modified dichotomous search frequency estimator", *IEEE Signal Process. Lett.*, vol. 11, no. 2, pp. 186–188, February 2004.

[19] B. Thoshkahna and K. R. Ramakrishnan, "A robust initialization scheme for faster convergence of the dichotomous search algorithm for single frequency estimation", in *Proc. IEEE ICSP'08*, Beijing, China, Oct. 2008, pp. 108–111.

[20] C. Yang, G. Wei, and F. Chen, "An estimation-range extended autocorrelation-based frequency estimator", *EURASIP Journal on Advances in Signal Processing*, vol. 2009, Article ID 961938, Oct. 2009.

[21] D. Tse and P. Viswanath, *Fundamentals of Wireless Communications*, Cambridge University Press, New York, 2005.

[22] J. G. Proakis, *Digital Communications*, McGraw-Hill, International Editions, 3rd edition, 1995.

[23] T. S. Rappaport, *Wireless Communications: Principles and Practice*, Prentice Hall PTR, Upper Saddle River, New Jersey, 2nd edition, 2002.

[24] M. Pätzold, *Mobile Fading Channels*, John Wiley & Sons, Chichester, 2002.

[25] M. G. Hebley and D. P. Taylor, "The effect of diversity on a burst-mode carrier-frequency estimator in the frequency-selective multipath channel", *IEEE Trans. Commun.*, vol. 46, no. 4, pp. 553–560, April 1998.

[26] J. K. Cavers, "Fast acquisition of carrier and timing in low SNR and fading using diversity antennas", in *Proc. IEEE VTC'97*, Phoenix, Arizona, USA, May 1997, pp. 1748–1752.

[27] K. W. Yip and T. S. Ng, "Efficient simulation of digital transmission over WSSUS channels", *IEEE Trans. Commun.*, vol. 43, no. 12, pp. 2907–2913, December 1995.

[28] M. Pätzold, U. Killat, F. Laue, and Y. Li, "On the statistical properties of deterministic simulation models for mobile fading channels", *IEEE Trans. Veh. Technol.*, vol. 2, pp. 254–269, February 1998.

[29] A. Sayeed and B. Aazhang, "Joint multipath-Doppler diversity in fast fading channels", in *Proc. IEEE ICASSP'98*, Seattle, Washington, USA, May 1998, vol. 6, pp. 3237–3240.

[30] A. M. Sayeed and B. Aazhang, "Joint multipath-Doppler diversity in Mobile wireless communications", *IEEE Trans. Commun.*, vol. 47, no. 1, pp. 123–132, January 1999.

[31] K. E. Scott and E. B. Olasz, "Simultaneous clock phase and frequency offset estimation", *IEEE Trans. Commun.*, vol. 43, no. 7, pp. 2263–2270, July 1995.

[32] M. Morelli and U. Mengali, "Joint frequency and timing recovery for MSK-type modulation", *IEEE Trans. Commun.*, vol. 47, no. 6, pp. 938–946, June 1999.

[33] M. Ghogho and A. Swami, "Estimation of frequency offset and Doppler rate in fading channels", in *Proc. IEEE ICPWC'99*, Jaipur, India, February 1999, vol. 3, pp. 105–109.

[34] W. Y. Kuo and M. P. Fitz, "Frequency offset compensation of pilot symbol assisted modulation in frequency flat fading", *IEEE Trans. Commun.*, vol. 45, no. 11, pp. 1412–1416, November 1997.

[35] M. Morelli, U. Mengali, and G. M. Vitetta, "Further results in carrier frequency estimation for transmissions over flat fading channels", *IEEE Commun. Lett.*, vol. 2, no. 12, pp. 327–330, December 1998.

[36] M. K. Tsatsanis and G. B. Giannakis, "Modeling and equalization of rapidly fading channels", *Int. J. Adaptive Control Signal Processing*, vol. 10, no. 2/3, pp. 159–176, Mar. 1996.

[37] P. Hoeher, S. Kaiser, and P. Robertson, "Two-dimensional pilot-symbol-aided channel estimation by Wiener filtering", in *Proc. IEEE ICASSP'98*, Munich, Germany, Apr. 1997, vol. 3, pp. 1845–1848.

[38] G. B. Giannakis and C. Tepedelenlioğlu, "Basis expansion models and diversity techniques for blind identification and equalization of time-varying channels", *Proc. IEEE*, vol. 86, no. 10, pp. 1969–1986, Oct. 1998.

[39] D. K. Borah and B. D. Hart, "Frequency-selective fading channel estimation with a polynomial time-varying channel model", *IEEE Trans. Commun.*, vol. 47, no. 6, pp. 862–873, Jun. 1999.

[40] X. Ma, G. B. Giannakis, and S. Ohno, "Optimal training for block transmissions over doubly selective wireless fading channels", *IEEE Trans. Signal Process.*, vol. 51, no. 5, pp. 1351–1366, May 2003.

[41] T. Zemen and C. F. Mecklenbräuker, "Time-variant channel estimation using discrete prolate spheroidal sequences", *IEEE Trans. Signal Process.*, vol. 53, no. 9, pp. 3597–3607, Sep. 2005.

[42] H. Mai, Y. V. Zakharov, and A. G. Burr, "Iterative channel estimation based on B-splines for fast flat fading channels", *IEEE Trans. Wireless Commun.*, vol. 6, no. 4, pp. 1224–1229, April 2007.

[43] Y. V. Zakharov, T. C. Tozer, and J. F. Adlard, "Polynomial spline-approximation of Clarke's model", *IEEE Trans. Signal Process.*, vol. 52, no. 5, pp. 1198–1208, May 2004.

[44] V. M. Baronkin, Y. V. Zakharov, and T. C. Tozer, "Maximum likelihood single tone frequency estimation in a multipath channel", *IEE Proc.-Commun.*, vol. 148, no. 6, pp. 400–404, December 2001.

[45] L. C. Palmer, "Coarse frequency estimation using the discrete Fourier transform", *IEEE Trans. Info. Theory*, vol. IT-20, no. 1, pp. 104–109, January 1974.

[46] M. Morelli and U. Mengali, "Carrier-frequency estimation for transmissions over selective channels", *IEEE Trans. Commun.*, vol. 48, no. 9, pp. 1580–1589, September 2000.

[47] Y. V. Zakharov, V. M. Baronkin, and T. C. Tozer, "DFT-based frequency estimators with narrow acquisition range", *IEE Proc.-Commun.*, vol. 148, no. 1, pp. 1–7, February 2001.

[48] V. M. Baronkin, Y. V. Zakharov, and T. C. Tozer, "Frequency estimation in slowly fading multipath channels", *IEEE Trans. Commun.*, vol. 50, no. 11, pp. 1848–1859, November 2002.

[49] R. N. Khal, Y. V. Zakharov, and J. Zhang, "Joint channel and frequency offset estimators for frequency-flat fast fading channels", in *Proc. 42nd Asilomar Conf. ACSSC'08*, Pacific Grove, California, USA, Oct. 2008, pp. 423–427.

[50] R. N. Khal, Y. V. Zakharov, and J. Zhang, "Robustness of joint Bayesian frequency offset and channel estimation based on basis expansion models", in *Proc. 43rd Asilomar Conf. ACSSC'09*, Pacific Grove, California, USA, Nov. 2009, pp. 957–961.

[51] Y. V. Zakharov, V. M. Baronkin, and J. Zhang, "Optimal and mismatched detection of QAM signals in fast fading channels with imperfect channel estimation", *IEEE Trans. Wireless Commun.*, vol. 8, no. 2, pp. 617–621, Feb. 2009.

[52] P. Ciblat, P. Bianchi, and M. Ghogho, "Training sequence optimization for joint channel and frequency offset estimation", *IEEE Trans. Signal Process.*, vol. 56, no. 8, pp. 3424–3436, Aug. 2008.

[53] T. Whitworth, M. Ghogho, and D. McLernon, "Optimized training and basis expansion model parameters for doubly-selective channel estimation", *IEEE Trans. Wireless Commun.*, vol. 8, no. 3, pp. 1490–1498, Mar. 2009.

[54] T. A. Kadous and A. M. Sayeed, "An integrated framework for MC-CDMA reception in the presence of frequency offsets, phase noise, and fast fading", *IEEE Trans. Wireless Commun.*, vol. 3, no. 4, pp. 1224–1235, Jul. 2004.

[55] J. Ylioinas and M. Juntti, "Iterative joint detection, decoding, and channel estimation in turbo-coded MIMO-OFDM", *IEEE Trans. Veh. Technol.*, vol. 58, no. 4, pp. 1784–1796, May 2009.

[56] Q. Yu and S. Lambotharan, "Iterative (turbo) estimation and detection techniques for frequency-selective channels with multiple frequency offsets", *IEEE Signal Process. Lett.*, vol. 14, no. 4, pp. 236–239, Apr. 2007.

[57] R. N. Khal and Y. V. Zakharov, "Iterative receivers with joint channel and frequency offset estimation in time-variant fading channels", in *Proc. IEEE ISWCS'10*, York, UK, Sep. 2010, pp. 844–848.

[58] R. N. Khal, "Comparison of accuracy and complexity of advanced frequency estimators", in *Proc. IEEE ISWCS'10*, York, UK, Sep. 2010, pp. 490–495.

[59] J. Zhang, R. N. Khal, and Y. V. Zakharov, "Sensitivity of channel estimation using B-splines to mismatched Doppler frequency", in *Proc. IEEE ISWCS'10*, York, UK, Sep. 2010, pp. 946–950.

[60] J. Zhang, Y. V. Zakharov, and R. N. Khal, "Optimum detection in spatially uncorrelated SIMO Rayleigh fast fading channels with imperfect channel estimation", in *Proc. IEEE ISWCS'10*, York, UK, Sep. 2010, pp. 476–479.

[61] R. N. Khal, Y. V. Zakharov, and J. Zhang, "B-spline based joint channel and frequency offset estimation in doubly-selective fading channels", in *Proc. IEEE ICASSP'10*, Dallas, Texas, USA, Mar. 2010, pp. 3214–3217.

[62] J. Zhang, Y. V. Zakharov, and R. N. Khal, "Optimal detection for STBC MIMO systems in spatially correlated Rayleigh fast fading channels with imperfect channel estimation", in *Proc. 43rd Asilomar Conf. ACSSC'09*, Pacific Grove, California, USA, Nov. 2009, pp. 1387–1391.

[63] R. H. Clarke, "A statistical theory of mobile-radio reception", *Bell Syst. Tech. J.*, vol. 47, no. 6, pp. 957–1000, July/August 1968.

[64] W. C. Jakes, *Microwave Mobile Communications*, Wiley-IEEE Press, reissue edition, 1994.

[65] Y. R. Zheng and C. Xiao, "Simulation models with correct statistical properties for Rayleigh fading channels", *IEEE Trans. on Commun.*, vol. 51, no. 6, pp. 920–928, 2003.

[66] P. Dent, G. E. Bottomley, and T. Croft, "Jakes fading model revisited", *Electron. Lett.*, vol. 29, no. 13, pp. 1162–1163, 1993.

[67] M. Patzold, U. Killat, F. Laue, and Y. Li, "On the statistical properties of deterministic simulation models for mobile fading channels", *IEEE Trans. on Veh. Technol.*, vol. 47, no. 1, pp. 254–269, 1998.

[68] Y. Li and X. Huang, "The simulation of independent Rayleigh faders", *IEEE Trans. on Commun.*, vol. 50, no. 9, pp. 1503–1514, 2002.

[69] K. W. Yip and T. S. Ng, "A simulation model for Nakagami-m fading channels, m<1", *IEEE Trans. on Commun.*, vol. 48, no. 2, pp. 214–221, 2000.

[70] Y. R. Zheng and C. Xiao, "Improved models for the generation of multiple uncorrelated Rayleigh fading waveforms", *IEEE Commun. Letters*, vol. 6, no. 6, pp. 256–258, 2002.

[71] C. Xiao, Y. R. Zheng, and N. C. Beaulieu, "Novel sum-of-sinusoids simulation models for Rayleigh and Rician fading channels", *IEEE Trans. on Wireless Commun.*, vol. 5, no. 12, pp. 3667—3679, 2006.

[72] D. J. Young and N. C. Beaulieu, "The generation of correlated Rayleigh random variates by inverse discrete Fourier transform", *IEEE Trans. on Commun.*, vol. 48, no. 7, pp. 1114–1127, 2000.

[73] K. E. Baddour and N. C. Beaulieu, "Accurate simulation of multiple cross-correlated Rician fading channels", *IEEE Trans. on Commun.*, vol. 52, no. 11, pp. 1980–1987, 2004.

[74] M. F. Pop and N. C. Beaulieu, "Limitations of sum-of-sinusoids fading channel simulators", *IEEE Trans. on Commun.*, vol. 49, no. 4, pp. 699–708, 2001.

[75] G. L. Stüber, *Principles of Mobile Communication*, Kluwer Academic Publishers, Boston, 2nd edition, 2001.

[76] I. S. Gradshteyn and I. M. Ryzhik, *Table of Integrals, Series, and Products*, Edited by A. Jeffrey and D. Zwillinger, Translated by Scripta Technica Inc., Academic Press, San Diego, 5th edition, 2007.

[77] M. Pätzold and F. Laue, "Statistical properties of Jakes' fading channel simulator", in *Proc. IEEE VTC'98*, Ottawa, Ontario, Canada, May 1998, vol. 2, pp. 712–718.

[78] M. F. Pop and N. C. Beaulieu, "Limitations of sum-of-sinusoids fading channel simulators", *IEEE Trans. Commun.*, vol. 49, no. 4, pp. 699–708, April 2001.

[79] Y. Li and Y. L. Guan, "Modified Jakes model for simulating multiple uncorrelated fading waveforms", in *Proc. IEEE ICC'00*, New Orleans, Louisiana, USA, June 2000, vol. 1, pp. 46–49.

[80] D. J. Young and N. C. Beaulieu, "The generation of correlated Rayleigh random variates by inverse discrete Fourier transform", *IEEE Trans. Commun.*, vol. 48, no. 7, pp. 1114–1127, July 2000.

[81] Y. R. Zheng and C. Xiao, "Simulation models with correct statistical properties for Rayleigh fading channels", *IEEE Trans. Commun.*, vol. 51, no. 6, pp. 920–928, June 2003.

[82] K. E. Baddour and N. C. Beaulieu, "Accurate simulation of multiple cross-correlated Rician fading channels", *IEEE Trans. Commun.*, vol. 52, no. 11, pp. 1980–1987, November 2004.

[83] C. Xiao and Y. R. Zheng, "Novel sum-of-sinusoids simulation models for Rayleigh and Rician fading channels", *IEEE Trans. Wireless Commun.*, vol. 5, no. 12, pp. 3667–3679, December 2006.

[84] G. Leus, "On the estimation of rapidly time-varying channels", in *Proc. European Signal Processing Conf. EUSIPCO'04*, Vienna, Austria, Sep. 2004, pp. 2227–2230.

[85] Z. Tang, R. C. Cannizzaro, G. Leus, and P. Banelli, "Pilot-assisted time-varying channel estimation for OFDM systems", *IEEE Trans. on Signal Process.*, vol. 55, no. 5, pp. 2226–2238, 2007.

[86] G. W. Wornell, "A Karhunen-Loeve-like expansion for 1/f processes via wavelets", *IEEE Trans. on Inf. Theory*, vol. 36, no. 4, pp. 859–861, 1990.

[87] M. Visintin, "Karhunen-Loève expansion of a fast Rayleigh fading process", *Electron. Lett.*, vol. 32, no. 18, pp. 1712–1713, Aug. 1996.

[88] D. Slepian, "Prolate spheroidal wave functions, Fourier analysis and uncertainty, V: The discrete case", *Bell Syst. Tech. J.*, vol. 43, no. 6, pp. 3009–3058, 1964.

[89] Z. Tang and G. Leus, "Time-multiplexed training for time-selective channels", *IEEE Signal Process. Lett.*, vol. 14, no. 9, pp. 585–588, 2007.

[90] P. Salvo Rossi and R. Muller, "Slepian-based two-dimensional estimation of time-frequency variant MIMO-OFDM channels", *IEEE Signal Process. Lett.*, vol. 15, 2008.

[91] Y. V. Zakharov and V. P. Kodanev, "Multipath-Doppler diversity of OFDM signals in an underwater acoustic channel", in *Proc. IEEE ICASSP'00*, Istanbul, Turkey, June 2000, vol. 5, pp. 2941–2944.

[92] D. Slepian, "Prolate spheroidal wave functions, Fourier analysis, and uncertainty. V- The discrete case", *Bell Syst. Tech. J.*, vol. 57, pp. 1371–1430, 1978.

[93] J. Kim, C. W. Wang, and W. E. Stark, "Frequency domain channel estimation for OFDM based on Slepian basis expansion", *Proc. IEEE ICC'07, Glasgow, Scotland*, pp. 3011–3015, 2007.

[94] M. Unser, A. Aldroubi, and M. Eden, "B-spline signal processing. I. Theory", *IEEE Trans. Signal Process.*, vol. 41, no. 2, pp. 821–833, February 1993.

[95] C. Berrou, A. Glavieux, and P. Thitimajshima, "Near Shannon limit error-correcting coding and decoding: Turbo-codes.", *Proc. IEEE ICC'93, Geneva, Switzerland*, vol. 2, pp. 1064–1070, 1993.

[96] G. White, "Optimised turbo codes for wireless Channels", *Ph.d. Thesis, University of York*, 2001.

[97] C. Berrou and A. Glavieux, "Near Optimum Error Correcting Coding And Decoding: Turbo-Codes", *IEEE Trans. on Commun.*, vol. 44, no. 10, pp. 1261, 1996.

[98] C. Berrou, "The ten-year-old turbo codes are entering into service", *IEEE Commun. Mag.*, vol. 41, no. 8, pp. 110–116, Aug. 2003.

[99] R. M. Pyndiah, "Near-optimum decoding of product codes: Block turbo codes", *IEEE Trans. on Commun.*, vol. 46, no. 8, pp. 1003–1010, 1998.

[100] J. Garcia-Frias, "Compression of correlated binary sources using turbo codes", *IEEE Commun. Lett.*, vol. 5, no. 10, pp. 417–419, 2001.

[101] S. Benedetto, R. Garello, and G. Montorsi, "A search for good convolutional codes to be used in the construction of turbo codes", *IEEE Trans. on Commun.*, vol. 46, no. 9, pp. 1101–1105, 1998.

[102] T. A. Summers and S. G. Wilson, "SNR mismatch and on–line estimation in turbo decoding", *IEEE Trans. on Commun.*, vol. 46, pp. 421–423, 1998.

[103] C. Berrou and M. Jezequel, "Non-binary convolutional codes for turbo coding", *Electron. Lett.*, vol. 35, no. 1, pp. 39–40, 1999.

[104] A. Burr, "Turbo-codes: the ultimate error control codes?", *Electronics & Communication Engineering Journal*, vol. 13, no. 4, pp. 155–165, 2001.

[105] D. Divsalar and F. Pollara, "Turbo codes for PCS applications", *Proc. IEEE ICC'95, Seattle, USA*, vol. 1, pp. 54–59, June 1995.

[106] B. Vucetic and J. Yuan, *Turbo codes: principles and applications*, Kluwer Academic Pub, 2000.

[107] L. Bahl, J. Cocke, F. Jelinek, and J. Raviv, "Optimal decoding of linear codes for minimizing symbol error rate", *IEEE Trans. on Inf. Theory*, vol. 20, no. 2, pp. 284–287, March 1974.

[108] M. M. Darmon and P. R. Sadot, "A new pseudo-random interleaving for antijamming applications", *Proc. IEEE MILCOM'89, Boston, MA, USA*, pp. 6–10, 1989.

[109] S. Dolinar and D. Divsalar, "Weight distributions for turbo codes using random and nonrandom permutations", *TDA Progress report*, vol. 42, no. 122, pp. 56–65, 1995.

[110] M. Ferrari, F. Scalise, S. Bellini, and D. E. e Inf, "Prunable s-random interleavers", *Proc. IEEE ICC'02, New York, USA*, vol. 3, pp. 1711–1715, 2002.

[111] L. Dinoi and S. Benedetto, "Design of fast-prunable S-random interleavers", *IEEE Trans. on Wireless Commun.*, vol. 4, no. 5, pp. 2540–2548, 2005.

[112] C. Heegard and S. B. Wicker, *Turbo coding*, Kluwer Academic Pub, 1999.

[113] P. Popovski, L. Kocarev, and A. Risteski, "Design of flexible-length S-random interleaver for turbo codes", *IEEE Commun. Lett.*, vol. 8, no. 7, pp. 461–463, 2004.

[114] S. Lin and D. J. Costello, *Error control coding*, Prentice-Hall Englewood Cliffs, NJ, 1983.

[115] P. Robertson, P. Hoeher, and E. Villebrun, "Optimal and sub-optimal maximum a posteriori algorithms suitable for turbo decoding", *Euro. Trans. on Telecom.*, vol. 8, no. 2, pp. 119–125, 1997.

[116] J. Vogt and A. Finger, "Improving the max-log-MAP turbo decoder", *Electron. lett.*, vol. 36, no. 23, pp. 1937–1939, 2000.

[117] A. Burr, *Modulation and coding: for wireless communications*, Prentice Hall, 2001.

[118] J. G. Proakis et al., *Digital Communication*, McGraw-Hill International 4th Editions, New York, 2001.

[119] J. Erfanian, S. Pasupathy, and G. Gulak, "Reduced complexity symbol detectors with parallel structure for ISI channels", *IEEE Trans. on Commun.*, vol. 42, no. 234 Part 3, pp. 1661–1671, 1994.

[120] W. Koch and A. Baier, "Optimum and sub-optimum detection of coded data disturbed by time-varying intersymbol interference", *Proc. IEEE Globecom'90, San Diego, CA, USA*, vol. 12, pp. 1679–1684, Nov. 1990.

[121] S. M. Kay, *Fundamentals of Statistical Signal Processing: Estimation Theory*, vol. I, Prentice Hall PTR, Upper Saddle River, New Jersey, 1993.

[122] T. K. Moon and W. C. Stirling, *Mathematical Methods and Algorithms for Signal Processing*, Prentice-Hall, Upper Saddle River, New Jersey, 2000.

[123] M. H. Hayes, *Statistical Digital Signal Processing and Modeling*, Wiley, New York, 1996.

[124] R. N. Khal, "DFT-based single frequency estimators for single-path and multipath channels", MSc by research thesis, University of York, York, UK, June 2007.

[125] C. H. Edwards and D. E. Penney, *Calculus*, Prentice-Hall, Upper Saddle River, New Jersey, 6th edition, 2002.

[126] F. Gini and G. B. Giannakis, "Frequency offset and symbol timing recovery in flat-fading channels: A cyclostationary approach", *IEEE Trans. Commun.*, vol. 46, no. 3, pp. 400–411, March 1998.

[127] B. G. Quinn, "Estimating frequency by interpolation using Fourier coefficients", *IEEE Trans. Signal Process.*, vol. 42, no. 5, pp. 1264–1268, May 1994.

[128] J. G. Proakis and D. G. Manolakis, *Digital Signal Processing: Principles, Algorithms, and Applications*, Prentice-Hall, Upper Saddle River, New Jersey, 3rd edition, 1996.

[129] Y. V. Zakharov, V. M. Baronkin, and J. Zhang, "Optimal detection of QAM signals in fast fading channels with imperfect channel estimation", in *Proc. IEEE ICASSP'08*, Las Vegas, Nevada, USA, March/April 2008, pp. 3205–3208.

[130] X. Wang and H. V. Poor, "Iterative (turbo) soft interference cancellation and decoding for coded CDMA", *IEEE Trans. Commun.*, vol. 47, no. 7, pp. 1046–1061, Jul. 1999.